UNIVERSITY OF CALIFORNIA
RIVERSIDE

Characterization of the DHH1/DDX6-Like RNA Helicase Family in *Arabidopsis thaliana*

A Dissertation submitted in partial satisfaction
of the requirements for the degree of

Doctor of Philosophy

in

Genetics, Genomics and Bioinformatics

by

Thanin Chantarachot

December 2018

Dissertation Committee:
Dr. Julia Bailey-Serres, Chairperson
Dr. Xuemei Chen
Dr. Fedor Karginov

The Dissertation of Thanin Chantarachot is approved:

Committee Chairperson

University of California, Riverside

Acknowledgements

I would like to express my sincere gratitude to my advisor, Dr. Julia Bailey-Serres, for welcoming me into her group. Without her patience, support, and insightful guidance, my PhD studies would not have been possible. To me, she is not only my advisor, but also a role model. I could not ask for a better mentor. I will cherish the memory of her wonderful mentorship and pass this on to my future students.

I would also like to thank the other members of my dissertation committee, Dr. Xuemei Chen and Dr. Fedor Karginov, for their helpful comments and suggestions on my dissertation project. I thank the faculty who served on my guidance and qualifying exam committees: Dr. Thomas Eulgem, Dr. Joel Sachs, Dr. Amy Litt, and Dr. Natasha Raikhel.

I thank current and former members of the Bailey-Serres lab for sharing with me their critical comments, encouragement, and ideas. Particularly, I thank Dr. Reed Sorenson who initiated this project and mentored me during the first two years of my PhD studies. I thank Dr. Maureen Hummel for her teaching and contribution on RNA-seq library preparation and analysis. I thank Dr. Jeremie Bazin, Dr. Mauricio Reynoso, Dr. Germain Pauluzzi, Dr. Anna Locke, Dr. Matthew Prior, Dr. Miguel Lopez, Dr. Erin Brinton, Dr. Rejbana Alam, Dr. Travis Lee, Dr. Lauren Dedow, Sonja Winte, and ALek Kettenburg for their help and support. I also thank Dr. Dawn Nagel and her group members, Dr. Titouan Bonnot, Emily Blair, and Tejasvinee Mody, for helpful comments on this project as well as encouragement.

I thank everyone at UCR that has helped me throughout my PhD studies: Dr. David Carter for his guidance and assistance with microscopy; Dr. Haiyan Ke for her

help with SA quantification; and members of the Dehesh and Chen lab for sharing ideas and reagents when needed.

I thank Dr. Leslie Sieburth for her guidance and technical support on the mRNA decay experiment during my visit to her lab at the University of Utah. I thank Alba González Hernando, Dr. Moritz Leber, and Dr. Malia Deshotel for their friendship during my time in Utah.

I thank my former mentors Dr. Upatham Meesawat and Prof. Choathip Purintavaragul at Prince of Songkla University, as well as Dr. Supachitra Chadchawan and Dr. Teerapong Buaboocha at Chulalongkorn University for laying the foundation and helping pave the way for my scientific career. It was indeed Dr. Meesawat's pigeon orchid that lured me into plant research, and in Dr. Chadchawan's lab that I fell in love with plant molecular biology.

I thank the Thailand's Institute for the Promotion of Teaching Science and Technology (IPST) for its full-scholarship through the Development and Promotion of Science and Technology Talents Project throughout 12 years of my educational career. Without its financial support, it would not have been possible for someone from my socioeconomic background to achieve highest education in the United States as I did today. This scholarship also provided me with wonderful mentors and friends that I am thankful for to the rest of my life. I am grateful to the administrative personnel at IPST and the Royal Thai embassy that has helped and taken care of me with kindness throughout this journey.

I thank my friends from college Dr. Supattra Thepnarong and Dr. Lompong Klinnawee for their continued friendship and moral support. I thank Bhanubhakta Kaan Jittiang for being there for me during my tough time. Thank you for being by people!

I thank my Royal Thai fellows and friends around the world for sending kind words and their friendship during this invaluable journey. I thank the Thai community and friends for their friendship and support: Dr. Yoothana Thanmongkhon, Dr. Supawadee Wichitchan, Dr. Parawee Pumwongpitak, Dr. Panu Suppatkul, Wipawee Leesutthiphonchai, and Nuttapol Pombubpa.

Finally, I thank my parents and my grandmother for their unconditional love and support. My parents did not have a chance to finish high school, but they have worked extremely hard to provide me and my brother and sister with the best educational opportunity they could possibly provide. Without their sacrifice, I would not have had this achievement. I thank my brother and sister, Joke and June, for being such wonderful siblings. I am lucky to be their brother.

Publications

Chantarachot T, Bailey-Serres J (2018) Polysomes, Stress Granules, and Processing Bodies: A Dynamic Triumvirate Controlling Cytoplasmic mRNA Fate and Function. Plant Physiol **176**: 254–269

ABSTRACT OF THE DISSERTATION

Characterization of the DHH1/DDX6-Like RNA Helicase Family in *Arabidopsis thaliana*

by

Thanin Chantarachot

Doctor of Philosophy, Graduate Program in Genetics, Genomics and Bioinformatics
University of California, Riverside, December 2018
Dr. Julia Bailey-Serres, Chairperson

General cytoplasmic mRNA turnover in eukaryotes is governed by two major pathways: 5'-to-3' decay initiated by the multi-subunit mRNA decapping complex and carried out by EXORIBONUCLEASE 1/4 and 3'-to-5' decay executed by the RNA exosome or the 3'-to-5' exoribonuclease SUPPRESSOR OF VARICOSE (SOV). In yeast and metazoa, DEAD-box RNA helicase DHH1/DDX6 proteins are associated with the decapping complex and involved in translational repression and/or mRNA degradation. In this dissertation, RNA HELICASE 6, 8 and 12 (RH6, RH8 and RH12) were identified as orthologs of the DHH1/DDX6 family in the plant *Arabidopsis thaliana*. Genetic analysis uncovered that the genes *RH6*, *RH8* and *RH12* are functionally redundant and indispensable for growth and development, as the triple homozygous *rh6 rh8 rh12* mutant displays pleiotropic phenotypes including delayed germination, altered vein patterning, and severe maturation defects including infertility. By use of confocal microscopy, we found that all the three RHs are nucleocytoplasmic proteins, with the cytoplasmic portion forming stress-inducible

cytoplasmic ribonucleoprotein complexes associated with both processing bodies (PBs) and stress granules (SGs). Evaluation of PB and SGs in the triple homozygous mutant *rh6 rh8 rh12* indicated that the RHs are required for PB but not SG formation. Genome-wide analysis of RNA decay kinetics in the *rh6 rh8 rh12* mutant by genome-scale RNA-sequencing revealed that the RHs mediate degradation of short-lived mRNAs with diverse biological functions, the majority of which are putative substrates of the 5' to 3' decapping-mediated decay pathway. Further genome-scale polyadenylated mRNA and polyadenylated ribosome-associated mRNA analysis revealed that co-disruption of these *RH*s perturbed transcriptome and translatome homeostasis, characterized by an increase in the steady-state mRNA abundance and translational status of stress- and defense-response transcripts and the simultaneous repression in accumulation of growth and development-associated transcripts. Genetic analysis determined that the growth defects of *rh6 rh8 rh12* are not related to small interfering RNA production, but caused by a constitutive immune response linked with stabilization and enhanced ribosome occupancy of defense-related mRNAs. The phenotypes, constitutive elevation of stress/defense-response mRNAs and repression of growth-related mRNAs was alleviated by (over)expression of a functional *SOV* allele. This study determined the plant DDH1/DDX6 orthologs are a variable component of the 5' to 3' decay machinery that accelerates decay of growth limiting defense-associated transcripts under non-stress conditions.

TABLE OF CONTENTS

LIST OF FIGURES

LIST OF TABLES

Chapter 1

Polysomes, Stress Granules and Processing Bodies: A Dynamic Triumvirate Controlling Cytoplasmic mRNA Fate and Function

1.1 ADVANCES

- Advancements in imaging and RNA-protein based ‘omic’ technologies reveal complex dynamics of mRNA activities and fate.
- mRNAs are selectively modulated in cytoplasmic translation, sequestration and turnover during development and in response to the environment.
- Multiple pathways of mRNA turnover are linked to translation.
- Processing bodies and stress granules are heterogeneous cytoplasmic sites of mRNA turnover and transient restriction from translation, respectively.
- mRNA sequestration and translation are rapidly and reversibly controlled by external and internal stimuli.

1.2 INTRODUCTION

The export of an mRNA from the nucleus to the cytoplasm begins an odyssey of dynamic regulation that determines the location, longevity and use of the transcript in the production of polypeptides by ribosomes in plant cells. Recent leveraging of mutants, imaging of fluorescent proteins and ‘omics’ of protein and ribosome association with mRNAs have significantly enriched our understanding of the intricate regulation of the fates of transcripts within the cytoplasm of plant cells. This Update explores the connections between translation, decay and storage of mRNAs that involve three heterogeneous mRNA-ribonucleoprotein (mRNP) complexes: polyribosomes

(polysomes), processing bodies (PBs) and stress granules (SGs) (Box 1). We begin with a brief overview of cellular surveillance of mRNA integrity during the first (pioneer) round of translation. Next, we consider mRNA decay initiated on translating ribosomes, including co-translational exonucleolytic decay and micro(mi)RNA-targeted decay. Then we detail the general decay process of mRNAs initiated by enzymatic deadenylation of the 3' poly(A) tail and removal of the 5'-^{7}mG-cap. Finally, we discuss the selective sequestration of translationally repressed mRNAs in SGs under severe environmental stress. This dynamic interplay between mRNA translation, stabilization and turnover fine-tunes the differential regulation of genes to enable developmental plasticity and effective environmental responses.

1.3 CONNECTIONS BETWEEN mRNA DECAY AND TRANSLATION

mRNA turnover occurs via multiple selective pathways that serve to modulate the abundance of transcripts and to eliminate those that are dysfunctional. Upon export from the nucleus to the cytoplasm, an mRNA may be bound at its 5'-terminus by the two-subunit nuclear cap-binding complex (CBP) comprised of CAP BINDING PROTEIN 20 (CBP20) and CAP BINDING PROTEIN 80 (CBP80) (Figure 1.2). It is not well understood how the CBP is exchanged for a cytoplasmic cap-binding complex, comprised of either eukaryotic initiation factor (eIF)4E and eIF4G or eIFiso4E and eIFiso4G. Both eIF4E and eIFiso4E bind directly to the 7-methyl guanosine (^{7}mG) cap structure at the 5' terminus and are tethered to the scaffold protein eIF4G and eIFiso4G, respectively, which directly interacts with a poly(A)-binding protein (PABP) among those bound to the polyadenylated (poly(A)) tail at the 3' terminus of the transcript (Browning and Bailey-Serres, 2015). This physical circularization of the polysome enhances

primary initiation or subsequent ribosome recycling events (Gallie, 2014; Browning and Bailey-Serres, 2015). It may also safeguard the transcript termini from enzymatic end-attacks that can commence its degradation.

1.3.1 mRNA surveillance-triggered decay

mRNAs exported through the nuclear pore undergo a quality control round of translation that routes transcripts with aberrant features to the nonsense-mediated decay (NMD) pathway (Figure 1.2). Several mRNA qualities that compromise the integrity of translation termination trigger NMD, including a premature termination codon (PTC) marked by the presence of an exon junction complex 3' of a stop codon (Reddy et al., 2013; Shaul, 2015). This is often a hallmark of incomplete or alternative splicing. Other mRNA features that trigger NMD include a ≥300 nt long 3' untranslated region (UTR), an intron in the 3′ UTR that is ≥50 nt downstream of the stop codon, an upstream open reading frame (uORF) that is out of frame with the start codon of the main (protein coding) ORF (mORF), a truncated transcript due to premature 3' polyadenylation, or an inefficient or absent stop codon (Reddy et al., 2013).

The early steps of PTC recognition and NMD complex formation in eukaryotes involve UP FRAMESHIFT 1 (UPF1), UPF2, UPF3 and SUPPRESSOR WITH MORPHOLOGICAL EFFECT ON GENITALIAs (SMGs) (reviewed by Shaul, 2015; Dai et al., 2016). The late steps of NMD involve translational repression and degradation of target mRNAs. In mammals, degradation of NMD targets is initiated by SMG6-mediated endonucleolytic cleavage followed by exonucleolytic degradation of the 3'- and 5'-cleavage products by the 5'-3' exoribonuclease EXORIBONUCLEASE 1 (XRN1) and the exosome (see below), respectively (Shaul, 2015). In *Arabidopsis* (*Arabidopsis thaliana*),

an ortholog of SMG6 has not been identified, but degradation of NMD substrates occurs in PBs and requires UPF1 and SMG7. It was proposed that AtSMG7 recruits the NMD complex to PBs for mRNA degradation through its interaction with phosphorylated AtUPF1. However, the mechanism by which NMD targets are fully degraded to nucleotides is unknown since AtXRN4, the functional cytoplasmic ortholog of mammalian XRN1, is not required (Kerényi et al., 2013; Mérai et al., 2013).

In addition to restricting the synthesis of nonfunctional proteins from PTC-containing mRNAs, NMD conditionally regulates the abundance and translation of a number of functional transcripts. For example, NMD controls the developmental transition to flowering by down-regulating a functional *FLOWERING LOCUS M* (*FLM*) transcript isoform under elevated temperatures in *Arabidopsis* (Sureshkumar et al., 2016). It also tempers levels of defense-related transcripts under normal growth conditions (Jeong et al., 2011; Gloggnitzer et al., 2014; Shaul, 2015), contributes to the repression of *EIN3-BINDING F BOX PROTEIN 2* (*EBF2*) mRNA translation in response to ethylene (Merchante et al., 2015), and promotes the acclimation response to salt stress in *Arabidopsis* (Vexler et al., 2016). A general dampening of NMD by stresses could be responsible for the increase in NMD-sensitive splicing variants in response to high salt (Drechsel et al., 2013) and prematurely polyadenylated transcripts under hypoxia (Lorenzo et al., 2017).

1.3.2 XRN4-mediated co-translational decay

As polysomes and the decay machinery act antagonistically in controlling the function and fate of cytoplasmic mRNAs, it has been generally thought that turnover takes place on ribosome-free mRNPs following translational repression and removal of

the 3’ poly(A) tail. Several new studies demonstrated that, in addition to a deadenylation-dependent mechanism (see below), cytoplasmic mRNA degradation can occur co-translationally in the 5’ to 3’ direction, in a deadenylation-independent manner (Figure 1.2). By selective purification of polyadenylated mRNAs with a free 5'-monophosphate, studies of *Arabidopsis*, rice (*Oryza sativa*) and soybean (*Glycine max*) show a global pervasiveness of 5’ decay-intermediate termini that display a 3-nt periodicity throughout the mORF, in the same register as the codon periodicity generated by RNAse digestion in ribosome footprinting analyses (Hou et al., 2016; Yu et al., 2016; Crisp et al. 2017). This in-frame periodicity in decay intermediates is dependent on XRN4 function, indicating that 5’ to 3’ mRNA degradation can accompany the codon-by-codon translocation of elongating ribosomes. This co-translational XRN4 activity most likely follows an inhibition of translational initiation before or as a consequence of removal of the 5’-^{7}mG-cap. Interestingly, co-translational mRNA degradation is associated with paused or stacked ribosomes on uORFs, within and at the stop codon of certain mORFs, and near to non-cleavable miRNA target sites (Hou et al., 2016; Yu et al., 2016). This suggests that co-translational XRN4-dependent decay may be linked to the kinetics of ribosome translocation, destabilizing mRNAs with sites of rate-limiting translational elongation or termination.

Ribosome pausing and co-translational decay may also serve as an efficient means for rapid transcriptome adjustment in response to environmental stimuli and transcriptome resetting during stress recovery. For example, co-translational decay appears to control rapid down regulation of excess-light-activated transcripts during stress recovery in *Arabidopsis* plants (Crisp et al., 2017). Moreover, within 15 minutes of pronounced heat stress (38 ^{o}C), approximately 25% of the *Arabidopsis* seedling

transcriptome is targeted for XRN4-dependent degradation, including both polysome-associated and polysome-released mRNAs (Merret et al., 2013). The heat-induced decay of polysomal mRNAs is dependent on LA RELATED PROTEIN 1A (LARP1A). High heat triggers the accumulation of XRN4 and decapping proteins DECAPPING1 (DCP1) and DCP2 in polysomes (Merret et al., 2013), and seems to coincide with ribosome pausing in 5' mRNA regions to elicit XRN4-dependent decay (Merret et al., 2015). It will be of interest to know how heat triggers the prerequisite mRNA decapping and whether the discrimination of mRNAs for heat-regulated turnover is integrated with the recently uncovered role of eIF5B1 in maintaining efficient translation of a subset of mRNAs, notably those that encode low molecular weight non-stress proteins, during heat stress in *Arabidopsis* (Zhang et al., 2017a).

1.3.3 miRNA-triggered decay of translating mRNAs

miRNA-mediated gene silencing regulates key biological processes in plants, including the plasticity of development in the context of the environment (reviewed by Ferdous et al., 2015; Fouracre and Poethig, 2016; D'Ario et al., 2017). The fully processed 21- or 22-nt miRNA and its effector ARGONAUTE 1 (AGO1) form a core RNA-induced silencing complex (RISC) that controls the fate of specific mRNAs through a mechanism that involves endonucleolytic cleavage and/or translational repression (Rogers and Chen, 2013). Slicing of miRNA targets by AGO1 generates two truncated cleavage products, termed RISC 5'- and 3'-cleaved fragments, which are further degraded by the cellular RNA decay machinery. In *Arabidopsis,* the RISC 3'-cleaved fragment contains a free 5'-monophosphate making it a substrate for XRN4 (Souret et al., 2004). RISC 5'-cleaved fragments undergo rapid turnover upon uridylation at their 3'

end by the miRNA nucleotidyl transferase HEN1 SUPPRESSOR 1 (HESO1) (Ren et al., 2014). The pathways participating in RISC 5'-cleaved fragment demise could include 5' to 3' decay by XRN4 (Ren et al., 2014), although the mechanism of the prerequisite removal of the 5' cap from these fragments is largely unknown. Alternatively, the uridylated fragments may be degraded in the 3' to 5' direction by the exosome (see below). This is supported by observation of their increased abundance in genotypes of *Arabidopsis* deficient in exosome cofactor SUPERKILLER (SKI) proteins (Branscheid et al., 2015). Recently, *Arabidopsis* RISC-INTERACTING CLEARING 3'-5' EXORIBONUCLEASE 1 and 2 (RICE1 and 2) were identified as AGO1- and AGO10-binding proteins that degrade uridylated RISC 5'-cleaved fragments and facilitate RISC recycling (Zhang et al., 2017b).

The co-purification of AGO1 and several miRNAs with *Arabidopsis* polysomes was reported some time ago (Lanet et al., 2009), but only recent coupling of mutant analyses, subcellular fractionation, and ribosome footprinting methods have clearly demonstrated their preferential association with membrane-bound polysomes (MBPs), including those at the endoplasmic reticulum (Li et al., 2013; Li et al., 2016). These studies show that both translational repression and cleavage of miRNA targets mainly occur in these subcellular domains. Notably, MBP association of AtAGO1 is required for miRNA-triggered production of phased secondary siRNAs (phasiRNAs) from select RNAs, *e.g. TRANS-ACTING SIRNA (TAS)* transcripts (Li et al., 2016). This is corroborated by the presence of two proteins required for phasiRNA biogenesis, SUPPRESSOR OF GENE SILENCING 3 (SGS3) and RNA-DEPENDENT RNA POLYMERASE 6 (RDR6), in specific granules called siRNA bodies that reside on the cytoplasmic side of membrane compartments (Jouannet et al., 2012). The position of

ribosome footprints generated from MBPs suggests that ribosome occupancy contributes to defining the site of phasiRNA biogenesis on these transcripts (Li et al., 2016). Indeed, functional translation of a positionally conserved short ORF of the *AtTAS3* transcript is critical to efficient *tasiRNA* production (Bazin et al., 2017).

The complex interactions between miRNA-targeted mRNAs and the translational and degradation apparatus raise new questions about the sub-compartments of the cytoplasm where these processes take place. Although miRNA-mediated translational repression involves MBPs, prior protein co-localization studies suggest these processes occur in PBs (Brodersen et al., 2008; Yang et al., 2012). The location of XRN4-mediated decay of the RISC 5'- and 3'-cleaved fragments could be in PBs or freely in the cytosol, since XRN4 is present in both locations (Weber et al., 2008).

1.4 GENERAL CYTOPLASMIC mRNA DEGRADATION

General cytoplasmic mRNA degradation in eukaryotic cells is initiated by the removal of 3' poly(A) tail, a reversible step known as deadenylation, followed by 5'-cap hydrolysis (decapping) and subsequent 5' to 3' mRNA decay by XRN1/4 (Siwaszek et al., 2014). Both processes may occur in but are not confined to PBs. Alternatively, deadenylated mRNAs can be degraded in the 3' to 5' direction by the exosome. This section summarizes our current understanding of deadenylation-dependent mRNA turnover machinery and mechanisms as well as the significance of their regulation in plants (Figure 1.2; Table 1.1).

1.4.1 Deadenylation

Progressive cytoplasmic mRNA poly(A) tail shortening displaces PABPs from the mRNA 3' end, likely disrupting the 5'-cap to 3'-tail (eIF4G-PABP) interaction that promotes translational re-initiation (Gallie, 2014), shifting mRNAs towards a translationally silent state and exposing the 3' terminus to exonucleases (Łabno et al., 2016). This first, rate-limiting step of mRNA decay is catalyzed by Mg^{2+}-dependent 3'-5' exoribonucleases called deadenylases that are classified into two superfamilies: EEP (exonuclease-endonuclease-phosphatase) and DEDD (Asp-Glu-Asp-Asp) nucleases (Siwaszek et al., 2014).

In yeast and metazoa, shortening and removal of the mRNA 3' poly(A) tail is performed by two major deadenylase complexes: poly(A)-nuclease PAN2-PAN3 and CARBON CATABOLITE REPRESSOR 4-NEGATIVE ON TATA (CCR4-NOT) (Wahle and Winkler, 2013). The PAN2-PAN3 complex is a heterotrimer of the DEDD-type PAN2 deadenylase interacting with a PAN3 homodimer (Siwaszek et al., 2014). Interestingly, the PAN2-PAN3 complex is present across higher eukaryotes including the green algae *Chlamydomonas*, but has not been recognized to date in flowering plants. The CCR4-NOT complex contains two catalytic subunits, *i.e.* CCR4 and CAF1, and at least seven additional proteins (NOT1-5, CAF40 and CAF130), with NOT1 serving as a scaffold (Miller and Reese, 2012). Of these, CCR4, CAF1 and NOT1 orthologs have been identified in plants (Table 1.1). *Arabidopsis* encodes two *CCR4* paralogs, *AtCCR4a and AtCCR4b*, both of which produce gene products that interact with the decapping complex proteins AtDCP1 and AtDCP2 within and outside of PBs (Suzuki et al., 2015). Mutant analyses have identified some important functions of these functionally redundant EEP deadenylases. For example, they appear to influence sucrose and

starch metabolism by controlling the poly(A) tail length and steady-state level of *GRANULE-BOUND STARCH SYNTHASE 1* (*GBSS1*) mRNA (Suzuki et al., 2015). The expansive *Arabidopsis CAF1* family includes 11 members. The products of two of these, CAF1a and CAF1b, exhibit 3'-5' exonucleolytic activity *in vitro* via their conserved DEDD domain, contribute to effective defense response (Liang et al., 2009), and regulate the poly(A) length of a defined set of stress-related transcripts rather than acting as general deadenylases (Liang et al., 2009; Walley et al., 2010).

Study of rice deadenylases has provided further insight. OsCCR4a and OsCCR4b are predominantly located in visible foci, presumably PBs, that include XRN4. The EEP domain of OsCCR4s is sufficient for *in vitro* 3'-5' exonuclease activity on poly(A), poly(U) and poly(C) substrates (Chou et al., 2017). Similarly, recombinant OsCAF1A, OsCAF1B, OsCAF1G, OsCAF1H are 3'-5' exonucleases, with at least OsCAF1B associating with XRN4 in PB-like foci (Chou et al., 2014). In yeast and mammals, CAF1 serves as a bridge between CCR4 and NOT1 via interactions between the N-terminal leucine-rich repeat (LRR) of CCR4 and MIF4G domain of NOT1. The rice CCR4-NOT complex appears to share this topology, although the N-terminal LRR domain of CCR4s is absent and the interaction with CAF1 is apparently replaced by an N-terminal zf-MYND-like domain of CCR4 (Chou et al., 2017).

Two other conserved deadenylases control turnover of specific transcripts. The first is the EEP-type deadenylase Nocturnin that is distinguished by its circadian clock-regulated transcript abundance in multicellular eukaryotes (Godwin et al., 2013). *Arabidopsis HESPERIN* (*AtHESP*) is closely related to mammalian *Nocturnin*, with maximal mRNA levels in the evening. Intriguingly, altered *AtHESP* expression affects rhythmicity of the core clock oscillator mRNAs *TIMING OF CAB EXPRESSION 1*

(*TOC1*) and *CIRCADIAN CLOCK ASSOCIATED 1* (*CCA1*) (Delis et al., 2016). The second is the homodimeric DEDD-class poly(A)-specific ribonucleases (PARNs) found in plants and humans, but apparently absent from budding yeast (*Saccharomyces cerevisiae*) and fruit flies (*Drosophila melanogaster*) (Godwin et al., 2013). *Arabidopsis* PARN (AtPARN)/ABA HYPERSENSITIVE GERMINATION 2 (AHG2) is required for the poly(A) tail shortening of select embryonic transcripts, affecting embryonic development and some stress responses (Chiba et al., 2004; Reverdatto et al., 2004; Nishimura et al., 2005). Altogether, the diversity of factors involved in deadenylation indicates significant control of deadenylation, the first step of general mRNA turnover.

1.4.2 Decapping

Removal of the mRNA 5′-^{7}mG-cap inhibits translation initiation and commits a deadenylated mRNA to complete degradation. mRNA decapping is carried out by DCP2, a conserved bi-lobed Nudix family enzyme that hydrolyzes the 5′-cap structure in a divalent cation (Mn^{2+}/Mg^{2+})-dependent manner, releasing ^{7}mGDP and a 5′-monophosphorylated mRNA (Arribas-Layton et al., 2013). DCP2 functions in a multi-subunit decapping complex, which includes cofactors that mediate its activity and regulators that coordinate decapping with translational repression, deadenylation and hydrolysis of the mRNA body (Table 1.1). In *Arabidopsis*, DCP1 and VARICOSE (VCS)/ENHANCER OF mRNA DECAPPING 4 (EDC4) directly modulate DCP2 activity (Xu et al., 2006). All three proteins are considered core decapping complex factors, indispensable for mRNA decapping and essential for post-embryonic development (Xu and Chua, 2011). Colocalization of AtDCP1 and AtDCP2 in macromolecular foci detectable by confocal microscopy is dynamically regulated by heat stress (Motomura et

al., 2015). Based on mutant analyses, the factor VCS regulates seed dormancy and germination in *Arabidopsis* (Basbouss-Serhal et al., 2017) and functions in plant-fungal pathogen interactions in *Nicotiana benthamiana* (Petre et al., 2016). Additionally, AtDCP5, an Sm-like (LSM) domain-containing RNA-binding protein (RBP), interacts with DCP1 and DCP2. Unlike DCP1 and VCS, DCP5 does not directly regulate DCP2 activity; however, it is required for PB formation, mRNA decapping and translational repression associated with mRNA decay. Attenuation of DCP5 function does not result in lethality, but causes developmental defects similar to loss-of-function mutants of core complex proteins including perturbation of germination and leaf venation (Xu and Chua, 2009), indicating that these developmental processes require tight regulation of mRNAs mediated by the decapping pathway.

Phosphorylation of specific residues of the core decapping proteins constitutes a crucial mechanism for osmotic stress response in plants. Under this stress, *Arabidopsis* DCP1 is phosphorylated by MITOGEN-ACTIVATED PROTEIN KINASE 6 (MPK6), leading to enhancement of its association with DCP5, which in turn promotes the RNA-binding capacity of DCP5 and mRNA decapping activity of DCP2 (Xu and Chua, 2012). By contrast, VCS is phosphorylated by the abscisic acid (ABA)-unresponsive osmotic stress-activated subclass I of SUCROSE NONFERMENTING 1-RELATED PROTEIN KINASE 2s (SnRK2s). Osmotic stress triggers SnRK2 localization in PBs where they appear to phosphorylate and regulate VCS function (Soma et al., 2017). Mutations that prevent DCP1 or VCS phosphorylation render *Arabidopsis* plants susceptible to osmotic stress (Xu and Chua, 2012; Soma et al., 2017). These observations firmly suggest that transcriptome adjustments mediated by mRNA decapping are relevant to stress resilience.

In yeast and metazoa, the heptameric LSM1-7 complex, in association with PROTEIN-ASSOCIATED WITH TOPOISOMERASE 1 (PAT1), binds to the 3'-end of deadenylated mRNAs and promotes decapping (Tharun, 2009; Haas et al., 2010). Simultaneously, PAT1 interacts with the DEAD-box RNA helicase DHH1/DDX6. Both PAT1 and DDH1 play a role in translational inhibition as well as PB formation (Coller and Parker, 2005; Ozgur et al., 2010; Sharif et al., 2013). This links deadenylation with translational repression and decapping. The LSM1-7 complex has been characterized in *Arabidopsis*. Genetic analysis of the paralogs *AtLSM1A* and *AtLSM1B* revealed their functional redundancy and importance in normal development (Perea-Resa et al., 2012; Golisz et al., 2013). Similar to DCP1, DCP2 and VCS, both LSM1A and LSM1B accumulate in PBs under heat, cold, drought and salt stress and are required for conditional PB assembly under these conditions (Perea-Resa et al., 2012; Perea-Resa et al., 2016). Intriguingly, the *Arabidopsis* LSM1s differentially regulate tolerance to abiotic stresses by dynamically controlling the decapping and degradation of a select group of stress-responsive transcripts, including those involved in ABA biosynthesis (Perea-Resa et al., 2016). Mutant analysis shows that the LSM5 component of the LSM1-7 complex is essential for heat tolerance in *Arabidopsis*, targeting both functional and aberrant transcripts for degradation during heat stress (Okamoto et al., 2016). A proteomic analysis revealed that AtLSM1A forms complexes with VCS, PAT1, DHH1/DDX6-like and NOT1-like proteins (Golisz et al., 2013), so its interaction with the deadenylation machinery or the 3' deadenylated mRNA remains somewhat unclear.

Arabidopsis PAT1 interacts with LSM1B and regulates decapping of select transcripts. It is a MPK4 phosphorylation target that accumulates in PBs in response to bacterial pathogen-associated molecular pattern (PAMP) flagellin 22. PAT1 and MPK4

suppress plant autoimmunity as loss of their function results in the ENHANCED DISEASE SUSCEPTIBILITY 1 (EDS1)-mediated constitutive immune response through a pathway downstream of the immune receptor SUPPRESSOR OF MKK1 MKK2 2 (SUMM2) (Roux et al., 2015). Studies of the *Arabidopsis* LSM1-7-PAT1 complex extend the contribution of mRNA decapping from abiotic to biotic stress signaling and suggest that both components and architecture of the mRNA decapping complex of yeast and metazoa is conserved in plants. An *Arabidopsis* DHH1-like protein has been identified and shown to localize in DCP1 and DCP2 granules (Xu et al., 2006; Bhullar et al., 2017), but whether this protein interacts with PAT1 and functions in translational repression and mRNA decapping is yet to be elucidated.

Arabidopsis also possesses non-canonical, condition-specific decapping activators important for abiotic and biotic stress responses. For example, BEACH domain-containing protein SPIRRIG (SPI) is a regulator of cellular membrane dynamics that localizes into PBs under salt stress via its interaction with DCP1. SPI function is required for salt stress-triggered PB assembly and it selectively stabilizes and destabilizes a subset of salt-responsive transcripts by regulating their translocation into PBs (Steffens et al., 2015). ASYMMETRIC LEAF 2 (AS2) is a transcription factor playing a role in leaf development. Intriguingly, AS2 co-localizes with PBs as a result of its trafficking there by the geminivirus nuclear shuttle protein BV1 (Ye et al., 2015). This apparently promotes DCP2 decapping activity to accelerate host mRNA decay, leading to suppression of the host antiviral gene silencing. There are numerous examples of viral conscription of the translational apparatus (Browning and Bailey-Serres, 2015); this example illustrates a bizarre means by which a virus manipulates mRNA turnover.

1.4.3 5’-3’ degradation

In eukaryotes, the hydrolysis of 5′-monophosphorylated (uncapped) transcripts into nucleotides is executed by Mg^{2+}-dependent 5’-3’ exoribonucleases of the XRN family, with XRN4 functioning as the cytoplasmic enzyme in *Arabidopsis* (Kastenmayer and Green, 2000). Unlike the core decapping proteins, disruption of AtXRN4 function only results in mild morphological defects under standard growth conditions. This may reflect reliance on AtXRN4 for degradation of specific transcripts (Rymarquis et al., 2011). Nevertheless, XRN4-mediated translational repression and mRNA decay exert a role on seed dormancy and germination (Basbouss-Serhal et al., 2017), ethylene signaling (Li et al., 2015; Merchante et al., 2015), heat stress response and tolerance (Merret et al., 2013; Nguyen et al., 2015) and viral defense (Jaag and Nagy, 2009; Peng et al., 2011; Lee et al., 2016). An alternative explanation is that in the absence of XRN4 function, the 3’ to 5’ degradation pathways described below may maintain homeostasis.

1.4.4 3’-5’ degradation

After deadenylation, the 3’ end of mRNAs can be directly hydrolyzed by an evolutionarily conserved complex of multiple 3′ to 5′ exoribonucleases called the exosome. In *Arabidopsis*, as in other eukaryotes, the exosome core complex is composed of nine subunits. Six are RNase PH domain-containing proteins (RIBOSOMAL RNA PROCESSING PROTEIN 41 (RRP41), RRP42, RRP43, RRP45, RRP46 and RRP41L/MTR3), that together form a hexameric core ring that is stabilized by attachment of a cap of three S1/KH-domain proteins (RRP4, RRP40 and CSL4) (Lange and Gagliardi, 2010). Whereas all nine core exosome subunits have equal contributions to the structural and functional integrity of the yeast and mammalian

exosome, each *Arabidopsis* exosome subunit appears to contribute a distinct and in some cases dispensable role suggesting target specificity (see Table 1.1). For example, AtCSL4 is apparently dispensable and AtRRP4 alone provides the 3'-5' exoribonuclease activity (Chekanova et al., 2002; Chekanova et al., 2007), whereas in yeast and mammals, exosome core subunits are catalytically inactive and additionally require RRP6 and/or RRP44 for the 3'-5' exoribonuclease activity.

The *Arabidopsis* genome encodes three *RRP6* paralogs: *AtRRP6L1*, *AtRRP6L2* and *AtRRP6L3*. Of these gene products, only RRP6L3 was shown to be cytosolic but its role in mRNA degradation is unknown (Lange et al., 2008). There are two *AtRRP44*-like genes: *AtRRP44A* and *AtRRP44B/SUPPRESSOR OF VARICOSE* (*SOV*). RRP44A is an active nuclear localized ribonuclease that functions in rRNA processing (Kumakura et al., 2016), whereas RRP44B is a cytosolic ribonuclease that forms microscopic PB-like particles. AtRRP44A and RRP44B/SOV fall into distinct phylogenetic clades present across the animal and plant kingdoms (Zhang et al., 2010). The latter lacks the N-terminal PIN domain required for binding to the exosome core and AtRRP44B/SOV is notably absent from the Col-0 ecotype. It is suggested that RRP44A is a component of the nuclear exosome whereas RRP44B is a solo cytoplasmic exoribonuclease (Kumakura et al., 2013). Notably, RRP44B can partially complement the function of VCS in cytoplasmic mRNA degradation (Zhang et al., 2010). This indicates a general functional redundancy of the 3'-5' decay apparatus, although it seems possible that the different complexes may have some specificity with respect to individual mRNAs, developmental stages or growth conditions.

The activity of the cytoplasmic exosome is dependent on the SKI complex, a tetrameric assembly of a SKI8 dimer and the RNA helicase SKI2 connected by their

mutual interaction with the scaffold protein SKI3, that unwinds and threads RNA substrates into the exosome for degradation (Halbach et al., 2013). *Arabidopsis* SKI2, SKI3 and SKI8 form a stable complex *in vivo*, with SKI2 and SKI3 also present in cytoplasmic foci (Dorcey et al., 2012; Zhang et al., 2015; Zhao and Kunst, 2016). Disruption of *AtSKI8* function results in stabilization of mRNAs targeted for degradation by the exosome (Dorcey et al., 2012). Similar to the exosome core components RRP45A and RRP45B, all three SKI proteins are required for the exosomal degradation of the *AtECERIFERUM 3* transcript during stem wax deposition (Zhao and Kunst, 2016).

1.5 mRNA SEQUESTRATION IN STRESS GRANULES – A TRANSIT DEPOT BETWEEN TRANSLATION, STORAGE AND DECAY?

Polysome disassembly as a consequence of translational repression induces the sequestration of mRNAs into translationally inactive mRNPs. SGs are one of such mRNPs that form in response to stress-induced inhibition of translation initiation, serving as triage centers for mRNA sorting to PBs or protection from degradation (Protter and Parker, 2016) (see Box 1). These heterogenous complexes are physically, compositionally and functionally linked with PBs (Buchan and Parker, 2009). Typically, mRNAs stored in SGs are translationally competent and can re-enter the translational pool once released. In plants, this is exemplified by *Arabidopsis* mRNAs encoding ribosomal proteins that are preferentially stored in SGs under heat shock stress and released and translated during recovery through a mechanism that requires HEAT SHOCK PROTEIN 101 (HSP101) (Merret et al., 2017).

In yeast and humans, SGs contain a diverse proteome (Jain et al., 2016). Some RBPs are essential for SG formation in these species, *e.g.* T-cell restricted intracellular

antigen-1 (TIA-1) and TIA-1-related (TIAR) proteins (Gilks et al., 2004), Ras-GTPase-activating protein SH3-domain-binding proteins (G3BPs) (Aulas et al., 2015), and Tudor Staphylococcal nucleases (TSNs) (Gao et al., 2015). Recent studies have unveiled the roles of related proteins in plants (Figure 1.2; Table 2).

TIA-1/TIARs are comprised of three N-terminal RNA recognition motifs (RRMs) that provide RNA/DNA binding specificity and a C-terminal prion-related domain (PRD) that confers self-aggregation, both of which are required for SG formation (Waris et al., 2014). In plants, RNA-BINDING PROTEIN 45 and 47 (RBP45/47) and OLIGOURIDYLATE BINDING PROTEIN 1 (UBP1) are the triple RRM families most closely related to the animal TIA-1/TIARs. Of the *Arabidopsis* RBP45/47 family, RBP47B is discernable in the nucleus under normal conditions and relocates to cytoplasmic foci detectable by confocal microscopy in response to heat, salt and hypoxia stress (Weber et al., 2008; Yan et al., 2014; Gutierrez-Beltran et al., 2015; Lokdarshi et al., 2015). The *Arabidopsis UBP1* family is comprised of three members, namely *AtUBP1A*, *AtUBP1B* and *AtUBP1C*. UBP1A and UBP1C reversibly aggregate into cytoplasmic poly(A) mRNA granules upon hypoxic and heat stress (Sorenson and Bailey-Serres, 2014). Similarly, UBP1B reversibly forms SGs under heat stress and plays a crucial role in ABA signaling and heat stress tolerance (Nguyen et al., 2016; Nguyen et al., 2017). An analysis of RNA decay kinetics suggested that UBP1B complexes (UBP1B-SGs) protect stress-related mRNAs from degradation during heat stress (Nguyen et al., 2016). Likewise, UBP1C is required for plant survival of low oxygen stress. UBP1C dynamically relocalizes from the nucleus to form cytoplasmic foci that are disassembled upon re-oxygenation. Intriguingly, RNA-ribonucleoprotein immunoprecipitation (RIP) followed by microarray analysis determined that AtUBP1C preferentially associates with mRNAs with U-rich 3′

UTRs under control conditions, but UBP1C-SGs collect mRNAs that are either stored or degraded as opposed to preferentially translated during hypoxia (Sorenson and Bailey-Serres, 2014).

G3BPs are phosphorylation-dependent, sequence-specific endoribonucleases that interact with Ras GTPase-activating proteins. In mammalian cells, G3BP1 is a potent SG-nucleating protein that constitutes stable cores of SGs (Jain et al., 2016). As such, G3BP1 is targeted and sequestered by several viral proteins to prevent SG assembly/sequestration of viral RNAs during infection (Reineke and Lloyd, 2013). The first plant G3BP-like protein was isolated from *N. benthamiana* together with other SG components as targets of the viral nonstructural protein 3 of Semliki Forest virus (Krapp et al., 2017). This protein is closely related to the NUCLEAR TRANSPORT FACTOR 2 (NTF2) family in *Arabidopsis*. This G3BP-like NTF2-RRM aggregates into SGs and interacts with the nuclear shuttle protein of the begomovirus abutilon mosaic virus and pea necrotic yellow dwarf virus upon heat stress (Krapp et al., 2017). The roles of plant G3BP-like proteins in SG nucleation and mRNA stabilization await further studies.

TSNs are evolutionarily conserved cytoskeletal-associated RBPs characterized by four complete N-terminal staphylococcal nuclease (SN) domains, followed by a central Tudor domain and a partial SN domain at the C-terminus (Gutierrez-Beltran et al., 2016). A plant TSN was first described in rice as an RBP required for transport of a sub-group of seed storage RNAs to a subdomain of the endosperm endoplasmic reticulum (Tian and Okita, 2014). *Arabidopsis thaliana* encodes functionally redundant *TSN1* and *TSN2*, which play a pivotal role in seed germination and response to high salinity and heat stress (Frey et al., 2010; Yan et al., 2014; Gutierrez-Beltran et al., 2015). Root transcriptome and mRNA decay data suggest that TSN1 and TSN2 protect

a specific set of transcripts from degradation during salinity stress, including mRNAs encoding GIBBERELLIN (GA) 20-OXIDASE 3 (GA20OX3), a key enzyme in GA biosynthesis (Yan et al., 2014). In contrast to animal TSNs that seem to exclusively localize to SGs (Gao et al., 2015), the *Arabidopsis* TSNs are targeted to both SGs and PBs, and function in mRNA decapping during heat stress, suggestive of a crucial role in the structural integrity as well as the molecular identity of both SGs and PBs (Gutierrez-Beltran et al., 2015).

Tandem CCCH zinc finger (TZF) proteins comprise another RBP family that associates with SGs and PBs. Plant TZFs are characterized by two zinc-binding CCCH motifs arranged in tandem, with an arginine rich (RR) motif upstream of the TZF motifs (Bogamuwa and Jang, 2014). *Arabidopsis* encodes 11 *TZFs*, encoding proteins localized to cytoplasmic granules when expressed heterologously in maize mesophyll protoplasts (Pomeranz et al., 2010b). AtTZFs play a diverse role in growth, development and stress responses (Pomeranz et al., 2010a; Lin et al., 2011; Bogamuwa and Jang, 2014). AtTZF1 shuttles between the nucleus and PBs under ambient temperatures, but relocalizes into SGs after heat shock (Pomeranz et al., 2010a). Through its RR and TZF motifs, AtTZF1 binds poly(U) RNAs in the presence of zinc, and triggers the decay of AU-rich element (ARE)-containing mRNAs (Qu et al., 2014). In rice, OsTZF1 is a negative regulator of leaf senescence under stress and also binds poly(U) RNAs. Its co-localization with SG and PB markers was enhanced after ABA and NaCl treatment (Jan et al., 2013). *AtTZF4*, *AtTZF5* and *AtTZF6* are specifically expressed in seeds and involved in seed germination (Bogamuwa and Jang, 2013). All three proteins physically interact in both SGs and PBs, along with MEDIATOR OF ABA-REGULATED DORMANCY 1 (MARD1) and RESPONSIVE TO DEHYDRATION 21A (RD21A)

(Bogamuwa and Jang, 2016). The dual localization of these proteins in SGs and PBs hints that they could be involved in the selective sorting of transcripts from a stable state to *en masse* degradation.

Apart from RBPs, *Arabidopsis* studies have uncovered proteins with diverse cellular functions as constituents of SGs. These include the purported calcium sensor CALMODULIN-LIKE 38 (CML38), which reversibly accumulates into SGs under hypoxic conditions in a Ca^{2+}-dependent manner (Lokdarshi et al., 2015), and the NAM (no apical meristem), ATAF (*Arabidopsis* transcription activation factor), CUC (cup-shaped cotyledon) (NAC)-family transcription factor VASCULAR PLANT ONE-ZINC-FINGER 2 (VOZ2) that translocates from the cytosol to the nucleus and SGs/PBs during heat stress (Koguchi et al., 2017). AtCML38 function contributes to hypoxia tolerance (Lokdarshi et al., 2015), but it remains to be discovered how AtVOZ2 incorporation into SGs/PBs under heat stress contributes to mRNA metabolism and if this influences heat stress tolerance.

1.6 HETEROGENEOUS MACROMOLECULAR HUBs OF CYTOPLASMIC mRNA TRANSLATION, TURNOVER AND SEQUESTRATION

Polyribosome (polysome): A complex of a 5'-^{7}mG-capped and 3'-polyadenylated mRNA and multiple 80S ribosomes, typically undergoing translation (see main text). Cytoplasmic ribosomes are composed of 81 ribosomal proteins (RPs) and four rRNAs. They catalyze the peptidyl transferase reaction of elongation, interacting with numerous soluble translation factors (Browning and Bailey-Serres, 2015). Often considered invariant, ribosomes can be distinguished by RPs produced by distinct gene paralogs and post-translational modifications (*i.e.*, phosphorylation) (Hummel et al.,

2015). In mammalian cells, ribosome that can be distinguished by the presence or absence of certain RPs translate different subsets of mRNAs (Shi et al., 2017). Translation involves the phases of initiation, elongation and termination that enable the ribosome to decode a transcript into a polypeptide (Browning and Bailey-Serres, 2015). In additional to global control of protein synthesis, the translation of individual mRNAs is regulated during development and as a rapid response to various internal and external cues (reviewed by Roy and von Arnim, 2013; Moore et al., 2016; Merchante et al., 2017). Because the major rate-limiting phase of translation is initiation, it has been thought that most polysomal mRNAs are actively undergoing decoding (Browning and Bailey-Serres, 2015). The discovery that mRNA decay can occur post-transcriptionally on poly(A) mRNAs indicates this interpretation is not fully accurate.

Processing body (PB): Dynamic cytoplasmic macromolecular assemblies of translationally inactive mRNAs and proteins involved in translation repression and mRNA turnover processes, including 3'-deadenylation, 5'-decapping, 5' to 3' exonucleolytic, nonsense-mediated decay, and miRNA-targeted gene silencing. PBs of > 0.1 μm are visible by imaging of fluorescent proteins confocal microscopy (Eulalio et al., 2007). In plants, PB markers include DCP1, DCP2, VCS and XRN4 (Maldonado-Bonilla, 2014). mRNP assemblies of DCP1 and other components of mRNA turnover can be detectable by confocal imaging under normal cellular states, and are enlarged by a variety of stimuli. PB formation requires mRNA release from polysomes as cycloheximide, a drug that stalls elongation mRNAs on elongating ribosomes, can inhibit their assembly. Mobility of PBs involves the actin cytoskeleton through an interaction between myosin XI-K and DCP1 (Steffens et al., 2014). Since PBs are heterogenous, this term is best used along with the names of specific proteins, transcripts and

biological activities studied, as in many cases mRNAs targeted to PBs in plant cells are stabilized rather than degraded despite the presence of mRNA decay factors (Li et al., 2015; Merchante et al., 2015; Steffens et al., 2015; Scarpin et al., 2017). This is supported by the recent discoveries that mRNAs localized to PBs are intact and not undergoing degradation in human cell lines (Horvathova et al., 2017; Hubstenberger et al., 2017), raising questions about the precise functions of PBs in mRNA fate.

Stress granule (SG): Multimolecular cytoplasmic complexes associated with mRNAs not undergoing translation that are ultimately stabilized or targeted for decay during stress. SGs are not typically discernable by confocal imaging unless cells or plants are exposed to acute environmental stress such as heat (Weber et al., 2008) and hypoxia (Sorenson and Bailey-Serres, 2014). SG assembly occurs through a mechanism that requires microtubule dynamics (Gutierrez-Beltran et al., 2015). Like PBs, this process is completely dependent on mRNA release from polysomes. SGs contain full-length polyadenylated mRNAs together with RNA-binding proteins, such as RBP47B, UBP1 and PABP. Although not well characterized in plants, SGs with stabilized mRNAs can include translation initiation factors (*e.g.* eIF3, eIF4E, eIF4A) and the 40S ribosomal subunit, indicating these complexes are in dynamic equilibrium with translating ribosomes. SG markers can overlap with other mRNPs, *e.g.* PBs or siRNA bodies, depending on the process of mRNP remodeling and environmental conditions (Jouannet et al., 2012; Gutierrez-Beltran et al., 2015). As for PBs, it is helpful to describe SGs in terms of the proteins and mRNAs under study.

1.7 CONCLUSION

The processes of mRNA translation, stabilization and turnover are intrinsically linked via highly complex and dynamic interactions of the macromolecular complexes that govern the function and fate of each transcript within the cytoplasm of plant cells. Recent studies have uncovered remarkable regulation of these processes, underscored strong conservation of mechanism across eukaryotes, and illuminated functions that may be limited to the plant lineage. As mRNAs are exported from the nucleus, the pioneer round of translation appears to be the default quality control pathway that licenses reiterative rounds of translation of a polysomal mRNA. It is now recognized that translation can be linked to mRNA decay or sequestration through co-translational degradation or a more complex process involving disassembly of a polysome complex and then advancement to decay or stabilization. Through mutant analyses, confocal microscopy and 'omics' technologies, the integration of mRNA translation, turnover and sequestration has become recognized as highly selective regulatory processes of individual mRNAs. Due to space limitations, we did not delve upon how mRNA decay protects the cellular transcriptome from inappropriate post-transcriptional silencing of endogenous genes (reviewed by Liu and Chen, 2016; Tsuzuki et al., 2017; Zhang and Guo, 2017). We also did not consider nuclear mechanisms of transcript turnover that can involve CBP80 (Yu et al., 2016). Nor did we consider N^6-methyladenosine (m^6A) and other modifications of specific nucleotides (the epitranscriptome) (Luo et al., 2014; Vandivier et al., 2015; Zuber et al., 2016; David et al., 2017), which may influence RNA-protein interactions and hence the nuclear or cytoplasmic fates of individual transcripts. The wealth of new discoveries of the dynamic cytoplasmic mRNP triumvirate has unearthed new challenging questions (see Outstanding Questions) that may provide

insights relevant to other eukaryotes or of value to crop improvement.

1.8 OUTSTANDING QUESTIONS

- Does ribosome translocation rate trigger co-translational decay of mRNAs with paused or stacked ribosomes?
- Is targeted turnover of mRNAs prevalent under optimal growth conditions? What role does turnover play in modulating the abundance and translation of stress-responsive transcripts under stress and recovery conditions?
- What signaling pathways link translational repression to the nucleation/assembly of SGs and PBs?
- What factors determine the targeting and fates of mRNAs in SGs and PBs?
- Following polysome disassembly, what determines whether a transcript is stabilized or degraded under a particular stress condition?
- Is the presence of some mRNA decay factors and SG components in the nucleus relevant to their functions in the cytoplasm?
- What are the mechanisms of mRNA release from SGs and clearance of their components after disassembly?
- Does codon use or RNA modifications (*e.g.*, uridylation and m^6A) impact cytoplasmic mRNA translation, sequestration or turnover?

1.9 OBJECTIVES OF THE DISSERTATION

The principal objective of this dissertation was to identify and characterize function of DHH1/DDX6-like proteins in *Arabidopsis thaliana* from the organismal, to the cellular and molecular levels.

In chapter 2, using phylogenetic analysis, we identified the genes *RNA HELICASE 6* (*RH6*), *RH8* and *RH12* of *Arabidopsis* as putative orthologs of the eukaryotic DHH1/DDX6 family. T-DNA insertion mutation and artificial microRNA-mediated gene silencing were leveraged to test functions of *RH6*, *RH8* and *RH12* in growth and development. We found that the triple homozygous mutant genotype *rh6 rh8 rh12* is a highly reduced and infertile plantlet with perturbations in development similar to some decapping complex mutants. The presence of one functional copy of an *Arabidopsis* DHH1/DDX6 gene is sufficient to increase plant rosette size and biomass. Next, we explored the subcellular localization of RH6, RH8, and RH12, showing that the proteins are localized to both the nucleus and cytoplasm. Moreover, protein co-localization studies uncovered that all the three RHs are components of PBs and can associate with SGs. We further demonstrated that RH6, RH8, and RH12 are indispensable for PB but not SG formation.

In chapter 3, we applied genetic and genomics approaches to elucidate the molecular functions of RH6, RH8, and RH12 in mRNA metabolism, and to identify the molecular underpinnings of the phenotypes associated with the loss of *RH6*, *RH8*, and *RH12* function. First, using the *rh6 rh8 rh12* mutant, we examined the role of these RHs in global mRNA degradation by use of cordycepin to block transcription followed by monitoring the change in mRNA abundance over time using RNA-seq. This revealed that attenuation of *RH6*, *RH8*, and *RH12* function results in stabilization of over 7,000

mRNAs that encode for proteins of diverse biological functions. Based on meta-analyses, most of these mRNAs are degraded via the 5'-to-3' decapping pathway. Despite that fact that the *rh6 rh8 rh12* is defective in mRNA decay, its reduced size phenotype is not associated with siRNA production. Next, we investigated the role of these RHs in translational control using Translating Ribosome Affinity Purification (TRAP) followed by RNA-seq. Based on the knowledge gleaned from the transcriptome and translatome data, we further demonstrated that loss of these RHs causes a salicylic acid-mediated constitutive immune response, a mechanism that is partially dependent on *PHYTOALEXIN DEFICIENT 4* (*PAD4*), but independent on *ENHANCED DISEASE SUSCEPTIBILITY 1* (*EDS1*) function. Finally, by use of genetic and RNA-seq analysis, we demonstrated that the function of RH6, RH8, and RH12 in mRNA degradation and control of growth-stress/defense transcriptome homeostasis can be complemented by a functional allele encoding the 3'-to-5' exoribonuclease SOV.

1.10 ACKNOWLEDGEMENTS

This work was supported by the United States National Science Foundation grant no. MCB-1716913 to J.B.-S. and a Royal Thai Government's Development and Promotion of Science and Technology Talents Project scholarship to T.C.

1.11 REFERENCES

Arribas-Layton M, Wu D, Lykke-Andersen J, Song H (2013) Structural and functional control of the eukaryotic mRNA decapping machinery. Biochim Biophys Acta **1829**: 580–589

Aulas A, Caron G, Gkogkas CG, Mohamed N-V, Destroismaisons L, Sonenberg N, Leclerc N, Parker JA, Vande Velde C (2015) G3BP1 promotes stress-induced RNA granule interactions to preserve polyadenylated mRNA. J Cell Biol **209**: 73–84

Basbouss-Serhal I, Pateyron S, Cochet F, Leymarie J, Bailly C (2017) 5' to 3' mRNA decay contributes to the regulation of *Arabidopsis* seed germination by dormancy. Plant Physiol 01933.2016

Bazin J, Baerenfaller K, Gosai SJ, Gregory BD, Crespi M, Bailey-Serres J (2017) Global analysis of ribosome-associated noncoding RNAs unveils new modes of translational regulation. Proc Natl Acad Sci USA. doi: 10.1073/pnas.1708433114

Bhullar DS, Sheahan MB, Rose RJ (2017) RNA processing body (P-body) dynamics in mesophyll protoplasts re-initiating cell division. Protoplasma **254**: 1627–1637

Bogamuwa S, Jang J-C (2013) The *Arabidopsis* tandem CCCH zinc finger proteins AtTZF4, 5 and 6 are involved in light-, abscisic acid- and gibberellic acid-mediated regulation of seed germination. Plant Cell Environ **36**: 1507–1519

Bogamuwa S, Jang J-C (2016) Plant tandem CCCH zinc finger proteins interact with ABA, drought, and stress response regulators in processing-bodies and stress granules. PLoS One **11**: e0151574

Bogamuwa SP, Jang J-C (2014) Tandem CCCH zinc finger proteins in plant growth, development and stress response. Plant Cell Physiol **55**: 1367–1375

Branscheid A, Marchais A, Schott G, Lange H, Gagliardi D, Andersen SU, Voinnet O, Brodersen P (2015) SKI2 mediates degradation of RISC 5′-cleavage fragments and prevents secondary siRNA production from miRNA targets in *Arabidopsis*. Nucleic Acids Res **43**: 10975–10988

Brodersen P, Sakvarelidze-Achard L, Bruun-Rasmussen M, Dunoyer P, Yamamoto YY, Sieburth L, Voinnet O (2008) Widespread translational inhibition by plant miRNAs and siRNAs. Science **320**: 1185–1190

Browning KS, Bailey-Serres J (2015) Mechanism of cytoplasmic mRNA translation. Arabidopsis Book **13**: e0176

Buchan JR, Parker R (2009) Eukaryotic stress granules: the ins and outs of translation. Mol Cell **36**: 932–941

Chekanova JA, Dutko JA, Mian IS, Belostotsky DA (2002) *Arabidopsis thaliana* exosome subunit AtRrp4p is a hydrolytic 3′→5′ exonuclease containing S1 and KH RNA-binding domains. Nucleic Acids Res **30**: 695–700

Chekanova JA, Gregory BD, Reverdatto SV, Chen H, Kumar R, Hooker T, Yazaki J, Li P, Skiba N, Peng Q, et al (2007) Genome-wide high-resolution mapping of exosome substrates reveals hidden features in the *Arabidopsis* transcriptome. Cell **131**: 1340–1353

Chiba Y, Johnson MA, Lidder P, Vogel JT, van Erp H, Green PJ (2004) AtPARN is an essential poly(A) ribonuclease in *Arabidopsis*. Gene **328**: 95–102

Chou W-L, Chung Y-L, Fang J-C, Lu C-A (2017) Novel interaction between CCR4 and CAF1 in rice CCR4–NOT deadenylase complex. Plant Mol Biol **93**: 79–96

Chou W-L, Huang L-F, Fang J-C, Yeh C-H, Hong C-Y, Wu S-J, Lu C-A (2014) Divergence of the expression and subcellular localization of CCR4-associated factor 1 (CAF1) deadenylase proteins in *Oryza sativa*. Plant Mol Biol **85**: 443–458

Coller J, Parker R (2005) General translational repression by activators of mRNA decapping. Cell **122**: 875–886

Crisp PA, Ganguly D, Smith AB, Murray KD, Estavillo GM, Searle IR, Ford E, Bogdanović O, Lister R, Borevitz JO, et al (2017) Rapid recovery gene downregulation during excess-light stress and recovery in *Arabidopsis*. Plant Cell. doi: 10.1105/tpc.16.00828

D'Ario M, Griffiths-Jones S, Kim M (2017) Small RNAs: big impact on plant development. Trends Plant Sci. doi: 10.1016/j.tplants.2017.09.009

Dai Y, Li W, An L (2016) NMD mechanism and the functions of Upf proteins in plant. Plant Cell Rep **35**: 5–15

David R, Burgess A, Parker B, Li J, Pulsford K, Sibbritt T, Preiss T, Searle IR (2017) Transcriptome-wide mapping of RNA 5-methylcytosine in *Arabidopsis* mRNAs and noncoding RNAs. Plant Cell **29**: 445–460

Delis C, Krokida A, Tomatsidou A, Tsikou D, Beta RAA, Tsioumpekou M, Moustaka J, Stravodimos G, Leonidas DD, Balatsos NAA, et al (2016) AtHESPERIN: a novel regulator of circadian rhythms with poly(A)-degrading activity in plants. RNA Biol **13**: 68–82

Dong OX, Meteignier L-V, Plourde MB, Ahmed B, Wang M, Jensen C, Jin H, Moffett P, Li X, Germain H (2015) *Arabidopsis* TAF15b localizes to RNA processing bodies and contributes to *snc1*-mediated autoimmunity. Mol Plant Microbe Interact **29**: 247–257

Dorcey E, Rodriguez-Villalon A, Salinas P, Santuari L, Pradervand S, Harshman K, Hardtke CS (2012) Context-dependent dual role of SKI8 homologs in mRNA synthesis and turnover. PLoS Genet **8**: e1002652

Drechsel G, Kahles A, Kesarwani AK, Stauffer E, Behr J, Drewe P, Rätsch G, Wachter A (2013) Nonsense-mediated decay of alternative precursor mRNA splicing variants is a major determinant of the *Arabidopsis* steady state transcriptome. Plant Cell **25**: 3726–3742

Eulalio A, Behm-Ansmant I, Izaurralde E (2007) P bodies: at the crossroads of post-transcriptional pathways. Nat Rev Mol Cell Biol **8**: 9–22

Ferdous J, Hussain SS, Shi B-J (2015) Role of microRNAs in plant drought tolerance. Plant Biotechnol J **13**: 293–305

Fouracre JP, Poethig RS (2016) The role of small RNAs in vegetative shoot development. Curr Opin Plant Biol **29**: 64–72

Frey NFD, Muller P, Jammes F, Kizis D, Leung J, Perrot-Rechenmann C, Bianchi MW (2010) The RNA binding protein Tudor-SN is essential for stress tolerance and stabilizes levels of stress-responsive mRNAs encoding secreted proteins in *Arabidopsis*. Plant Cell **22**: 1575–1591

Gallie DR (2014) The role of the poly(A) binding protein in the assembly of the Cap-binding complex during translation initiation in plants. Translation (Austin) **2**: e959378

Gao X, Fu X, Song J, Zhang Y, Cui X, Su C, Ge L, Shao J, Xin L, Saarikettu J, et al (2015) Poly(A)(+) mRNA-binding protein Tudor-SN regulates stress granules aggregation dynamics. FEBS J **282**: 874–890

Gilks N, Kedersha N, Ayodele M, Shen L, Stoecklin G, Dember LM, Anderson P (2004) Stress granule assembly is mediated by prion-like aggregation of TIA-1. Mol Biol Cell **15**: 5383–5398

Gloggnitzer J, Akimcheva S, Srinivasan A, Kusenda B, Riehs N, Stampfl H, Bautor J, Dekrout B, Jonak C, Jiménez-Gómez JM, et al (2014) Nonsense-mediated mRNA decay modulates immune receptor levels to regulate plant antibacterial defense. Cell Host Microbe **16**: 376–390

Godwin AR, Kojima S, Green CB, Wilusz J (2013) Kiss your tail goodbye: the role of PARN, Nocturnin, and Angel deadenylases in mRNA biology. Biochim Biophys Acta **1829**: 571–579

Goeres DC, Van Norman JM, Zhang W, Fauver NA, Spencer ML, Sieburth LE (2007) Components of the *Arabidopsis* mRNA decapping complex are required for early seedling development. Plant Cell **19**: 1549–1564

Golisz A, Sikorski PJ, Kruszka K, Kufel J (2013) *Arabidopsis thaliana* LSM proteins function in mRNA splicing and degradation. Nucleic Acids Res **41**: 6232–6249

Gutierrez-Beltran E, Denisenko TV, Zhivotovsky B, Bozhkov PV (2016) Tudor staphylococcal nuclease: biochemistry and functions. Cell Death Differ **23**: 1739–1748

Gutierrez-Beltran E, Moschou PN, Smertenko AP, Bozhkov PV (2015) Tudor staphylococcal nuclease links formation of stress granules and processing bodies with mRNA catabolism in *Arabidopsis*. Plant Cell **27**: 926-943

Haas G, Braun JE, Igreja C, Tritschler F, Nishihara T, Izaurralde E (2010) HPat provides a link between deadenylation and decapping in metazoa. J Cell Biol **189**: 289–302

Halbach F, Reichelt P, Rode M, Conti E (2013) The yeast ski complex: crystal structure and RNA channeling to the exosome complex. Cell **154**: 814–826

Hooker TS, Lam P, Zheng H, Kunst L (2007) A Core subunit of the RNA-processing/degrading exosome specifically influences cuticular wax biosynthesis in *Arabidopsis*. Plant Cell **19**: 904–913

Horvathova I, Voigt F, Kotrys AV, Zhan Y, Artus-Revel CG, Eglinger J, Stadler MB, Giorgetti L, Chao JA (2017) The dynamics of mRNA turnover revealed by single-molecule imaging in single cells. Mol Cell. doi: 10.1016/j.molcel.2017.09.030

Hou C-Y, Lee W-C, Chou H-C, Chen A-P, Chou S-J, Chen H-M (2016) Global analysis of truncated RNA ends reveals new insights into ribosome stalling in Plants. The Plant Cell Online **28**: 2398–2416

Hubstenberger A, Courel M, Bénard M, Souquere S, Ernoult-Lange M, Chouaib R, Yi Z, Morlot J-B, Munier A, Fradet M, et al (2017) P-body purification reveals the condensation of repressed mRNA regulons. Mol Cell. doi: 10.1016/j.molcel.2017.09.003

Hummel M, Dobrenel T, Cordewener J, Davanture M, Meyer C, Smeekens S, Bailey-Serres J, America T, Hanson J (2015) Proteomic LC–MS analysis of *Arabidopsis* cytosolic ribosomes: Identification of ribosomal protein paralogs and re-annotation of the ribosomal protein genes. J Proteomics **128**: 436–449

Jaag HM, Nagy PD (2009) Silencing of *Nicotiana benthamiana* Xrn4p exoribonuclease promotes tombusvirus RNA accumulation and recombination. Virology **386**: 344–352

Jain S, Wheeler JR, Walters RW, Agrawal A, Barsic A, Parker R (2016) ATPase-modulated stress granules contain a diverse proteome and substructure. Cell **164**: 487–498

Jan A, Maruyama K, Todaka D, Kidokoro S, Abo M, Yoshimura E, Shinozaki K, Nakashima K, Yamaguchi-Shinozaki K (2013) OsTZF1, a CCCH-tandem zinc finger protein, confers delayed senescence and stress tolerance in rice by regulating stress-related genes. Plant Physiol **161**: 1202–1216

Jeong H-J, Kim YJ, Kim SH, Kim Y-H, Lee I-J, Kim YK, Shin JS (2011) Nonsense-mediated mRNA decay factors, UPF1 and UPF3, contribute to plant defense. Plant Cell Physiol **52**: 2147–2156

Jouannet V, Moreno AB, Elmayan T, Vaucheret H, Crespi MD, Maizel A (2012) Cytoplasmic *Arabidopsis* AGO7 accumulates in membrane-associated siRNA bodies and is required for ta-siRNA biogenesis. EMBO J **31**: 1704–1713

Kastenmayer JP, Green PJ (2000) Novel features of the XRN-family in *Arabidopsis*: evidence that AtXRN4, one of several orthologs of nuclear Xrn2p/Rat1p, functions in the cytoplasm. Proc Natl Acad Sci USA **97**: 13985–13990

Kerényi F, Wawer I, Sikorski PJ, Kufel J, Silhavy D (2013) Phosphorylation of the N- and C-terminal UPF1 domains plays a critical role in plant nonsense-mediated mRNA decay. Plant J **76**: 836–848

Koguchi M, Yamasaki K, Hirano T, Sato MH (2017) Vascular plant one-zinc-finger protein 2 is localized both to the nucleus and stress granules under heat stress in *Arabidopsis*. Plant Signal Behav **12**: e1295907

Krapp S, Greiner E, Amin B, Sonnewald U, Krenz B (2017) The stress granule component G3BP is a novel interaction partner for the nuclear shuttle proteins of the nanovirus pea necrotic yellow dwarf virus and geminivirus abutilon mosaic virus. Virus Res **227**: 6–14

Kumakura N, Otsuki H, Ito M, Nomoto M, Tada Y, Ohta K, Watanabe Y (2016) *Arabidopsis* AtRRP44 has ribonuclease activity that is required to complement the growth defect of yeast rrp44 Mutant. Plant Biotechnol **33**: 77–85

Kumakura N, Otsuki H, Tsuzuki M, Takeda A, Watanabe Y (2013) *Arabidopsis* AtRRP44A is the functional homolog of Rrp44/Dis3, an exosome component, is essential for viability and is required for RNA processing and degradation. PLoS One **8**: e79219

Łabno A, Tomecki R, Dziembowski A (2016) Cytoplasmic RNA decay pathways - Enzymes and mechanisms. Biochim Biophys Acta **1863**: 3125–3147

Lanet E, Delannoy E, Sormani R, Floris M, Brodersen P, Crété P, Voinnet O, Robaglia C (2009) Biochemical evidence for translational repression by *Arabidopsis* microRNAs. Plant Cell **21**: 1762–1768

Lange H, Gagliardi D (2010) The exosome and 3′–5′ RNA degradation in Plants. RNA Exosome. Springer, New York, NY, pp 50–62

Lange H, Holec S, Cognat V, Pieuchot L, Le Ret M, Canaday J, Gagliardi D (2008) Degradation of a polyadenylated rRNA maturation by-product involves one of the three RRP6-like proteins in *Arabidopsis thaliana*. Mol Cell Biol **28**: 3038–3044

Lee C-C, Lin T-L, Lin J-W, Han Y-T, Huang Y-T, Hsu Y-H, Meng M (2016) Promotion of bamboo mosaic virus accumulation in *Nicotiana benthamiana* by 5′→3′ exonuclease NbXRN4. Front Microbiol. doi: 10.3389/fmicb.2015.01508

Liang W, Li C, Liu F, Jiang H, Li S, Sun J, Wu X, Li C (2009) The *Arabidopsis* homologs of CCR4-associated factor 1 show mRNA deadenylation activity and play a role in plant defence responses. Cell Res **19**: 307–316

Lin P-C, Pomeranz MC, Jikumaru Y, Kang SG, Hah C, Fujioka S, Kamiya Y, Jang J-C (2011) The *Arabidopsis* tandem zinc finger protein AtTZF1 affects ABA- and GA-mediated growth, stress and gene expression responses. Plant J **65**: 253–268

Li S, Le B, Ma X, Li S, You C, Yu Y, Zhang B, Liu L, Gao L, Shi T, et al (2016) Biogenesis of phased siRNAs on membrane-bound polysomes in *Arabidopsis*. eLife Sciences **5**: e22750

Li S, Liu L, Zhuang X, Yu Y, Liu X, Cui X, Ji L, Pan Z, Cao X, Mo B, et al (2013) MicroRNAs inhibit the translation of target mRNAs on the endoplasmic reticulum in *Arabidopsis*. Cell **153**: 562–574

Liu L, Chen X (2016) RNA quality control as a key to suppressing RNA silencing of endogenous genes in plants. Mol Plant **9**: 826–836

Li W, Ma M, Feng Y, Li H, Wang Y, Ma Y, Li M, An F, Guo H (2015) EIN2-directed translational regulation of ethylene signaling in *Arabidopsis*. Cell **163**: 670–683

Lokdarshi A, Conner WC, McClintock C, Li T, Roberts D (2015) *Arabidopsis* CML38, a calcium sensor that localizes to ribonucleoprotein complexes under hypoxia stress. Plant Physiol **170**: 01407.2015

Lorenzo L de, Sorenson R, Bailey-Serres J, Hunt AG (2017) Noncanonical alternative polyadenylation contributes to gene regulation in response to hypoxia. Plant Cell tpc.00746.2016

Luo G-Z, MacQueen A, Zheng G, Duan H, Dore LC, Lu Z, Liu J, Chen K, Jia G, Bergelson J, et al (2014) Unique features of the m^6A methylome in *Arabidopsis thaliana*. Nat Commun **5**: ncomms6630

Maldonado-Bonilla LD (2014) Composition and function of P bodies in *Arabidopsis thaliana*. Front Plant Sci **5**: 201

Matsui H, Nomura Y, Egusa M, Hamada T, Hyon G-S, Kaminaka H, Watanabe Y, Ueda T, Trujillo M, Shirasu K, et al (2017) The GYF domain protein PSIG1 dampens the induction of cell death during plant-pathogen interactions. PLoS

Genet **13**: e1007037

Mérai Z, Benkovics AH, Nyikó T, Debreczeny M, Hiripi L, Kerényi Z, Kondorosi É, Silhavy D (2013) The late steps of plant nonsense-mediated mRNA decay. Plant J **73**: 50–62

Merchante C, Brumos J, Yun J, Hu Q, Spencer KR, Enríquez P, Binder BM, Heber S, Stepanova AN, Alonso JM (2015) Gene-specific translation regulation mediated by the hormone-signaling molecule EIN2. Cell **163**: 684–697

Merchante C, Stepanova AN, Alonso JM (2017) Translation regulation in plants: an interesting past, an exciting present and a promising future. Plant J **90**: 628–653

Merret R, Carpenier M-C, Favory J-J, Picart C, Descombin J, Bousquet-Antonelli C, Tillard P, Lejay L, Deragon J-M, Charng Y-Y (2017) Heat-shock protein HSP101 affects the release of ribosomal protein mRNAs for recovery after heat shock. Plant Physiol 00269.2017

Merret R, Descombin J, Juan Y-T, Favory J-J, Carpentier M-C, Chaparro C, Charng Y-Y, Deragon J-M, Bousquet-Antonelli C (2013) XRN4 and LARP1 are required for a heat-triggered mRNA decay pathway involved in plant acclimation and survival during thermal stress. Cell Rep **5**: 1279–1293

Merret R, Nagarajan VK, Carpentier M-C, Park S, Favory J-J, Descombin J, Picart C, Charng Y-Y, Green PJ, Deragon J-M, et al (2015) Heat-induced ribosome pausing triggers mRNA co-translational decay in *Arabidopsis thaliana*. Nucleic Acids Res **43**: 4121–4132

Miller JE, Reese JC (2012) Ccr4-Not complex: the control freak of eukaryotic cells. Crit Rev Biochem Mol Biol **47**: 315–333

Moore M, Gossmann N, Dietz K-J (2016) Redox regulation of cytosolic translation in plants. Trends Plant Sci **21**: 388–397

Motomura K, Le QTN, Hamada T, Kutsuna N, Mano S, Nishimura M, Watanabe Y (2015) Diffuse decapping enzyme DCP2 accumulates in DCP1 foci under heat stress in *Arabidopsis thaliana*. Plant Cell Physiol **56**: 107–115

Nguyen AH, Matsui A, Tanaka M, Mizunashi K, Nakaminami K, Hayashi M, Iida K, Toyoda T, Nguyen DV, Seki M (2015) Loss of *Arabidopsis* 5′–3′ exoribonuclease AtXRN4 function enhances heat stress tolerance of plants subjected to severe heat stress. Plant Cell Physiol **56**: 1762–1772

Nguyen CC, Nakaminami K, Matsui A, Kobayashi S, Kurihara Y, Toyooka K, Tanaka M, Seki M (2016) Oligouridylate binding protein 1b plays an integral role in plant heat stress tolerance. Front Plant Sci. doi: 10.3389/fpls.2016.00853

Nguyen CC, Nakaminami K, Matsui A, Watanabe S, Kanno Y, Seo M, Seki M (2017) Overexpression of oligouridylate binding protein 1b results in ABA hypersensitivity. Plant Signal Behav **12**: e1282591

Nishimura N, Kitahata N, Seki M, Narusaka Y, Narusaka M, Kuromori T, Asami T, Shinozaki K, Hirayama T (2005) Analysis of ABA hypersensitive germination 2 revealed the pivotal functions of PARN in stress response in *Arabidopsis*. Plant J **44**: 972–984

Okamoto M, Matsui A, Tanaka M, Morosawa T, Ishida J, Iida K, Mochizuki Y, Toyoda T, Seki M (2016) Sm-like protein-mediated RNA metabolism is required for heat stress tolerance in *Arabidopsis*. Front Plant Sci. doi: 10.3389/fpls.2016.01079

Ozgur S, Chekulaeva M, Stoecklin G (2010) Human Pat1b connects deadenylation with mRNA decapping and controls the assembly of processing bodies. Mol Cell Biol **30**: 4308–4323

Peng J, Yang J, Yan F, Lu Y, Jiang S, Lin L, Zheng H, Chen H, Chen J (2011) Silencing of NbXrn4 facilitates the systemic infection of Tobacco mosaic virus in *Nicotiana benthamiana*. Virus Res **158**: 268–270

Perea-Resa C, Carrasco-López C, Catalá R, Turečková V, Novak O, Zhang W, Sieburth L, Jiménez-Gómez JM, Salinas J (2016) The LSM1-7 complex differentially regulates *Arabidopsis* tolerance to abiotic stress conditions by promoting selective mRNA decapping. Plant Cell **28**: 505–520

Perea-Resa C, Hernández-Verdeja T, López-Cobollo R, Castellano M del M, Salinas J (2012) LSM proteins provide accurate splicing and decay of selected transcripts to ensure normal *Arabidopsis* development. Plant Cell **24**: 4930–4947

Petre B, Saunders DGO, Sklenar J, Lorrain C, Krasileva KV, Win J, Duplessis S, Kamoun S (2016) Heterologous expression screens in *Nicotiana benthamiana* identify a candidate effector of the wheat yellow rust pathogen that associates with processing bodies. PLoS One **11**: e0149035

Pomeranz MC, Hah C, Lin P-C, Kang SG, Finer JJ, Blackshear PJ, Jang J-C (2010a) The *Arabidopsis* tandem zinc finger protein AtTZF1 traffics between the nucleus and cytoplasmic foci and binds both DNA and RNA. Plant Physiol **152**: 151–165

Pomeranz M, Lin P-C, Finer J, Jang J-C (2010b) AtTZF gene family localizes to cytoplasmic foci. Plant Signal Behav **5**: 190–192

Potuschak T, Vansiri A, Binder BM, Lechner E, Vierstra RD, Genschik P (2006) The exoribonuclease XRN4 is a component of the ethylene response pathway in *Arabidopsis*. Plant Cell **18**: 3047–3057

Protter DSW, Parker R (2016) Principles and properties of stress granules. Trends Cell Biol **26**: 668–679

Qu J, Kang SG, Wang W, Musier-Forsyth K, Jang J-C (2014) The *Arabidopsis thaliana* tandem zinc finger 1 (AtTZF1) protein in RNA binding and decay. Plant J **78**: 452–467

Reddy ASN, Marquez Y, Kalyna M, Barta A (2013) Complexity of the alternative splicing landscape in plants. Plant Cell **25**: 3657–3683

Reineke LC, Lloyd RE (2013) Diversion of stress granules and P-bodies during viral infection. Virology **436**: 255–267

Ren G, Xie M, Zhang S, Vinovskis C, Chen X, Yu B (2014) Methylation protects microRNAs from an AGO1-associated activity that uridylates 5′ RNA fragments generated by AGO1 cleavage. Proc Natl Acad Sci USA **111**: 6365–6370

Reverdatto SV, Dutko JA, Chekanova JA, Hamilton DA, Belostotsky DA (2004) mRNA deadenylation by PARN is essential for embryogenesis in higher plants. RNA **10**: 1200–1214

Rogers K, Chen X (2013) Biogenesis, turnover, and mode of action of plant microRNAs. Plant Cell **25**: 2383–2399

Roux ME, Rasmussen MW, Palma K, Lolle S, Regué ÀM, Bethke G, Glazebrook J, Zhang W, Sieburth L, Larsen MR, et al (2015) The mRNA decay factor PAT1 functions in a pathway including MAP kinase 4 and immune receptor SUMM2. EMBO J **34**: 593–608

Roy B, von Arnim AG (2013) Translational regulation of cytoplasmic mRNAs. Arabidopsis Book **11**: e0165

Rymarquis LA, Souret FF, Green PJ (2011) Evidence that XRN4, an *Arabidopsis* homolog of exoribonuclease XRN1, preferentially impacts transcripts with certain sequences or in particular functional categories. RNA **17**: 501–511

Sarowar S, Oh HW, Cho HS, Baek K-H, Seong ES, Joung YH, Choi GJ, Lee S, Choi D (2007) *Capsicum annuum* CCR4-associated factor CaCAF1 is necessary for plant development and defence response. Plant J **51**: 792–802

Scarpin MR, Sigaut L, Temprana SG, Boccaccio GL, Pietrasanta LI, Muschietti JP (2017) Two *Arabidopsis* late pollen transcripts are detected in cytoplasmic granules. Plant Direct. doi: 10.1002/pld3.12

Sharif H, Ozgur S, Sharma K, Basquin C, Urlaub H, Conti E (2013) Structural analysis of the yeast Dhh1-Pat1 complex reveals how Dhh1 engages Pat1, Edc3 and RNA in mutually exclusive interactions. Nucleic Acids Res **41**: 8377–8390

Shaul O (2015) Unique aspects of plant nonsense-mediated mRNA decay. Trends Plant Sci **20**: 767–779

Shi Z, Fujii K, Kovary KM, Genuth NR, Röst HL, Teruel MN, Barna M (2017)

Heterogeneous ribosomes preferentially translate distinct subpools of mRNAs genome-wide. Mol Cell **67**: 71–83.e7

Siwaszek A, Ukleja M, Dziembowski A (2014) Proteins involved in the degradation of cytoplasmic mRNA in the major eukaryotic model systems. RNA Biol **11**: 1122–1136

Soma F, Mogami J, Yoshida T, Abekura M, Takahashi F, Kidokoro S, Mizoi J, Shinozaki K, Yamaguchi-Shinozaki K (2017) ABA-unresponsive SnRK2 protein kinases regulate mRNA decay under osmotic stress in plants. Nature Plants **3**: nplants2016204

Sorenson R, Bailey-Serres J (2014) Selective mRNA sequestration by OLIGOURIDYLATE-BINDING PROTEIN 1 contributes to translational control during hypoxia in *Arabidopsis*. Proc Natl Acad Sci USA **111**: 2373–2378

Souret FF, Kastenmayer JP, Green PJ (2004) AtXRN4 degrades mRNA in *Arabidopsis* and its substrates include selected miRNA targets. Mol Cell **15**: 173–183

Stauffer E, Westermann A, Wagner G, Wachter A (2010) Polypyrimidine tract-binding protein homologues from *Arabidopsis* underlie regulatory circuits based on alternative splicing and downstream control. Plant J **64**: 243–255

Steffens A, Bräutigam A, Jakoby M, Hülskamp M (2015) The BEACH domain protein SPIRRIG is essential for *Arabidopsis* salt stress tolerance and functions as a regulator of transcript stabilization and localization. PLoS Biol **13**: e1002188

Steffens A, Jaegle B, Tresch A, Hülskamp M, Jakoby M (2014) Processing-body movement in *Arabidopsis* depends on an interaction between myosins and DECAPPING PROTEIN1. Plant Physiol **164**: 1879–1892

Sureshkumar S, Dent C, Seleznev A, Tasset C, Balasubramanian S (2016) Nonsense-mediated mRNA decay modulates FLM-dependent thermosensory flowering response in *Arabidopsis*. Nat Plants **2**: 16055

Suzuki Y, Arae T, Green PJ, Yamaguchi J, Chiba Y (2015) AtCCR4a and AtCCR4b are involved in determining the poly(A) length of granule-bound starch synthase 1 transcript and modulating sucrose and starch metabolism in *Arabidopsis thaliana*. Plant Cell Physiol **56**: 863–874

Tharun S (2009) Lsm1-7-Pat1 complex: A link between 3’ and 5’-ends in mRNA decay? RNA Biol **6**: 228–232

Tian L, Okita TW (2014) mRNA-based protein targeting to the endoplasmic reticulum and chloroplasts in plant cells. Curr Opin Plant Biol **22**: 77–85

Tsuzuki M, Motomura K, Kumakura N, Takeda A (2017) Interconnections between mRNA degradation and RDR-dependent siRNA production in mRNA turnover in

plants. J Plant Res **130**: 211–226

Vandivier LE, Campos R, Kuksa PP, Silverman IM, Wang L-S, Gregory BD (2015) Chemical modifications mark alternatively spliced and uncapped messenger RNAs in *Arabidopsis*. Plant Cell **27**: 3024–3037

Vexler K, Cymerman MA, Berezin I, Fridman A, Golani L, Lasnoy M, Saul H, Shaul O (2016) The *Arabidopsis* NMD factor UPF3 is feedback-regulated at multiple levels and plays a role in plant response to salt stress. Front Plant Sci **7**: 1376

Wahle E, Winkler GS (2013) RNA decay machines: Deadenylation by the Ccr4–Not and Pan2–Pan3 complexes. Biochimica et Biophysica Acta (BBA) - Gene Regulatory Mechanisms **1829**: 561–570

Walley JW, Kelley DR, Nestorova G, Hirschberg DL, Dehesh K (2010) *Arabidopsis* deadenylases AtCAF1a and AtCAF1b play overlapping and distinct roles in mediating environmental stress responses. Plant Physiol **152**: 866–875

Wang S, Okamoto T (2009) Involvement of polypyrimidine tract-binding protein (PTB)-related proteins in pollen germination in *Arabidopsis*. Plant Cell Physiol **50**: 179–190

Waris S, Wilce MCJ, Wilce JA (2014) RNA recognition and stress granule formation by TIA proteins. Int J Mol Sci **15**: 23377–23388

Weber C, Nover L, Fauth M (2008) Plant stress granules and mRNA processing bodies are distinct from heat stress granules. Plant J **56**: 517–530

Xu J, Chua N-H (2011) Processing bodies and plant development. Curr Opin Plant Biol **14**: 88–93

Xu J, Chua N-H (2009) *Arabidopsis* decapping 5 is required for mRNA decapping, P-body formation, and translational repression during postembryonic development. Plant Cell **21**: 3270–3279

Xu J, Chua N-H (2012) Dehydration stress activates *Arabidopsis* MPK6 to signal DCP1 phosphorylation. EMBO J **31**: 1975–1984

Xu J, Yang J-Y, Niu Q-W, Chua N-H (2006) *Arabidopsis* DCP2, DCP1, and VARICOSE form a decapping complex required for postembryonic development. Plant Cell **18**: 3386–3398

Yan C, Yan Z, Wang Y, Yan X, Han Y (2014) Tudor-SN, a component of stress granules, regulates growth under salt stress by modulating GA20ox3 mRNA levels in *Arabidopsis*. J Exp Bot **65**: 5933–5944

Yang L, Wu G, Poethig RS (2012) Mutations in the GW-repeat protein SUO reveal a developmental function for microRNA-mediated translational repression in *Arabidopsis*. Proc Natl Acad Sci USA **109**: 315–320

Yang M, Zhang B, Jia J, Yan C, Habaike A, Han Y (2013) RRP41L, a putative core subunit of the exosome, plays an important role in seed germination and early seedling growth in *Arabidopsis*. Plant Physiol **161**: 165–178

Ye J, Yang J, Sun Y, Zhao P, Gao S, Jung C, Qu J, Fang R, Chua N-H (2015) Geminivirus activates ASYMMETRIC LEAVES 2 to accelerate cytoplasmic DCP2-mediated mRNA turnover and weakens RNA silencing in *Arabidopsis*. PLoS Pathog **11**: e1005196

Yu X, Willmann MR, Anderson SJ, Gregory BD (2016) Genome-wide mapping of uncapped and cleaved transcripts reveals a role for the nuclear mRNA cap-binding complex in co-translational RNA decay in *Arabidopsis*. The Plant Cell Online tpc.00456.2016

Zhang L, Liu X, Gaikwad K, Kou X, Wang F, Tian X, Xin M, Ni Z, Sun Q, Peng H, et al (2017a) Mutations in eIF5B confer thermosensitive and pleiotropic phenotypes via translation defects in *Arabidopsis thaliana*. Plant Cell. doi: 10.1105/tpc.16.00808

Zhang W, Murphy C, Sieburth LE (2010) Conserved RNaseII domain protein functions in cytoplasmic mRNA decay and suppresses *Arabidopsis* decapping mutant phenotypes. Proc Natl Acad Sci USA **107**: 15981–15985

Zhang X, Guo H (2017) mRNA decay in plants: both quantity and quality matter. Curr Opin Plant Biol **35**: 138–144

Zhang X, Zhu Y, Liu X, Hong X, Xu Y, Zhu P, Shen Y, Wu H, Ji Y, Wen X, et al (2015) Suppression of endogenous gene silencing by bidirectional cytoplasmic RNA decay in *Arabidopsis*. Science **348**: 120–123

Zhang Z, Hu F, Sung MW, Shu C, Castillo-González C, Koiwa H, Tang G, Dickman M, Li P, Zhang X (2017b) RISC-interacting clearing 3'- 5' exoribonucleases (RICEs) degrade uridylated cleavage fragments to maintain functional RISC in *Arabidopsis thaliana*. eLife Sciences **6**: e24466

Zhao L, Kunst L (2016) SUPERKILLER complex components are required for the RNA exosome-mediated control of cuticular wax biosynthesis in *Arabidopsis* inflorescence Stems. Plant Physiol **171**: 960–973

Zuber H, Scheer H, Ferrier E, Sement FM, Mercier P, Stupfler B, Gagliardi D (2016) Uridylation and PABP cooperate to repair mRNA deadenylated ends in *Arabidopsis*. Cell Rep **14**: 2707–2717

Figure 1.2. mRNA surveillance-triggered decay during the pioneer round of translation.
An mRNA is exported from the nucleus to the cytoplasm as a messenger ribonucleoprotein particle (mRNP) with the nuclear CBP20/CBP80 cap-binding complex (CBC) bound to the 5'-cap and poly(A)-binding proteins (PABPs) bound to the 3' polyadenylated tail. Within minutes after export, the mRNA undergoes a pioneer round of translation as a quality control (QC) mechanism (*A*). After the first round of translation and replacement of CBP20 by the eukaryotic translation initiation factor 4E (eIF4E), only mRNAs that pass the QC check can enter into active translation as templates for bulk protein synthesis (*B*). mRNAs with defects in translation are subjected to degradation via different pathways. mRNAs containing a sequence feature that causes premature translation termination, *e.g.* a premature termination codon (PTC) upstream of an exon junction complex (EJC), are targeted for nonsense-mediated decay (NMD). mRNAs with stalled translating ribosomes in the coding region or lacking a termination codon may be targeted to the no-go decay (NGD) and non-stop decay (NSD) pathways, respectively. In contrast to NMD, which has been characterized, it is less clear if NGD and NSD pathways function in plants (*C*). Abbreviations: AUG, translation initiation codon; STOP, termination codon.

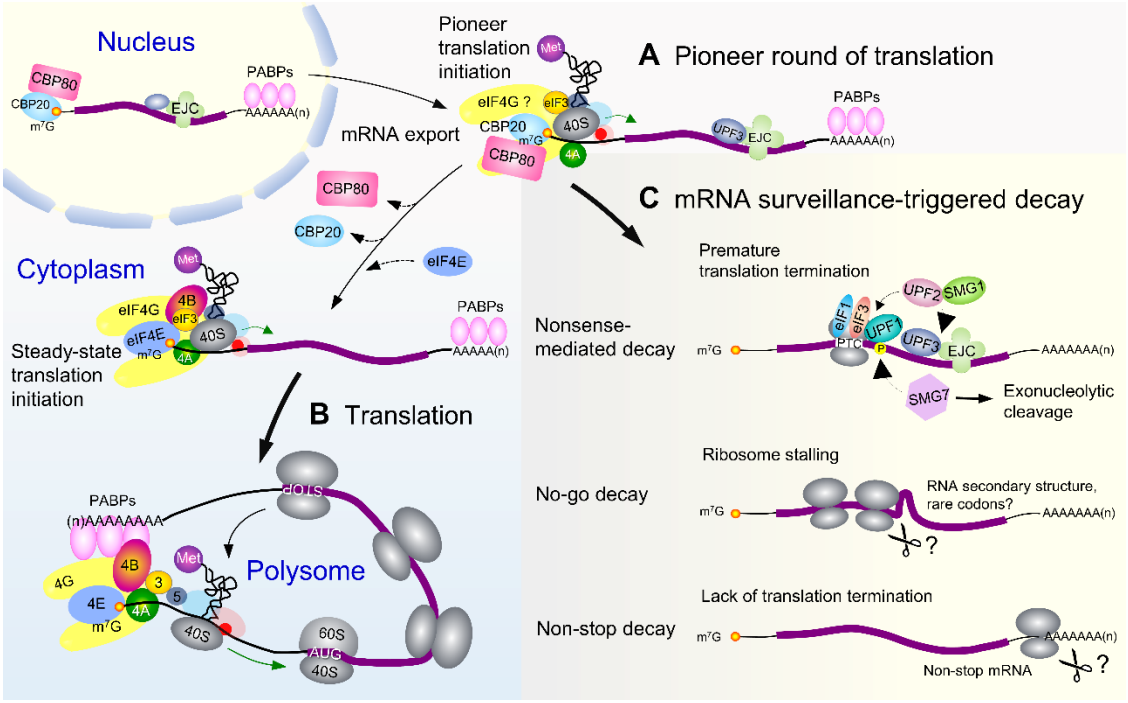
Nucleus
CBP80
CBP20
m7G
EJC
PABPs
AAAAAA(n)
mRNA export
Pioneer translation initiation
Met
eIF4G ?
eIF3
CBP20
40S
CBP80
4A
A Pioneer round of translation
UPF3
EJC
PABPs
AAAAAA(n)
CBP80
CBP20
eIF4E
Cytoplasm
Met
eIF4G
4B
eIF3
eIF4E
m7G
4A
40S
PABPs
AAAAA(n)
Steady-state translation initiation
B Translation
PABPs
(n)AAAAAAAA
eIF4G
4B
3
4E
4A
5
m7G
Met
40S
Polysome
60S
AUG
40S
C mRNA surveillance-triggered decay
Premature translation termination
Nonsense-mediated decay
eIF1
eIF3
PTC
UPF1
P
UPF2
SMG1
UPF3
EJC
m7G
AAAAAAA(n)
SMG7
Exonucleolytic cleavage
Ribosome stalling
No-go decay
m7G
RNA secondary structure, rare codons?
AAAAAAA(n)
?
Lack of translation termination
Non-stop decay
m7G
AAAAAAA(n)
Non-stop mRNA
?

Figure 1.2. Overview of cytoplasmic mRNA translation, storage and decay in plants.

Cytoplasmic mRNAs undergoing active translation form polysomes and remain in a translationally active state until damaged or translationally repressed (*A*). Repression can result from multiple causes (*i.e.*, altered abundance or phosphorylation of specific translation factors or RNA binding proteins and ribosome stalling) that limits translational initiation or ribosome translocation, promoting transition into a translationally repressed mRNP, where the mRNA is either sequestered by RNA-binding proteins (*e.g.*, UBP1, G3BP, and RBP45/47) or degraded via different pathways (*B*). mRNA sequestration is typically triggered by cellular stress, serving as a sorting nucleation point for mRNP assembly into stress granules (SGs) for storage or processing bodies (PBs) for degradation (*C*). During a stress-recovery period, intact mRNAs stored in SGs can re-enter translation via a process facilitated by a chaperone (*e.g.* HSP101 during heat stress recovery). Some mRNAs released from SGs may be targeted for degradation after stress (*D*). In general mRNA decay, the 3' protective poly(A) tail is removed by different classes of deadenylases (Nocturnin, Poly(A)-specific ribonuclease (PARN) and CCR-NOT complex), then degradation proceeds in the 3' to 5' direction by the multimeric SKI-exosome complex and/or the RRP44B/SOV exonuclease. After deadenylation, mRNA degradation can also occur from the 5' to 3' direction. mRNAs degraded via this mode could be localized in the cytosol and/or PBs where the multi-protein mRNA decapping complex removes the protective 5'-cap, and subsequently the 5'-3' XRN4 exoribonuclease catalyzes nucleotide hydrolysis (*E*). In addition to the deadenylation-dependent decay pathway, translationally repressed mRNAs can be degraded directly in the 5' to 3' direction while in association with elongating ribosomes via XRN4-mediated co-translational decay. This mode of degradation bypasses deadenylation but requires mRNA decapping. The progressive 5'-3' exonucleolytic destruction of the mRNA by XRN4 yields a codon-by-codon 3-nucleotide signature that is thought to reflect the movement of the most 5' ribosome along the transcript (*F*). Abbreviations: AUG, translation initiation codon; STOP, termination codon.

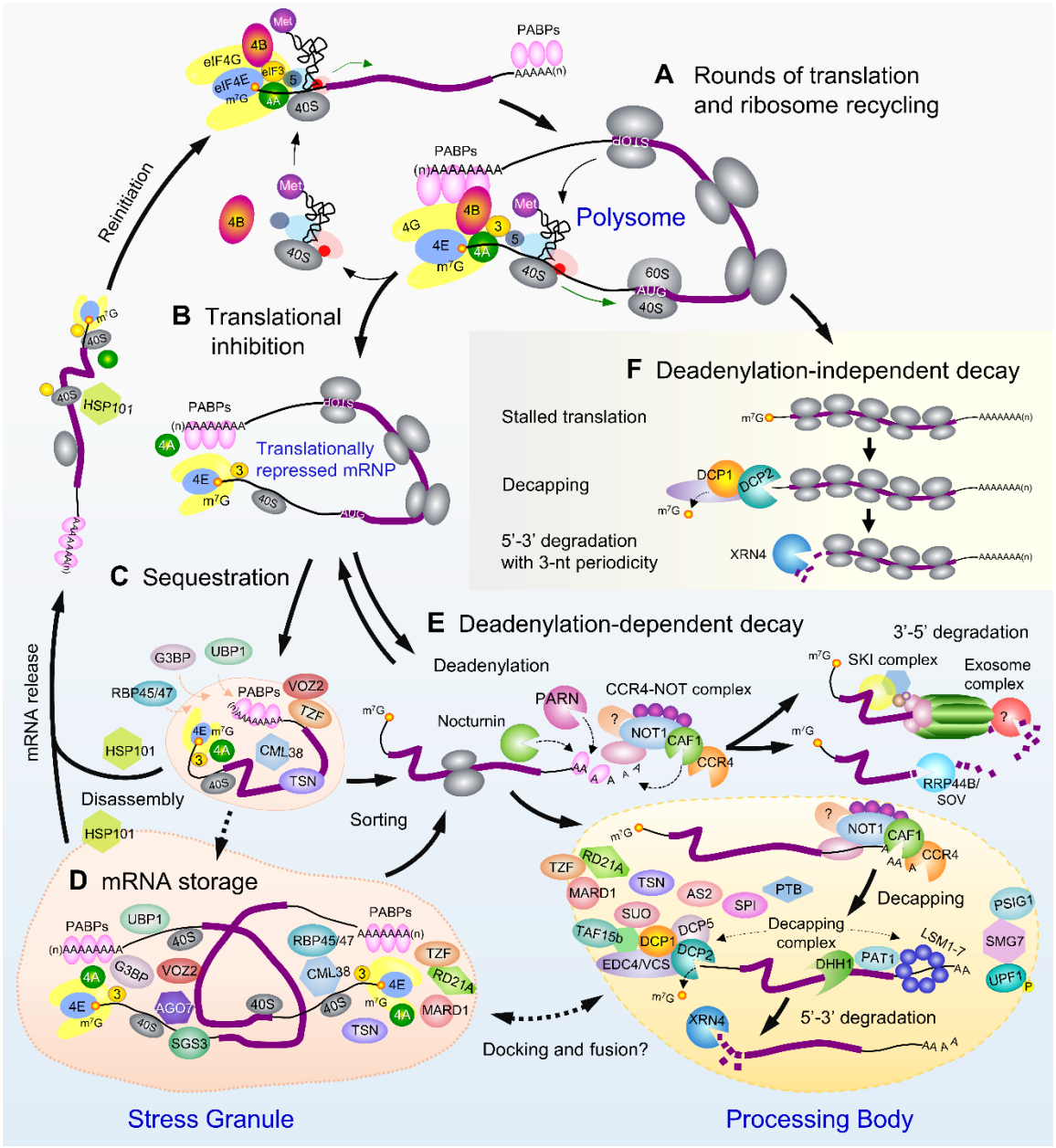
A Rounds of translation and ribosome recycling
Reinitiation
Polysome
B Translational inhibition
Translationally repressed mRNP
C Sequestration
HSP101
D mRNA storage
Stress Granule
Disassembly
mRNA release
Sorting
E Deadenylation-dependent decay
Deadenylation
Nocturnin
PARN
CCR4-NOT complex
3'-5' degradation
SKI complex
Exosome complex
RRP44B/ SOV
Decapping
Decapping complex
5'-3' degradation
XRN4
Docking and fusion?
Processing Body
F Deadenylation-independent decay
Stalled translation
Decapping
5'-3' degradation with 3-nt periodicity
PABPs
eIF4G
eIF4E
eIF3
40S
60S
Met
G3BP
UBP1
RBP45/47
VOZ2
TZF
CML38
TSN
AGO2
SGS3
RD21A
MARD1
NOT1
CAF1
CCR4
DCP1
DCP2
DCP5
TAF15b
EDC4/VCS
DHH1
PAT1
LSM1-7
SMG7
PSIG1
UPF1
SUO
AS2
SPI
PTB

Table 1.1. Proteins involved in the regulation of bulk cytoplasmic mRNA degradation in plants

Protein	Molecular function	Gene symbol	Gene ID	Biological functions	References
Deadenylation					
CCR4-NOT complex					
Carbon catabolite repressor 4	3′–5′ exoribonuclease, EEP superfamily	*AtCCR4a*	AT3G58560	Sucrose and starch metabolism	Suzuki et al. (2015)
		AtCCR4b	AT3G58580		
		OsCCR4a	Os10g27230	Unknown	Chou et al. (2017)
		OsCCR4b	Os03g07080		
CCR4-associated factor 1	3′–5′ exoribonuclease, DEDD superfamily	*AtCAF1a*	AT3G44260	Defense response to bacterial pathogens; abiotic stress response	Liang et al. (2009); Walley et al. (2010)
		AtCAF1b	AT5G22250		
		OsCAF1A	Os08g34170	Unknown	Chou et al. (2014); Chou et al. (2017)
		OsCAF1B	Os04g58810		
		OsCAF1G	Os09g24990		
		OsCAF1H	Os02g55300		
		CaCAF1		Development and defense response	Sarowar et al. (2007)
Negative on TATA 1	CCR4-NOT complex scaffold	*OsNOT1*	Os10g40780	Unknown	Chou et al. (2017)
Nocturnin	Poly(A)-specific 3′–5′ exoribonuclease, EEP superfamily	*AtHESP*	AT1G31500	Circadian clock regulation	Delis et al. (2016)
Poly(A) ribonuclease	Poly(A)-specific 3′–5′ exoribonuclease, DEDD superfamily	*AtPARN/ AHG2*	AT1G55870	Embryogenesis; ABA sensitivity; abiotic stress response	Reverdatto et al. (2004); Nishimura et al. (2005)
5'-3' mRNA decay					
Decapping complex					
Decapping 1	Decapping cofactor	*AtDCP1*	AT1G08370	Post-embryonic development; dehydration and heat stress response	Xu et al. (2006); Xu and Chua (2012); Motomura et al. (2015)
Decapping 2	Decapping enzyme	*AtDCP2/ TDT*	AT5G13570	Post-embryonic development; heat stress response	Xu et al. (2006); Motomura et al. (2015)
Decapping 5	Decapping enhancer	*AtDCP5*	AT1G26110	Post-embryonic development; osmotic stress response	Xu and Chua (2009); Xu and Chua (2012)
Enhancer of mRNA decapping 4	Core decapping complex scaffold	*AtEDC4/ VCS*	AT3G13300	Post-embryonic development; osmotic stress response; seed dormancy and germination	Xu et al. (2006); Goeres et al. (2007); Soma et al. (2017)
		TaEDC4	Traes_6DL_3FBA5B70E	Plant-fungal pathogen interaction	Petre et al. (2016)
LSM1-7 complex	Decapping enhancer	*AtLSM1a*	AT1G19120	Post-embryonic development; heat stress tolerance; ABA-mediated response to cold, drought, and salt tolerance	Perea-Resa et al. (2012); Golisz et al. (2013); Okamoto et al. (2016); Perea-Resa et al. (2016)
		AtLSM1b	AT3G14080		
		AtLSM2	AT1G03330		
		AtLSM3a	AT1G21190		
		AtLSM3b	AT1G76860		
		AtLSM4	AT5G27720		
		AtLSM5	AT5G48870		
		AtLSM6a	AT2G43810		
		AtLSM6b	AT3G59810		

		AtLSM7	AT2G03870		
Protein-associated with topoisomerase 1	Decapping enhancer, translation repressor?	*AtPAT1*	AT1G79090	Immune response	Roux et al. (2015)
DEAD-box RNA helicase		*AtDHH1*	AT3G61240	Unknown	Xu et al. (2006); Bhullar et al. (2017)
Asymmetric leaf 2	Decapping activator	*AtAS2*	AT1G65620	Plant-virus interaction	Ye et al. (2015)
5′-3′ mRNA decay					
Exoribonuclease 4	5′-3′ exoribonuclease	*AtXRN4/ EIN5*	AT1G54490	Ethylene response/signaling; heat stress response	Potuschak et al. (2006); Merret et al. (2013)
		NbXRN4	gi|242037819	Defense response to viral pathogen	Peng et al. (2011); Lee et al. (2016)
La-related protein 1A	Heat-specific cofactor of AtXRN4	*AtLARP1A*	AT5G21160	Heat stress response	Merret et al. (2013)
3′-5′ mRNA decay					
Cytoplasmic exosome					
Ribosomal RNA processing proteins	RNase PH domain-containing proteins; hexameric core ring subunits of Exosome	*AtRRP41*	AT3G61620	Female gametogenesis	Chekanova et al. (2007)
		AtRRP42	AT3G07750	Unknown	Chekanova et al. (2007)
		AtRRP43	AT1G60080	Unknown	Chekanova et al. (2007)
		AtRRP45A *AtRRP45B /CER7*	AT3G12990 AT3G60500	Essential for viability; cuticular wax biosynthesis	Hooker et al. (2007)
		AtRRP46	AT3G46210	Unknown	Chekanova et al. (2007)
		AtRRP41L/ MTR3	AT4G27490	Germination and seedling development	Yang et al. (2013)
	S1/KH domain-containing proteins; ‘cap’ structure subunits of core Exosome	*AtRRP4*	AT1G03360	Post-zygotic development	Chekanova et al. (2007)
		AtRRP40A	AT2G25355	Unknown	Chekanova et al. (2007)
		AtRRP40B	AT4G32175	Unknown	Chekanova et al. (2007)
		AtCSL4	AT5G38885	Unknown	Chekanova et al. (2007)
	RNase II-type 3′-5′ exoribonuclease	*AtRRP44B /SOV*	AT1G77680	Compensation of VCS function in post-embryonic development	Zhang et al. (2010); Kumakura et al. (2013)
	RNase D-type 3′-5′ exoribonuclease, DEDD superfamily	*AtRRP6L3*	AT2G32415	Unknown	Lange et al. (2008)
Superkiller (SKI) complex					
Superkiller proteins	Auxiliary factors of the exosome	*AtSKI2* *AtSKI3* *AtSKI8/ VIP3*	AT3G46960 AT1G76630 AT4G29830	Cuticular wax biosynthesis	Zhao and Kunst (2016)

At, *Arabidopsis thaliana*; *Ca*, *Capsicum annuum*; *Nb*, *Nicotiana benthamiana*; *Os*, *Oryza sativa*; *Te*, *Triticum aestivum*
AtRRP44A, AtRRP6L1 and AtRRP6L2 are components of the exosome complex, but they are not included in this table because subcellular localization data suggest that they are nuclear proteins, hence being components of the nuclear exosome (Lange et al., 2008; Zhang et al. 2010).

Table 1.2. Proteins associated with stress granules and processing bodies in plants

Protein	Symbol	Gene ID	mRNP	Biological functions	Reference
Eukaryotic translation initiation factors	AteIF4E AteIF3b1	AT4G18040 AT5G27640	SG SG	Heat stress response	Weber et al. (2008) Suzuki et al. (2015)
Poly(A)-binding proteins	AtPABP2 AtPABP8	AT4G34110 AT1G49760	SG SG	Hypoxia stress response Heat stress response	Weber et al. (2008); Sorenson and Bailey-Serres, (2014)
RNA-binding proteins 45 and 47	AtRBP47B	AT1G19130	SG	Heat stress response	Weber et al. (2008)
Oligouridylate binding proteins 1	AtUBP1A	AT1G54080	SG	Hypoxia stress response	Sorenson and Bailey-Serres (2014)
	AtUBP1B	AT1G17370	SG	Salt, osmotic and heat stress response/tolerance; ABA sensitivity	Weber et al. (2008); Nguyen et al. (2016); Nguyen et al. (2017)
	AtUBP1C	AT3G14100	SG	Hypoxia stress response/ tolerance; sucrose-reversible seedling growth arrest	Sorenson and Bailey-Serres (2014)
Ras-GAP SH3 domain-binding protein	AtG3BP-like	AT5G43960	SG	Plant-virus interaction	Krapp et al. (2017)
Tudor Staphylococcal nucleases	AtTSN1	AT5G07350	SG, PB	GA-mediated growth response under salt stress; heat stress response	Yan et al. (2014); Gutierrez-Beltran et al. (2015)
	AtTSN2	AT5G61780	SG, PB		
Tandem zinc finger proteins	AtTZF1	AT2G25900	SG, PB	Sugar and ABA−mediated stress response; GA−dependent growth response	Pomeranz et al. (2010); Lin et al. (2011)
	OsTZF1	Os05s10670	SG, PB	Salt and drought stress tolerance	Jan et al. (2013)
	AtTZF4	AT1G03790	SG, PB	ABA-, GA-, and phytochrome-mediated seed germination	Bogamuwa and Jang (2013); Bogamuwa and Jang (2016)
	AtTZF5	AT5G44260	SG, PB		
	AtTZF6	AT5G07500	SG, PB		
	AtTZF9	AT5G58620	PB	PAMP-triggered immunity	Maldonado-Bonilla et al. (2014)
Mediator of ABA-regulated dormancy 1	AtMARD1	AT3G63210	SG, PB	Interacting partner of AtTZF4, AtTZF5 and AtTZF6	Bogamuwa and Jang (2016)
Responsive to dehydration 21A	AtRD21A	AT1G47128	SG, PB	Interacting partner of AtTZF4, AtTZF5 and AtTZF6	Bogamuwa and Jang (2016)
Calmodulin-like 38	AtCML38	AT1G76650	SG	Hypoxia response/tolerance	Lokdarshi et al. (2016)
Vascular plant one-zinc-finger protein 2	AtVOZ2	AT2G42400	SG, PB	Heat stress response	Koguchi et al. (2017)
Heat-shock protein 101	AtHSP101	AT1G74310	SG	Heat stress response	Merret et al. (2017)
Suppressor of gene silencing 3	AtSGS3	AT5G23570	SG	Heat stress response	Jouannet et al. (2012)
Argonaute 7	AtAGO7	AT1G69440	SG	Heat stress response	Jouannet et al. (2012)
BEACH domain containing protein	AtSPIRRIG/ AtSPI	AT1G03060	PB	Salt stress tolerance	Steffens et al. (2015)
GW-repeat protein	AtSUO	AT3G48050	PB	miRNA-mediated translational repression; control of vegetative phase change	Yang et al. (2012)

Table 1.2. Proteins associated with stress granules and processing bodies in plants (continued)

Protein	Symbol	Gene ID	mRNP	Biological functions	Reference
TBP-associated factor 1b	AtTAF15b	AT5G58470	PB	TNL-mediated plant immunity	Dong et al. (2016)
Plant SMY2-type ILE-GYF domain-containing protein 1	AtPSIG1	AT5G42950	PB	Regulation of cell death during plant-pathogen interaction	Matsui et al. (2017)
Polypyrimidine tract-binding proteins	AtPTB1 AtPTB2	AT3G01150 AT5G53180	PB PB	Pollen germination	Wang and Okamoto (2009); Stauffer et al. (2010)
Ethylene insensitive 2	AtEIN2	AT5G03280	PB	Ethylene response	Li et al. (2015); Merchante et al. (2015)
Up frameshift 1	AtUPF1	AT5G47010	PB	Nonsense-mediated decay; ethylene response	Kerényi et al. (2013); Merchante et al. (2015)
Suppressor with morphological effect on genitalia 7	AtSMG7	AT5G19400	PB	Nonsense-mediated decay; TNL-mediated plant immunity	Mérai et al. (2013); Gloggnitzer et al. (2014)

CCR4s, CAF1s, XRN4 and components of mRNA decapping complex are localized PBs, but are only presented in Table 1.1. AtLARP1A, a heat-specific cofactor of XRN4-mediated cotranslational decay, also accumulates in SGs and PBs under heat-shock stress, and is presented in Table 1.1. All 11 *Arabidopsis* tandem zinc finger proteins are localized to cytoplasmic granules; however, only ones with demonstrated co-localizations with known SG and/or PB components are included. AtSGS3 and AtAGO7 are typically present in distinct siRNA bodies, but become positive for SG markers during heat stress. SG, stress granules; PB, processing bodies; *At, Arabidopsis thaliana; Os, Oryza sativa*

Chapter 2

Functional Characterization of DHH1/DDX6-like Proteins of *Arabidopsis* at the Whole Plant and Subcellular Levels

2.1 ABSTRACT

RNA helicases are motor proteins that unwind nucleotide duplexes in an ATP-dependent manner. Their roles have been implicated in every step of RNA metabolism, including cytoplasmic mRNA degradation. In yeast and metazoa, DEAD-box RNA helicases of the DHH1/DDX6 family are associated with translationally repressed cytoplasmic mRNA-ribonucleoprotein (mRNP) complexes, and play a role in translational repression, mRNA protection, or decapping and degradation. However, orthologs of the DHH1/DDX6 family are not well established in plants. In this chapter, we identified a near-constitutively family of genes encoding three closely related DHH1/DDX6-like proteins in *Arabidopsis thaliana*, *RNA HELICASE 6*, *8* and *12* (*RH6*, *RH8* and *RH12*). Genetic analyses of T-DNA insertion alleles of these genes unveiled their functional redundancy. Single and double mutants of *rh6*, *rh8* and *rh12* exhibit only minor developmental alterations, whereas the triple homozygous *rh6 rh8 rh12* mutant displays pleiotropic phenotypes including delayed germination and seedling growth, altered vein patterning, diminutive organs and severe maturation defects. The requirement for *RH6*, *RH8*, and *RH12* in plant growth and development was further confirmed by use of artificial microRNA-mediated gene silencing. Subcellular localization analysis of fluorescently labeled RH6, RH8, and RH12 expressed via their endogenous promoters demonstrated that all the three are nucleocytoplasmic proteins, with the cytoplasmic fraction forming mRNPs that are inducible by mild hypoxic stress. These RH complexes

overlapped with cytoplasmic foci containing the 5'-to-3' mRNA decay apparatus proteins, DECAPPING PROTEIN 2 (DCP2) and VARICOSE (VCS), suggesting that they are a component of processing bodies (PBs). RH6, RH8, and RH12 complexes overlapped with with the OLIGOURIDYLATE BINDING PROTEIN 1C (UBP1C) stress granules (SGs), indicating that they associate with more than one type of mRNPs. Evaluation of DCP2, VCS, and UBP1C localization in the triple *rh6 rh8 rh12* mutant revealed that the RHs are required for PB but not SG formation.

2.2 INTRODUCTION

Gene expression is the outcome of the multiscale process that involves regulatory activity of individual genes encompassing dynamics in chromatin architecture and the epigenetic DNA landscape, initiation and elongation of transcription, pre-mRNA processing, export, pioneer and steady-state mRNA translation, mRNA transport, sequestration and decay. Almost, if not all of these steps require RNA helicases, enzymes that utilize ATP to catalyze the separation of RNA duplexes and/or remodeling of RNA-ribonucleoprotein (RNP) complexes (Linder and Jankowsky, 2011). RNA helicases are present in all three domains of life, as well as in viruses (Kadaré and Haenni, 1997). Helicases are classified into superfamilies (SFs) including SF3-6 that form hexameric rings and SF1-2 that do not (Fairman-Williams et al., 2010). SF1 and SF2 helicases share a conserved helicase core comprising two tandem protein domains that resemble the fold of the bacterial recombination protein recombinase A (RecA) (Singleton et al., 2007). The helicase core contains sequence motifs required for ATP-binding, ATP-hydrolysis, RNA-binding, and RNA-remodeling (Bourgeois et al., 2016). Based on primary sequence motif composition, SF1 is divided into three families

including UvrD/Rep, Pif1-like, and Upf1-like. By the same criterion, the SF2 is classified into nine families and one group, *i.e.* RecG-like, RecQ-like, Rad3/XPD, Ski2-like, T1R, Swi/Snf, RIG-I-like, DEAD-box, DEAH/RHA, and NS3/NPH-II (Fairman-Williams et al., 2010). Of these, DEAD box proteins represent the largest family, with 40 members in humans and 26 in the yeast *Saccharomyces cerevisiae* (Fairman-Williams et al., 2010; Linder and Jankowsky, 2011; Bourgeois et al., 2016).

The DEAD-box RNA helicase family is characterized by the presence of 12 conserved motifs in the helicase core, one of which is motif II that contains Asp-Glu-Ala-Asp (DEAD) residues, providing the moniker DEAD box (Linder and Fuller-Pace, 2013) first characterized for the eukaryotic initiation factor 4A (eIF4A) required to remove mRNA secondary structure during the initiation phase of translation (Andreou and Klostermeier, 2013). In addition to the dual RecA-like catalytic core domains, most DEAD-box family members contain highly variable amino- and carboxyl-terminal extensions. It is thought that these variable regions contribute to the functional diversification among DEAD-box proteins through interactions with different partners. Since the characterization of eIF4A, roles of DEAD-box RNA helicases have been implicated in every step of RNA metabolism, including nuclear transcription, pre-mRNA splicing, ribosome biogenesis, RNA nuclear export, translation initiation, and RNA decay (Cordin et al., 2006). Closely related to eIF4A are DBP5/DDX19-like proteins important for mRNA export and translation termination (Gross et al., 2007; Tran et al., 2007; Okamura et al., 2018), and DHH1/DDX6-like proteins with roles in translational repression, mRNA storage, and degradation in various eukaryotes (Presnyak and Coller, 2013).

Eukaryotic DHH1/DDX6-like proteins constitute a single DEAD-box RNA helicase family that functions in diverse biological contexts that include conserved roles in translational repression associated with mRNA storage and/or degradation. In the yeast *Saccharomyces. cerevisiae*, DHH1 is essential for normal growth (Hata et al., 1998; Tseng-Rogenski et al., 2003), and required for efficient removal of the 5' terminal m^7Gppp cap (decapping) and subsequent 5' to 3' turnover of mRNAs (Coller et al., 2001). DHH1 physically interacts with DECAPPING 1 (DCP1), SM-LIKE PROTEIN 1 (LSM1), PROTEIN ASSOCIATED WITH TOPOISOMERASE 1 (PAT1), CCR4-ASSOCIATED FACTOR 1 (CAF1), and EXORIBONUCLEASE 1 (XRN1) (Hata et al., 1998; Coller et al., 2001; Fischer and Weis, 2002; Sheth and Parker, 2003). Together with its interacting partner PAT1, DHH1 is required for the general translational repression of mRNAs in response to glucose deprivation. These two proteins promote PB formation and repress translation of both capped and uncapped mRNAs (Coller and Parker, 2005).

In the nematode *Caenorhabditis elegans*, CGH-1 is required for oocyte and sperm functions (Navarro et al., 2001). CGH-1 forms cytoplasmic granules in both somatic and germ cells, with apparent antithetical function. In somatic cells, the formation of CGH-1 granules is dependent on PAT1 function, and the granules are involved in mRNA degradation. In germ cells, the formation of CGH-1 granules is independent of PAT1, and these granules are sites of mRNA storage along with translation factors (Boag et al., 2008). This indicates that the single DHH1/DDX6 protein CGH-1 functions in both mRNA storage and decay, involving distinct mRNPs and determined by tissue type. CGH-1 controls mRNA storage by promoting mRNP granule

stability during late oocyte development, and stabilizing maternal mRNAs during oogenesis (Noble et al., 2008).

In *Xenopus* oocytes, the DHH1/DDX6 protein Xp54 functions as an integral component of stored (maternal) mRNPs (Ladomery et al., 1997). Similar to the role of yeast DHH1 in translational repression, Xp54 binding and helicase action on deadenylated firefly luciferase mRNA represses translation *in vivo* (Minshall et al., 2001; Minshall et al., 2009). Moreover, Xp54 interacts with the cap-binding protein eIF4E. It is hypothesized that Xp54 sequesters eIF4E from the translational machinery, thereby promoting and maintaining the translational silencing of stored mRNAs in oocytes (Minshall and Standart, 2004).

DHH1/DDX6 proteins are involved in translational repression and recruitment of mRNAs to PBs in animals. In the fruitfly *Drosophila melanogaster*, the DHH1/DDX6 protein Me13B is essential for oogenesis.The protein forms cytoplasmic mRNP complexes containing oocyte-localized mRNAs, and mediates translational silencing of the mRNAs during transport from nurse cells to the oocyte (Nakamura et al., 2001). Me13B colocalizes with the 5’ to 3’ decay machinery proteins DCP1 and XRN1 in both maternal RNP granules and PBs of testis cells (Barbee et al., 2006; Zabolotskaya et al., 2008). In humans, DDX6 (also known as Rck/p54) is required for the proliferation of some cancer cell lines (Akao et al., 1995; Lin et al., 2008), and is involved in the replication and encapsidation of some viruses (Jangra et al., 2010; Yu et al., 2011; Reed et al., 2012). DDX6 preferentially binds single-stranded RNA of random sequence in a manner not requiring ATP-hydrolysis (Ernoult-Lange et al., 2012). DDX6 interacts with the CCR4-NOT deadenylation complex and functions microRNA (miRNA)-mediated gene silencing (Mathys et al., 2014; Rouya et al., 2014). The conserved core helicase

core of DDX6 is strictly required for PB assembly, and its carboxy-terminal domain alone is sufficient for translational repression and its accumulation in PBs (Minshall et al., 2009). DDX6 is proposed to act downstream of translational repressors to maintain the repressed state of mRNAs via a mechanism that triggers their localization in PBs, in a manner that sustains their repression and guides ultimate decay (Ernoult-Lange et al., 2012). In summary, DHH1/DDX6 proteins are frequently associated with translational repression and subsequent targeting of mRNAs for 5' to 3' mediated turnover.

The DEAD-box RNA helicase family is greatly expanded in plants, with an estimated 50 members in *Arabidopsis*, 51 in rice (*Oryza sativa*), 57 in maize (*Zea mays*), and 87 in soybean (*Glycine max*) (Xu et al., 2013a). Among the 50 DEAD-box proteins in *Arabidopsis*, RH12 was identified as a putative ortholog of yeast DHH, and shown to colocalize with *Arabidopsis* DCP2 in tobacco leaf epidermal cells (Xu et al., 2006). However, the function of this protein was not demonstrated. In this chapter, a multi-species and multi-kingdom phylogenetics analysis identified RH12 and two additional closely related proteins, RH6 and RH8, as putative *Arabidopsis* DHH1/DDX6 orthologs. The analysis of development of multigenic DDH1/DDX6-like *RH* mutants determined that these three RHs carry out redundant roles in plant growth and development. Subcellular localization of fluorescent translational fusion proteins expressed under the regulation of native promoters demonstrated that RH6, RH8, and RH12 are components of PBs and SGs, and are required for PB but not SG formation.

2.3 RESULTS

2.3.1 Identification of DHH1/DDX6-like RNA helicases in plants

To determine whether the DHH1/DDX6 protein family is conserved in plants, we performed a comprehensive phylogenetic analysis using amino acid sequences of DEAD-box RNA helicases from representative genomes across eukaryotic lineages. These include: yeast (*Saccharomyces cerevisiae*); animals, roundworm (*Caenorhabditis elegans*), fruit fly (*Drosophila melanogaster*), and human (*Homo sapiens*); and land plants, *Arabidopsis* (*Arabidopsis thaliana*), soybean (*Glycine max*), tomato (*Solanum lycopersicum*), rice (*Oryza sativa*), and maize (*Zea mays*). We found that at least three DEAD-box RNA helicases from each plant species were grouped into the same clade with known members of the DHH1/DDX6 family from yeast and animals, including yeast DHH1, roundworm CGH-1, fruit fly DDX6/ME31B, and human DDX6. These plant DHH1/DDX6-like RNA helicases include: RH6 (At2g45810), RH8 (At4g00660) and RH12 (At3g61240) from *Arabidopsis*; Glyma09g39710, Glyma03g01500, Glyma03g01530, Glyma08g26950, and Glyma17g27250 from soybean; DEAD18 (Solyc05g048850), DEAD4 (Solyc01g094350), and DEAD33 (Solyc10g017530) from tomato; RH6 (LOC_Os04g45040), RH8 (LOC_Os02g42860), and RH12 (LOC_Os10g35990) from rice; and DHH1 (Zm00001d032526), Zm00001d013910, and Zm00001d017384 from maize **(Figure 2.1A and 2.1B)**. This analysis suggests that the DHH1/DDX6 RNA helicase family is conserved and may have expanded as a result of genome duplication in land plants.

To understand the evolutionary relationships between members of the DDH1/DDX6 RNA helicase family, multiple sequence alignment and phylogenetic analysis were performed with full-length amino acid sequences of DHH1/DDX6-like

proteins from multiple eukaryotic species. The analysis was extended to other fungal DHH1 and animal DDX6 orthologs. To represent all *Viridiplantae* lineages, DHH1/DDX6-like proteins were included from green algae, bryophytes, and angiosperms. The results revealed that eukaryotic DHH1/DDX6-like proteins clustered into three major clades corresponding to the major eukaryotic branches of life. All DHH1/DDX6-like proteins analyzed shared a central characteristic helicase core comprising the two Rec-A like domains connected by a linker region **(Figure 2.2)**. Notably, the amino acid sequences of the N- and C-terminal extensions were variable both within and across the lineages, with long N- or C-extensions typically associated with glutamine- and proline-rich sequences. Nevertheless, conservation could be assumed in regard to the lengths of the N- and C-terminal extensions within each lineage. In this regard, fungal DDH1-like helicases generally possessed short N-terminal (7-23 amino acids) but long C-terminal extensions (67-150 amino acids), with an exception for *Thanatephorus cucumeris* DHH1-like protein (AG1IA_04085), of which both the N- and C-terminal extensions were short (17 amino acids) **(Figure 2.2)**. Animal DDX6-like helicases, on the other hand, contained long N-terminal extensions (21-77 amino acids) but short C-terminal extensions (12-27 amino acids). Like the animal DDX6-like proteins, plant DHH1/DDX6-like helicases had long N-terminal extensions (30-141 amino acids). However, the C-terminal extensions were altogether absent in both plant and algal DHH1/DDX6-like helicases, with shorter N-terminal regions (8-19 amino acids) in algal DDX6-like proteins compared to their plant and animal counterparts **(Figure 2.2)**.

2.3.2 *Arabidopsis RH6*, *RH8* and *RH12* encode DHH1/DDX6-like proteins with redundant roles in plant growth and development

As a representative of the plant DHH1/DDX6-like proteins, we were interested in characterizing the functions of *Arabidopsis* RH6, RH8 and RH12. A survey of tissue-specific expression profiles of *RH6*, *RH8*, and *RH12* transcripts from online sources, *i.e*. the *Arabidopsis* eFP browser (Winter et al., 2007) and Transcriptome Variation Analysis (TraVa) database (Klepikova et al., 2015; Klepikova et al., 2016), provided the consistent view that all three *RH* transcripts accumulate in all tissues examined **(Figure 2.3A and 2.3B)**, although one or another of them may have higher transcript levels in some tissues, suggesting some tissue specificity. For example, *RH6* transcripts are higher than those of *RH8* and *RH12* in mature leaves, whereas *RH8* transcripts predominate in mature pollen and seeds, and *RH12* transcripts are most abundant in shoot and floral meristems. These data indicate that *RH6*, *RH8* and *RH12* genes are generally active and ubiquitously expressed.

To study the physiological and molecular functions of RH6, RH8 and RH12, we obtained a T-DNA insertion mutant in each of the *RHs*. We designated these alleles *rh6-1* (Sail_111_H08), *rh8-1* (Salk_016830C), and *rh12-2* (Salk_016921C) **(Figure 2.4A)**. The *rh6-1* contains a T-DNA in the first exon; *rh8-1* contains a T-DNA in the 5' UTR region; and *rh12-2* contains a T-DNA in the sixth exon. Plants homozygous for the specific insertion alleles were confirmed by use of T-DNA- and allele-specific PCR **(Figure 2.4B)**. The steady-state levels of *RH6*, *RH8* and *RH12* transcripts were then evaluated in each homozygous mutant using end-point RT-PCR with primers flanking the T-DNA insertion sites. The results demonstrated the absence of PCR products for *RH6* and *RH8* transcripts in cDNA prepared from *rh6-1* and *rh8-1* seedlings, respectively

(Figure 2.4C). On the other hand, the PCR products for *RH12* transcripts were still detectable in cDNA prepared from *rh12-2* seedlings, although at smaller than expected sizes. It is possible that truncated *RH12* transcripts are produced in *rh12-2* mutant as a consequence of the T-DNA insertion. Next, the steady-state levels of *RH6*, *RH8*, and *RH12* transcripts in *rh6-1*, *rh8-1* and *rh12-2* mutants were measured by quantitative RT-PCR (RT-qPCR) using allele-specific primers that bind downstream of the T-DNA. This confirmed a significant decrease in *RH6* and *RH12* transcripts in *rh6-1* and *rh12-2* mutants, respectively, as compare to the wild-type Col-0 **(Figure 2.4D)**. *RH8* transcripts were not detectable in *rh8-1* mutant. Hence, we concluded that the *rh8-1* is a null allele, whereas *rh6-1* and *rh12-2* are knock-down alleles, although it is unclear if their transcripts are translated into functional proteins.

Phenotypic analysis of the individual *rh6-1*, *rh8-1* and *rh12-2* mutants did not unveil any obvious morphological abnormality typical of mRNA decapping-related mutants (Xu et al., 2006; Goeres et al., 2007; Xu and Chua, 2009; Perea-Resa et al., 2012; Roux et al., 2015), except a slight, but significant reduction in rosette size and fresh weight at the rosette stage **(Figure 2.4E and 2.4F)**. As *RH6*, *RH8* and *RH12* are closely related, with the gene products sharing 79-86% sequence identity, we hypothesized that these proteins may be functionally redundant. The lack of clear morphological phenotypes in *rh6-1*, *rh8-1* and *rh12-2* mutants may be due to genetic compensations between the family members as *RH12* transcripts were significantly increased in the null *rh8-1* mutant **(Figure 2.4D)**. To test these hypotheses, the *rh6-1*, *rh8-1* and *rh12-2* alleles were crossed with one another to generate the double *rh6 rh8*, *rh6 rh12* and *rh8 rh12* mutants, and finally the triple *rh6 rh8 rh12* mutant. All three double mutants exhibited a further reduction in rosette size and fresh weight **(Figure 2.4E and**

2.4F). Strikingly, the triple *rh6 rh8 rh12* mutant manifested pleiotropic developmental phenotypes, including diminished statue with defects in petiole and leaf expansion, and inhibition of overall growth and reproduction **(Figure 2.4E and 2.4F)**. The effect of *RH6*, *RH8* and *RH12* mutations on rosette growth phenotypes is dose-dependent as the rosette size and fresh weight of the mutants decreased as the wild-type *RH* allele number decrease. For example, the double homozygous heterozygous genotypes *rh6*$^{(+/-)}$ *rh8 rh12*, *rh6 rh8*$^{(+/-)}$ *rh12*, and *rh6 rh8 rh12*$^{(+/-)}$ had intermediate developmental phenotypes relative to the three double mutants and the triple mutant **(Figure 2.4E and 2.4F)**. To confirm that growth and developmental defects in the triple *rh6 rh8 rh12* mutant are caused by the *RH6*, *RH8*, and *RH12* mutations, a 3.3-kb genomic fragment corresponding to the *RH6* promoter and genic region, modified by insertion of a FLAG epitope sequence directly 5′ upstream of the stop codon (*gRH6-FLAG*) was transformed into the double homozygous single heterozygous *rh6*$^{(+/-)}$ *rh8 rh12*. The transgenic homozygous *gRH6-FLAG* in the triple *rh6 rh8 rh12* mutant background (*rh6 rh8 rh12_gRH6-FLAG*) displayed a rescued phenotype, with the rosette growth similar to that of the double *rh8 rh12* mutant **(Figure 2.4E and 2.4F)**. This confirmed that the phenotypes of the triple *rh6 rh8 rh12* mutant were due to the severe reduction or absence of *RH6*, *RH8*, and *RH12* functions. Taken together, the data indicate that *RH6*, *RH8*, and *RH12* are functionally redundant and required for plant growth and development.

At the seedling stage, the single *rh6-1*, *rh8-1*, and *rh12-2* mutants as well as the three double mutants appeared to have longer primary roots as compared to the wild-type, especially *rh12-2* and *rh8 rh12*, of which the roots were significantly longer than that of the wild-type **(Figure 2.4G and 2.4H)**. Conversely, primary roots of the triple *rh6*

rh8 rh12 mutant were significantly shorter relative to the wild-type. This short-root phenotype was also rescued in the complemented *rh6 rh8 rh12_gRH6-FLAG* line, which had primary roots lengths similar to that of the double *rh8 rh12* mutant **(Figure 2.4G and 2.4H)**. Root developmental defects are typical in mutants defective in the mRNA decapping machinery, including the core decapping proteins DCP1, DCP2 and VCS (Xu et al., 2006; Goeres et al., 2007), the decapping activator DCP5 (Xu and Chua, 2009), and the LSM1-7 complex (Perea-Resa et al., 2012). However, comparison of the triple *rh6 rh8 rh12* mutant with the decapping mutants *dcp2-1* and *vcs-7* (Xu et al., 2006; Goeres et al., 2007) revealed that primary roots of the triple mutant were significantly longer **(Figure 2.4G and 2.4H)**. Nonetheless, the triple *rh6 rh8 rh12* mutant shared other developmental defects with *dcp2-1* and *vcs-7*, such as chlorotic, curvy and small cotyledons with disorganized cotyledonary veins **(Figure 2.4I and 2.4J)**.

2.3.3 Mutations in *RH6*, *RH8* and *RH12* delay seed germination

Expression profiles of *RH6*, *RH8* and *RH12* from publicly available microarray and RNA-seq datasets indicated that all *RH6*, *RH8*, and *RH12* transcripts increase in imbibed and germinating seeds relative to dry seeds **(Figure 2.3A and 2.3B)**. We hypothesized that RH6, RH8 and RH12 may play a role in seed germination. As a first step, we confirmed by RT-qPCR that *RH6*, *RH8*, and *RH12* transcripts rise dramatically in wild-type Col-0 seeds after release from the cold temperature used for stratification and retained at the same levels during germination and seedling growth on plates for 8 days **(Figure 2.5A)**. Next, we tested whether mutations in *RH6*, *RH8*, and *RH12* affect seed germination. To this end, we compared germination rates of non-dormant (2-month-old stored) seeds of the progeny of the double homozygous single heterozygous

mutants *rh6*$^{(+/-)}$ *rh8 rh12*, *rh6 rh8*$^{(+/-)}$ *rh12*, and *rh6 rh8 rh12*$^{(+/-)}$ with the wild-type. Interestingly, without prior stratification, the progeny of all the three mutants germinated more slowly than the wild-type **(Figure 2.5B)**. However, since the progeny of *rh6*$^{(+/-)}$ *rh8 rh12*, *rh6 rh8*$^{(+/-)}$ *rh12*, and *rh6 rh8 rh12*$^{(+/-)}$ mutants are segregating populations of the double mutants (*rh6 rh8*, *rh6 rh12*, and *rh8 rh12*), the double homozygous single heterozygous mutants (*rh6*$^{(+/-)}$ *rh8 rh12*, *rh6 rh8*$^{(+/-)}$ *rh12*, and *rh6 rh8 rh12*$^{(+/-)}$) and the triple *rh6 rh8 rh12* mutant, it was unclear if the delayed germination in the populations was caused by which genotypes. To further investigate this phenotype, we compared germination rates of the triple mutant *rh6 rh8 rh12* with its siblings *rh8 rh12* and *rh6*$^{(+/-)}$ *rh8 rh12* by recording germination times of all the F1 progeny of the genotype *rh6*$^{(+/-)}$ *rh8 rh12*, then later scoring genotypes based on the phenotype of the *rh6 rh8 rh12* seedlings. Since the initial experiment was performed without stratification of the seed (4^{o} C for 2 days), it was unclear whether cold treatment that normally induces and synchronizes germination would alleviate the delayed germination of the mutants. Therefore, this experiment was repeated with and without stratification. For the non-stratified seeds, only 45% of the triple *rh6 rh8 rh12* seeds germinated after two days, whereas their siblings *rh8 rh12* and *rh6*$^{(+/-)}$ *rh8 rh12*, the wild-type, as well as the complemented *rh6 rh8 rh12_gRH6-FLAG* line reached 79.3%, 90%, and 91.8% germination at this time, respectively **(Figure 2.5C)**. Stratification slightly alleviated the delayed germination of the triple *rh6 rh8 rh12* mutant, as 53.5% of these seeds germinated after two days. However, germination rates of the triple mutant were still clearly delayed by comparison to their siblings *rh8 rh12* and *rh6*$^{(+/-)}$ *rh8 rh12*, the wild-type, and the complemented *rh6 rh8 rh12_gRH6-FLAG* line which had 86.9%, 93.1%, and 96.3% germination, respectively **(Figure 2.5C)**.

Germination is associated with the degradation of stored mRNAs that accumulate during seed development (Nakabayashi et al., 2005). It has been shown that the decapping mutant *dcp5-1* accumulates more mRNAs encoding seed storage proteins in seedlings (Xu and Chua, 2009). Consistent with the delayed germination of the triple mutant, the reduction of two seed-stored mRNAs, *OLEOSIN1* (*OLEO1*) and *OLEO2*, was also delayed during germination of the F1 progeny of the genotype *rh6*$^{(+/-)}$ *rh8 rh12* **(Figure 2.5D)**.

2.3.4 RH6/8/12-knockdown mutants are defective in plant growth

To obtain an additional, hypomorphic allele of *rh6*, we generated transgenic lines expressing an artificial miRNA targeting *RH6* transcripts in the double *rh8 rh12* mutant background using the miRNA319a precursor driven by the 35S promoter **(Figure 2.6A)**. We named this genotype *amiRH6 rh8 rh12*. Three independent *amiRH6 rh8 rh12* lines with strong suppression of *RH6* transcript abundance were obtained, including lines #21, #77, and #84 **(Figure 2.6B)**. At the seedling stage, none of the *amiRH6 rh8 rh12* lines displayed obvious developmental alterations as compared to those of the double mutant *rh8 rh12*. Quantification of the mature miRNA in the seedlings by pulsed stem-loop RT-qPCR confirmed the presence of *amiRH6* in all the three *amiRH6 rh8 rh12* lines, with the line #77 showing the highest *amiRH6* level as compared to the lines #21 and #84 **(Figure 2.6C)**. Concomitantly, *RH6* transcript levels were reduced to approximately 37%, 32% and 39% in line #21, #77, and #84, respectively, relative to the double mutant *rh8 rh12* and the wild-type **(Figure 2.6D)**. Notably, *RH12* transcripts were also significantly reduced in lines #77 and #84 as compared to *rh8 rh12,* suggesting that the artificial miRNA *amiRH6* may silence *RH12* as well or promote *RH12* transcript turnover.

Examination of the rosette growth phenotypes of the *amiRH6 rh8 rh12* lines revealed a significant decrease in rosette diameter and fresh weight as compared to the *rh8 rh12* and wild-type genotypes **(Figure 2.6E, 2.6F and 2.6G)**. These results further underscore the significance of RH6, RH8 and RH12 in plant growth and development.

2.3.5 Subcellular localization of RH6, RH8 and RH12

To determine the subcellular localization of *Arabidopsis* DHH1/DDX6-like proteins, transgenic *Arabidopsis* lines expressing C-terminal translational fusion of genomic *RH6*, *RH8*, and *RH12* with red fluorescent protein (*proRH6:RH6-RFP*, *proRH8:RH8-RFP*, and *proRH12:RH12-RFP*) were generated. In root tissues of *proRH6:RH6-RFP* seedlings grown under normal growth conditions, RH6 was localized in both the nucleus and cytoplasm **(Figure 2.7A, 2.7B and 2.7C)**. Similar results were obtained with the seedlings of *proRH8:RH8-RFP* **(Figure 2.7D, 2.7E and 2.7F)**, and *proRH12:RH12-RFP* lines **(Figure 2.7G, 2.7H and 2.7I)**. Based on these results, we conclude that the *Arabidopsis* DHH1/DDX6-like proteins are nucleocytoplasmic proteins.

Members of the DHH1/DDX6 family in other organisms have been shown to associate with cytoplasmic macromolecular RNA-protein assemblies, including germ granules (Ladomery et al., 1997; Nakamura et al., 2001; Navarro et al., 2001), neuronal granules (Barbee et al., 2006; Hillebrand et al., 2010), and processing bodies (PBs) and stress granules (SGs) (Buchan et al., 2008; Swisher and Parker, 2010). The N-terminal extensions of *Arabidopsis* RH6, RH8, and RH12 contain glutamine- and proline-rich sequences predicted to be intrinsically disordered, an important biophysical property facilitating the formation of macromolecular condensates, such as mRNP granules, through liquid-liquid phase separation (Boeynaems et al., 2018) **(Figure 2.8A)**.

Therefore, we evaluated the localization of RH6, RH8, and RH12 in the root basal meristem region of the *Arabidopsis* seedlings, where the cortex cells are cytoplasmically dense and vacuoles are small. When the seedlings were submerged in water under a coverslip and the protein localization was examined within 2 minutes of specimen preparation, all three RHs were dispersed across the cytoplasm, with a small fraction appearing to be in cytoplasmic granules. Strikingly, incubation of seedlings under the coverslip for up to 30 minutes, sufficient to cause mild hypoxia and/or mechanical stress, redistributed RH6, RH8, RH12 into large cytoplasmic foci **(Figure 2.8B)**. Next, we asked whether the RH6, RH8 and RH12 foci represent mRNP complexes, or simply unfolded protein aggregates caused by stresses. To answer this question, we repeated the same experiments with the seedlings treated with cycloheximide (CHX), an inhibitor of translation elongation that traps translating mRNAs on polysomes, thereby blocking PB and SG assembly (Weber et al., 2008). Indeed, we found that CHX treatment inhibited the formation of RH6, RH8 and RH12 foci altogether, whereas in seedlings treated with DMSO (mock control), all three RHs formed foci after 2 and 30 min of submergence **(Figure 2.8B)**. Based on these results, we conclude that RH6, RH8, and RH12 are nucleocytoplasmic and form macromolecular cytoplasmic mRNPs, of which the formation requires mRNA release from the ribosome.

Next, as our genetic data indicated that *RH6*, *RH8*, and *RH12* are functionally redundant, we asked whether their gene products are targeted to the same mRNPs. To this end, we tested if RH6 and RH12 colocalize in the same cytoplasmic foci by use of transgenic plants that coexpress C-terminally RFP-tagged RH6 and C-terminally CFP-tagged RH12, both of which were driven by their native promoter (*proRH6:RH6-RFP*; *proRH12:RH12-CFP*). Indeed, RH6 and RH12 had overlapping fluorescence in almost

all the cytoplasmic foci observed **(Figure 2.9)**, suggesting that the two proteins are targeted to the same mRNPs.

2.3.6 RH6, RH8 and RH12 associate with both processing bodies and stress granules

As RH6, RH8 and RH12 form cytoplasmic mRNP complexes upon submergence, we asked whether these structures are PBs or SGs, two major conserved translationally repressed cytoplasmic mRNPs in eukaryotic cells that can be induced by stresses (Decker and Parker, 2012). Like in yeast and animals, plant SGs are typically not discernible while PB components may diffuse throughout the cytoplasm or form distinct cytoplasmic foci under standard growth conditions, depending on the proteins studied. Nevertheless, both complexes are induced by stresses (Lokdarshi et al., 2015; Motomura et al., 2015). To this end, transgenic *Arabidopsis* coexpressing a pairwise combination of RH6, RH8 and RH12 with the PB markers DCP2 and VCS were generated by transformation of the genomic construct of *RH6*, *RH8*, and *RH12* C-terminally tagged with *RFP* (*proRH6:RH6-RFP*, *proRH8:RH8-RFP*, and *proRH12:RH12-RFP*) into native promoter-driven DCP2-GFP and VCS-GFP lines (*proDCP2:DCP2-GFP*, (Motomura et al., 2015); *proVCS:VCS-GFP*, (Roux et al., 2015)). In the root basal meristem of seedlings coexpressing RH6-RFP and DCP2-GFP, DCP2 was readily visible in granules after 2 minutes of submergence, whereas the majority of RH6 was dispersed in the cytoplasm with some proportion forming visible foci. Nevertheless, some of RH6 foci colocalized with those of DCP2 **(Figure 10A)**, with increased colocalization in the enlarged RH6 and DCP2 granules visible 30 minutes after sample preparation (**Figure 10A)**. Although RH6 and DCP2 granules clearly overlapped, a

number of granules were predominantly RH6 or DCP2, strongly suggesting that RH6 and DCP2 granules may constitute distinct mRNPs that can be dynamically associated or disassociated from one other. The same patterns of colocalization were observed in seedlings coexpressing RH8-RFP and DCP2-GFP as well as those coexpressing RH12-RFP and DCP2-GFP **(Figure 10B and 10C)**, confirming that all three RH complexes associate with DCP2 complexes. Next, we tested whether RH6 foci also overlap with those of the core decapping protein VCS. In transgenic seedlings coexpressing RH6-RFP and VCS-GFP, as observed for DCP2, VCS was localized to the cytoplasm in small foci visible within 2 minutes of submergence. At this time point, RH6 was distributed mainly in small cytoplasmic foci, but clearly colocalized with VCS in some of these macromolecular assemblies. Both VCS and RH6 complexes were enlarged and colocalized after 30 min **(Figure 11A)**. Similar colocalization was observed for RH8-RFP and RH12-RFP with VCS-GFP **(Figure 11B and 11C)**. In all, these data demonstrate that RH6, RH8, and RH12 are components of PBs.

As RH6, RH8, and RH12 complexes are induced by submergence, it is possible that these complexes also represent SGs. Therefore, we tested whether RH6, RH8, and RH12 complexes overlap with those of the SG marker UBP1C (Sorenson and Bailey-Serres, 2014). Transgenic seedlings coexpressing RH6-RFP, RH8-RFP, and RH12-RFP (*proRH6:RH6-RFP*, *proRH8:RH8-RFP*, and *proRH12:RH12-RFP*) with UBP1C-GFP (*pro35S:UBP1C-GFP*, (Sorenson and Bailey-Serres, 2014)) were individually generated. Although SGs are generally formed in response to stress, UBP1C foci were already visible in the root basal meristem of seedlings coexpressing RH6-RFP and UBP1C-GFP with 2 minutes of submergence. At this time point, although most of RH6 was dispersed, a small fraction was present in small visible foci, that included a subset that partially to

completely overlapped with those of UBP1C **(Figure 12A)**. The colocalization of RH6 and UBP1C macromolecular complexes was more evident after 30 minutes, when both the sizes and number of RH6 and UBP1C foci increased **(Figure 12A)**. These showed coalescence of RH6 and UBP1C complexes as the granule borders were typically enriched in one or the other protein. Similar results were obtained with colocalization analysis of RH8-RFP with UBP1C-GFP **(Figure 12B)**, and RH12-RFP with UBP1C-GFP **(Figure 12C)**. We conclude that RH6, RH8, and RH12 complexes can associate with small to large SGs to form a hybrid PB and SG complex.

2.3.7 *Arabidopsis* DHH1/DDX6-like RHs are required for the assembly of PB but not SG complexes

Since RH6, RH8, and RH12 localize to both PBs and SGs, we asked whether loss/depletion of their function affects the formation of these complexes. To this end, *proDCP2:DCP2-GFP*, *proVCS:VCS-GFP*, and *pro35S:UBP1C-GFP* lines were crossed with the double homozygous single heterozygous *rh6*$^{(+/-)}$ *rh8 rh12* mutant to obtain homozygous triple mutants that express DCP2-GFP, VCS-GFP, or UBP1C-GFP. These were compared with the parental lines (*proDCP2:DCP2-GFP/dcp2-1*, *proVCS:VCS-GFP/*Col-0 and *pro35S:UBP1C-GFP/ubp1c-1*) with functional (wild-type Col-0) *RH6*, *RH8*, and *RH12* alleles. Analysis of DCP2 localization in the root basal meristem of the parental wild-type plants showed small cytoplasmic foci after 2 minutes of incubation under a coverslip that increased in size and number after 30 minutes **(Figure 2.13A)**. In the triple mutant background, on the other hand, DCP2 was more dispersed across the cytoplasm with few foci discernible within 2 minutes of sample preparation. After 30 minutes, the number of large DCP2 foci increased in the triple

mutant, but to a far lesser extent than wild-type seedlings **(Figure 2.13A)**. Similarly, VCS signals in the root basal meristem of the wild-type seedlings appeared in visible discrete foci after two minutes of incubation, and were further induced in number and enlarged after 30 minutes. Conversely, VCS signals in the root basal meristem of the triple mutant seedlings were distributed in the cytoplasm with the number and size of foci clearly diminished after 2 and 30 minutes of incubation relative to the wild-type **(Figure 2.13B)**. Unlike DCP2 and VCS, UBP1C signals in the triple mutant seedlings were visible as cytoplasmic granules after 2 minutes of incubation, increasing in size and number after 30 minutes, similar to what was observed in wild-type seedlings **(Figure 2.13B)**. Taken together, these data demonstrate that RH6, RH8 and RH12 contribute to formation of the vast majority of PBs, but are dispensable for SG formation.

2.4 DISCUSSION

2.4.1 *Arabidopsis* DHH1/DDX6-like proteins have an essential role in plant growth and development

Although the role of DHH1/DDX6-like RNA helicases has been well established in yeast and animals (Presnyak and Coller, 2013), nothing is known about the function of these proteins in plants. In this study, we performed a comprehensive phylogenetic analysis of DEAD-box RNA helicases across eukaryotic species and inferred their evolutionary relationship. We demonstrated that, like in yeast and animals, the DHH1/DDX6 family is conserved in the *Viridiplantae* lineage, and have been expanded in land plants as a result of genome duplication events. Based on this analysis, we identified RH6, RH8, and RH12 from *Arabidopsis thaliana* as members of the DHH1/DDX6 family. Evaluation of the exon-intron organization of the *RH6*, *RH8*, and

RH12 genes revealed that all three have 9 exons, and an intron in the 3' UTR **(Figure 2.4)**. Notably, the sizes of exons 2 to 9 are equal among the three genes, likely reflecting recent duplications. At the protein level, RH6 and RH12 share 86% identity, both of which are 79% identical to RH8. These proteins are 61-62% and 54-55% identical to the yeast DHH1 and human DDX6, respectively, and share the essential and conserved helicase core with its 12 characteristic motifs.

Our genetic analysis of the single *rh6*, *rh8*, and *rh12* mutants as well as their high-ordered mutant combinations established that RH6, RH8, and RH12 exert a redundant, indispensable function in plant growth and development. This is indicated by the fact that each of the single mutants was indistinguishable from the wild-type at the seedling stage and only showed minor growth reduction at the rosette stage, whereas the triple *rh6 rh8 rh12* mutant displayed severe growth and developmental defects. The demonstration that the triple mutant phenotype was complemented by a re-introduction of the functional *RH6* gene further supports the conclusion that these highly co-expressed genes are functionally redundant. Additionally, the intermediate rosette size and fresh weight presented in the double *rh6 rh8*, *rh6 rh12*, and *rh8 rh12* genotypes as well as the *amiRH6 rh8 rh12* mutant combination indicate that plant growth is regulated by the DDH1/DDX6-like RHs in a dose-dependent manner. Yet, each double homozygous single heterozygous genotype was distinct in appearance. The contribution of each RH on growth may not be fully equivalent due to variation in gene activity in individual cell types or subtle but specific, non-overlapping functions.

The homozygous triple *rh6 rh8 rh12* mutant displayed a pleiotropic developmental alteration, including delayed germination, impaired root development, chlorotic cotyledon with altered venation, diminished growth, and infertility. In

Arabidopsis, it is well recognized that mRNA decapping factors play a crucial role in plant development, with loss of their function resulting in post-embryonic lethality for the core proteins DCP1, DCP2, VCS, and DCP5, or in severe growth alterations for the decapping activators LSM1 and PAT1 (Xu et al., 2006; Goeres et al., 2007; Xu and Chua, 2009; Perea-Resa et al., 2012; Roux et al., 2015). The loss (or severe reduction) of *RH6*, *RH8*, and *RH12* yielded phenotypes intermediate between the core decapping *dcp1*, *dcp2*, and *vcs* mutants and the decapping activators *pat1* and *lsm1a lsm1b* mutants. Unlike *dcp1*, *dcp2*, and *vcs* mutants, the triple *rh6 rh8 rh12* mutant is not embryonic lethal. However, its growth and development were more defective than those of *pat1* and *lsm1a lsm1b* mutants. Nevertheless, *rh6 rh8 rh12* seedlings share a number of phenotypes with all other characterized decapping-related mutants, as defective primary root, chlorotic cotyledon, and incomplete dicotyledonous vein have been observed in *dcp1*, *dcp2*, *dcp5*, *vcs*, and *lsm1a lsm1b*, whereas delayed germination has been reported *dcp5* and *lsm1a lsm1b* (Perea-Resa et al., 2012; Wawer et al., 2018). Delayed germination in the triple *rh6 rh8 rh12* mutant seeds might be associated with abscisic acid (ABA) response in the same manner as in *dcp5-1* mutant, where it was shown have increased ABA sensitivity during germination (Wawer et al., 2018). Collectively, the phenotype displayed by the triple *rh6 rh8 rh12* mutant is consistent with the putative role of RH6, RH8, and RH12 as DHH1/DDX6 orthologs that function in mRNA decapping and degradation.

2.4.2 RH6, RH8, and RH12 are nucleocytoplasmic proteins

Nuclear localization of DHH1/DDX6 proteins is conserved

Subcellular localization of RH6, RH8, and RH12 expressed under the control of their endogenous promoters determined that all the three are localized to both the nucleus and cytoplasm. Although most studies thus far focus on the cytoplasmic roles of DHH1/DDX6-like proteins, their nuclear localization has been observed in several organisms, including the yeast *S. cerevisiae* (Kruk et al., 2011; Haimovich et al., 2013), the planarian *Dugesia japonica* (Yoshida-Kashikawa et al., 2007), *Xenopus laevis* (Smillie and Sommerville, 2002), the brown rat *Rattus norvegicus* (Kawahara et al., 2014), and different human cell lines (Pettersson et al., 2014; Mück et al., 2016; Huang et al., 2017). It has been proposed that human DDX6 is shuttled between the nucleus and cytoplasm by dual mechanisms: one is through its association with mitotic chromosomes during mitosis and the other is mediated by its interacting partner nuclear shuttling protein, 4E-Transporter (4E-T) (Huang et al., 2017). Nuclear functions of DHH1/DDX6-like proteins have been implicated in both transcriptional and posttranscriptional control of gene expression. At the transcriptional level, yeast DHH1, as part of the CCR4-NOT complex, associates with RNA polymerase II and promotes transcriptional elongation(Kruk et al., 2011). Similarly, human DDX6 associates with the AF4/AF4N super elongation complex, and promotes transcription (Mück et al., 2016). In yeast, apart from DHH1, other 5'-to-3' decay machinery including PAT1, DCP2, LSM1, and XRN4 shuttle between the nucleus and cytoplasm. Directly associated with their roles in mRNA decay, the nuclear presence of these factors is required for efficient transcription (Haimovich et al., 2013). At the post transcriptional level, human DDX6 has been shown to unwind CUG-RNA duplexes of the nuclear-accumulated *MYOTONIC*

DYSTROPHY PROTEIN KINASE mRNAs and reduce the nuclear CUG-mRNP foci associated the Myotonic Dystrophy type 1 disease in human (Pettersson et al., 2014). In line with our observation of nuclear localized of RH6, RH8 and RH12, a study has shown that RH8 interacts with PROTEIN PHOSPHATASE 2CA (PP2CA) in the nucleus (Baek et al., 2018). In this regard, RH8 inhibits PP2CA phosphatase activity, hence positively regulating ABA signaling and drought stress response. However, it is unclear whether this process involves the RNA helicase function of RH8. Future work can address the functional relevance of the nuclear localization of RH6, RH8, RH12 with respect to their role in RNA metabolism.

RH6/8/12 localize with cytoplasmic macromolecular complexes associated with mRNA decay and storage

Cytoplasmic mRNA translation, storage, and degradation are highly dynamic interconnected processes modulated by a cohort of RNA-binding proteins. Under certain cellular states including stress conditions, these proteins can form macromolecular mRNP assemblies through liquid-liquid phase separation, a process mediated by high-affinity interactions of low-complexity protein sequences, weak/intermediate interactions between low-complexity protein domains or intrinsically disordered regions, and multivalent interactions between RNA and proteins (Standart and Weil, 2018). SGs and PBs are the generic terms for the two major conserved translationally repressed mRNP complexes in the cytoplasm of eukaryotic cells formed by this mechanism (Kroschwald et al., 2015; Molliex et al., 2015; Protter et al., 2018). SGs are involved in mRNA storage and protection, characterized by the presence of poly(A)-binding proteins and translation initiation factors (Protter and Parker, 2016). PBs are enriched with translational

repressors and the 5′ to 3′ mRNA degradation machinery including components of the decapping complexes and the exoribonuclease XRN1/4 (Luo et al., 2018). PBs are thought to be sites of mRNA decay and/or storage, although overall their function remains an enigma. In yeast and humans, the DHH1/DDX6 orthologs have been shown to associate with both PBs and SGs. In SGs, DHH1 interacts with the translational regulator PAB1-BINDING PROTEIN 1 (PBP1) and DDX6 interacts with Ataxin-2 (PBP1 ortholog) (Wilczynska et al., 2005; Nonhoff et al., 2007; Swisher and Parker, 2010). In PBs, on the other hand, DHH1 interacts with several 5'-to-3' mRNA decay factors (Hata et al., 1998; Coller et al., 2001; Fischer and Weis, 2002; Sheth and Parker, 2003), and regulates PB dynamics through its ATPase activity (Mugler et al., 2016). Similarly, DDX6 interacts with eIF4E and eIF4E-T in PBs (Andrei et al., 2005).

In the root basal meristem of *Arabidopsis* seedlings, we demonstrated that, while the majority of RH6, RH8, and RH12 are cytoplasmic, the proteins are also present in cytoplasmic foci that can be further induced by mild hypoxia under a coverslip. By use of cycloheximide to stall elongating ribosome on mRNAs, we confirmed that these foci are mRNP complexes, of which the formation is dependent on mRNA substrates that disengage from translating ribosomes. The localization of RH6, RH8, and RH12 in mRNP complexes is supported by the presence of intrinsically disordered regions (IDRs) in their N-terminal extensions, that generally drive mRNP assembly. Unlike RH6, RH8, and RH12, yeast DHH1 lacks an N-terminal IDRs but this is replaced by the C-terminal extension. A recent study showed that the C-terminal DIRs of DHH1 are not sufficient for the protein to form macromolecular complexes and losing these regions does not affect the formation of granules (Protter et al., 2018). It is yet to be determined whether the N-

terminal IDRs of RH6, RH8, and RH12 participate in the formation of these macromolecular complexes.

Similar to what observed in yeast and humans, our colocalization analysis of RH6, RH8, and RH12 foci with the PB markers DCP2, and VCS as well as the SG marker UBP1C revealed that all the three RHs are localized to both type of mRNPs. Corroborated with our results, a recent study showed that all RH6, RH8, and RH12 form complexes with the NMD factor UP-FRAMESHIFT 1 (UPF1), along with other decapping factors including DCP1, DCP5 and VCS, as well as the eukaryotic translation initiation factor eIF4G, ARGONAUTE 1, and several POLY(A) BINDING PROTEINs (PABPs) (Chicois et al., 2018). Associations of RH6, RH8, and RH12 with UPF1 occur in an RNA-independent manner. Additionally, this study showed that, in addition to UPF1, all the three RHs directly associate with the translational repressor and decapping activator DCP5. Collectively, these data confirm that RH6, RH8, and RH12 are components of the mRNA decay machinery. The overlap of RH6, RH8, and RH12 foci with UBP1C SGs suggests that the RHs might also function in translationally repressed mRNPs that involve in mRNA storage, or a hybrid mRNP that mediates the transition of mRNA from storage to decay. This is supported by the presence of eIF4G and several PABPs, which typically bind intact non-degraded mRNAs, in the UPF1-RH6/8/12 complexes (Chicois et al., 2018). Moreover, the role of UPF1 in translation repression without affecting mRNA stability has been demonstrated for *EIN3-BINDING F BOX PROTEIN 1* (*EBF1*) and *EBF2* transcripts during ethylene signaling (Li et al., 2015; Merchante et al., 2015)

Finally, our evaluation of DCP2, VCS, and UBP1C localization in the triple *rh6 rh8 rh12* mutant indicates that not only do RH6, RH8 and RH12 associate with DCP2 and VCS complexes, but they also play a crucial role in DCP2 and VCS granule

formation. At this point it is unclear how the RHs contribute to this process, and whether they are required for PB nucleation or the complex stability. Future work can address these question by probing the dynamics of individual complexes over time upon the induction. Nevertheless, our results show that the impairment in PB formation is not due to pleiotropic effects, as a result of severe developmental defects in the triple *rh6 rh8 rh12,* since the formation of UBP1C-SG complexes is unaffected. As such, we conclude that the *Arabidopsis* DHH1/DDX6-like RHs are indispensable for PB but not SG formation. The role of DHH1/DDX6 proteins in PB assembly and dynamics has been demonstrated in other organisms. Depletion of DDX6 in HeLa cells causes strong reduction of arsenite-induced DCP1 bodies, but does not affect eIF3 bodies, which are considered SGs (Serman et al., 2007). In another case, mutation of DDX6 in HeLa cells prevents the formation of Ge-1 (human VCS ortholog) complexes (Minshall et al., 2009). Notably, the role of DDX6 in PB formation is coupled with translational repression as DDX6 forms complexes with the translational repressor 4E-Transporter (4E-T), and DDX6-4E-T interaction is required for *de novo* PB assembly (Ayache et al., 2015; Kamenska et al., 2016). Intriguingly, point mutations in the yeast DDH1 that inhibits its ATPase activity or interaction with the CCR4-NOT deadenylation complex cause constitutive PB formation (Mugler et al., 2016).

The findings of this chapter lead to key questions: (1) Do the functionally redundant RH6/8/12 proteins of *Arabidopsis* target the turnover of specific mRNAs? (2) Are RH6/8/12 involved in translation-coupled turnover of RNAs? These two questions were addressed in Chapter 3 of this dissertation.

2.5 MATERIALS and METHODS

2.5.1 Database search and *in silico* sequence analysis

Evolutionary analysis of DEAD-box RNA helicases was conducted in MEGA7 (Kumar et al., 2016). Amino acid sequences of DEAD-box RNA helicases from yeast (*Saccharomyces cerevisiae*), roundworm (*Caenorhabditis elegans*), fruit fly (*Drosophila melanogaster*), and human (*Homo sapiens*), were downloaded from Saccharomyces Genome Database (https://www.yeastgenome.org/), WormBase (https://parasite.wormbase.org/index.html), FlyBase (http://flybase.org/), and GeneCards Human Database (http://www.genecards.org/), respectively. Amino acid sequences of DEAD-box proteins from rice (*Oryza sativa*), maize (*Zea mays*), *Arabidopsis* (*Arabidopsis thaliana*), soybean (*Glycine max*), and tomato (*Solanum lycopersicum*) were retrieved from MSU Rice Genome Annotation Project (RGAP7; http://rice.plantbiology.msu.edu/index.shtml), Maize Genetics and Genomics database (B73 Reference Version 4.0; https://www.maizegdb.org/gbrowse/maize_v4), The Arabidopsis Information Resource (TAIR10; https://www.arabidopsis.org/), SoyBase (JGI Wm82.a1; https://soybase.org/search/index.php), and Sol Genomics Network (ITAG3.20; https://solgenomics.net/), respectively. A total of 427 full-length DEAD-box protein sequences collected were aligned using the MUSCLE function in the MEGA7 software (Edgar, 2004). Only 383 sequences (22 from yeast, 30 roundworm, 27 fruit fly, 33 human, 47 *Arabidopsis*, 47 rice, 52 maize, 83 soybean, 42 tomato) with the canonical "DEAD" motif were used for phylogenetic analysis. The evolutionary history was inferred by using the Maximum Likelihood method following the Le_Gascuel_2008 model with 1000 bootstrap replicates (Le and Gascuel, 2008). Initial tree(s) for the heuristic search were obtained by applying Neighbor-Join and BioNJ algorithms to a matrix of pairwise

distances estimated using Jones-Taylor-Thorton (JTT) model (Jones et al., 1992). A discrete Gamma distribution was used to model evolutionary rate differences among sites (5 categories (+G, parameter = 1.1984)). All positions with less than 95% site coverage were eliminated. That is, fewer than 5% alignment gaps, missing data, and ambiguous bases were allowed at any position. There was a total of 349 positions in the final dataset. The tree was visualized and drawn using the Interactive Tree Of Life (iTOL) software (Letunic and Bork, 2016).

Putative DHH1 orthologs from fungi were identified using the orthoDB database (Zdobnov et al., 2017), and their corresponding amino acid sequences were downloaded from UniProt database (https://www.uniprot.org/). Amino acid sequences of DDX6 orthologs from vertebrates were downloaded from the Emsembl genome browser (http://uswest.ensembl.org/index.html). Amino acid sequences of DHH1/DDX6-like proteins from green algae and land plants were obtained from the Phytozome database (https://phytozome.jgi.doe.gov/pz/portal.html) following a BLASTP search of the yeast DHH1 sequence. Amino acid sequences of DHH1/DDX6-like proteins from the yeast *Saccharomyces cerevisiae*, roundworm, fruit fly, human, rice, maize, *Arabidopsis*, soybean, and tomato were as identified in the above phylogenetic analysis of DEAD-box RNA helicase. Two soybean sequences, Glyma08g26950.1 and Glyma17g27250.1, were excluded due to the lack the N-terminal region and the incomplete core helicase domain. In total, full-length amino acid sequences of 58 representative DHH1/DDX6-like proteins from fungi (12), animals (14), green algae (5), and land plants (27) were aligned using the MUSCLE algorithm in MEGA7. The alignment was used to infer evolutionary relationship of the proteins using the same methods and parameters as in the analysis of the DEAD-box RNA helicases, with a total of 403 positions in the final dataset.

2.5.2 Genetic material and growth conditions

The plant material used in this study include wild-type *Arabidopsis thaliana* ecotype Columbia-0 (Col-0) and T-DNA insertion mutants *rh6-1* (Sail_111_H08), *rh8-1* (Salk_016830C), and *rh12-2* (Salk_016921C), *dcp2-1* (Salk_000519), and *vcs-7* (Salk_032031). The T-DNA insertion lines were all in Col-0 background, and obtained from the *Arabidopsis* Biological Resource Center (ABRC), and have been described previously (Goeres et al., 2007; Sorenson, 2012). Genotyping primers used are listed in **Table 2.1**. The homozygous double *rh6 rh8*, *rh6 rh12* and *rh8 rh12*, and triple *rh6 rh8 rh12* mutant combination lines were generated by Dr. Reed Sorenson through crossing of the *rh6-1*, *rh8-1* and *rh12-2* alleles. *proDCP2:DCP2-GFP* in *dcp2-1* was kindly provided by Dr. Yuichiro Watanabe (Motomura et al., 2015). *proVCS:VCS-GFP* in Col-0 was a gift from Dr. Leslie Sieburth (Roux et al., 2015). *pro35S:UBP1C-GFP* in *ubp1c-1* was previously described (Sorenson and Bailey-Serres, 2014). Seeds were surface-sterilized by incubation in 70% (v/v) ethanol for 5 minutes, 20 % (v/v) household bleach plus 0.01 % (v/v) Tween-20 for 5 minutes, and rinsed 5 times with sterile water. Seeds were plated on sterile solid Murashige and Skoog (MS) medium containing 0.5x MS salts (Caisson Laboratories), 0.5 % (w/v) Sucrose, 0.4 % (w/v) Phytagel (Sigma-Aldrich) [pH 5.7-5.8], followed by stratification at 4^{o}C in complete darkness for 2 days before vertically grown in a growth chamber under a 16-hour light and 8-hour dark cycle (long-day) at constant 23°C. 7-day-old seedlings were transferred to soil containing Sunshine LC1 soil mix (JM McConkey) with 1.87 g/L Marathon insecticide (Crop Production Services, Riverside, California) and 1.4 g/ L osmocote 14-14-14 fertilizer, and grown in a growth room under long-day conditions. Alternatively, seeds were directly sown in soil, and stratified at 4^{o}C in the dark for 2 days before transferred to a growth room and grown

under the same conditions. Plants were imaged using a Canon camera (Canon USA). Images were processed using Fiji software (Schindelin et al., 2012). Primary root lengths were measured from photographic images using Fiji software.

2.5.3 RNA isolation, RT-PCR, and quantitative RT-PCR

Total RNA was extracted from indicated tissues using TRIzol™ reagent (Invitrogen), and purified using the Direct-zol™ RNA MiniPrep (Zymo Research) according to the manufacturer's instructions. Total RNA was treated with DNase I (New England Biolabs), and cDNAs were prepared from 2 µg of DNase-free total RNA using an oligo(dT) primer or gene-specific/stem-loop primers (Integrated DNA Technologies) and Maxima Reverse Transcriptase (Thermo Fisher Scientific) following the manufacturer's instructions. End-point PCR was performed using 3 µL of 5x diluted cDNA solution with Taq DNA polymerase (G-Biosciences) and the appropriate primers (**Table 2.1**) according to the manufacturer's instructions. PCR was conducted in a thermocycler with an initial step at 94°C for 3 minutes followed by 30 cycles at 94°C for 30 seconds, at ~Tm-3 for 30 seconds, and at 72°C for 1 kb/minutes. *UBIQUITIN 10* (At4g05320) was used as an internal control. RT-PCR fragments were analyzed using 2% agarose Tris-acetate (TAE, 40 mM Tris, 20 mM acetate, 1 mM EDTA, pH 8.0) gels and ethidium bromide staining followed by visualization under UV irradiation. For RT-qPCR analysis, amplification was performed in technical duplicate in the CFX Connect™ Real-Time PCR Detection System (Bio-Rad Laboratories) using 2 µL of 5× diluted cDNA. Real-time PCR was performed using iQ™ SYBR® Green Supermix (Bio-Rad Laboratories) in a 15-µL reaction volume with 0.67 µm of each primer (**Table 2.1**). The program for running qPCR was initiated at 95°C for 3 minutes followed by 40 cycles at 95°C for 15 seconds, at Tm for 15 seconds, and at 72°C for 15 seconds. *PP2AA2*

(At3g25800) fragments were amplified as a reference. Relative transcript fold-change was calculated by the ΔΔCt method (Pfaffl, 2001).

2.5.4 Plasmid construction and complementation of the triple *rh6 rh8 rh12* mutant

A 3.3 kb *RH6* genomic fragment, spanning the upstream intergenic (promoter, 836 bp upstream of the start codon) region and gene transcript sequence without the stop codon, was amplified from of Col-0 wild-type genomic DNA using the primer pair proRH6-F (5'CAC CTT TCT CTC TTT CTT TCG GAT GTT A-3') and RH6(-stop)-R (5'-CTG ACA GTA GAT TGC CTT GT-3') and introduced into pENTR/D-TOPO (Invitrogen) to generate a genomic *RH6* entry clone. The DNA fragment was then introduced into the gateway-FH-OCST (*nptII*) T-DNA vector (Mustroph et al., 2009) to generate C-terminally FLAG tagged RH6 under its native promoter (*gRH6-FLAG*) via LR reaction. The construct was transformed into *Agrobacterium tumefaciens* strain GV3101 and then transformed into *rh6 rh8 rh12*$^{(+/-)}$ plants by the floral dip method (Clough and Bent, 1998). Transgenic T1 and T2 seeds were selected on 0.5x MS medium supplemented with 50 μg/mL kanamycin. The selected homozygous *gRH6-FLAG* plants were then subjected to genotyping for the homozygous *rh12-2* allele.

2.5.5 Generation of transgenic plants and crossing

An artificial miRNA targeting *RH6* transcripts was designed using the WMD3-Web MicroRNA Designer (Ossowski et al., 2008). The 404-bp *MIR319a* precursor was engineered by replacing the original miR319a with the artificial sequence targeting *RH6* (amiRH6, 5'-TTA ATA TTG GGT AAC ACC CAG-3'), and the miR319a* with amiRH6* (5'-CTA GGT GTT ACC CTA TAT TAT-3'). The engineered *MIR319a-amiRH6* precursor

with the *att*B1 and *att*B2 flanking sequences was synthesized and placed in the pIDTSMART-AMP vector (Integrated DNA Technologies). The *MIR319a-amiRH6* sequence was transferred by *in vitro* recombination into pDONR-zeo using BP clonase (Invitrogen), and then further transferred into the pMDC32 binary vector (Curtis and Grossniklaus, 2003) using LR clonase (Invitrogen). The resulting *pro35S:amiRH6* construct was introduced into the double *rh8 rh12* mutant via *Agrobacterium tumefaciens* GV3101 using the floral dip method (Clough and Bent, 1998). T1 and T2 seeds were selected on 0.5x MS medium supplemented with 0.5% (w/v) sucrose and 50 µg/mL Hygromycin B (Sigma).

A 5.0 kb fragment of *RH8* genomic region (including 2.2 kb upstream of the start codon and the gene body without the stop codon) was amplified from of Col-0 wild-type genomic DNA using the primer pair proRH8-F (5'-ggg gac aag ttt gta caa aaa agc agg ctC TCT ACG GCG ATT GAT CTA AGC-3') and RH8(-stop)-R (5'-ggg gac cac ttt gta caa gaa agc tgg gtA TTG GCA ATA AAT TGC CTG ATC G-3') and introduced into pDONR-zeo vector (Invitrogen) to generate a genomic *RH8* entry clone. Similarly, a 3.5 kb RH12 genomic region spanning 992 bp upstream of the start codon and the genic region without the stop codon was amplified from of Col-0 wild-type genomic DNA using the primer pair proRH12-F (5'CAC CTC AAG GTT TGT TTT GCC ATC A-3') and RH12(-stop)-R (5'-ATC GAT CAA GCA ATC TAC TGT CAG-3') and introduced into pENTR/D-TOPO (Invitrogen) to generate a genomic *RH12* entry clone. To generate transgenic lines expressing fluorescently tagged RH6, RH8, RH12 under their native promoters, genomic entry clones of *RH6* (as generated for the complementation of *rh6 rh8 rh12* mutant), *RH8*, and *RH12* were transferred into the pGWB653 gateway vector (Nakagawa et al., 2007) by *in vitro* recombination using LR clonase (Invitrogen) to

generate *proRH6:RH6-RFP*, *proRH8:RH8-RFP*, and *proRH12:RH12-RFP* constructs. Additionally, the genomic entry clone of *RH12* was transferred into pGWB643 to generate the *proRH12:RH12-CFP* construct. All fusions were verified by sequencing before introduced into *Agrobacterium tumefaciens* strain GV3101 and then transformed into different *Arabidopsis* genotypes using the floral dip method: *proRH6:RH6-RFP* was transformed into Col-0 wild-type; *proRH8:RH8-RFP* was transformed into *rh8-1*; *proRH12:RH12-RFP* was transformed into *rh12-2*. Transgenic T1 seeds were harvested after 1 month and selected on 0.5x MS medium supplemented with 0.5% sucrose and 10 µg/mL ammonium glufosinate (Basta, Sigma).

Transgenic *Arabidopsis* lines coexpressing individual RFP-tagged RHs and DCP2-GFP were generated by transformation of *proRH6:RH6-RFP*, *proRH8:RH8-RFP*, and *proRH12:RH12-RFP* constructs into the *proDCP2:DCP2-GFP* genotype. Transgenic lines coexpressing RH6-RFP and VCS-GFP as well as RH12-RFP and VCS-GFP were generated by crossing of T2 *proRH6:RH6-RFP* and *proRH12:RH12-RFP* lines with the *proVCS:VCS-GFP* genotype, whereas transgenic lines coexpressing RH8-RFP and VCS-GFP were generated by transformation of *proRH8:RH8-RFP* construct into the *proVCS:VCS-GFP* genotype. Transgenic lines coexpressing RH6-RFP and UBP1C-GFP as well as RH12-RFP and UBP1C-GFP were generated by crossing of T2 *proRH6:RH6-RFP* and *proRH12:RH12-RFP* lines with the *pro35S:UBP1C-GFP* genotype, whereas transgenic lines coexpressing RH8-RFP and UBP1C-GFP were generated by transformation of *proRH8:RH8-RFP* construct into the *pro35S:UBP1C-GFP* genotype. Generation of *rh6 rh8 rh12; proDCP2:DCP2-GFP*, *rh6 rh8 rh12; proVCS:VCS-GFP*, and *rh6 rh8 rh12; pro35S:UBP1C-GFP* genotypes was performed by crossing of

proDCP2:DCP2-GFP, *proVCS:VCS-GFP*, and *pro35S:UBP1C-GFP* genotypes with *rh6*$^{(+/-)}$ *rh8 rh12* plants.

2.5.6 Confocal microscopy

Confocal microscopy images were collected using a Leica SP5 laser scanning confocal microscope (Leica Microsystems) and processed with Fiji software (Schindelin et al., 2012). Subcellular localization of fluorescent tagged proteins in transgenic *Arabidopsis* was performed in 4-day-old seedlings grown in a vertical position on solid 0.5x MS medium supplemented with 0.5% (w/v) sucrose. RH6-RFP, RH8-RFP and RH12-RFP fusion proteins within the root tissues were imaged using a 543 nm excitation wavelength with 25% Ar laser power, and RFP emission was collected at 608-672 nm. Visualization of the nucleus was accomplished by counter-staining of the root with 1 µg/mL 4',6-diamidino-2-phenylindole (DAPI). For DAPI fluorescence detection, excitation light was provided by a 405 nm laser line at 5% power, and 440-540 nm fluorescent light was collected as DAPI signal. Cycloheximide treatment was performed by transfer of seedlings into a 1.5 mL tube containing 1 mL of 200 ng/µl cycloheximide or 0.001% (v/v) DMSO (for mock control treatment) and application of vacuum infiltration for 3 minutes. Visualization of protein localization under a microscope was performed within minutes after infiltration. All colocalization experiments were performed using a sequential scan mode, beginning with the detection of protein with longer excitation wavelength. Colocalization analysis of RH6-RFP and RH12-CFP was performed with excitation of RFP and CFP by 543 and 458 nm laser lines at 20% power, and collection of fluorescent emission at 608-672 nm and 465-538, respectively. Colocalization analysis between RFP and GFP fusion proteins was performed using 543 nm and 488 nm laser lines at

20% power for RFP and GFP excitation, respectively. RFP and GFP emissions were collected at 577-672 nm and 494-541 nm, respectively. For comparison of DCP2-GFP, VCS-GFP, and UBP1C-GFP localization in the triple mutant *rh6 rh8 rh12* and the wild-type, germination of *rh6 rh8 rh12* seeds was started 12 hours before those of the wild-type to compensate for their overall delayed germination. For GFP detection, a 488 nm laser at 20-35% power was used for excitation. GFP emission was captured at 494-541 nm.

2.5.7 Statistical analysis

Statistical analysis was performed in R software using *agricolae* package (De Mendiburu and Simon, 2015).

2.6 ACKNOWLEDGEMENTS

The *rh6 rh8*, *rh6 rh12* and *rh8 rh12*, and *rh6 rh8 rh12* genotypes were generated by Reed Sorenson. We thank Dr. Yuichiro Watanabe and Dr. Leslie Sieburth for kindly providing the *proDCP2:DCP2-GFP* and *proVCS:VCS-GFP* lines, respectively. This work was supported by the United States National Science Foundation grant no. MCB-1716913 to J.B.-S. and a Royal Thai Government's Development and Promotion of Science and Technology Talents Project scholarship to T.C.

2.7 REFERENCES

Akao Y, Marukawa O, Morikawa H, Nakao K, Kamei M, Hachiya T, Tsujimoto Y (1995) The rck/p54 Candidate Proto-oncogene Product Is a 54-Kilodalton D-E-A-D Box Protein Differentially Expressed in Human and Mouse Tissues. Cancer Res **55**: 3444–3449

Andrei MA, Ingelfinger D, Heintzmann R, Achsel T, Rivera-Pomar R, Lührmann R (2005) A role for eIF4E and eIF4E-transporter in targeting mRNPs to mammalian processing bodies. RNA **11**: 717–727

Andreou AZ, Klostermeier D (2013) The DEAD-box helicase eIF4A: paradigm or the odd one out? RNA Biol **10**: 19–32

Ayache J, Bénard M, Ernoult-Lange M, Minshall N, Standart N, Kress M, Weil D (2015) P-body assembly requires DDX6 repression complexes rather than decay or Ataxin2/2L complexes. Mol Biol Cell **26**: 2579–2595

Baek W, Lim CW, Lee SC (2018) A DEAD-box RNA helicase, RH8, is critical for regulation of ABA signalling and the drought stress response via inhibition of PP2CA activity. Plant Cell Environ **41**: 1593–1604

Barbee SA, Estes PS, Cziko A-M, Hillebrand J, Luedeman RA, Coller JM, Johnson N, Howlett IC, Geng C, Ueda R, et al (2006) Staufen- and FMRP-Containing Neuronal RNPs Are Structurally and Functionally Related to Somatic P Bodies. Neuron **52**: 997–1009

Boag PR, Atalay A, Robida S, Reinke V, Blackwell TK (2008) Protection of specific maternal messenger RNAs by the P body protein CGH-1 (Dhh1/RCK) during Caenorhabditis elegans oogenesis. J Cell Biol **182**: 543–557

Boeynaems S, Alberti S, Fawzi NL, Mittag T, Polymenidou M, Rousseau F, Schymkowitz J, Shorter J, Wolozin B, Van Den Bosch L, et al (2018) Protein Phase Separation: A New Phase in Cell Biology. Trends Cell Biol **28**: 420–435

Bourgeois CF, Mortreux F, Auboeuf D (2016) The multiple functions of RNA helicases as drivers and regulators of gene expression. Nat Rev Mol Cell Biol. doi: 10.1038/nrm.2016.50

Buchan JR, Muhlrad D, Parker R (2008) P bodies promote stress granule assembly in Saccharomyces cerevisiae. J Cell Biol **183**: 441–455

Cai J, Meng X, Li G, Dong T, Sun J, Xu T, Li Z, Han Y, Zhu M (2018) Identification, expression analysis, and function evaluation of 42 tomato DEAD-box RNA helicase genes in growth development and stress response. Acta Physiol Plant **40**: 94

Chicois C, Scheer H, Garcia S, Zuber H, Mutterer J, Chicher J, Hammann P, Gagliardi D, Garcia D (2018) The UPF1 interactome reveals interaction networks between RNA degradation and translation repression factors in Arabidopsis. Plant J.

doi: 10.1111/tpj.14022

Clough SJ, Bent AF (1998) Floral dip: a simplified method forAgrobacterium-mediated transformation ofArabidopsis thaliana: Floral dip transformation of Arabidopsis. Plant J **16**: 735–743

Coller JM, Tucker M, Sheth U, Valencia-Sanchez MA, Parker R (2001) The DEAD box helicase, Dhh1p, functions in mRNA decapping and interacts with both the decapping and deadenylase complexes. RNA **7**: 1717–1727

Coller J, Parker R (2005) General Translational Repression by Activators of mRNA Decapping. Cell **122**: 875–886

Cordin O, Banroques J, Tanner NK, Linder P (2006) The DEAD-box protein family of RNA helicases. Gene **367**: 17–37

Curtis MD, Grossniklaus U (2003) A gateway cloning vector set for high-throughput functional analysis of genes in planta. Plant Physiol **133**: 462–469

Decker CJ, Parker R (2012) P-bodies and stress granules: possible roles in the control of translation and mRNA degradation. Cold Spring Harb Perspect Biol **4**: a012286

De Mendiburu F, Simon R (2015) Agricolae - Ten years of an open source statistical tool for experiments in breeding, agriculture and biology. doi: 10.7287/peerj.preprints.1404v1

Edgar RC (2004) MUSCLE: a multiple sequence alignment method with reduced time and space complexity. BMC Bioinformatics **5**: 113

Ernoult-Lange M, Baconnais S, Harper M, Minshall N, Souquere S, Boudier T, Bénard M, Andrey P, Pierron G, Kress M, et al (2012) Multiple binding of repressed mRNAs by the P-body protein Rck/p54. RNA **18**: 1702–1715

Fairman-Williams ME, Guenther U-P, Jankowsky E (2010) SF1 and SF2 helicases: family matters. Curr Opin Struct Biol **20**: 313–324

Fischer N, Weis K (2002) The DEAD box protein Dhh1 stimulates the decapping enzyme Dcp1. EMBO J **21**: 2788–2797

Goeres DC, Van Norman JM, Zhang W, Fauver NA, Spencer ML, Sieburth LE (2007) Components of the Arabidopsis mRNA decapping complex are required for early seedling development. Plant Cell **19**: 1549–1564

Gross T, Siepmann A, Sturm D, Windgassen M, Scarcelli JJ, Seedorf M, Cole CN, Krebber H (2007) The DEAD-box RNA helicase Dbp5 functions in translation termination. Science **315**: 646–649

Haimovich G, Medina DA, Causse SZ, Garber M, Millán-Zambrano G, Barkai O, Chávez S, Pérez-Ortín JE, Darzacq X, Choder M (2013) Gene expression is circular: factors for mRNA degradation also foster mRNA synthesis. Cell **153**: 1000–

1011

Hata H, Mitsui H, Liu H, Bai Y, Denis CL, Shimizu Y, Sakai A (1998) Dhh1p, a Putative RNA Helicase, Associates with the General Transcription Factors Pop2p and Ccr4p from Saccharomyces cerevisiae. Genetics **148**: 571–579

Hillebrand J, Pan K, Kokaram A, Barbee S, Parker R, Ramaswami M (2010) The Me31B DEAD-Box Helicase Localizes to Postsynaptic Foci and Regulates Expression of a CaMKII Reporter mRNA in Dendrites of Drosophila Olfactory Projection Neurons. Front Neural Circuits **4**: 121

Huang J-H, Ku W-C, Chen Y-C, Chang Y-L, Chu C-Y (2017) Dual mechanisms regulate the nucleocytoplasmic localization of human DDX6. Sci Rep **7**: 42853

Jangra RK, Yi M, Lemon SM (2010) DDX6 (Rck/p54) Is Required for Efficient Hepatitis C Virus Replication but Not for Internal Ribosome Entry Site-Directed Translation. J Virol **84**: 6810–6824

Jones DT, Taylor WR, Thornton JM (1992) The rapid generation of mutation data matrices from protein sequences. Comput Appl Biosci **8**: 275–282

Kadaré G, Haenni AL (1997) Virus-encoded RNA helicases. J Virol **71**: 2583–2590

Kamenska A, Simpson C, Vindry C, Broomhead H, Bénard M, Ernoult-Lange M, Lee BP, Harries LW, Weil D, Standart N (2016) The DDX6-4E-T interaction mediates translational repression and P-body assembly. Nucleic Acids Res **44**: 6318–6334

Kawahara C, Yokota S, Fujita H (2014) DDX6 localizes to nuage structures and the annulus of mammalian spermatogenic cells. Histochem Cell Biol **141**: 111–121

Klepikova AV, Kasianov AS, Gerasimov ES, Logacheva MD, Penin AA (2016) A high resolution map of the Arabidopsis thaliana developmental transcriptome based on RNA-seq profiling. Plant J **88**: 1058–1070

Klepikova AV, Logacheva MD, Dmitriev SE, Penin AA (2015) RNA-seq analysis of an apical meristem time series reveals a critical point in Arabidopsis thaliana flower initiation. BMC Genomics **16**: 466

Kroschwald S, Maharana S, Mateju D, Malinovska L, Nüske E, Poser I, Richter D, Alberti S (2015) Promiscuous interactions and protein disaggregases determine the material state of stress-inducible RNP granules. Elife **4**: e06807

Kruk JA, Dutta A, Fu J, Gilmour DS, Reese JC (2011) The multifunctional Ccr4-Not complex directly promotes transcription elongation. Genes Dev **25**: 581–593

Kumar S, Stecher G, Tamura K (2016) MEGA7: Molecular Evolutionary Genetics Analysis Version 7.0 for Bigger Datasets. Mol Biol Evol **33**: 1870–1874

Ladomery M, Wade E, Sommerville J (1997) Xp54, the Xenopus Homologue of Human RNA Helicase p54, is an Integral Component of Stored mRNP Particles in Oocytes. Nucleic Acids Res **25**: 965–973

Le SQ, Gascuel O (2008) An improved general amino acid replacement matrix. Mol Biol Evol **25**: 1307–1320

Letunic I, Bork P (2016) Interactive tree of life (iTOL) v3: an online tool for the display and annotation of phylogenetic and other trees. Nucleic Acids Res **44**: W242–5

Linder P, Fuller-Pace FV (2013) Looking back on the birth of DEAD-box RNA helicases. Biochimica et Biophysica Acta (BBA) - Gene Regulatory Mechanisms **1829**: 750–755

Linder P, Jankowsky E (2011) From unwinding to clamping — the DEAD box RNA helicase family. Nat Rev Mol Cell Biol **12**: 505–516

Lin F, Wang R, Shen J-J, Wang X, Gao P, Dong K, Zhang H-Z (2008) Knockdown of RCK/p54 expression by RNAi inhibits proliferation of human colorectal cancer cells in vitro and in vivo. Cancer Biol Ther **7**: 1669–1676

Li W, Ma M, Feng Y, Li H, Wang Y, Ma Y, Li M, An F, Guo H (2015) EIN2-Directed Translational Regulation of Ethylene Signaling in Arabidopsis. Cell **163**: 670–683

Lokdarshi A, Conner WC, McClintock C, Li T, Roberts D (2015) *Arabidopsis* CML38, a calcium sensor that localizes to ribonucleoprotein complexes under hypoxia stress. Plant Physiol **170**: 01407.2015

Luo Y, Na Z, Slavoff SA (2018) P-Bodies: Composition, Properties, and Functions. Biochemistry **57**: 2424–2431

Mathys H, Basquin J, Ozgur S, Czarnocki-Cieciura M, Bonneau F, Aartse A, Dziembowski A, Nowotny M, Conti E, Filipowicz W (2014) Structural and biochemical insights to the role of the CCR4-NOT complex and DDX6 ATPase in microRNA repression. Mol Cell **54**: 751–765

Merchante C, Brumos J, Yun J, Hu Q, Spencer KR, Enríquez P, Binder BM, Heber S, Stepanova AN, Alonso JM (2015) Gene-Specific Translation Regulation Mediated by the Hormone-Signaling Molecule EIN2. Cell **163**: 684–697

Minshall N, Kress M, Weil D, Standart N (2009) Role of p54 RNA Helicase Activity and Its C-terminal Domain in Translational Repression, P-body Localization and Assembly. Mol Biol Cell **20**: 2464–2472

Minshall N, Standart N (2004) The active form of Xp54 RNA helicase in translational repression is an RNA-mediated oligomer. Nucleic Acids Res **32**: 1325–1334

Minshall N, Thom G, Standart N (2001) A conserved role of a DEAD box helicase in mRNA masking. RNA **7**: 1728–1742

Molliex A, Temirov J, Lee J, Coughlin M, Kanagaraj AP, Kim HJ, Mittag T, Taylor JP (2015) Phase separation by low complexity domains promotes stress granule assembly and drives pathological fibrillization. Cell **163**: 123–133

Motomura K, Le QTN, Hamada T, Kutsuna N, Mano S, Nishimura M, Watanabe Y (2015) Diffuse Decapping Enzyme DCP2 Accumulates in DCP1 Foci Under Heat Stress in Arabidopsis thaliana. Plant Cell Physiol **56**: 107–115

Mück F, Bracharz S, Marschalek R (2016) DDX6 transfers P-TEFb kinase to the AF4/AF4N (AFF1) super elongation complex. Am J Blood Res **6**: 28–45

Mugler CF, Hondele M, Heinrich S, Sachdev R, Vallotton P, Koek AY, Chan LY, Weis K (2016) ATPase activity of the DEAD-box protein Dhh1 controls processing body formation. Elife **5**: e18746

Mustroph A, Zanetti ME, Jang CJH, Holtan HE, Repetti PP, Galbraith DW, Girke T, Bailey-Serres J (2009) Profiling translatomes of discrete cell populations resolves altered cellular priorities during hypoxia in Arabidopsis. Proceedings of the National Academy of Sciences **106**: 18843–18848

Nakabayashi K, Okamoto M, Koshiba T, Kamiya Y, Nambara E (2005) Genome-wide profiling of stored mRNA in Arabidopsis thaliana seed germination: epigenetic and genetic regulation of transcription in seed. Plant J **41**: 697–709

Nakagawa T, Suzuki T, Murata S, Nakamura S, Hino T, Maeo K, Tabata R, Kawai T, Tanaka K, Niwa Y, et al (2007) Improved Gateway Binary Vectors: High-Performance Vectors for Creation of Fusion Constructs in Transgenic Analysis of Plants. Biosci Biotechnol Biochem **71**: 2095–2100

Nakamura A, Amikura R, Hanyu K, Kobayashi S (2001) Me31B silences translation of oocyte-localizing RNAs through the formation of cytoplasmic RNP complex during Drosophila oogenesis. Development **128**: 3233–3242

Navarro RE, Shim EY, Kohara Y, Singson A, Blackwell TK (2001) cgh-1, a conserved predicted RNA helicase required for gametogenesis and protection from physiological germline apoptosis in C. elegans. Development **128**: 3221–3232

Noble SL, Allen BL, Goh LK, Nordick K, Evans TC (2008) Maternal mRNAs are regulated by diverse P body-related mRNP granules during early Caenorhabditis elegans development. J Cell Biol **182**: 559–572

Nonhoff U, Ralser M, Welzel F, Piccini I, Balzereit D, Yaspo M-L, Lehrach H, Krobitsch S (2007) Ataxin-2 interacts with the DEAD/H-box RNA helicase DDX6 and interferes with P-bodies and stress granules. Mol Biol Cell **18**: 1385–1396

Okamura M, Yamanaka Y, Shigemoto M, Kitadani Y, Kobayashi Y, Kambe T, Nagao M, Kobayashi I, Okumura K, Masuda S (2018) Depletion of mRNA export regulator DBP5/DDX19, GLE1 or IPPK that is a key enzyme for the production of IP6, resulting in differentially altered cytoplasmic mRNA expression and specific cell

defect. PLoS One **13**: e0197165

Ossowski S, Schwab R, Weigel D (2008) Gene silencing in plants using artificial microRNAs and other small RNAs: Engineering small RNA-mediated gene silencing. Plant J **53**: 674–690

Perea-Resa C, Hernández-Verdeja T, López-Cobollo R, Castellano M del M, Salinas J (2012) LSM Proteins Provide Accurate Splicing and Decay of Selected Transcripts to Ensure Normal Arabidopsis Development. Plant Cell **24**: 4930–4947

Pettersson OJ, Aagaard L, Andrejeva D, Thomsen R, Jensen TG, Damgaard CK (2014) DDX6 regulates sequestered nuclear CUG-expanded DMPK-mRNA in dystrophia myotonica type 1. Nucleic Acids Res **42**: 7186–7200

Pfaffl MW (2001) A new mathematical model for relative quantification in real-time RT-PCR. Nucleic Acids Res **29**: e45

Presnyak V, Coller J (2013) The DHH1/RCKp54 family of helicases: An ancient family of proteins that promote translational silencing. Biochimica et Biophysica Acta (BBA) - Gene Regulatory Mechanisms **1829**: 817–823

Protter DSW, Parker R (2016) Principles and Properties of Stress Granules. Trends Cell Biol **26**: 668–679

Protter DSW, Rao BS, Van Treeck B, Lin Y, Mizoue L, Rosen MK, Parker R (2018) Intrinsically Disordered Regions Can Contribute Promiscuous Interactions to RNP Granule Assembly. Cell Rep **22**: 1401–1412

Reed JC, Molter B, Geary CD, McNevin J, McElrath J, Giri S, Klein KC, Lingappa JR (2012) HIV-1 Gag co-opts a cellular complex containing DDX6, a helicase that facilitates capsid assembly. J Cell Biol **198**: 439–456

Roux ME, Rasmussen MW, Palma K, Lolle S, Regué ÀM, Bethke G, Glazebrook J, Zhang W, Sieburth L, Larsen MR, et al (2015) The mRNA decay factor PAT1 functions in a pathway including MAP kinase 4 and immune receptor SUMM2. EMBO J **34**: 593–608

Rouya C, Siddiqui N, Morita M, Duchaine TF, Fabian MR, Sonenberg N (2014) Human DDX6 effects miRNA-mediated gene silencing via direct binding to CNOT1. RNA **20**: 1398–1409

Schindelin J, Arganda-Carreras I, Frise E, Kaynig V, Longair M, Pietzsch T, Preibisch S, Rueden C, Saalfeld S, Schmid B, et al (2012) Fiji: an open-source platform for biological-image analysis. Nat Methods **9**: 676–682

Serman A, Le Roy F, Aigueperse C, Kress M, Dautry F, Weil D (2007) GW body disassembly triggered by siRNAs independently of their silencing activity. Nucleic Acids Res **35**: 4715–4727

Sheth U, Parker R (2003) Decapping and decay of messenger RNA occur in

cytoplasmic processing bodies. Science **300**: 805–808

Singleton MR, Dillingham MS, Wigley DB (2007) Structure and Mechanism of Helicases and Nucleic Acid Translocases. Annu Rev Biochem **76**: 23–50

Smillie DA, Sommerville J (2002) RNA helicase p54 (DDX6) is a shuttling protein involved in nuclear assembly of stored mRNP particles. J Cell Sci **115**: 395–407

Sorenson R, Bailey-Serres J (2014) Selective mRNA sequestration by OLIGOURIDYLATE-BINDING PROTEIN 1 contributes to translational control during hypoxia in Arabidopsis. Proceedings of the National Academy of Sciences **111**: 2373–2378

Sorenson RS (2012) Role of the RNA-Binding Protein UBP1C in Translational Repression During Hypoxia in Arabidopsis thaliana.

Standart N, Weil D (2018) P-Bodies: Cytosolic Droplets for Coordinated mRNA Storage. Trends Genet. doi: 10.1016/j.tig.2018.05.005

Swisher KD, Parker R (2010) Localization to, and effects of Pbp1, Pbp4, Lsm12, Dhh1, and Pab1 on stress granules in Saccharomyces cerevisiae. PLoS One **5**: e10006

Tran EJ, Zhou Y, Corbett AH, Wente SR (2007) The DEAD-box protein Dbp5 controls mRNA export by triggering specific RNA:protein remodeling events. Mol Cell **28**: 850–859

Tseng-Rogenski SS-I, Chong J-L, Thomas CB, Enomoto S, Berman J, Chang T-H (2003) Functional conservation of Dhh1p, a cytoplasmic DExD/H-box protein present in large complexes. Nucleic Acids Res **31**: 4995–5002

Wawer I, Golisz A, Sulkowska A, Kawa D, Kulik A, Kufel J (2018) mRNA Decapping and 5′-3′ Decay Contribute to the Regulation of ABA Signaling in Arabidopsis thaliana. doi: 10.3389/fpls.2018.00312

Weber C, Nover L, Fauth M (2008) Plant stress granules and mRNA processing bodies are distinct from heat stress granules. Plant J **56**: 517–530

Wilczynska A, Aigueperse C, Kress M, Dautry F, Weil D (2005) The translational regulator CPEB1 provides a link between dcp1 bodies and stress granules. J Cell Sci **118**: 981–992

Winter D, Vinegar B, Nahal H, Ammar R, Wilson GV, Provart NJ (2007) An "Electronic Fluorescent Pictograph" browser for exploring and analyzing large-scale biological data sets. PLoS One **2**: e718

Xu J, Chua N-H (2009) Arabidopsis decapping 5 is required for mRNA decapping, P-body formation, and translational repression during postembryonic development. Plant Cell **21**: 3270–3279

Xu J, Yang J-Y, Niu Q-W, Chua N-H (2006) Arabidopsis DCP2, DCP1, and VARICOSE

Form a Decapping Complex Required for Postembryonic Development. Plant Cell **18**: 3386–3398

Xu R, Zhang S, Huang J, Zheng C (2013a) Genome-Wide Comparative In Silico Analysis of the RNA Helicase Gene Family in Zea mays and Glycine max: A Comparison with Arabidopsis and Oryza sativa. PLoS One **8**: e78982

Xu R, Zhang S, Lu L, Cao H, Zheng C (2013b) A genome-wide analysis of the RNA helicase gene family in Solanum lycopersicum. Gene **513**: 128–140

Yoshida-Kashikawa M, Shibata N, Takechi K, Agata K (2007) DjCBC-1, a conserved DEAD box RNA helicase of the RCK/p54/Me31B family, is a component of RNA-protein complexes in planarian stem cells and neurons. Dev Dyn **236**: 3436–3450

Yu SF, Lujan P, Jackson DL, Emerman M, Linial ML (2011) The DEAD-box RNA Helicase DDX6 is Required for Efficient Encapsidation of a Retroviral Genome. PLoS Pathog **7**: e1002303

Zabolotskaya MV, Grima DP, Lin M-D, Chou T-B, Newbury SF (2008) The 5′–3′ exoribonuclease Pacman is required for normal male fertility and is dynamically localized in cytoplasmic particles in Drosophila testis cells. Biochem J **416**: 327

Zdobnov EM, Tegenfeldt F, Kuznetsov D, Waterhouse RM, Simão FA, Ioannidis P, Seppey M, Loetscher A, Kriventseva EV (2017) OrthoDB v9.1: cataloging evolutionary and functional annotations for animal, fungal, plant, archaeal, bacterial and viral orthologs. Nucleic Acids Res **45**: D744–D749

Figure 2.1. Phylogenetic analysis reveals conservation of the DHH1/DDX6 family of RNA helicases in plants. (A) Evolutionary analysis was performed on 383 canonical DEAD-box RNA Helicases from yeast (*Saccharomyces cerevisiae*), roundworm (*Caenorhabditis elegans*), fruit fly (*Drosophila melanogaster*), human (*Homo sapiens*), rice (*Oryza sativa*), maize (*Zea mays*), *Arabidopsis* (*Arabidopsis thaliana*), soybean (*Glycine max*), and tomato (*Solanum lycopersicum*). DEAD-box RNA helicases from yeast were as identified by Fairman-Williams et al. (Fairman-Williams et al., 2010) and Bourgeois et al. (Bourgeois et al., 2016), and the sequences were retrieved from *Saccharomyces* Genome Database (https://www.yeastgenome.org/). DEAD-box RNA helicases from roundworm, fruit fly and human were as identified by Bourgeois et al. (Bourgeois et al., 2016), and their sequences were downloaded from WormBase (https://parasite.wormbase.org/index.html), FlyBase (http://flybase.org/), and GeneCards Human Database (http://www.genecards.org/), respectively. DEAD-box proteins from rice, maize, *Arabidopsis* and soybean were as identified by Xu et al. (2013a)(Xu et al., 2013a), and their sequences were downloaded from MSU Rice Genome Annotation Project (RGAP7; http://rice.plantbiology.msu.edu/index.shtml), Maize Genetics and Genomics database (B73 Reference Version 4.0; https://www.maizegdb.org/gbrowse/maize_v4), The Arabidopsis Information Resource (TAIR10; https://www.arabidopsis.org/), and SoyBase (JGI Wm82.a1; https://soybase.org/search/index.php) databases, respectively. Sequences from tomato were as identified by (Xu et al., 2013b; Cai et al., 2018) and were obtained from Sol Genomics Network (ITAG3.20; https://solgenomics.net/). The sequences were aligned using the Muscle algorithm and the phylogenetic tree was generated with the Maximum Likelihood method with 1000 bootstrap replicates using Neighbor-Join and BioNJ algorithms in MEGA7 software (Kumar et al., 2016). Evolutionary rate differences among sites were modelled with a discrete Gamma distribution. The tree is drawn to scale, with branch lengths measured as the number of substitution per site. Black rectangular boxes on the tree branches represent bootstrap values greater than 50%, with the sizes of the boxes being proportional to the bootstrap values. Blue strip denotes the DHH1/DDX6-like clade, with its members from yeast and animals being presented by blue letters whereas members from plants presented by green letters. The sister clades of the DHH1/DDX6-like family include the eIF4A and DBP5/DDX19 families presented by pink and orange strips, respectively. (B) A zoom-in view of the DHH1/DDX6-like family presented in (A).

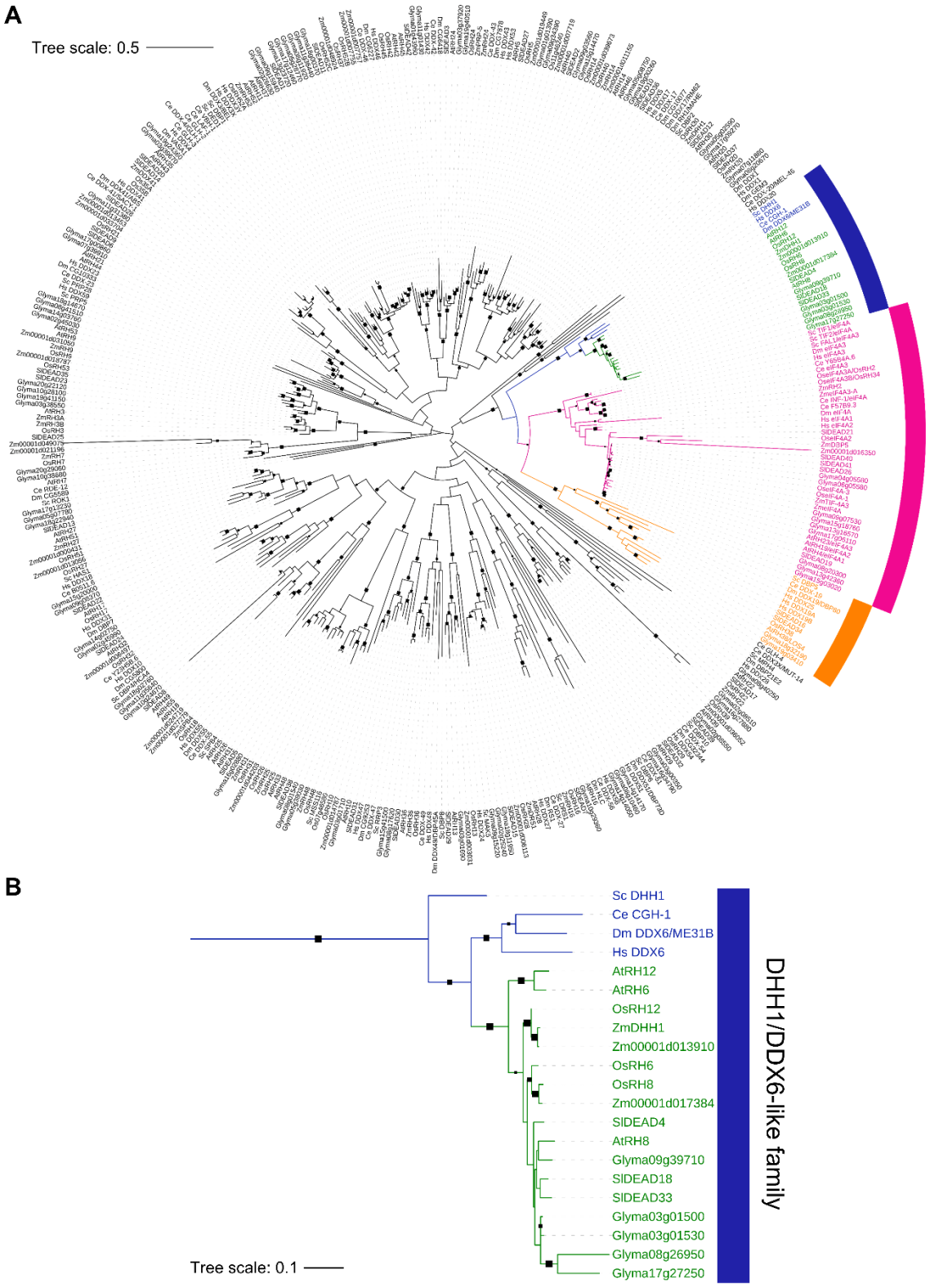
A
Tree scale: 0.5
B
Sc DHH1
Ce CGH-1
Dm DDX6/ME31B
Hs DDX6
AtRH12
AtRH6
OsRH12
ZmDHH1
Zm00001d013910
OsRH6
OsRH8
Zm00001d017384
SlDEAD4
AtRH8
Glyma09g39710
SlDEAD18
SlDEAD33
Glyma03g01500
Glyma03g01530
Glyma08g26950
Glyma17g27250
DHH1/DDX6-like family
Tree scale: 0.1

Figure 2.2. Phylogenetic relationship and schematic representation of primary sequence structure of eukaryotic DHH1/DDX6-like DEAD-box RNA helicases. Evolutionary history was inferred from 58 representative DHH1/DDX6-like helicases across different eukaryotic lineages. Amino acid sequences of their representative isoforms were obtained from public databases. The sequences were aligned using the Muscle algorithm and the phylogenetic tree was generated with the Maximum Likelihood method with 1000 bootstrap replicates using Neighbor-Join and BioNJ algorithms in MEGA7 software (Kumar et al., 2016). Evolutionary rate differences among sites were modelled with a discrete Gamma distribution. The tree is shown to scale, with branch lengths measured as the number of substitution per site. Black rectangular boxes on the tree branches depict bootstrap values greater than 50%, with the sizes of the boxes being proportional to the bootstrap values. DHH1/DDX6-like proteins from fungi, roundworm (*Caenorhabditis elegans*), and fruit fly (*Drosophila melanogaster*) were downloaded from UniProt database with sequence identifiers as follow: *Schizosaccharomyces pombe* STE13, Q09181; *Thanatephorus cucumeris* AG1IA_04085, L8WUS4; *Aspergillus clavatus* DHH1, A1CJ18; *Botrytis cinerea* BofuT4_P074000, G2XPI2; *Fusarium graminearum* DHH1, Q4HW67; *Neurospora crassa* DRH-10, Q7S5D9; *Kluyveromyces lactis* DHH1, Q6CSZ7; *Eremothecium gossypii* DHH1, Q75BS4; *Zygosaccharomyces rouxii* ZYRO0F11440p, C5DYA2; *Candida glabrata* DHH1, Q6FQU5; *Saccharomyces cerevisiae* DHH1, P39517; *Saccharomyces arboricola* SU7_0473, J8Q9Y5; *C. elegans* CGH-1, Q95YF3; *D. melanogaster* DDX6/ME31B, P23128. Vertebrate DDX6-like sequences were obtained from the Emsembl genome browser with the following identifiers: *Petromyzon marinus* ENSPMAT00000007938.1; *Oreochromis niloticus* DDX61, ENSONIT00000014381.1; *Danio rerio* DDX61, ENSDART00000155899.3; *O. niloticus* DDX6, ENSONIT00000007261.1; *D. rerio* DDX6, ENSDART00000185638.1; *Homo sapiens* DDX6, ENSG00000110367.12; *Gallus gallus* DDX6, ENSGALT00000058124.1; *Monodelphis domestica* DDX6, ENSMODT00000017036.3; *Mus musculus* DDX6, ENSMUST00000170489.1; *Bos taurus* DDX6, ENSBTAT00000011952.4; *Canis lupus familiaris* DDX6, ENSCAFT00000019743.3; *Felis catus* DDX6, ENSFCAT00000041628.2. DHH1-like sequences from rice (*Oryza sativa*), maize (*Zea mays*), *Arabidopsis* (*Arabidopsis thaliana*), soybean (*Glycine max*) and tomato (*Solanum lycopersicum*) were obtained from the sources as in Figure 2.1 with the following identifiers: *O. sativa* RH6, LOC_Os04g45040.1; *O. sativa* RH8, LOC_Os02g42860.1; *O. sativa* RH12 LOC_Os10g35990.1; *Z. mays* DHH1; Zm00001d032526; *Z. mays* Zm00001d013910; *Z. mays* Zm00001d017384; *A. thaliana* RH6, At2g45810.1; *A. thaliana* RH8, At4g00660.1; *A. thaliana* RH12, At3g61240.1; *G. max* Glyma09g39710.1; *G. max* Glyma03g01500.1; *G. max* Glyma03g01530.1; *S. lycopersicum* DEAD18, Solyc05g048850.1.1; *S. lycopersicum* DEAD4, Solyc01g094350.1.1; *S. lycopersicum* DEAD33, Solyc10g017530.1.1. Two soybean sequences, Glyma08g26950.1 and Glyma17g27250.1, clustered into the DDH1-like clade in Figure 1 were excluded from this analysis since the proteins lack the N-terminal region and contain the incomplete core helicase domain. Other green algae and plant sequences were collected from the Phytozome database with the identifiers as follow: *Coccomyxa subellipsoidea* 24291; *Dunaliella salina* Dusal.0443s00010.1; *Chlamydomonas reinhardtii* DEH1, Cre04.g223850.t1.2; *Volvox carteri* Vocar.0049s0041.1; *Micromonas pusilla* 161518; *Marchantia polymorpha* Mapoly0009s0142.1; *Physcomitrella patens* Pp3s121_40V3.1; *P. patens* Pp3c11_17170V3.1; *Sphagnum fallax* Sphfalx0022s0104.1; *S. fallax*

Sphfalx0022s0103.1; *S. fallax* Sphfalx0008s0043.1; *S. fallax* Sphfalx0009s0268.1; *Amborella trichopoda* evm_27.model.AmTr_v1.0_scaffold00029.296; *Aquilegia coerulea* Aqcoe7G038300.1; *Eucalyptus grandis* Eucgr.D02270.1; *Fragaria vesca* mrna19070.1-v1.0-hybrid; *Citrus sinensis* orange1.1g011065m. Grey boxes represent the N- and C-terminal extensions; blue boxes, RecA-like domains; yellow boxes, linker regions.

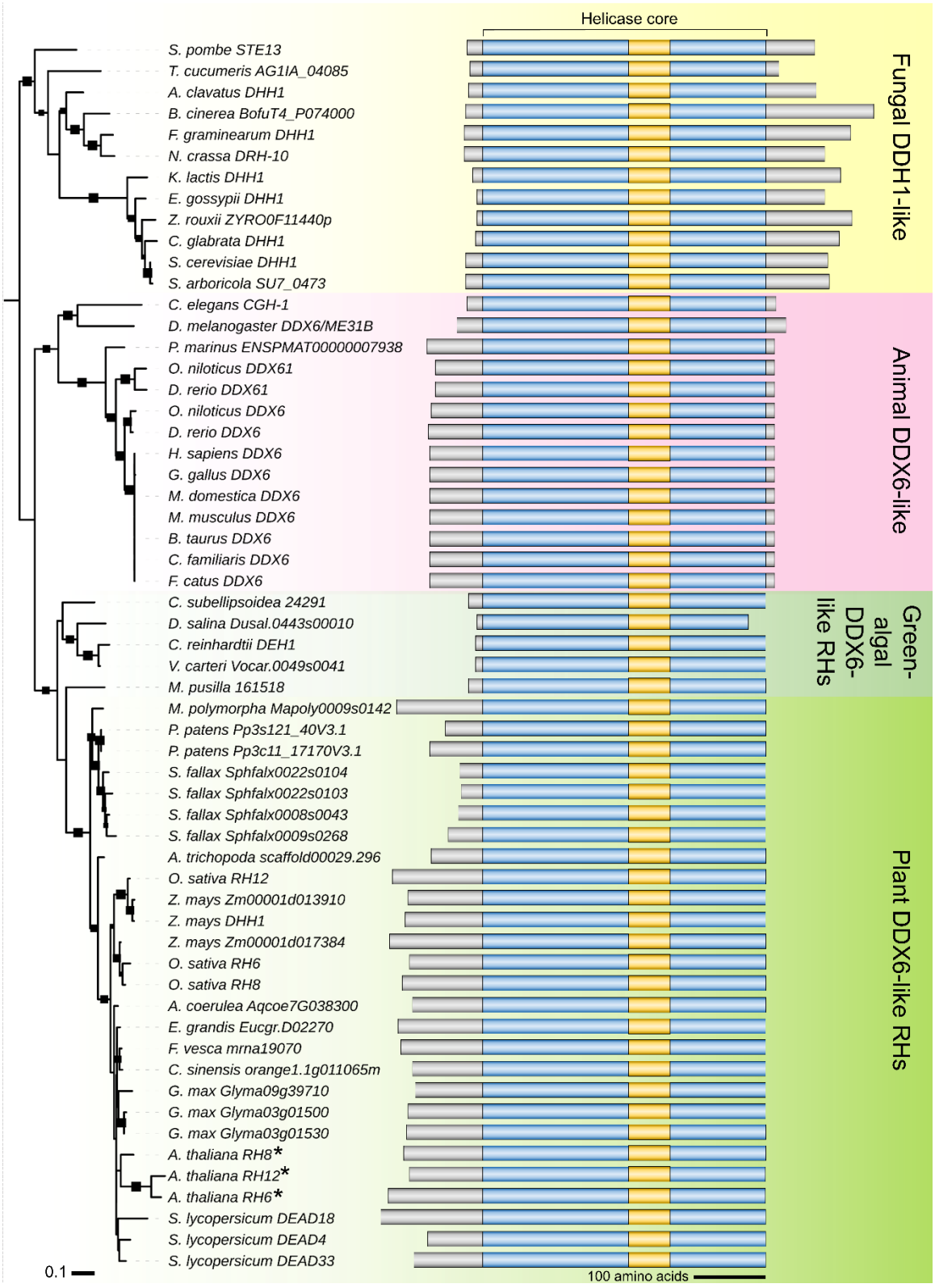
Helicase core
S. pombe STE13
T. cucumeris AG1IA_04085
A. clavatus DHH1
B. cinerea BofuT4_P074000
F. graminearum DHH1
N. crassa DRH-10
K. lactis DHH1
E. gossypii DHH1
Z. rouxii ZYRO0F11440p
C. glabrata DHH1
S. cerevisiae DHH1
S. arboricola SU7_0473
C. elegans CGH-1
D. melanogaster DDX6/ME31B
P. marinus ENSPMAT00000007938
O. niloticus DDX61
D. rerio DDX61
O. niloticus DDX6
D. rerio DDX6
H. sapiens DDX6
G. gallus DDX6
M. domestica DDX6
M. musculus DDX6
B. taurus DDX6
C. familiaris DDX6
F. catus DDX6
C. subellipsoidea 24291
D. salina Dusal.0443s00010
C. reinhardtii DEH1
V. carteri Vocar.0049s0041
M. pusilla 161518
M. polymorpha Mapoly0009s0142
P. patens Pp3s121_40V3.1
P. patens Pp3c11_17170V3.1
S. fallax Sphfalx0022s0104
S. fallax Sphfalx0022s0103
S. fallax Sphfalx0008s0043
S. fallax Sphfalx0009s0268
A. trichopoda scaffold00029.296
O. sativa RH12
Z. mays Zm00001d013910
Z. mays DHH1
Z. mays Zm00001d017384
O. sativa RH6
O. sativa RH8
A. coerulea Aqcoe7G038300
E. grandis Eucgr.D02270
F. vesca mrna19070
C. sinensis orange1.1g011065m
G. max Glyma09g39710
G. max Glyma03g01500
G. max Glyma03g01530
A. thaliana RH8*
A. thaliana RH12*
A. thaliana RH6*
S. lycopersicum DEAD18
S. lycopersicum DEAD4
S. lycopersicum DEAD33
0.1
100 amino acids
Fungal DDH1-like
Animal DDX6-like
Green-algal DDX6-like RHs
Plant DDX6-like RHs

Figure 2.3. Tissue-specific expression profiles of *RH6*, *RH8* and *RH12* transcripts. Expression pattern of *RH6*, *RH8*, and *RH12* across different organs and developmental stages based on the publicly available collection of microarray (A) and RNA-seq (B) data. Microarray and RNA-seq data were extracted from the *Arabidopsis* eFP browser (http://bar.utoronto.ca/efp/cgi-bin/efpWeb.cgi) and TraVa database (http://travadb.org/), respectively.

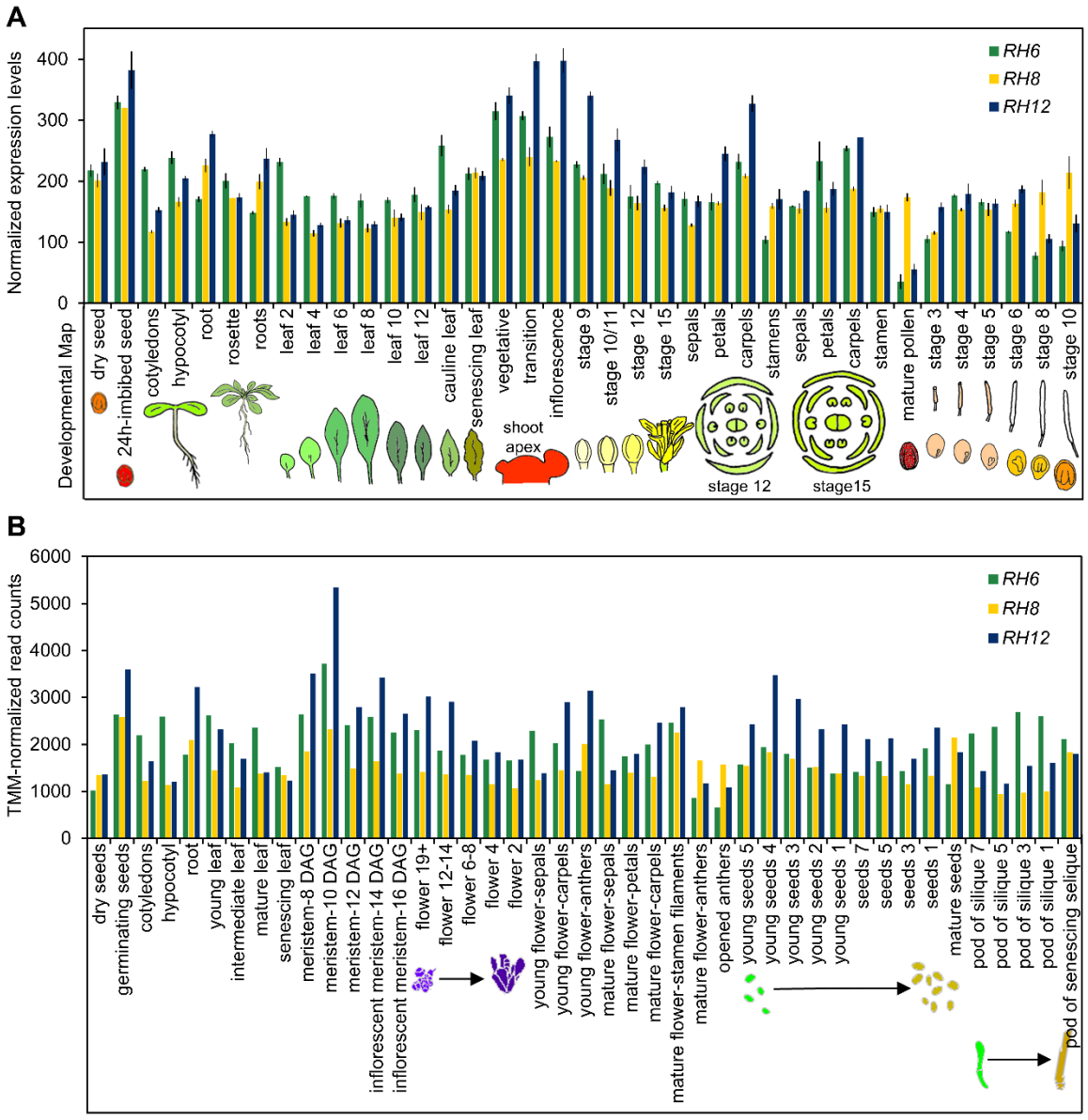
A
Normalized expression levels
0
100
200
300
400
RH6
RH8
RH12
Developmental Map
dry seed
24h-imbibed seed
cotyledons
hypocotyl
root
rosette
roots
leaf 2
leaf 4
leaf 6
leaf 8
leaf 10
leaf 12
cauline leaf
senescing leaf
vegetative
shoot apex
transition
inflorescence
stage 9
stage 10/11
stage 12
stage 15
sepals
petals
carpels
stamens
sepals
petals
carpels
stamen
mature pollen
stage 3
stage 4
stage 5
stage 6
stage 8
stage 10
stage 12
stage15
B
TMM-normalized read counts
0
1000
2000
3000
4000
5000
6000
RH6
RH8
RH12
dry seeds
germinating seeds
cotyledons
hypocotyl
root
young leaf
intermediate leaf
mature leaf
senescing leaf
meristem-8 DAG
meristem-10 DAG
meristem-12 DAG
inflorescent meristem-14 DAG
inflorescent meristem-16 DAG
flower 19+
flower 12-14
flower 6-8
flower 4
flower 2
young flower-sepals
young flower-carpels
young flower-anthers
mature flower-sepals
mature flower-petals
mature flower-carpels
mature flower-stamen filaments
mature flower-anthers
opened anthers
young seeds 5
young seeds 4
young seeds 3
young seeds 2
young seeds 1
seeds 7
seeds 5
seeds 3
seeds 1
mature seeds
pod of silique 7
pod of silique 5
pod of silique 3
pod of silique 1
pod of senescing silique

Figure 2.4. *Arabidopsis RH6*, *RH8* and *RH12* are functionally redundant and required for plant growth and development. (A) Schematic representation of the *RH6*, *RH8* and *RH12* loci and their associated T-DNA insertion alleles. Untranslated and coding regions are depicted as white and black boxes, respectively. Introns are depicted as lines. "ATG" and "TAA" indicate the translational initiation and stop codon, respectively. Inverted white triangles refer to the positions of T-DNA insertions in the *rh6-1*, *rh8-1* and *rh12-2* alleles. Arrows indicate the orientations and approximate positions of primers used for molecular genotyping of the genes or the T-DNAs: blue, forward primers; red, reverse primers. (B) PCR-based genotyping of the homozygous *rh6-1*, *rh8-1* and rh*12-2* alleles. Gene and T-DNA-specific primers represented in (A) were used for PCR amplification of genomic DNA from Col-0 wild-type, and homozygous *rh6-1*, *rh8-1* and *rh12-2* insertion alleles. (C) RT-PCR analysis of *RH6*, *RH8*, and *RH12* transcripts. Primers flanking the T-DNAs as indicated in (A) were used for PCR-based specific detection of *RH6*, *RH8* and *RH12* transcripts from the homozygous *rh6-1*, *rh8-1* and rh*12-2* alleles in comparison to the wild-type Col-0. *UBQ10* was used as an internal control. (D) RT-qPCR analysis of *RH6*, *RH8* and *RH12* transcript levels in 7-day-old seedlings of the homozygous *rh6-1*, *rh8-1* and *rh12-2* mutants. Gene-specific primers located downstream of the T-DNA as indicated in (A) were used. Relative transcript fold-change was calculated by the ΔΔCt method (Pfaffl, 2001) using *PP2AA2* as a reference. Error bars represent the standard deviation (SD) of three biological replicates. Statistical significance was determined by ANOVA, followed by a Tukey's Honest Significant Difference (HSD) test (n = 3). Means that are significantly different from each other (p < 0.05) are denoted by different letters. (E) Rosette growth phenotype of 39-day-old plants of Col-0 wild-type in comparison to the single *rh6-1*, *rh8-1* and *rh12-2* mutants as well their double (*rh6 rh8*, *rh6 rh12* and *rh8 rh12*), double homozygous single heterozygous (*rh6*$^{(+/-)}$ *rh8 rh12*, *rh6 rh8*$^{(+/-)}$ *rh12* and *rh6 rh8 rh12* $^{(+/-)}$) and triple (*rh6 rh8 rh12*; inset) mutant combinations, and a transgenic line homozygous for the *rh6 rh8 rh12* triple mutant alleles with an introduced genomic *RH6* wild-type allele C-terminally tagged with the FLAG peptide (*rh6 rh8 rh12_gRH6-FLAG*). All plants were germinated directly on soil; representative plants were selected to demonstrate the effect on growth and development of the different mutant combinations. (F) Rosette diameters and fresh weights of 39-day-old plants in (E). Statistical significance was determined by ANOVA, followed by a Tukey's HSD test. Means that are significantly different from each other (p < 0.05) are denoted by different letters. n = 28 and 30 for rosette diameters and fresh weights, respectively. (G) Seedlings (7-day-old) of Col-0 wild-type, *rh6-1*, *rh8-1*, *rh12-2*, *rh6 rh8*, *rh6 rh12*, *rh8 rh12*, *rh6 rh8 rh12*, *rh6 rh8 rh12*, and *rh6 rh8 rh12_gRH6-FLAG* lines in comparison with the homozygous decapping mutants *dcp2-1* and *vcs-7*. (H) Primary root length of 7-day-old seedlings of the genotypes illustrated in (H). Statistical significance was determined by ANOVA, followed by a Tukey's HSD test (n = 15). Means significantly different between genotypes (p < 0.05) are indicated by different letters. (I) Representative photographs of 7-day-old seedlings of the triple *rh6 rh8 rh12* mutant in comparison to the wild-type Col-0 as well as homozygous *dcp2-1* and *vcs-7* mutants. Bar = 1 cm. (J) Representative images of the cotyledon vasculature of 7-day-old seedlings of Col-0 wild-type, *rh6 rh8 rh12*, *dcp2-1* and *vcs-7* mutants. Bar = 0.3 mm.

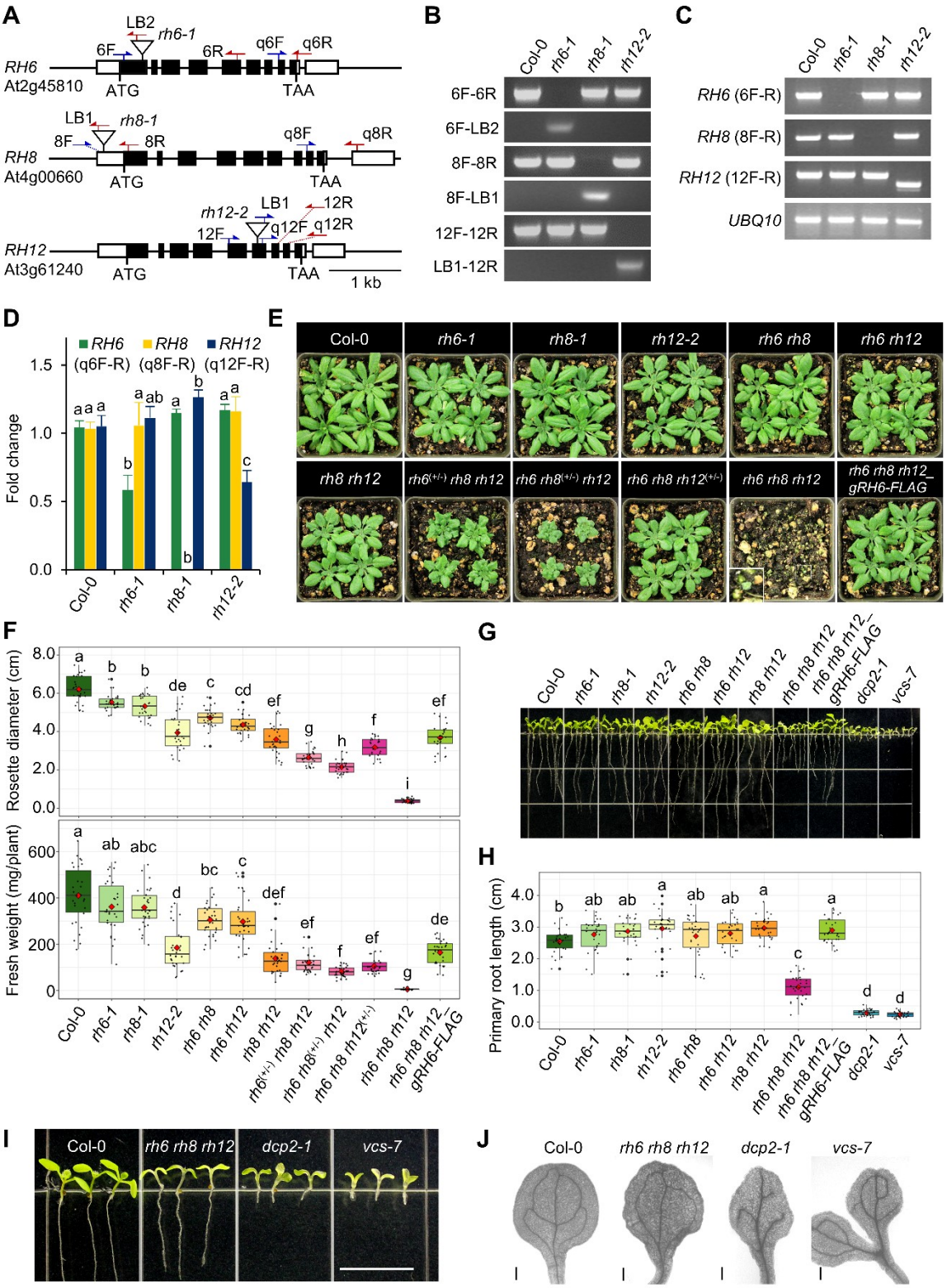
A
LB2
rh6-1
6F
6R
q6F
q6R
RH6
At2g45810
ATG
TAA
LB1
rh8-1
8F
8R
q8F
q8R
RH8
At4g00660
rh12-2
LB1
12R
12F
q12F
q12R
RH12
At3g61240
1 kb
B
Col-0
rh6-1
rh8-1
rh12-2
6F-6R
6F-LB2
8F-8R
8F-LB1
12F-12R
LB1-12R
C
RH6 (6F-R)
RH8 (8F-R)
RH12 (12F-R)
UBQ10
D
RH6 (q6F-R)
RH8 (q8F-R)
RH12 (q12F-R)
Fold change
E
Col-0
rh6-1
rh8-1
rh12-2
rh6 rh8
rh6 rh12
rh8 rh12
rh6(+/-) rh8 rh12
rh6 rh8(+/-) rh12
rh6 rh8 rh12(+/-)
rh6 rh8 rh12
rh6 rh8 rh12_ gRH6-FLAG
F
Rosette diameter (cm)
Fresh weight (mg/plant)
G
dcp2-1
vcs-7
H
Primary root length (cm)
I
J

Figure 2.5. The triple *rh6 rh8 rh12* mutant exhibits delayed germination. (A) RT-qPCR analysis of *RH6*, *RH8* and *RH2* transcripts during germination. Non-dormant Col-0 wild-type seeds were surface-sterilized and stratified at 4ºC in the dark for 2 days before being transferred to 0.5x MS media with 0.5% (w/v) sucrose and grown under long-day (16-hour light/8-hour dark) conditions. Tissues were sampled at 6 and 12 hours, 1 day, 2 days, 3 days, 6 days and 10 days after imbibition. Transcript fold-change was calculated by the ΔΔCt method using *PP2AA2* as a reference. Error bars represent the standard error (SE) of three biological replicates. Shaded area represents stratification at 4ºC in the dark. (B) Germination rates of Col-0 wild-type and the progeny of the double homozygous single heterozygous *rh6*$^{(+/-)}$ *rh8 rh12*, *rh6 rh8*$^{(+/-)}$ *rh12* and *rh6 rh8 rh12*$^{(+/-)}$ mutant seeds. The seeds were surface-sterilized and plated on agar medium (water) without stratification before being grown under long-day conditions. Error bars represent the SD of three biological replicates (*n* = 100 seeds). (C) Germination rates of *rh6 rh8 rh12* in comparison with siblings *rh8 rh12* and *rh6*$^{(+/-)}$ *rh8 rh12* (1:2) seeds, *rh6 rh8 rh12_gRH6-FLAG*, and wild-type Col-0 seeds. The seeds were surface-sterilized and grown on 0.5x MS media with 0.5% (w/v) sucrose under long-day conditions with or without prior stratification. The F1 of genotype *rh6*$^{(+/-)}$ *rh8 rh12* were used to determine germination rates of *rh6 rh8 rh12* and their siblings. Germination times of all *rh6*$^{(+/-)}$ *rh8 rh12* progeny were recorded and their genotypes later determined after 7 days of germination based on the phenotype of the *rh6 rh8 rh12* seedlings. (D) RT-qPCR analysis of *OLEO1* and *OLEO2* transcripts of stored seed (2-month-old) during germination for Col-0 wild-type and the progeny of *rh6*$^{(+/-)}$ *rh8 rh12* mutant. The seeds were prepared and germinated as in (A). *rh6 rh8 rh12* seedlings were distinguished after 6 days of imbibition/germination based on phenotype. Transcript fold-change was calculated by the ΔΔCt method using *PP2AA2* as an internal control. Error bars represent the SE of three biological replicates. Shaded area represents stratification at 4ºC in the dark.

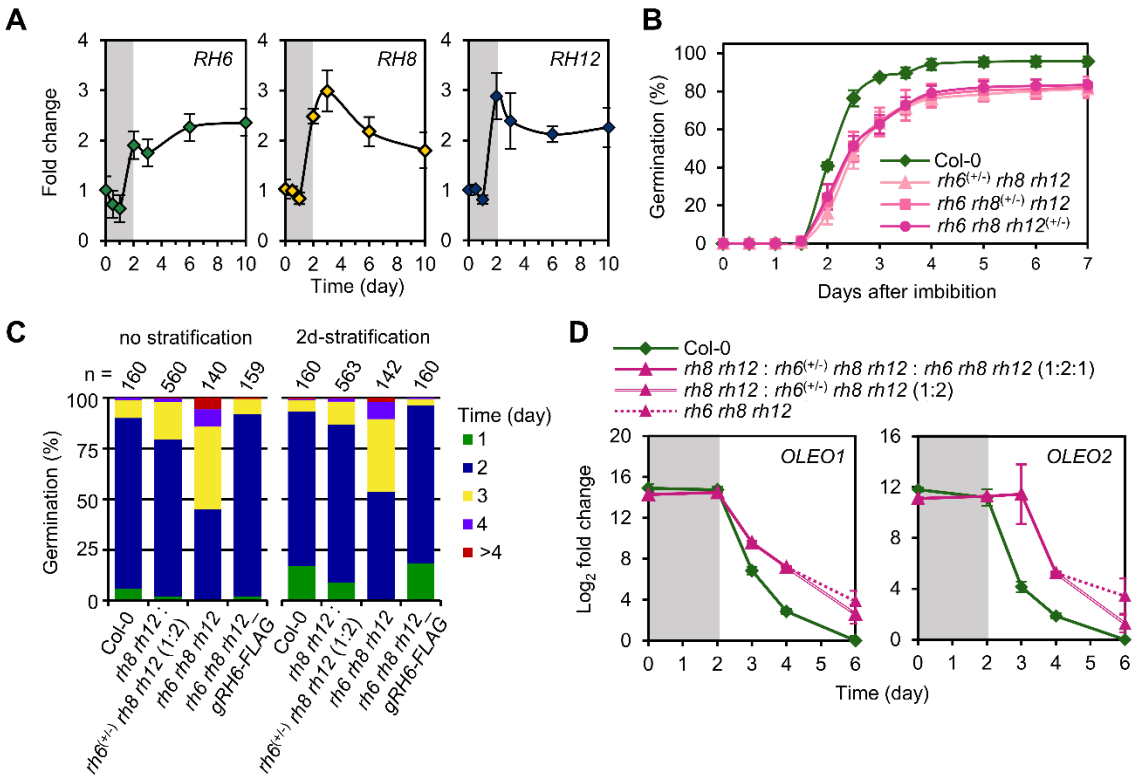
A
RH6
RH8
RH12
Fold change
Time (day)
B
Germination (%)
Col-0
rh6(+/-) rh8 rh12
rh6 rh8(+/-) rh12
rh6 rh8 rh12(+/-)
Days after imbibition
C
no stratification
2d-stratification
n =
160
560
140
159
160
563
142
160
Germination (%)
Time (day)
1
2
3
4
>4
Col-0
rh8 rh12 : rh6(+/-) rh8 rh12 (1:2)
rh6 rh8 rh12
rh6 rh8 rh12_gRH6-FLAG
D
Col-0
rh8 rh12 : rh6(+/-) rh8 rh12 : rh6 rh8 rh12 (1:2:1)
rh8 rh12 : rh6(+/-) rh8 rh12 (1:2)
rh6 rh8 rh12
Log2 fold change
OLEO1
OLEO2
Time (day)

Figure 2.6. Reduced expression of *Arabidopsis* DHH1/DDX6-like *RHs* affects plant growth. (A) Schematic diagram and sequences of an artificial miRNA and its target site on *RH6*. Design of a 21-nucleotide artificial miRNA specifically targeting *RH6* transcripts and produced within the *Arabidopsis MIR319a* gene under the 35S promoter. (B) Phenotype of 7-day-old seedlings of Col-0 wild-type, the double *rh8 rh12* mutant, and three independent *amiRH6* lines generated in *rh8 rh12* background (*amiRH6 rh8 rh12*). (C) Levels of the artificial miRNA *amiRH6* in three independent lines determined by pulsed stem-loop RT-qPCR. miRNA fold-change was calculated by the ΔΔCt method relative to line #21 using *U6* RNA as a reference. Error bars represent the SD of three biological replicates. Statistical significance was determined by ANOVA, followed by a Tukey's HSD test. Means that are significantly different from each other ($p < 0.05$) are indicated by different letters. n.d. = not detectable. (D) RT-qPCR analysis of *RH6*, *RH8* and *RH12* transcript levels in 7-day-old seedlings of Col-0 wild-type, *rh8 rh12* and three *amiRH6 rh8 rh12* lines. Relative transcript fold-change of each transcript was calculated by the ΔΔCt method using *PP2AA2* as a reference. Error bars represent the SD of three biological replicates. Statistical significance was determined by ANOVA, followed by a Tukey's HSD test. Means that are significantly different from each other ($p < 0.05$) are indicated by different letters. (E) Rosette growth phenotype of 28-day-old plants of Col-0 wild-type, *rh8 rh12* and three *amiRH6/rh8 rh12* lines. The plants were germinated on 0.5x MS media with 0.5% (w/v) sucrose for 7 days before being transferred to soil and grown for another 21 days. (F-G) Rosette diameters and fresh weights of 28-day-old plants of the genotypes presented in (E). Statistical significance was determined by ANOVA (n = 18-24), followed by a Tukey's HSD test. Means that are significantly different from each other ($p < 0.05$) are denoted by different letters.

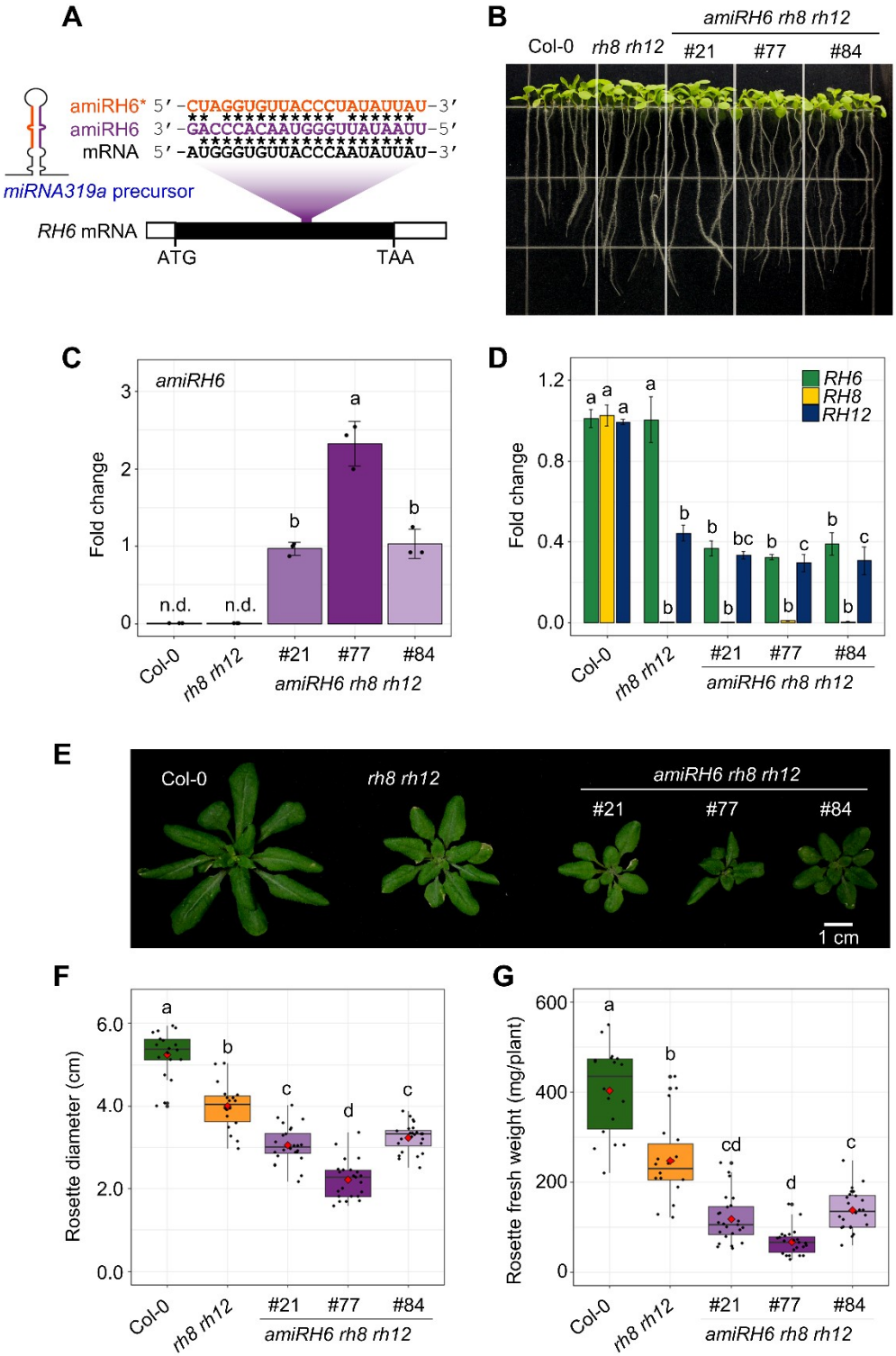
A
amiRH6* 5′-CUAGGUGUUACCCUAUAUUAU-3′
amiRH6 3′-GACCCACAAUGGGUUUAUAAUU-5′
mRNA 5′-AUGGGUGUUACCCAAUAUUAU-3′
miRNA319a precursor
RH6 mRNA
ATG
TAA
B
amiRH6 rh8 rh12
Col-0
rh8 rh12
#21
#77
#84
C
amiRH6
Fold change
n.d.
n.d.
Col-0
rh8 rh12
#21
#77
#84
amiRH6 rh8 rh12
D
RH6
RH8
RH12
Fold change
Col-0
rh8 rh12
#21
#77
#84
amiRH6 rh8 rh12
E
Col-0
rh8 rh12
amiRH6 rh8 rh12
#21
#77
#84
1 cm
F
Rosette diameter (cm)
Col-0
rh8 rh12
#21
#77
#84
amiRH6 rh8 rh12
G
Rosette fresh weight (mg/plant)
Col-0
rh8 rh12
#21
#77
#84
amiRH6 rh8 rh12

Figure 2.7. *Arabidopsis* RH6, RH8 and RH12 are nucleocytoplasmic proteins. (A) Confocal images of RFP fluorescence in root tissues of transgenic 4-day-old seedlings expressing C-terminally tagged RH6-RFP under control of its native promoter. Left panel illustrates a maximum projection of RFP fluorescence over 12 *z*-planes for a total volume of 55 µm; right panel displays an overlay of RFP fluorescence from the left panel with a bright field image. Bars = 100 µm. (B) RFP fluorescence of the root apical meristem region of the plants described in (A) counter-stained with 4',6-diamidino-2-phenylindole (DAPI) for visualization of the nucleus. (C) Magnified images of framed areas in (B). Bars in (B) and (C) = 10 µm. Confocal images of C-terminally tagged RH8-RFP (D-F) and RH12-RFP (G-I) are presented in the same manner as for RH6-RFP (A-C).

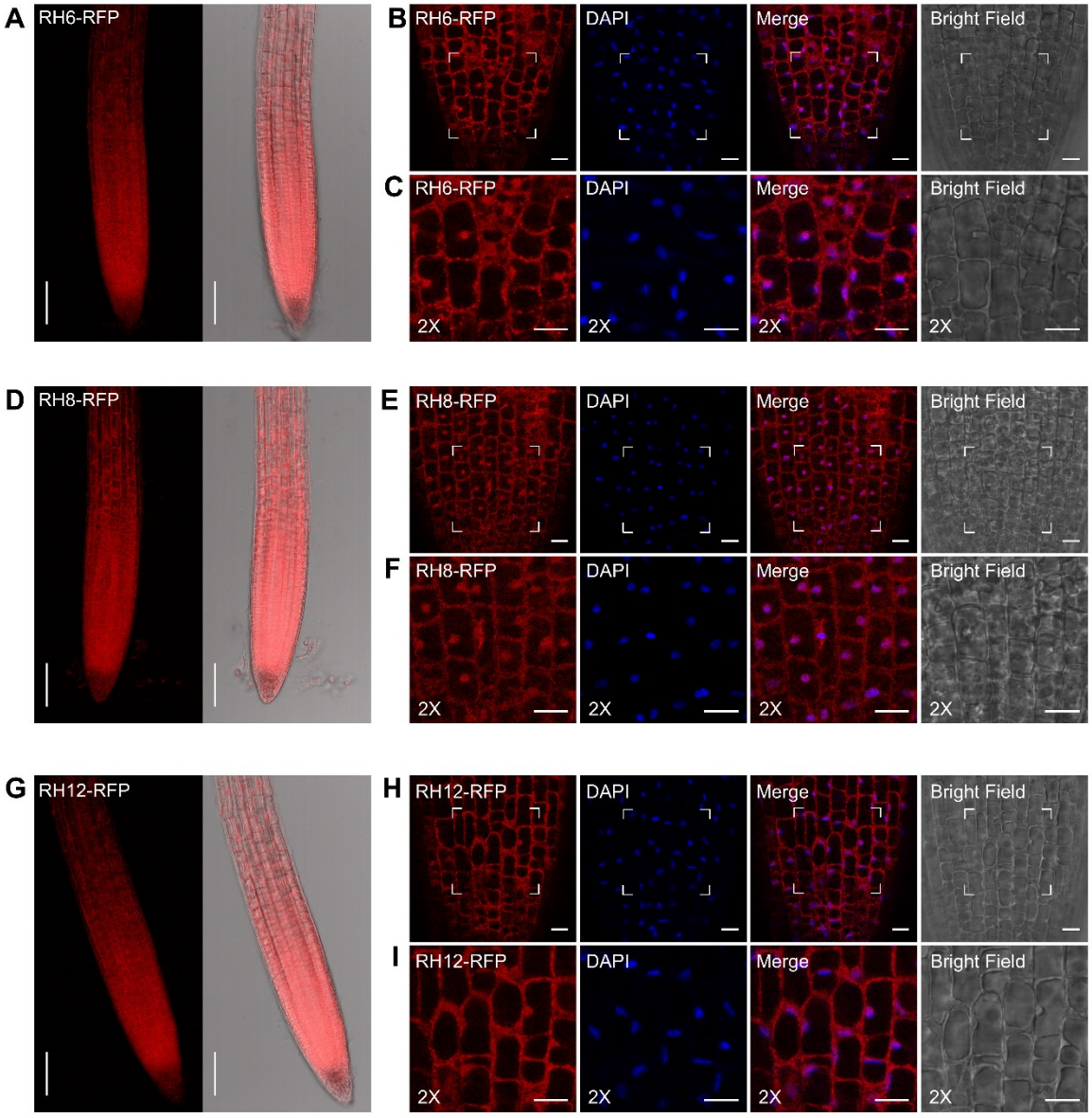
A
RH6-RFP
B
RH6-RFP
DAPI
Merge
Bright Field
C
RH6-RFP
DAPI
Merge
Bright Field
2X
2X
2X
2X
D
RH8-RFP
E
RH8-RFP
DAPI
Merge
Bright Field
F
RH8-RFP
DAPI
Merge
Bright Field
2X
2X
2X
2X
G
RH12-RFP
H
RH12-RFP
DAPI
Merge
Bright Field
I
RH12-RFP
DAPI
Merge
Bright Field
2X
2X
2X
2X

Figure 2.8. RH6, RH8 and RH12 localize into cytoplasmic foci in a translation-dependent manner. (A) Prediction of disordered regions on the N-terminus of RH6, RH8 and RH12 proteins based on VL3 scores of PONDR® (Predictor of Naturally Disordered Regions) software (http://www.pondr.com/). (B) Confocal images of RFP fluorescence in the root basal meristem regions of transgenic seedlings expressing C-terminally RFP-tagged RH6, RH8 or RH12. Top panel: 4-day-old seedlings grown on 0.5x MS media with 0.5% (w/v) sucrose were submerged in water under coverslip for approximately 2 minutes before imaging. Changes in protein localization in the same regions were re-imaged after 30 minutes of incubation. Middle and bottom panels: seedlings grown under the same conditions were pre-treated with 0.001% (v/v) dimethyl sulfoxide (DMSO, solvent) with or without cycloheximide (CHX; 200 ng μl^{-1}) for 3 minutes by vacuum infiltration before being submerged under the same solutions and imaged after 2 and 30 minutes of incubation. At least three seedlings were examined per genotype and treatment with similar results. Bars = 10 μm.

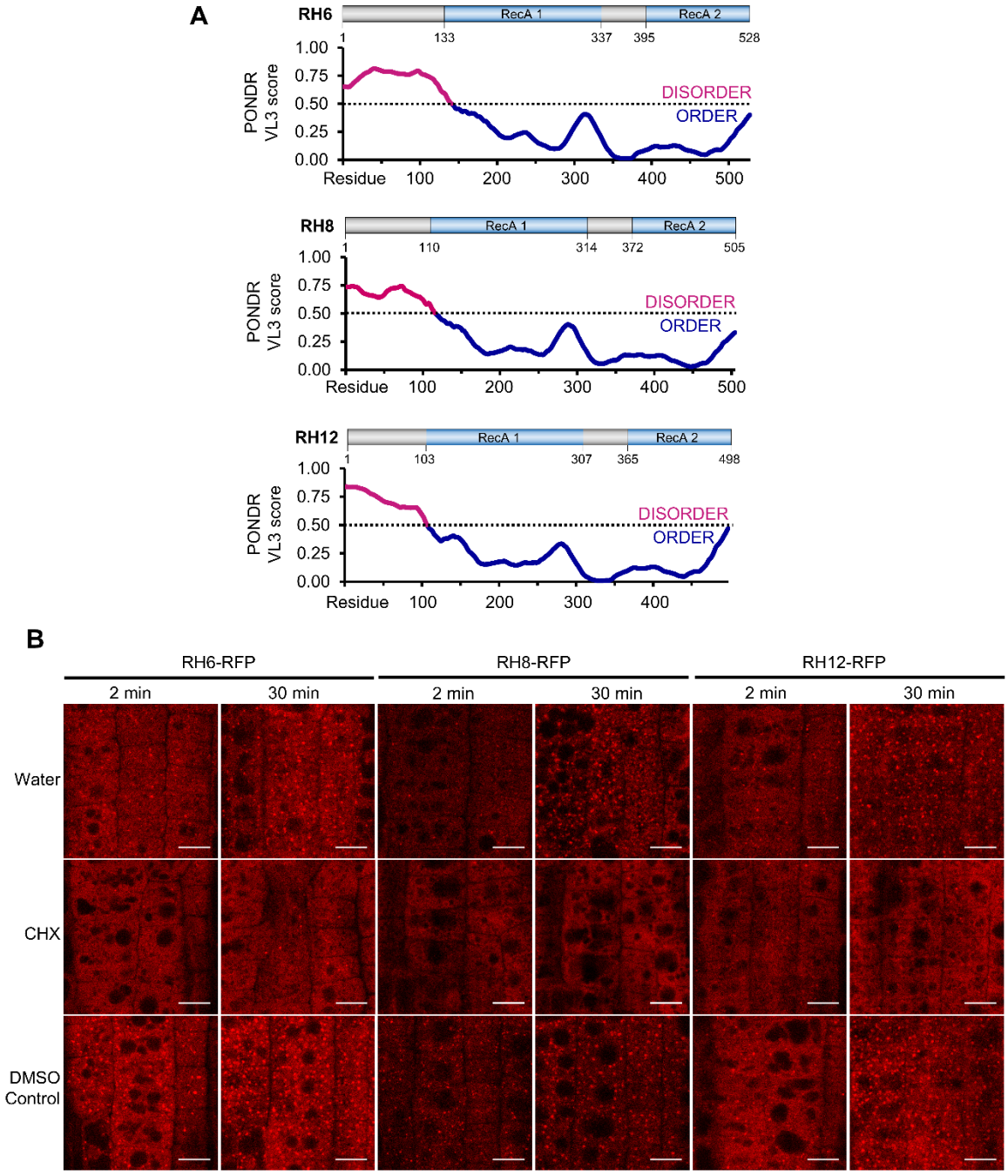
A
RH6
RecA 1
RecA 2
1
133
337
395
528
PONDR VL3 score
1.00
0.75
0.50
0.25
0.00
DISORDER
ORDER
Residue
100
200
300
400
500
RH8
110
314
372
505
RH12
103
307
365
498
B
RH6-RFP
RH8-RFP
RH12-RFP
2 min
30 min
Water
CHX
DMSO
Control

Figure 2.9. RH6 and RH12 localize to the same cytoplasmic complexes. Confocal images of RFP and CFP fluorescence in the root basal meristem of 4-day-old seedlings co-expressing C-terminally tagged RH6-RFP and RH12-CFP under their native promoters. The seedlings grown on 0.5x MS media with 0.5% (w/v) sucrose were submerged in water under coverslip, and visualization of RH6-RFP and RH12-CFP was determined after 2 and 30 minutes of submergence. For visualization, RFP and CFP signals were false-colored into magenta and green, respectively. Framed areas in the upper panels are magnified below. Arrowheads denote examples of foci in which RH6-RFP and RH12-CFP colocalize. Bars = 10 μm.

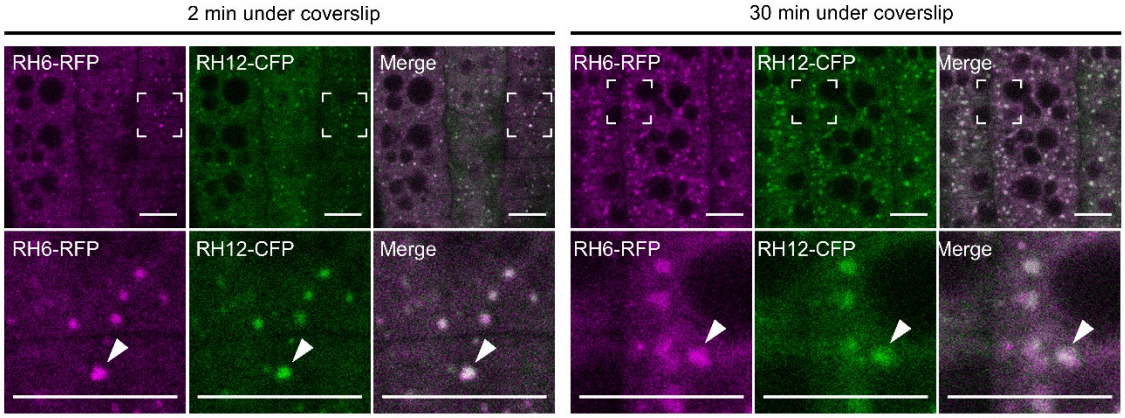
2 min under coverslip
30 min under coverslip
RH6-RFP
RH12-CFP
Merge
RH6-RFP
RH12-CFP
Merge
RH6-RFP
RH12-CFP
Merge
RH6-RFP
RH12-CFP
Merge

Figure 2.10. RH6, RH8 and RH12 foci can colocalize with those of the decapping enzyme DCP2. (A) Confocal images of RFP and GFP fluorescence in the root basal meristem of 4-day-old seedlings co-expressing C-terminally tagged RH6-RFP and DCP2-GFP under their endogenous promoters. The seedlings grown on 0.5x MS media with 0.5% (w/v) sucrose were submerged in water under coverslip, and subcellular localization of RH6-RFP and DCP2-GFP was determined within approximately 2 minutes. The plants were incubated under coverslip for a total period of 30 minutes before the protein localization was re-imaged in the same regions. For visualization, RFP and GFP signals were false-colored into magenta and green, respectively. Framed areas in the upper panels are magnified below. Arrowheads denote an example of foci where RH6-RFP and DCP2-GFP colocalize. Bars = 10 μm. (B) Confocal images of 4-day-old seedlings co-expressing C-terminally tagged RH8-RFP and DCP2-GFP under their native promoters. (C) Confocal images of 4-day-old seedlings co-expressing C-terminally tagged RH12-RFP and DCP2-GFP. Data in (B) and (C) are presented the same way as in (A).

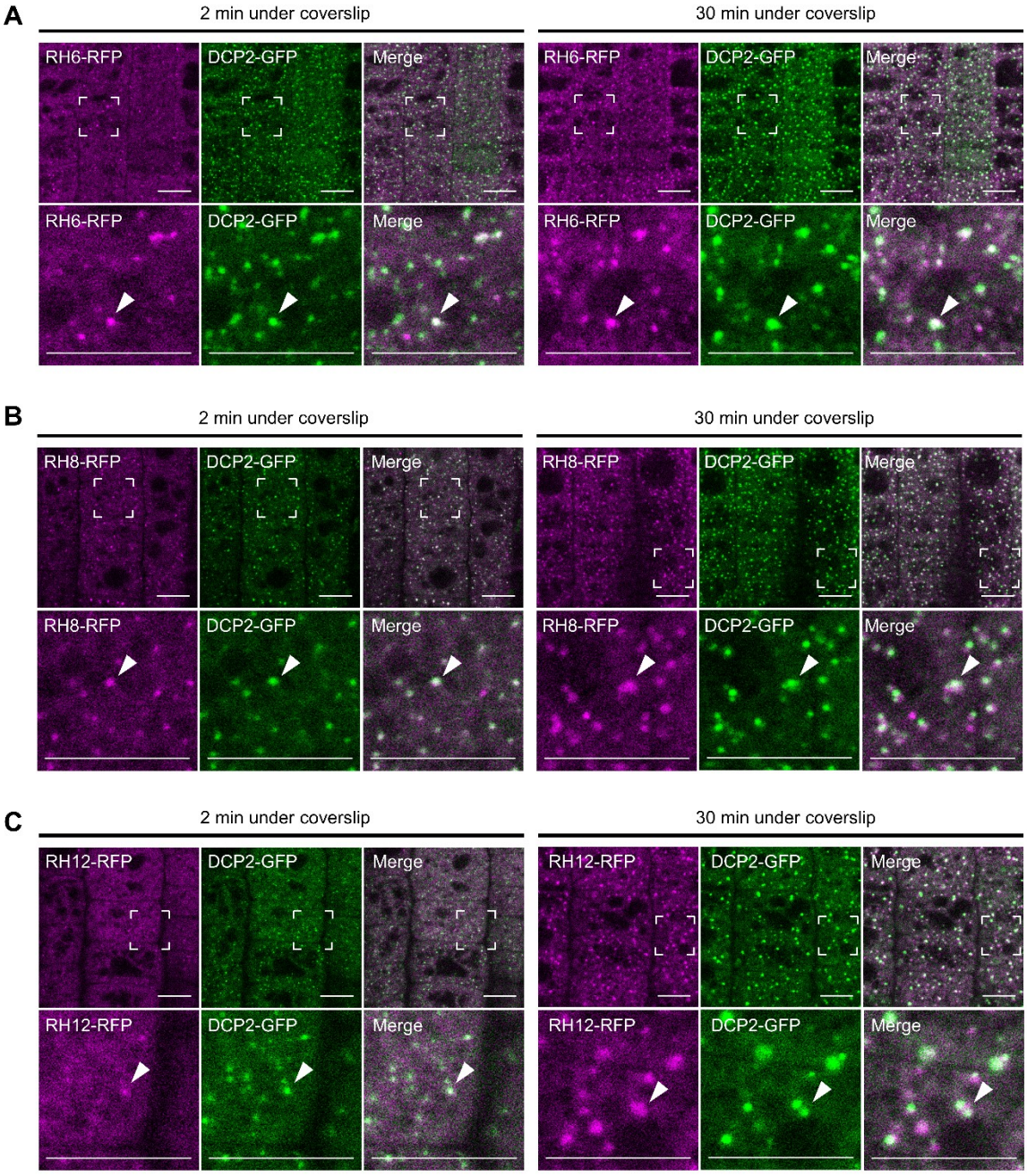
A
2 min under coverslip
30 min under coverslip
RH6-RFP
DCP2-GFP
Merge
B
2 min under coverslip
30 min under coverslip
RH8-RFP
DCP2-GFP
Merge
C
2 min under coverslip
30 min under coverslip
RH12-RFP
DCP2-GFP
Merge

Figure 2.11. RH6, RH8 and RH12 complexes can colocalize with those of the core decapping protein VCS. (A) Fluorescence microscopy images of 4-day-old seedlings co-expressing C-terminally tagged RH6-RFP and VCS-GFP under their native promoters. The seedlings grown on ½ MS + 0.5% sucrose were submerged in water under coverslip, and subcellular localization of RH6-RFP and VCS-GFP was determined in the root basal meristem regions within 2 minutes of submergence. The plants were left under coverslip and the protein localization was re-imaged after 30 minutes of incubation. For visualization, RFP and GFP signals were false-colored in magenta and green, respectively. Framed areas in the upper panels are magnified below. Arrowheads indicate representative foci where RH6-RFP and VCS-GFP colocalize. Bars = 10 μm. (B) Confocal images of 4-day-old seedlings co-expressing C-terminally tagged RH8-RFP and VCS-GFP under their native promoters. (C) Confocal images of 4-day-old seedlings co-expressing C-terminally tagged RH12-RFP and VCS-GFP. Data in (B) and (C) are presented the same way as in (A).

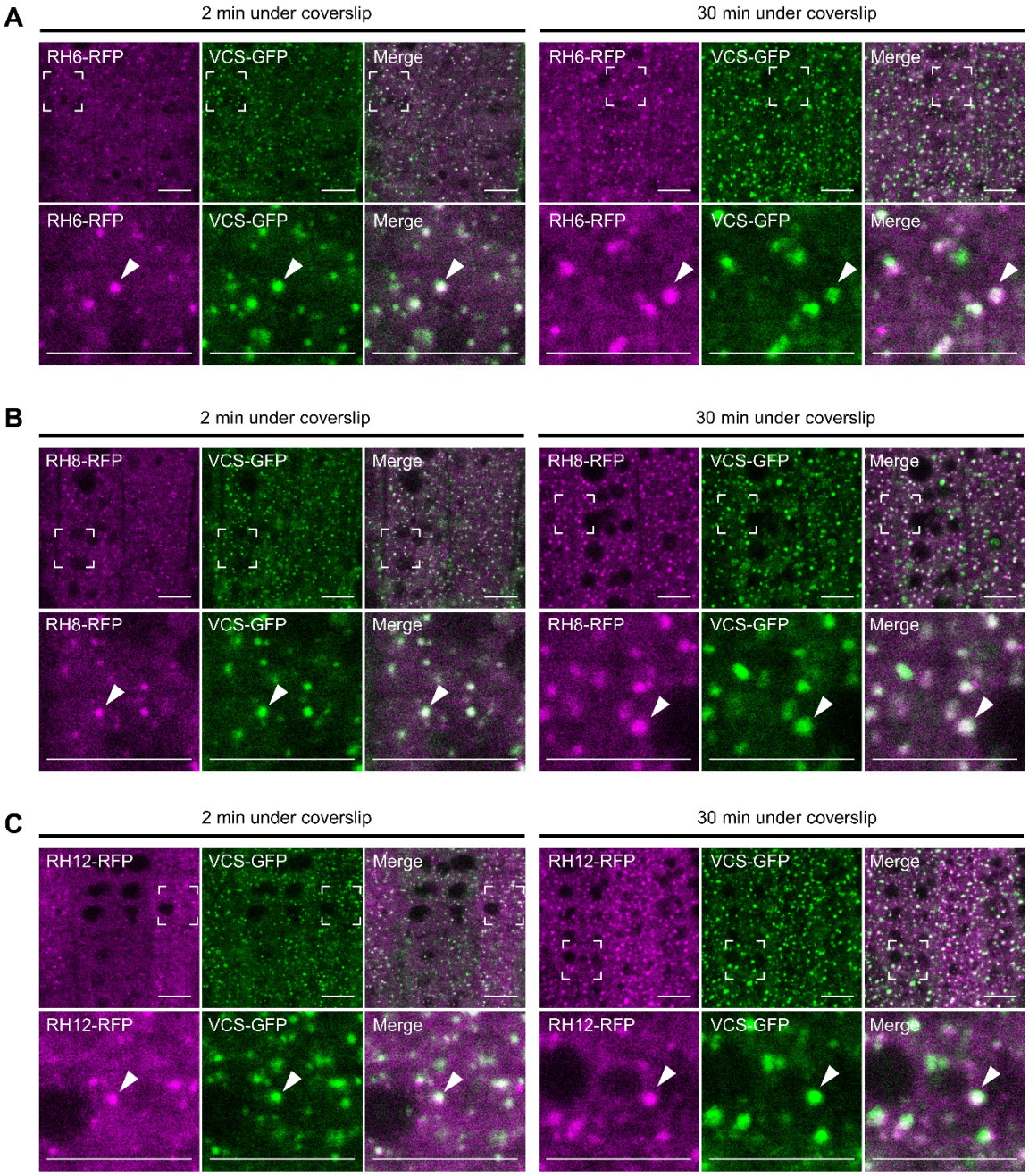
A
2 min under coverslip
30 min under coverslip
RH6-RFP
VCS-GFP
Merge
B
2 min under coverslip
30 min under coverslip
RH8-RFP
VCS-GFP
Merge
C
2 min under coverslip
30 min under coverslip
RH12-RFP
VCS-GFP
Merge

Figure 2.12. RH6, RH8 and RH12 foci can colocalize with UBP1C stress granules. (A) Confocal images of 4-day-old seedlings co-expressing C-terminally tagged RH6-RFP and UBP1C-GFP (Sorenson and Bailey-Serres, 2014). Seedlings grown on 0.5x MS media with 0.5% (w/v) sucrose were submerged in water under coverslip, and subcellular localization of RH6-RFP and UBP1C-GFP was determined within approximately 2 minutes of submergence. Plants were further incubated under coverslip for a total period of 30 minutes before the protein localization was re-imaged in the same region. For visualization, RFP and GFP signals were false-colored into magenta and green, respectively. Framed areas in the upper panels are magnified below. Arrowheads point to a representative complex where RH6-RFP and UBP1C-GFP colocalize. Bars = 10 µm. (B) Confocal images of 4-day-old seedlings co-expressing C-terminally tagged RH8-RFP and UBP1C-GFP. (C) Confocal images of 4-day-old seedlings co-expressing C-terminally tagged RH12-RFP and UBP1C-GFP. In all figures, the RHs were expressed with their native promoters; UBP1C-GFP was expressed with the 35S promoter.

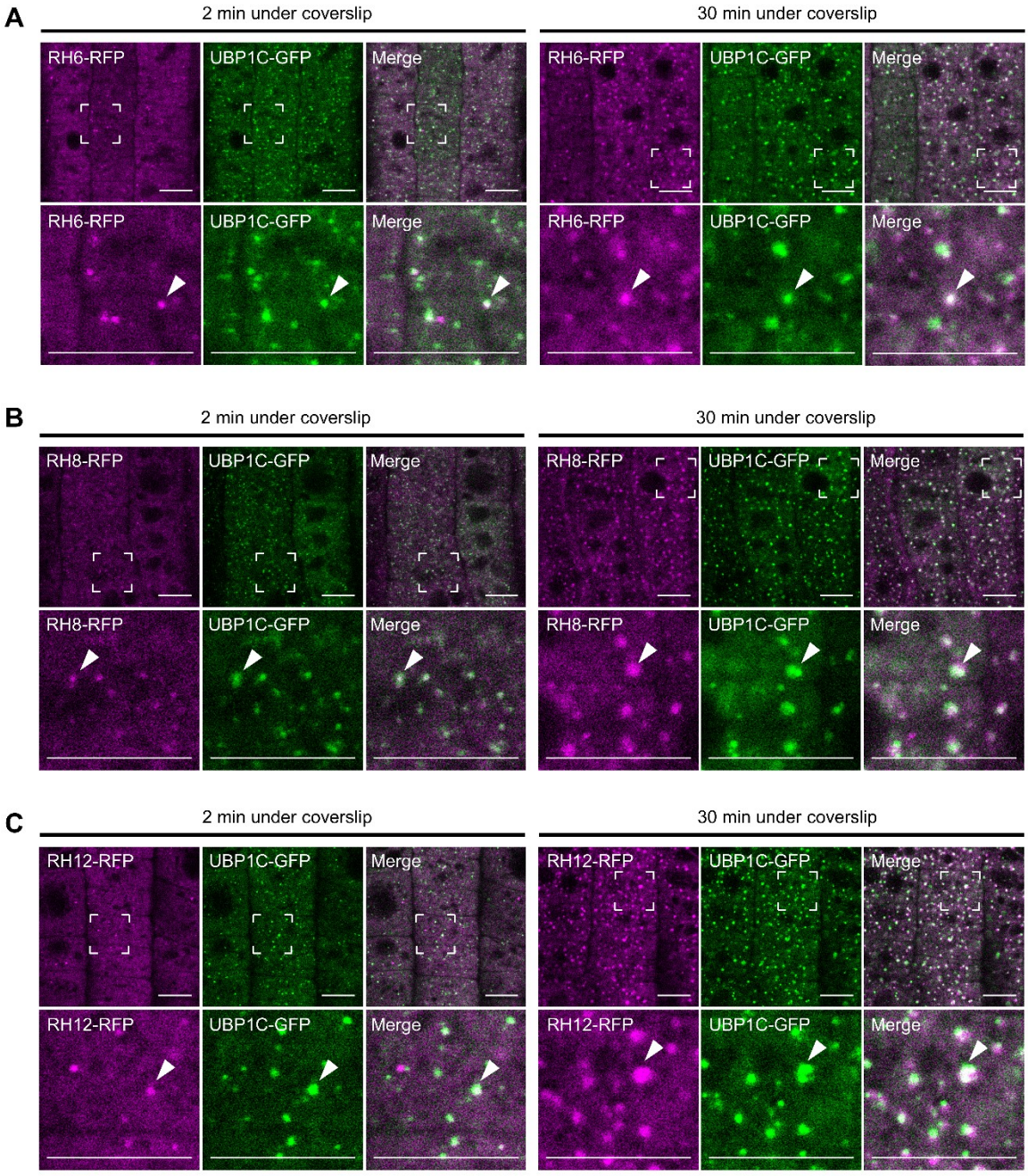
A
2 min under coverslip
30 min under coverslip
RH6-RFP
UBP1C-GFP
Merge
B
2 min under coverslip
30 min under coverslip
RH8-RFP
UBP1C-GFP
Merge
C
2 min under coverslip
30 min under coverslip
RH12-RFP
UBP1C-GFP
Merge

Figure 2.13. *Arabidopsis* DDX6-like RHs are required for processing body but not stress granule formation. Confocal images of GFP fluorescence in the root basal meristem of the Processing Body (PB) markers DCP2-GFP (A) and VCS-GFP (B), and Stress Granule (SG) marker UBP1C-GFP (C) in the wild-type Col-0 or triple *rh6 rh8 rh12* mutant. The DCP2-GFP (*proDCP2:DCP2-GFP*) carried *dcp2-1(Motomura et al., 2015)*, VCS-GFP (*proVCS:VCS-GFP*) was in wild-type Col-0 (Roux et al., 2015) and UBP1C-GFP (*pro35S:UBP1C-GFP-16*) was in *ubp1c-1* (Sorenson and Bailey-Serres, 2014). Developmental age-matched 4-day-old seedlings grown on 0.5x MS media with 0.5% (w/v) sucrose were submerged in water under a coverslip, and PB/SG formation was first imaged within 2 minutes of submergence. Coverslip-submergence was continued for a total period of 30 minutes before plants were re-imaged. At least six plants were examined per genotype with similar results. Bars = 10 μm.

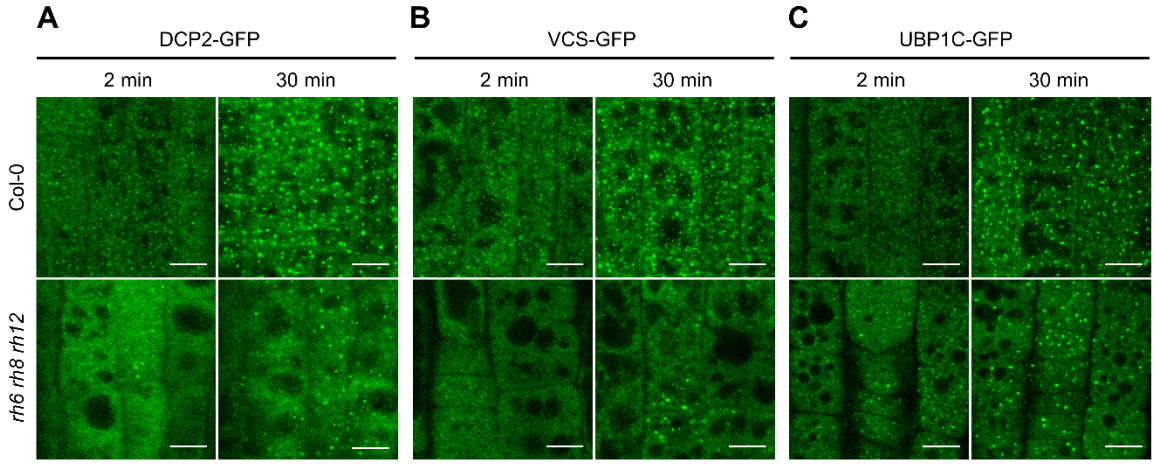
A
DCP2-GFP
2 min
30 min
B
VCS-GFP
2 min
30 min
C
UBP1C-GFP
2 min
30 min
Col-0
rh6 rh8 rh12

Table 2.1. Primers used for genotyping, RT-PCR and qPCR

Primer name	Sequence (5'-3')	Associated gene/loci	Application	Tm (ºC)
6F	CTCAACAGTACCTTCAGTCACG	*RH6*	Genotyping, RT-PCR	55.1
6R	GCTTCTTGAGATACCGATCCTTG	*RH6*	Genotyping, RT-PCR	55.2
8F	GTCTCTCTGTCTCACGCGAGAA	*RH8*	Genotyping, RT-PCR	58.2
8R	GCCAATTCCAGGAGGGT	*RH8*	Genotyping, RT-PCR	54.8
12F	TCACTGCCTCAACACACTTTTCTC	*RH12*	Genotyping, RT-PCR	57.4
12R	AGTTGCCTCATCTCCTCCCCTC	*RH12*	Genotyping, RT-PCR	60.5
LB1	TCAAACAGGATTTTCGCCTGCT	T-DNA left border; SALK lines	Genotyping	57.4
LB2	GCTTCCTATTATATCTTCCCAAATT ACCAATACA	T-DNA left border; SAIL lines	Genotyping	56.7
q6F	GGTAGGCAGATCAGGACGATT	*RH6*	qPCR	56.4
q6R	CGATAAGTGAAGGTATGGGCTTG	*RH6*	qPCR	55.5
q8F	GTTGGACGATCAGGAAGGTTTGG	*RH8*	qPCR	58.0
q8R	AGGTAAGAGGCAGAATGTGAAGC	*RH8*	qPCR	57.0
q12F	CAGAGTATTCCACGAGTTCCGC	*RH12*	qPCR	57.5
q12F	TTCACAGCCAATCCAAGGTGTC	*RH12*	qPCR	57.7
UBQ10-F	CACACTCCACTTGGTCTTGCGT	*UBQ10*	RT-PCR	59.8
UBQ10-R	TGGTCTTTCCGGTGAGAGTCTTCA	*UBQ10*	RT-PCR	59.6
PP2AA2-F	AATCGGTTGTGGAGAAGACG	*PP2AA2*	qPCR	54.9
PP2AA2-R	GCGAAAAACCTGACATCAACAT	*PP2AA2*	qPCR	54.2
amiRH6-F	GCGGCGTTAATATTGGGTAAC	*amiRH6*	qPCR	54.2
amiRH6-R	GTGCAGGGTCCGAGGT	Universal stem-loop primer	qPCR	57.5
U6-F	GATAAAATTGGAACGATACAG	*U6*	qPCR	46.8
U6-R	GGACCATTTCTCGATTTATGCG	*U6*	qPCR	54.1

Chapter 3

Elucidation of the Molecular Function of the DHH1/DDX6-like RHs in mRNA Metabolism

3.1 ABSTRACT

mRNA turnover is an essential process in the regulation of gene expression. As it controls both the quantity and quality of cellular mRNAs, this post-transcriptional process is critical for plant survival and development. In the general pathway of cytoplasmic mRNA degradation, decay of the majority of deadenylated mRNAs is initiated by the multi-subunit decapping complex that removes the the 5′-^{7}mG-cap, exposing the mRNA 5’ end for a hydrolysis by EXORIBONUCLEASE 1/4. Alternatively, the mRNA can be degraded from the 3’ end by the RNA exosome or the 3’-to-5’ exoribonuclease SUPPRESSOR OF VARICOSE (SOV). In Chapter 1, we identified RNA HELICASE 6 (RH6), RH8, and RH12 in A*rabidopsis thaliana* as orthologs of the DHH1/DDX6 family. Genetic analysis established that all the three RHs have redundant function in plant growth and development, as the triple *rh6 rh8 rh12* mutant exhibited severe growth and developmental defects typical of mRNA decapping mutants. Subcellular localization data showed that the DHH1/DDX6-like RHs are components of stress granules and processing bodies, suggesting that they are involved in mRNA degradation and/or decay. In this chapter, to elucidate the molecular functions of RH6, RH8, and RH12 in mRNA decay, we performed a genome-wide analysis of mRNA decay rates after transcriptional arrest in the triple *rh6 rh8 rh12* mutant seedlings using RNA-sequencing (RNA-seq). We found that loss/severe reduction of RH6/8/12 function confers an overall increase in mRNA stability, with 7,277 transcripts stabilized in the triple mutant as

compared to the wild-type. These putative RH6/8/12 decay substrates encode proteins with diverse functions. The degradation of 84% of them requires the VARICOSE (VCS) subunit of the 5'-to-3 decapping pathway. RH6/8/12 substrates were generally short-lived, short-length and less likely to have introns. Genetic analysis revealed that the growth defect of the triple mutant is not associated with RDR6 function. By contrast, transcriptome and translatome analysis of the triple mutant seedlings by use of translating ribosome affinity purification followed by RNA-seq demonstrated that loss of RH6/8/12 function shifts transcriptome and translatome homeostasis to that of constitutive immune response, characterized by an accumulation and enhanced translation of stress- and defense-responsive transcripts under optimal growth conditions, with simultaneous depletion of mRNAs encoding proteins important for growth, development, and primary metabolisms. This alteration was associated with an increased stability, abundance, and ribosome-association of 397 mRNAs related to stress and defense response including immune receptors of the Toll-like/Interleukin 1 receptor and the coiled-coil families, supported by an overaccumulation of the defense hormone salicylic acid (SA) in the triple *rh6 rh8 rh12* mutant. Genetic analysis indicated that the autoimmune phenotype of the triple mutant is partially dependent on PHYTOALEXIN DEFICIENT 4, but not dependent on ENHANCED DISEASE SUSCEPTIBILITY 1. Manipulation of SA accumulation and perception confirmed the autoimmunity displayed by the triple mutant occurs through a SA-partially dependent, but NONEXPRESSER OF PR GENES 1-independent pathway. Finally, we demonstrated that the growth defect as well as constitutive immune response and repression of growth-related mRNAs in the triple mutant was mitigated by expression of a functional *SOV* allele. Our data determined that the *Arabidopsis* DHH1/DDX6-like

RH6, RH8, and RH12 control mRNA decay to suppress stress- and defense-responsive transcripts and augment expression of growth- and development-promoting transcripts to maintain mRNA homeostasis required for plant growth under standard growth conditions.

3.2 INTRODUCTION

Regulation of translation, decay and sequestration is fundamental to cellular cytoplasmic mRNA dynamics. mRNA turnover, in particular, is integral for plant survival and development as it regulates both the quantity and quality of the mRNA pool (Zhang and Guo, 2017; Chantarachot and Bailey-Serres, 2018). In eukaryotes including plants, while some mRNAs are turned over by such specialized pathways as nonsense-mediated decay (NMD) and micro (mi)RNA-mediated silencing (Shaul, 2015; Yu et al., 2017), most cytoplasmic mRNAs are degraded by the general mRNA decay machinery initiated by removal of the poly(A) tail by deadenylases, via a process called deadenylation. The majority of deadenylated mRNAs are attacked at the 5′-^{7}mG-cap by the decapping enzyme DECAPPING 2 (DCP2) mediated by the core decapping factors DCP1 and VARICOSE (VCS, also known as ENHANCER OF DECAPPING 4 [EDC4], HEDLS, or GE-1) and other decapping activators such as EDC3, DCP5 (also known as SCD6, LSM14, RAP55, TRAL, and CAR-1), PROTEIN ASSOCIATED WITH TOPOISOMERASE 1 (PAT1), the LSM1-7 complex, and DHH1/DDX6. Uncapped mRNAs then can be hydrolyzed by the 5’-to-3’ exoribonuclease XRN1/4. Alternatively, deadenylated mRNAs are degraded by the 3’-to-5’ exoribonuclease SUPPRESSOR OF VARICOSE (SOV, also known as RRP44B or DIS3L2), or the multimeric exoribonucleases RNA exosome. In *Arabidopsis*, it has been shown that when one

mRNA decay pathway is not not functional, another pathway can compensate the function to control mRNA turnover, hence homeostasis (Zhang et al., 2010; Sorenson et al., 2018).

DHH1/DDX6 is an ancient family of DEAD-box RNA helicases. Members of this protein family have been described in a wide range of eukaryotic organisms, including the yeast *Saccharomyces cerevisiae* DHH1 (Westmoreland et al., 2003), *Schizosaccharomyces pombe* STE13 (Maekawa et al., 1994), *Caenorhabditis elegans* CGH-1 (Navarro et al., 2001), *Drosophila melanogaster* ME31B (de Valoir et al., 1991), *Xenopus laevis* XP54 (Ladomery et al., 1997), and human DDX6/P54/RCK (Akao et al., 1995). These proteins are remarkably similar in sequence, with human DDX6 sharing 69% identity with yeast DHH1, and able to complement the phenotypes of the *dhh1Δ* mutant (Bergkessel and Reese, 2004), suggesting that they play conserved roles in mRNA metabolism. Like other DEAD-box helicases, DHH1 possess an ATPase activity conferred by the two RecA-like helicase domain, and binds RNA with high nanomolar affinity but without sequence specificity (Ernoult-Lange et al., 2012). Whereas other DEAD-box helicases bind RNA substrates in an ATP-dependent manner (Linder and Jankowsky, 2011), DHH1 binds RNA in the absence of ATP, although its RNA unwinding activity is dependent on ATP binding but not ATP hydrolysis (Ernoult-Lange et al., 2012). Furthermore, DHH1 has a significantly weaker RNA-dependent ATPase activity than other well characterized DEAD-box proteins, most likely due to intermolecular interactions between the N- and C-terminal RecA-like domains that restrict the conformational flexibility, hence the competency of ATP hydrolysis (Cheng et al., 2005; Dutta et al., 2011). It is postulated that the ATPase activity of DHH1 is regulated by other factors that can alter the conformation of its two RecA domains

(Sharif et al., 2013).

The role of DHH1/DDX6 family proteins in mRNA metabolism has been established at the nexus between translation and decay, where the proteins mediate translational repression and initiate mRNA degradation (Presnyak and Coller, 2013). Whether DHH1/DDX6 binding results in translational repression and/or decay of mRNA substrates is primarily dictated by its interacting partners and the composition of mRNA-ribonucleoprotein (mRNPs) complexes with which it associates.

The role of DHH1/DDX6 in translational repression is linked with the conserved translational repressor eIF4E transporter (4E-T) (Nakamura et al., 2004; Nelson et al., 2004; Sengupta et al., 2013). 4E-T binds the cap-binding protein eIF4E at the same site as eIF4G; therefore, 4E-T-DDX6 complex disrupts the eIF4E–eIF4G interaction and inhibits translation initiation (Kinkelin et al., 2012). A study in *Xenopus* oocytes have shown that 4E-T forms complexes with XP54, PAT1, LSM14, and eIF4E in translationally silenced mRNPs required for maternal mRNA storage (Minshall et al., 2007). In the *Drosophila* embryo, the 4E-T ortholog CUP forms complexes with ME31B through an adapter protein TRAL that interacts with the C-terminal RecA-like domain (RecA2) of ME31B through its Phe-Asp-Phe (FDF) motifs (Nakamura et al., 2004; Tritschler et al., 2008). In general, CUP induces translational repression, and maintains mRNA targets in a repressed state by promoting their deadenylation and protects deadenylated mRNAs from further degradation (Igreja and Izaurralde, 2011). During the maternal-to-zygotic transition (MZT) of *Drosophila* embryos, ME31B binds to and represses translation of thousands of maternal mRNAs, but its binding confers different outcomes depending on developmental stages of the embryo. Prior to zygotic genome activation, ME31B binding results in translational repression; however, binding of ME31B

triggers mRNA degradation during the MZT as the abundance CUP, TRAL and ME31B itself decreases (Wang et al., 2017).

Promotion of adenylation by CUP (4E-T) may be mediated by the CCR4-NOT deadenylation complex through an interaction between ME31B (DDX6) and NOT1, a scaffold subunit of the CCR4-NOT complex. In humans, 4E-T directly interacts with the RecA2 domain of DDX6 via its conserved CUP-homology domain (CHD) (Ozgur et al., 2015). Similarly, the RecA2 domain of DDX6 also serves as binding surface for the central MIF4G domain of NOT1 (Chen et al., 2014; Mathys et al., 2014).This DDX6-NOT1 binding surface is also conserved in yeast (Rouya et al., 2014). Nevertheless, the 4E-T-DDX6 interaction can occur both in the presence and absence of NOT1, indicating that DDX6 can bind 4E-T and the CNOT1 subunit of the CCR4-NOT complex simultaneously (Ozgur et al., 2015). Given that DDX6 RecA2 domain used for 4E-T interaction is the same as the surface for DDX6 interactions with the decapping activators EDC3 and PAT1, and that NOT1 binding inhibits the interaction of DDX6 with EDC3 and PAT1, formation of the 4E-T/DDX6/CNOT1 complex likely promotes deadenylation while impairs decapping. In fact, NOT1 binding primes DDX6 toward its active conformation, inducing the ATPase activity (Mathys et al., 2014). ATP hydrolysis by DDX6, in turn, contributes to 4E-T mediated translational repression (Kamenska et al., 2016). Additionally, the role of DDX6-4E-T interaction is extended to miRNA-dependent translational repression and the formation of new processing bodies (PBs), suggesting that translational repression and *de novo* PB assembly are coupled processes (Kamenska et al., 2014; Kamenska et al., 2016). Nonetheless, another study has demonstrated that, instead of stabilizing mRNAs, 4E-T induces turnover of mRNAs targeted by the CCR4-NOT complex, including those mediated by the RNA-binding

protein tristetraprolin and miRNAs (Nishimura et al., 2015). This could represent another mRNP state that DDX6-4E-T complexes bridge translational repression with decay.

The role of DHH1/DDX6 in mRNA decay is most likely modulated by its interaction with different decapping factors. In yeast, DHH1 interacts with the decapping activators LSM1 and PAT1, and the decapping holoenzyme DCP1-DCP2 through DCP1 (Coller et al., 2001). Interaction of DHH1 with PAT1 connects translational repression with decay, as yeast strains lacking both DHH1 and PAT1 are severely impaired in mRNA decapping, and translational repression (Coller and Parker, 2005). As previously mentioned, the RecA2 domain of DHH1/DDX6 interacts with TRAL, EDC3, and PAT1 through their FDF motifs. Apart from 4E-T, binding of PAT1 and EDC3 on the DDX6 RecA2 domain is also mutually exclusive, and this phenomenon is conserved from yeast to humans (Sharif et al., 2013). Similarly, the interaction of DDX6 (ME31B) with EDC3 and TRAL is mutually exclusive (Tritschler et al., 2009). While TRAL and EDC3 are structurally closely related, TRAL associates with CUP and involves in translational repression and/or decay but EDC3 associates with the decapping enzyme DCP2, hence specifically promoting mRNA degradation (Tritschler et al., 2008). PAT1, on the other hand, interacts with the LSM2 and LSM3 subunits of the LSM1-7 complex (Sharif and Conti, 2013). The LSM1-7 complex preferentially associates with the 3' end of polyadenylated mRNAs to protect the last 20-30 nucleotides of the message, and promote mRNA decapping, thereby coupling deadenylation with the 5'-to-3' degradation pathway (Tharun et al., 2000; He and Parker, 2001). Apart from decay factors, DHH1 also associates with ribosomes and senses the codon-dependent rate of translational elongation to trigger decay of non-optimal mRNAs cotranslationally, representing another mode of mRNA turnover (Radhakrishnan et al., 2016). Based on these complex

interactions between DDX6 and different partners, it has been proposed that the DHH1/DDX6 family proteins function as general general regulatory factors, of which the repressive function in translational attenuation and/or mRNA decay, depends on its interacting partners and biological context (Wang et al., 2017).

In Chapter 2, we identified *Arabidopsis* RH6, RH8, and RH12 as members of the DHH1/DDX6 family. Genetic analysis unveiled the role of these proteins in plant growth and development, with the triple *rh6 rh8 rh12* mutant phenocopying several developmental traits observed in mutants of other genes associated with mRNA decapping. Subcellular localization analysis of the DHH1/DDX6-like RHs determined they are components of PBs and SGs, and regulators of PB formation, suggesting that they may exert an important role in mRNA storage and/or degradation. In this chapter, to determine the role of DHH1/DDX6-like RHs in mRNA metabolism, we performed an integrative genome-wide analysis of mRNA decay rate, transcriptome, and translatome comparisons in the triple *rh6 rh8 rh12* mutant and the wild-type seedlings. Our data demonstrate that RH6, RH8, and RH12 play an indispensable role in mRNA degradation and the regulation of transcriptome and translatome homeostasis. Loss of the *RH* function dramatically reconfigures the transcriptome and translatome profiles associated with a depletion and translational repression of mRNAs encoding proteins important for growth and developmental progression, with an ectopic expression of stress- and defense-responsive transcripts under optimal growth conditions as a result of impairment in mRNA decay and translational regulation. Finally, using genetic and transcriptomic approaches, we demonstrate that disruption of transcriptome homeostasis caused by *RH6*, *RH8*, and *RH12* mutations can be reinstated by expression of the 3'-to-5' exoribonuclease *SOV*.

3.3 RESULTS

3.3.1 The triple *rh6 rh8 rh12* mutant is defective in global mRNA decay

To elucidate whether the *Arabidopsis* DHH1/DDX6-like family plays a role in mRNA degradation, we performed genome-wide mRNA decay analysis comparing seedlings of the triple homozygous mutant *rh6 rh8 rh12* and the wild-type (Col-0). As *RH6*, *RH8*, and *RH12* are functionally redundant, we used the *rh6 rh8 rh12* genotype to aviod the functional compensation between the *RH* genes in mRNA decay. This was accomplished by treating 5-day-old seedlings with the transcription inhibitor cordycepin, collectioned after 0, 15, 30, 60 and 120 minutes in 3 independent biological replicates, followed by RNA-seq analysis **(Figure 3.1A)**. To include deadenylated mRNAs and decay intermediates, RNA-seq libraries were prepared from ribosomal RNA-depleted total RNA. Multiplexed sequencing of the libraries provided an average of 22.7 million single-hit mapped reads per sample. Read counts of individual genes were normalized to the library size, and scaled with a decay factor for each library using 30 abundant and stable RNAs to account for the increase in their abundance as RNA decay proceeds (Sorenson et al., 2018). After normalization of the data with the mean abundance of the corresponding initial (T_0) sample, and removal of low abundance transcripts [0 reads in the T_0 of any genotype, and those with a sum of the mean T_0 counts per million (CPM) from both genotypes ≤ 4], the difference in mRNAs decay rates of 18,092 individual genes between the two genotypes was determined using the maximum likelihood functions developed previously (Sorenson et al., 2018). The estimated parameter for variance (σ^2) was used to evaluate the quality of fit of the decay model. We obtained 16,025 genes with $\sigma^2 < 0.0625$, demonstrating a high-quality dataset that was used for subsequent analyses.

Gene-specific initial primary decay rates (α) provided a global view of estimated mRNA half-life ($t_{1/2}$) distributions across 16,025 transcripts. In the wild-type Col-0, mRNA $t_{1/2}$ ranged from 3.8 to 6,931.5 minutes (115.52 hours), with the median $t_{1/2}$ = 160.9 minutes **(Figure 3.1B, Table S1)**. In the triple *rh6 rh8 rh12* mutant, on the other hand, while the estimated maximum $t_{1/2}$ was similar to the wild-type, the minimum $t_{1/2}$ increased to 5.2 minutes, and the median $t_{1/2}$ shifted to 314.1 minutes. This indicates that loss of the RHs promotes an overall increase in mRNA stability. Comparison of the α decay rates of individual mRNAs allowed classification of 16,025 genes into three groups based on their relative decay rate or mRNA $t_{1/2}$ in the triple *rh6 rh8 rh12* mutant and the wild-type. The first group (group 1) included 7,277 mRNAs of which the decay was compromised in the triple mutant, hence a longer $t_{1/2}$ relative to the wild-type (*rh6 rh8 rh12* $t_{1/2}$ > Col-0 $t_{1/2}$) **(Figure 3.1C and 3D, Table S1)**. This group was considered putative RH6/8/12 substrates. The second group represented transcripts (group 2, 487 mRNAs) with accelerated decay, hence a shorter mRNA $t_{1/2}$ in the triple mutant relative to the wild-type (*rh6 rh8 rh12* $t_{1/2}$ < Col-0 $t_{1/2}$). The remainder (group 3) were mRNAs with decay that is independent of RH6/8/12 function as their $t_{1/2}$ was unchanged in the triple mutant (*rh6 rh8 rh12* $t_{1/2} \simeq$ Col-0 $t_{1/2}$) **(Figure 3.1C and 3D, Table S1)**. Gene ontology (GO) enrichment analysis of 7,277 RH6/8/12 substrates revealed an enrichment of over 300 functional categories that encompass a wide range of biological processes including primary metabolic process (GO:0044238, 3,465 genes, adjusted *p*-value [Padj] 2.25E-26), RNA processing (GO:0006396, 385 genes, 4.10E-18), response to abiotic stimulus (GO:0044238, 900 genes, 3.25E-16), post-embryonic development (GO:0009791, 687 genes, 4.30E-14), chromatin organization (GO:0009791, 245 genes, 2.64E-11), response to stimulus (GO:0050896, 2,012 genes, 4.12E-11), and rhythmic process

(GO:0048511, 77 genes, 9.58E-05) **(Figure 3.1E, Table S2)**. This indicates that the *Arabidopsis* DHH1/DDX6-like RHs regulate decay of mRNAs encoding proteins of diverse functions. Next, we were interested to know whether RH6, RH8, and RH12 function in specialized mRNA decay pathways; human DDX6 contributes to micro (mi)RNA-mediated gene silencing (Rouya et al., 2014). Comparison of 72 validated miRNA targets detectable in the 5-day-old seedling transcriptome with RH6/8/12 substrates revealed that only 21 were stabilized in the triple mutant **(Figure 3.1F)**. This was not significant compared to random chance (p = 0.9984, hypergeometric test), suggesting that degradation of miRNA targets may not require RH6, RH8, and RH12 function. Because all the three RHs co-immunoprecipitated with the core nonsense-mediated decay (NMD) factor UP-FRAMESHIFT 1 (UPF1) in *Arabidopsis* (Chicois et al., 2018), we asked whether NMD targets are stabilized in the *rh6 rh8 rh12* genotype. To answer this question, we compared RH6/8/12 substrates with those degraded by the NMD pathway. Among the 391 confirmed NMD substrates (Drechsel et al., 2013) present in our dataset, 197 showed increased mRNA $t_{1/2}$ in the triple *rh6 rh8 rh12* mutant. This is more than expected by random chance (p = 0.0259, hypergeometric test), suggesting that RH6, RH8, RH12 might play a role in NMD.

Next, we explored the characteristics associated with mRNAs of which the decay requires RH6, RH8, and RH12 function. First, we found that RH6/8/12 substrates (group 1) had shorter wild-type mRNA $t_{1/2}$ than mRNAs that do not require the RH function for degradation (group 2 and group 3) **(Figure 3.2A)**. The median wild-type $t_{1/2}$ for RH6/8/12 substrates was 108 minutes, whereas the median wild-type $t_{1/2}$ of those with reduced or unchanged decay rates in the triple mutant were 263 and 299 minutes, respectively. Thus, RH6, RH8, and RH12 regulate turnover of the most short-lived or high-flux

mRNAs of seedlings. Next, we explored mRNA features associated with RH6/8/12 substrates, including number of codons (amino acids) and introns, as well as the length of transcripts, 5' untranslated region (UTR), and 3' UTR. For comparison, the 16,025 genes analyzed were divided into 6 subgroups based on their wild-type mRNA $t_{1/2}$; mRNAs with accelerated decay (group 2) in the triple mutant were excluded as they represent a small group of genes with a special decay profile **(Figure 3.2B)**. For mRNAs with $t_{1/2}$ more than 60 minutes, RH6/8/12 substrates (group 1) had fewer codons, typically fewer introns and shorter transcripts than non-substrate mRNAs (group 3) **(Figure 3.2C)**. The length of the 5' and 3' UTRs appeared inconsequential to the function of these RNA helicases.

Finally, since subcellular localization data showed that all the three RH complexes associate with the core decapping factors DCP2 and VCS, it is most likely that RH6/8/12 substrates are degraded through the 5'-to-3', decapping pathway. To test this hypothesis, we sought to compare RH6/8/12 substrates with those of VCS. To this end, we re-analyzed our previously published mRNA decay data of the *vcs-7* mutant (Sorenson et al., 2018), using the same parameters, time-points, and number of replicates as in the triple *rh6 rh8 rh12* mutant data. We limited the analysis to mRNAs with the wild-type $t_{1/2}$ less than 12 hours as the maximum $t_{1/2}$ of RH6/8/12 substrates was 11.5 hours. Based on these criteria, we recognized 12,697 transcripts, of which 6,941 were identified as RH6/8/12 substrates whereas 9,694 were VCS substrates **(Figure 3.3A)**. Among 6,941 RH6/8/12 substrates identified in the triple mutant decay analysis, 5,832 (84%) overlapped with those of VCS, indicating that they are degraded by the decapping pathway **(Figure 3.3A)**. Comparison of the wild-type mRNA $t_{1/2}$ revealed that mRNAs that require the RHs but not VCS and those that require both the RHs and VCS

for their decay had a shorter $t_{1/2}$ than those that only required VCS but not the RHs or those that require neither the RHs nor VCS for decay **(Figure 3.3B)**. This further supports the notion that RH6/8/12 accelerate the decay of short-lived and high-flux mRNAs.

3.3.2 Mutation of *RNA-DEPENDENT RNA POLYMERASE 6* (*RDR6*) and *SUPPRESSOR OF GENE SILENCING 3* (*SGS3*) did not rescue the triple *rh6 rh8 rh12* mutant

In plants, it is well established that, apart from controlling transcript levels to fine tune protein synthesis, the general mRNA decay pathways also safeguard the transcriptome from undergoing posttranscriptional gene silencing (PTGS) (Liu and Chen, 2016; Tsuzuki et al., 2017; Zhang and Guo, 2017). As nearly half of the seedling transcriptome are not properly degraded in the *rh6 rh8 rh1*2 mutant, it is possible the stabilized transcripts become substrates for double-stranded RNA biosynthesis by RDR6/SGS3, and subsequently siRNA production by DICER-LIKE 2/4 thereby causing PTGS. This might explain growth defects of the triple *rh6 rh8 rh12* mutant. To test whether the triple *rh6 rh8 rh12* mutant phenotype is caused by siRNA-mediated gene silencing, the double homozygous single heterozygous *rh6*$^{(+/-)}$ *rh8 rh12* mutant was crossed with *rdr6*$^{sgs2\text{-}1}$ and *sgs3-1* (Mourrain et al., 2000; Martínez de Alba et al., 2015) to generate the quadruple *rh6 rh8 rh12; rdr6*$^{sgs2\text{-}1}$ and *rh6 rh8 rh12; sgs3-1* genotypes, respectively. Surprisingly, phenotypic analysis revealed that loss of either *RDR6* or *SGS3* function did not alter the *rh6 rh8 rh12* phenotype **(Figure 3.4A and 3.4B)**. This indicates that the effect of RDR6-mediated PTGS on the triple *rh6 rh8 rh12* mutant phenotypes, if any, is negligible.

3.3.3 Loss/reduction of *RH6*, *RH8*, and *RH12* function disrupts seedling transcriptome and translatome homeostasis

The evidence that the growth and developmental defects of the *rh6 rh8 rh12* genotype are independent of RDR6 function led us to hypothesize that these phenotypes might be associated with the dysregulation of mRNA abundance and translation connected with increased stability of a subset of cellular mRNAs. To determine whether and how attenuation of *RH6*/*8*/*12* function affects the steady-state mRNA abundance and translational states at the genome-wide scale, the genotype *rh6*$^{(+/-)}$ *rh8 rh12* was crossed with a wild-type (Col-0) transgenic line expressing His-FLAG-GFP tagged RIBOSOMAL PROTEIN L18 (*pro35S:HF-GFP-RPL18*) (Mustroph et al., 2009b) that enables Translating RIbosome Affinity Purification (TRAP). Five-day-old seedlings of the homozygous triple *rh6 rh8 rh12; pro35S:HF-GFP-RPL18* mutant, together with the parental control line *pro35S:HF-GFP-RPL18*, were used for polysomal RNA isolation by TRAP. Ribosome-associated poly(A)$^+$ mRNAs (henceforth TRAP mRNAs) were used for global translatome analysis by RNA-seq. In parallel, total poly(A)$^+$ mRNAs (henceforth TOTAL mRNAs) isolated from the same samples were used for transcriptome analysis **(Figure 3.5A)**.

Sequencing of multiplexed RNA-seq libraries provided an average of 6.5 million unique mapped reads per library. A principal components analysis of normalized read counts [20,041 genes, ≥ 2 CPMs in any two samples] obtained using the package edgeR (Robinson et al., 2010). showed the reproducibility of the libraries within the genotype and mRNA population **(Figure 3.5B)**. After filtering genes with very low mRNA abundance [≤ 5 reads per kilobase of transcript per million mapped reads (RPKM) in any two samples], genes with a significant change in TOTAL or TRAP mRNA abundance

between the triple *rh6 rh8 rh12; pro35S:HF-GFP-RPL18* mutant and the wild-type *pro35S:HF-GFP-RPL18* seedlings were identified using the differential expression analysis functions of edgeR. In the TOTAL population, ~1,870 mRNAs were enriched, whereas ~1,240 mRNAs were depleted in the triple mutant relative to the wild-type **(Figure 3.5C, Table S3)**. Relatively similar numbers of mRNAs (~1,789) were enriched in the TRAP fraction. However, 36% more mRNAs (~1,687) were depleted in the TRAP fraction as compared to those depleted in the TOTAL mRNA population of the triple mutant, yet these groups were largely overlapping **(Figure 3.5C)**.

Of the differentially expressed genes, the change in TOTAL mRNA abundance correlated well with the change in TRAP mRNA abundance (Pearson correlation = 0.93), suggesting alterations of the steady-state transcriptome were reflected in the translatome in the triple mutant **(Figure 3.5D)**. In this regard, 1,403 (75%) of 1,870 mRNAs enriched in the TOTAL fraction were found enriched in the TRAP fraction **(Figure 3.5E)**. Similarly, among 1,240 transcripts depleted in the TOTAL mRNA population of the triple mutant, 1,003 (81%) were also depleted in the TRAP fraction. However, there was disparity in the change in TOTAL and TRAP mRNA abundance, as a considerable number of genes were enriched or depleted in one fraction but not in the other **(Figure 3.5E)**. These may represent a subset of transcripts that are regulated, directly or indirectly, by RH6, RH8 and RH12 through translational repression and/or decay.

Interestingly, GO enrichment analysis on mRNAs enriched in the TOTAL and TRAP populations of the triple mutant showed consistent overrepresentation of genes in the same classes including response to stress [GO:0006950, 551 genes in TOTAL (1.78E-59), 564 genes in TRAP (3.09E-71)], defense response [GO:0006952, 276

TOTAL (9.05E-33), 287 TRAP (1.07E-44)], immune system process [GO:0002376, 171 TOTAL (1.69E-31), 187 TRAP (1.69E-42)], response to abiotic stimulus [GO:0009628, 326 TOTAL (4.00E-30), 320 TRAP (9.41E-31)], and programmed cell death [GO:0012501, 87 TOTAL (6.42E-17), 95 TRAP (1.46E-22)] **(Figure 3.5F, Table S4)**. Transcripts depleted in the TOTAL mRNA fraction of the triple mutant were overrepresented with GO terms related to general growth and development, such as response to monosaccharide (GO:0034284, 34 genes, 1.83E-11), rhythmic process (GO:0048511, 32 genes, 2.09E-10), regulation of hormone levels (GO:0010817, 56 genes, 3.83E-10), multidimensional cell growth (GO:0009825, 20 genes, 4.16E-08), pigment accumulation in tissues (GO:0043480, 20 genes, 1.20E-05), auxin-activated signaling pathway (GO:0009734, 19 genes, 1.12E-02), epidermis development (GO:0008544, 50 genes, 2.22E-02), and brassinosteroid metabolic process (GO:0016131, 16 genes, 2.32E-02) **(Figure 3.5F, Table S4)**.

Transcripts depleted in the TRAP fraction of the triple mutant were generally represented by the same functional categories as those depleted in the TOTAL mRNA population, but with more number of genes and some additional terms uniquely presented, such as root system development (GO:0022622, 84 genes, 3.08E-11), root hair cell differentiation (GO:0048765, 55 genes, 1.81E-10), cell wall organization or biogenesis (GO:0071554, 108 genes, 2.00E-08), auxin polar transport (GO:0009926, 22 genes, Padj 6.31E-06), and regulation of meristem development (GO:0048509, 36 genes, 1.72E-05) **(Figure 3.5F, Table SAA)**. Overall, these data indicate that, under standard growth conditions, disruption of *RH6*, *RH8*, and *RH12* functions results in an alteration of the seedling transcriptome and translatome profiles into a direction that favors stress/defense responses over growth and development.

3.3.4 Loss of *RH6*/8/*12* function results in mis-regulation and a global decrease in mRNA translation

We further investigated how well each mRNA is translated within each of the two genotypes by comparing the the abundance of mRNAs in the TRAP fraction to the TOTAL mRNA population. These data provided evidence on the translational status of individual mRNAs. In the wild-type Col-0, we found that ~723 mRNAs were translationally enhanced, whereas ~1,306 were translationally repressed **(Figure 3.6A, Table S3)**. Similarly, 533 and 1,289 mRNAs of the triple *rh6 rh8 rh12* mutant were translationally enhanced and repressed, respectively **(Figure 3.6A)**. We were particularly interested in mRNAs that showed enhanced or repressed translational status specifically in the triple mutant as these have mis-regulated translation. Among 533 mRNAs showing an enhanced translational status in the triple mutant, 317 also had enhanced translation in the wild-type, leaving 216 mRNAs with altered translation status as a consequence of the disruption of RH6/8/12 function **(Figure 3.6B)**. GO enrichment analysis revealed that these were enriched for stress-related functional categories, including defense response, incompatible interaction (GO:0009814, 20 genes, 5.10E-07), carboxylic acid metabolic process (GO:0019752, 38 genes, 6.95E-06), systemic acquired resistance (GO:0009627, 15 genes, 1.97E-04), innate immune response (GO:0045087, 20 genes, 1.05E-03), and defense response to other organism (GO:0098542, 25 genes, 1.96E-03) **(Figure 3.6C, Table S5)**.

By performing a similar analysis on the 1,289 mRNAs with repressed translational status in the triple mutant, we found 865 (67.1%) were also translationally repressed in the wild-type, whereas 424 (32.9%) were translationally repressed specifically in the triple mutant **(Figure 3.6B)**. The latter cohort encodes proteins

involved in cell wall organization or biogenesis (GO:0071554, 47 genes, 2.99E-04), tissue development (GO:0009888, 51 genes, 4.73E-03), polysaccharide metabolic process (GO:0005976, 39 genes, 9.21E-03), and post-embryonic morphogenesis (GO:0009886, 25 genes, 3.53E-02) **(Figure 3.6D, Table S5)**. Collectively, these results indicate that, regardless of abundance, the *rh6 rh8 rh12* mutant prioritizes translation of mRNAs encoding proteins related to stress and/or defense response over those required for primary metabolism and development.

Next, we asked how increased mRNA stability of RH6/8/12 substrates affects their translational status in the triple *rh6 rh8 rh12* mutant. We hypothesized that mRNAs that are stabilized in the triple mutant will be more likely to be associated with ribosomes, hence having increased translational status in the triple mutant. To test this hypothesis, meta-analysis of mRNA decay and transcriptome-translatome datasets was performed to compare translational status of mRNAs in the triple mutant with that in the wild-type between the RH6/8/12 substrates (group 1, *rh6 rh8 rh12* $t_{1/2}$ **>** Col-0 $t_{1/2}$) and the rest of the transcriptome (group 2 and 3, *rh6 rh8 rh12* $t_{1/2}$ **≤** Col-0 $t_{1/2}$). Unexpectedly, there was no discernible increase in translational status of RH6/8/12 substrates in the triple mutant relative to the rest of the transcriptome (group 2 and 3) **(Figure 3.6E)**. On the other hand, translational status of both mRNA populations was lower in the triple mutant than in the wild-type, although within the genotype RH6/8/12 substrates had higher ribosome occupancy than those non-substrate mRNAs **(Figure 3.6F)**. Based on these data, we conclude that RH6/8/12 substrates are generally well translated, but loss of *RH6*/8/*12* function does not enhance translation of these mRNAs, rather, loss of *RH6*/*8*/*12* function results in a global decline of mRNA translation.

3.3.5 Stress/defense-related mRNAs are stabilized and well translated in the triple *rh6 rh8 rh12* mutant

Next, we asked whether an increase in stability of RH6/8/12 substrates affects the steady-state abundance of TOTAL and/or TRAP mRNAs in the triple *rh6 rh8 rh12* mutant. To answer this question, a meta-analysis was performed on a combined dataset of mRNA decay and differential expression analysis of transcriptome and translatome data. From a total of 12,351 genes in the combined dataset, ~5,819 mRNAs were identified as RH6/8/12 substrates. The majority of these mRNAs were unchanged in their TOTAL and TRAP mRNA abundance in the triple mutant relative to Col-0 **(Figure 3.7A)**. Only 516 and 529 of them were enriched (log_2 FC > 1, FDR < 0.01) in their TOTAL and TRAP mRNA abundance, respectively. Similarly, 531 and 713 transcripts were depleted (log_2 FC < 1, FDR < 0.01) in the TOTAL and TRAP fractions of the triple mutant, respectively **(Figure 3.7A)**. We were especially interested in transcripts that had increased stability and were simultaneously enriched in abundance, both in the TOTAL and TRAP fractions, in the triple mutant given that this population may provide a clue on the molecular processes underlying the triple mutant phenotype. Comparison of mRNAs that were enriched in these populations with those that were stabilized in the triple mutant identified 397 transcripts with increased stability as well as TOTAL and TRAP mRNA abundance in the triple mutant **(Figure 3.7B)**. Next, we determined whether translation status of these transcripts increased in the triple mutant relative to the wild-type. As a control we compared translation status of these mRNAs with those that were enriched in both TOTAL and TRAP populations but found their stability were unaffected in the triple mutant. Although we previously showed that the overall ribosome association of mRNAs was lower in the triple mutant as compared to the wild-type

(Figure 3.6F), mRNAs that were enriched in their TOTAL and TRAP abundance in the triple mutant had increased translational status both in RH6/8/12 substrates and non-substrates **(Figure 3.7C)**. However, RH6/8/12 substrates were more translationally enriched in the triple mutant than those non-substrate mRNAs, whereas translational status of these two mRNA populations were not different in the wild-type **(Figure 3.7C)**. These data indicate that, despite a global decline in mRNA-ribosome association in the triple mutant, a subset of transcripts, specifically those with increased abundance concomitant with increased stability, are more actively engaged in translation in the triple mutant. GO enrichment analysis demonstrated that this particular group of mRNAs encode for proteins involved in stress response-related functional categories, such as response to stress (GO:0006950, 115 genes, 2.67E-07), response to abiotic stimulus (GO:0009628, 80 genes, 3.05E-07), response to wounding (GO:0009611, 23 genes, 4.56E-07), defense response (GO:0006952, 61 genes, 6.76E-06), response to jasmonic acid (GO:0009753, 25 genes, 3.18E-05), and immune system process (GO:0002376, 37 genes, 9.88E-05) **(Figure 3.7D, Table S5).** Many of these stabilized and well-translated mRNAs encoded for regulators of plant immunity, *e.g. PLANT DEFENSIN 2.1* (*PDF2.1*), *PHYTOALEXIN DEFICIENT 4* (*PAD4*), *CORONATINE-INDUCED PROTEIN 1* (*CORI1*), *WRKY DNA-BINDING PROTEIN 33* (*WRKY33*), and *CYTOCHROME P450 FAMILY 81 SUBFAMILY D POLYPEPTIDE 11* (*CYP81D11*) **(Figure 3.7E)**. This suggests that defense/stress-related mRNAs are preferably translated in the triple mutant. This is mostly likely facilitated by the increase in their stability and abundance, but may also reflect a decline in translation-coupled turnover of these transcripts.

3.3.6 The *rh6 rh8 rh12* mutant displays a constitutive autoimmune response through a pathway partially dependent on *PHYTOALEXIN DEFICIENT 4*, but independent of *ENHANCED DISEASE SUSCEPTIBILITY 1*

Differential expression analysis of steady-state mRNA abundance and translational status indicates that *rh6 rh8 rh12* mutant seedlings exhibit a constitutive immune response. In the absence of pathogens, transcripts involved in pathogen defense and systemic acquired resistance (SAR) were enriched in both the transcriptome and translatome of the triple mutant **(Figure 3.8A)**. Among the most highly induced transcripts were the salicylic acid (SA) inducible SAR markers *PATHOGENESIS-RELATED 1* (*PR1*), *PR2* and *PR5* (Malamy et al., 1990) **(Figure 3.8A)**. Consistently, the defense hormone SA was significantly elevated in the triple mutant as compared to the wild-type **(Figure 3.8B)**, supported by an enrichment of *ISOCHORISMATE SYNTHASE 1* (*ICS1*) transcripts encoding a key enzyme in SA biosynthesis **(Figure 3.8A)**. This was not surprising as the disruption of *RH6*/*8*/*12* resulted in stabilization and a concomitant increased translation status of several transcripts involved in defense **(Figure 3.7D and 3.7E)**. Inhibition of growth attributed to autoimmunity have been demonstrated in other mRNA decay mutants, including *upf1* and *smg7* defective in the NMD pathway, and *protein-associated with topoisomerase 1* (*pat1*) with impair in mRNA decapping (Riehs-Kearnan et al., 2012; Roux et al., 2015). The autoimmune phenotypes in these mutants can be suppressed by inactivation of the immune regulator ENHANCED DISEASE SUSCEPTIBILITY 1 (EDS1) and/or PAD4 (Riehs-Kearnan et al., 2012; Gloggnitzer et al., 2014; Roux et al., 2015). These pathways are likely to be regulated by RH6/8/12 based on two observations. *PAD4* transcripts were stabilized and well translated with transcript enrichment in both TOTAL

and TRAP populations of the triple mutant **(Figure 3.7E and 3.8A)**. Additionally, the majority of EDS1/PAD4-induced mRNAs were enriched in the triple mutant transcriptome and translatome **(Figure 3.8C)**.

As PAT1 orthologs of yeast and humans form complexes with DHH1/DDX6 to mediate translational repression and promote mRNA decapping (Sharif et al., 2013; Ozgur et al., 2015), we hypothesized that these functions might be conserved in plants, and that the autoimmune phenotypes of the triple *rh6 rh8 rh12* mutant could be mediated by a similar mechanism as in the *pat1* and *upf1* mutants. To determine whether inactivation of *EDS1* and *PAD4* functions attenuates the constitutive immunity of the triple mutant, we crossed *rh6*$^{(+/-)}$ *rh8 rh12* with *eds1-2* and *pad4-1* mutants (Col-0 background). Interestingly, comparison of the growth phenotypes revealed a significant improvement in growth, based on rosette size and fresh weight, of the homozygous *rh6 rh8 rh12; pad4-1* genotype as compared to the triple *rh6 rh8 rh12* and the quadruple *rh6 rh8 rh12; eds1-2* mutants **(Figure 3.8D and 3.8E)**. This was more evident in the triple homozygous single heterozygous *rh6*$^{(+/-)}$ *rh8 rh12*; *pad4-1* plants, as their improved rosette growth was more apparent whereas growth phenotypes of *rh6*$^{(+/-)}$ *rh8 rh12*; *eds1-2* plants were not different from those of the diminutive *rh6 rh8 rh12* mutant **(Figure 3.8D and 3.8E)**.

Consistent with the rescued growth phenotypes, the elevation of *PR1* transcripts was diminished in seedlings of the *rh6 rh8 rh12; pad4-1* genotype relative to its levels in *rh6 rh8 rh12* and *rh6 rh8 rh12; eds1-2* **(Figure 3.8F)**. However, *PR1* transcripts in the *rh6 rh8 rh12; pad4-1* genotype remained higher than those in the wild type Col-0 and the control *eds1-2* and *pad4-1* mutants. Disruption of *EDS1* function, on the other hand, did not attenuate the constitutive elevation of *PR1* transcripts in *rh6 rh8 rh12* seedlings

(Figure 3.8F). Rather, loss of *EDS1* function resulted in higher accumulation of SA in the *rh6 rh8 rh12; eds1-2* seedlings as compared to *rh6 rh8 rh12* and *rh6 rh8 rh12; pad4-1* seedlings **(Figure 3.8G)**. Despite a decrease in *PR1* transcript induction, SA content in the *rh6 rh8 rh12; pad4-1* genotype remained as high as in *rh6 rh8 rh12* **(Figure 3.8G)**. These data indicate that constitutive immunity exhibited by the triple *rh6 rh8 rh12* mutant occurs in an EDS1-independent manner, and that inactivation of *PAD4* function is not sufficient to prevent the autoimmune response in the triple *rh6 rh8 rh12* mutant.

3.3.7 Ectopic expression of the bacterial salicylate hydroxylase *NahG* rescues the triple *rh6 rh8 rh12* mutant phenotype

Given that a constitutive immune response in the triple *rh6 rh8 rh12* mutant does not require *EDS1* or *PAD4* function, we hypothesized that the autoimmunity may result from additive effects of multiple pathways, leading to the overaccumulation of SA and activation of the downstream responses. Therefore, we tested whether manipulation of SA metabolism could suppress this constitutive immune response **(Figure 3.9A)**. In this regard, we asked whether a reduction in SA biosynthesis by mutation of *ICS1* would suppress the immune response and reduce the inhibition of growth displayed in the *rh6 rh8 rh12* mutant. Also, we asked whether mutation of *NONEXPRESSER OF PR GENES 1* (*NPR1*), a SA receptor, as well as ectopic overexpression of the bacterial salicylate hydroxylase *NahG*, which hydrolyzes SA into the inactive compound cetachol, would suppress the autoimmunity and developmental phenotypes of *rh6 rh8 rh12*. To answer these questions, the *rh6*$^{(+/-)}$ *rh8 rh12* genotype was crossed with *ics1* and *npr1-3* mutants as well as the wild-type transgenic *Arabidopsis* expressing *NahG* to generate the quadruple *rh6 rh8 rh12; ics1* and *rh6 rh8 rh12; npr1-3* mutants, and the triple *rh6 rh8*

rh12 mutant with the transgene *NahG* (*rh6 rh8 rh12; NahG*) genotypic combinations. Phenotypic analysis revealed that rosette growth (rosette diameter and fresh weight) of the *rh6 rh8 rh12; ics1* and *rh6 rh8 rh12; npr1-3* genotypes were not significantly different from that of the triple *rh6 rh8 rh12* mutant **(Figure 3.9B and 3.9C)**. On the other hand, a significant increase in rosette growth was seen for *rh6 rh8 rh12; NahG* plants as compared to *rh6 rh8 rh12* **(Figure 3.9B and 3.9C)**. This change in phenotype was concomitant with reduced *PR1* transcript abundance in the quadruple *rh6 rh8 rh12; ics1* and *rh6 rh8 rh12; npr1-3* mutants, and the triple *rh6 rh8 rh12; NahG* mutants **(Figure 3.9D)**. Nevertheless, *PR1* mRNA levels in the *rh6 rh8 rh12; ics1* and *rh6 rh8 rh12; npr1-3* genotypes were still significantly higher than in the wild-type Col-0, *ics1* and *npr1-3* mutants, and the wild-type Col-0 with the *NahG* transgene. By contrast, *PR1* transcripts in the *rh6 rh8 rh12; NahG* genotype were reduced to the same levels as in the wild-type Col-0, *ics1* and *npr1-3* mutants, and the wild-type Col-0 expressing the *NahG* transgene **(Figure 3.9D)**. However, although *PR1* transcript levels in the *rh6 rh8 rh12; NahG* genotype were reduced to the wild-type levels, the rosette sizes and fresh weights of *rh6 rh8 rh12; NahG* plants were still significantly lower than those of the wild-types. These data indicate that the attenuation of growth of *rh6 rh8 rh12* is partly but not entirely due to a SA-mediated constitutive immune response.

3.3.8 Expression of the Landsberg *erecta* (L.*er*) allele of *SUPPRESSOR OF VARICOSE* (*SOV*$^{L.er}$) rescues the triple *rh6 rh8 rh12* mutant

Arabidopsis SOV, also known as RRP44 HOMOLOG B (RRP45B), is a conserved 3'-to-5' exoribonuclease orthologous to the yeast DIS3-like exonuclease 2 (DIS3L2) (Zhang et al., 2010; Kumakura et al., 2013). In wild-type seedings, SOV is

responsible for degradation of approximately 1,825 transcripts (Sorenson et al., 2018). We performed a meta-analysis on 12,697 genes (Col-0 $t_{1/2}$ < 12 hours) comparing transcripts that are stabilized in the *rh6 rh8 rh12* mutant (RH6/8/12 substrates, *n* = 6,941) with those that are substrates of SOV (*n* = 1,170), and found the overlap of 622 genes (8.96%) **(Figure 3.10A)**. Degradation of these 622 transcripts could be mediated by RH6/8/12 and/or SOV. Interestingly, SOV has lost its catalytic activity in some *Arabidopsis* ecotypes, including Col-0. Previous work has shown that expression of the catalytically active L.*er* allele of *SOV* can suppress developmental defects of the decapping mutant *vcs-7* as $SOV^{L.er}$ can compensate VCS function in mRNA degradation (Zhang et al., 2010; Sorenson et al., 2018). In our meta-analysis, comparison of RH6/8/12 substrates (*n* = 6,941) with those of VCS that can be degraded by SOV in the *vcs-7* mutant (*n* = 5,344) identified 3,112 transcripts that overlap between the two populations **(Figure 3.10A)**, suggesting that these mRNAs might as well be degraded by SOV in the triple *rh6 rh8 rh12* mutant. Due to the overlap between RH6/8/12 and SOV substrates from the above comparisons, we assumed that SOV might be able to compensate RH6, RH8, and RH12 function in mRNA decay. However, we were not able to see this effect since the triple *rh6 rh8 rh12* mutant was in the Col-0 background, which contains the catalytically inactive SOV. Therefore, we crossed the double homozygous single heterozygous $rh6^{(+/-)}$ *rh8 rh12* mutant with the wild-type Col-0 containing the L.*er* allele of *SOV* [Col-0 $SOV^{L.er}$, driven by the native promoter (Zhang et al., 2010)] to generate the triple *rh6 rh8 rh12* mutant with the L.*er* allele of *SOV* (*rh6 rh8 rh12;* $SOV^{L.er}$), with the hypothesis that if $SOV^{L.er}$ could compensate RH6/8/12 function, the *rh6 rh8 rh12;* $SOV^{L.er}$genotype would show rescued growth phenotypes. Indeed, phenotypic analysis of the homozygous *rh6 rh8 rh12;* $SOV^{L.er}$ plants revealed that their

rosette diameter and fresh weight were significantly higher than those of the triple *rh6 rh8 rh12* plants **(Figure 3.10B, 3.10C and 3.10D)**. This supports our hypothesis that SOV can compensate RH6/8/12 function.

Next, we asked whether complementation of the triple *rh6 rh8 rh12* mutant phenotype by SOV would be more efficient if $SOV^{L.er}$ is expressed under a constitutive promoter. To answer this question, we crossed the $rh6^{(+/-)}$ *rh8 rh12* plants with a transgenic line expressing a translational fusion of $SOV^{L.er}$*-CFP* under the 35S promoter ($SOV^{L.er}$*-OX*). This construct has been shown to rescue the *vcs-7* mutant (Zhang et al., 2010). Strikingly, we found that the rosette growths of the homozygous *rh6 rh8 rh12;* $SOV^{L.er}$*-OX* genotype were significantly improved as compared to the *rh6 rh8 rh12* and *rh6 rh8 rh12;* $SOV^{L.er}$ genotypes **(Figure 3.10E, 3.10F and 3.10G)**. Collectively, these data indicate that $SOV^{L.er}$, especially when overexpressed, can complement the triple *rh6 rh8 rh12* mutant phenotype, suggesting that the 3'-to-5' mRNA decay pathway mediated by SOV is able to compensate RH6/8/12 function. As *SOV* encodes a cytoplasmic ribonuclease, these data further accentuate that the growth and developmental defect present in the triple *rh6 rh8 rh12* mutant is directly associated with the loss of RH6, RH8, and RH12 function in cytoplasmic mRNA decay.

3.3.9 Comparative transcriptome profiling of the triple *rh6 rh8 rh12* and the rescued triple *rh6 rh8 rh12;* $SOV^{L.er}$*-OX* mutants

It is interesting that the triple *rh6 rh8 rh12* and the rescued triple *rh6 rh8 rh12;* $SOV^{L.er}$*-OX* mutants had relatively similar size and appearance at the seedling stage **(Figure 3.11A)**, but the *rh6 rh8 rh12;* $SOV^{L.er}$*-OX* genotype partially rescued rosette stage leaf expansions and fecundity, whereas the triple *rh6 rh8 rh12* mutant remained

miniscule and sterile. As the *rh6 rh8 rh12* mutant exhibits transcriptome and translatome profiles of a stress-responsive state, we hypothesized that *SOV* overexpression might alleviate this effect by reducing abundance of transcripts that limit growth. To test this hypothesis and gain more insight into the underpinnings of the rescued *rh6 rh8 rh12; $SOV^{L.er}$-OX* phenotype, we performed poly(A)$^+$-selected RNA-seq on 7-day-old seedlings comparing the rescued triple *rh6 rh8 rh12; $SOV^{L.er}$-OX* genotype with its severely defective counterpart *rh6 rh8 rh12* and the control genotypes Col-0 and *$SOV^{L.er}$-OX* **(Figure 3.11A)**. The RNA-seq analysis was performed in three biological replicates, yielding an average of 13.7 million single-mapped reads per library. A PCA of edgeR-normalized read counts [19,894 genes, ≥ 2 CPMs in any two samples] confirmed the reproducibility of the RNA-seq libraries of the four genotypes **(Figure 3.11B)**. Based on PCA, overexpression of *$SOV^{L.er}$* did not have any obvious impact on the Col-0 wild-type transcriptome. Conversely, the *$SOV^{L.er}$* overexpression strongly influenced the *rh6 rh8 rh12* mutant transcriptome, as the rescued triple *rh6 rh8 rh12; $SOV^{L.er}$-OX* genotype plotted separately from the triple mutant as well as the control genotypes Col-0 and *$SOV^{L.er}$-OX* **(Figure 3.11B)**.

After removing genes with very low transcript abundance, differential expression analysis was performed across the genotypes on 14,476 genes [> 5 reads RPKM in any two samples]. Transcripts with $|\log_2 FC| \geq 1$ and FDR < 0.01 were considered differentially expressed. In line with PCA, only 25 genes were differentially expressed in the *$SOV^{L.er}$-OX* line relative to Col-0. As expected, *SOV* was enriched in the *$SOV^{L.er}$-OX* line relative to Col-0 ($\log_2$ FC = 4.45, FDR = 3.37E-205) **(Figure 3.11C, Table S6)**. Similar to what was observed in the 5-day-old seedling transcriptome, ~1841 transcripts were found enriched ($\log_2$ FC ≥ 1, FDR < 0.01) and ~1060 transcripts were depleted

(log_2 FC ≤ 1, FDR < 0.01) in the triple mutant relative to the wild-type Col-0. Similarly, ~1,865 transcripts were enriched and ~1,136 transcripts were depleted in the triple mutant relative to *SOV$^{L.er}$-OX*. GO enrichment analysis on transcripts enriched in the triple mutant relative to the wild-type Col-0 and *SOV$^{L.er}$-OX* confirmed our 5-day-old seedling transcriptome and translatome data, showing an overrepresentation of genes involved in defense and stress responses, with prominent GO terms including response to stress [GO:0006950, 656 genes (Padj 4.91E-106) in the triple mutant relative to Col-0, 646 genes (Padj 5.96E-99) in the triple mutant relative to *SOV$^{L.er}$-OX*], defense response [GO:0006952, 377 genes (4.99E-89) in the triple mutant relative to Col-0, 359 genes (5.33E-77) in the triple mutant relative to *SOV$^{L.er}$-OX*] and systemic acquired resistance [GO:0009627, 153 genes (5.09E-67) in the triple mutant relative to Col-0, 144 genes (1.54E-58) in the triple mutant relative to *SOV$^{L.er}$-OX*] **(Table S7)**. Likewise, transcripts depleted in the triple mutant relative to Col-0 and *SOV$^{L.er}$-OX* were enriched in those associated with primary metabolisms and plant development, including rhythmic process [GO:0048511, 28 genes (1.78E-09) in the triple mutant relative to Col-0, 25 genes (1.91E-06) in the triple mutant relative to *SOV$^{L.er}$-OX*], response to monosaccharide [GO:0034284, 26 genes (1.30-8.80E-07) in the triple mutant relative to Col-0 and *SOV$^{L.er}$-OX*], polysaccharide metabolic process [GO:0005976, 69 genes (8.21E-09) in the triple mutant relative to Col-0, 73 genes (9.78E-09) in the triple mutant relative to *SOV$^{L.er}$-OX*], multidimensional cell growth [GO:0009825, 13 genes (1.66E-03) in the triple mutant relative to Col-0, 14 genes (8.30E-04) in the triple mutant relative to *SOV$^{L.er}$-OX*], stomatal complex morphogenesis [GO:0010103, 19 genes (3.66E-04) in the triple mutant relative to Col-0, 18 genes (5.43E-03) in the triple mutant relative to *SOV$^{L.er}$-OX*], and primary metabolic process [GO:0044238, 452 genes (1.49E-02) in the

triple mutant relative to Col-0, 492 genes (1.20E-02) in the triple mutant relative to *SOV$^{L.er}$-OX*] **(Table S7)**. Overexpression of *SOV$^{L.er}$* in the triple mutant resulted in a reduction in the number of differentially expressed genes. A large cohort of ~1,245 transcripts were enriched and ~561 were depleted in the rescued triple *rh6 rh8 rh12; SOV$^{L.er}$-OX* mutant relative to Col-0. Similarly, ~1,222 transcripts were enriched and ~556 were depleted relative to the *SOV$^{L.er}$-OX* line **(Figure 3.11C)**. GO functional categories of mRNAs differentially expressed in the rescued triple *rh6 rh8 rh12; SOV$^{L.er}$-OX* mutant were generally similar to those differentially expressed in the triple *rh6 rh8 rh12* mutant, but in most cases with a reduction in the number of genes presented and the level of significance (Padj). These include the terms response to stress [463 genes relative to Col-0 (4.79E-80), 447 genes relative to *SOV$^{L.er}$-OX* (3.41E-75)], defense response [276 genes relative to Col-0 (4.99E-89), 261 genes relative to *SOV$^{L.er}$-OX* (3.18E-71)] and systemic acquired resistance [106 genes relative to Col-0 (6.05E-45), 100 genes relative to *SOV$^{L.er}$-OX* (9.47E-41)] among those that are enriched, and the terms rhythmic process [20 genes relative to Col-0 (5.05E-09), 19 genes relative to *SOV$^{L.er}$-OX* (5.48E-08)] and response to monosaccharide [17 genes relative to Col-0 (3.57E-06), 20 genes relative to *SOV$^{L.er}$-OX* (1.38E-08)] among those that are depleted in the rescued triple *rh6 rh8 rh12; SOV$^{L.er}$-OX* mutant **(Table S7)**. Comparison of genes differentially expressed in the rescued triple *rh6 rh8 rh12; SOV$^{L.er}$-OX* mutant relative to its counterpart *rh6 rh8 rh12* identified ~212 enriched and ~384 depleted transcripts **(Figure 3.11C)**. Transcripts that were enriched in the rescued line represent genes involved in cellular response to chemical stimulus (GO:0070887, 33 genes, 3.06E-05), response to hormone (GO:0009725, 30 genes, 3.48E-04), cellular response to hydrogen peroxide (GO:0070301, 8 genes, Padj 2.81E-03), and rhythmic process (GO:0048511, 8

genes, 4.86E-03) **(Table S7)**. A group of 384 transcripts depleted in the rescued line had enrichment for defense-related GO functional categories, including defense response incompatible interaction (GO:0009814, 63 genes, 3.03E-38), salicylic acid biosynthetic process (GO:0009697, 43 genes, 9.18E-36), and systemic acquired resistance (GO:0009627, 56 genes, 3.19E-35) **(Table S7)**. Overall, the presence of *SOV*$^{L.er}$ minimized the number of genes that are differentially expressed in the triple *rh6 rh8 rh12* mutant, demonstrating that 3' to 5' decay of high fluence transcripts can be carried out by SOV when RH6/8/12 function is handicapped.

3.3.10 *SOV*$^{L.er}$ overexpression restores the transcriptome homeostasis of the *rh6 rh8 rh12* triple mutant

To gain further insight into the effect of *SOV*$^{L.er}$ overexpression on the triple *rh6 rh8 rh12* mutant transcriptome, clustering was performed on a set of 3,611 differentially expressed genes using the Partitioning Around Medoids (PAM) algorithm. PAM clustering identified 8 gene clusters based on the patterns of change in transcript abundance in the triple *rh6 rh8 rh12* mutant and the rescued triple *rh8 rh8 rh12; SOV*$^{L.er}$*-OX* genotype relative to the wild-type Col-0 and the control *SOV*$^{L.er}$*-OX* line **(Figure 3.12A)**. Clusters 1 (*n* = 118) and 2 (*n* = 299) represent transcripts that were highly induced in the triple mutant relative to the control genotypes Col-0 (mean $\log_2$ FC = 6.29 and 3.16, respectively) and *SOV*$^{L.er}$*-OX* (mean $\log_2$ FC = 6.18 and 3.17, respectively). However, the elevation of transcripts in these clusters was lessened in the rescued triple *rh6 rh8 rh12; SOV*$^{L.er}$*-OX* genotype (mean $\log_2$ FC = 4.60 and 2.45 relative to Col-0, and 4.49 and 2.47 relative to *SOV*$^{L.er}$*-OX*). In other words, these transcripts were depleted in *rh6 rh8 rh12; SOV*$^{L.er}$*-OX* relative to the triple *rh6 rh8 rh12* mutant (mean $\log_2$ FC = -1.70

and -0.71, respectively) **(Figure 3.12A)**. Not unexpectedly, the clusters were enriched for genes encoding proteins involved in defense response, with several GO categories shared by the two clusters, such as innate immune response [GO:0045087, 33 genes (1.32E-21) in cluster 1, 52 genes (1.38E-22) in cluster 2], salicylic acid biosynthetic process [GO:0009697, 20 genes (5.00E-20) in cluster 1, 21 genes (1.78E-12) in cluster 2], and response to biotic stimulus [GO:0009607, 37 genes (2.72E-16) in cluster 1, 77 genes (7.97E-27) in cluster 2] **(Figure 3.12B, Table S8)**. Similar to those in clusters 1 and 2, cluster 3 (*n* =543) and cluster 4 (*n* = 779) transcripts were also increased when RH6/8/12 function was compromised, although to lower magnitudes, in the triple mutant relative to Col-0 (mean $\log_2$ FC = 1.91 and 1.15, respectively) and *SOV$^{L.er}$-OX* (mean $\log_2$ FC = 1.90 and 1.21, respectively). *SOV$^{L.er}$* seedlings reduced constitutive levels of these transcripts (mean $\log_2$ FC *rh6 rh8 rh12; SOV$^{L.er}$-OX*/Col-0 = 1.33 and 0.51 in cluster 3 and cluster 4, respectively; mean $\log_2$ FC *rh6 rh8 rh12; SOV$^{L.er}$-OX*/*SOV$^{L.er}$-OX* = 1.31 and 0.57 in cluster 3 and cluster 4, respectively) **(Figure 3.12A)**. The majority of genes in these two clusters were also associated with response to chemical [GO:0042221, 184 genes (3.56E-33) in cluster 3, 219 genes (1.16E-22) in cluster 4], response to stress [GO:0006950, 197 genes (1.50E-25) in cluster 3, 235 genes (1.16E-22) in cluster 4], and defense response [GO:0006950, 103 genes (5.53E-31) in cluster 3, 116 genes (3.55E-13) in cluster 4] **(Figure 3.12B, Table S8)**. By contrast, cluster 5 transcripts (*n* =450) were enriched in the triple mutant relative to Col-0 and the *SOV$^{L.er}$-OX* genotype (mean $\log_2$ FC = 1.02 and 0.94, respectively), but remained at the same levels or further enriched in the rescued triple in comparison to Col-0 and *SOV$^{L.er}$-OX* (mean $\log_2$ FC = 1.33 and 1.25, respectively). Thus, these transcripts were slightly enriched in the rescued triple relative to the triple mutant (mean $\log_2$ FC = 0.31) **(Figure**

3.12A). These transcripts were enriched with stress-related GO categories, such as response to wounding (GO:0009611, 33 genes, 1.60E-14), response to stimulus (GO:0050896, 185 genes, 2.68E-14), defense response (GO:0006952, 80 genes, 3.65E-13), jasmonic acid biosynthetic process (GO:0009695, 20 genes, 1.72E-11), response to jasmonic acid (GO:0009753, 30 genes, 8.34E-08), programmed cell death (GO:0012501, 27 genes, 2.98E-06), and response to salicylic acid (GO:0009751, 25 genes, 8.26E-05) **(Figure 3.12B, Table S8)**.

Cluster 6 represented 310 transcripts that were depleted in the triple mutant relative to Col-0 and *SOV*$^{L.er}$*-OX* genotypes (mean $\log_2$ FC = -2.06 and -2.13, respectively), but were less depleted in the rescued triple genotype (mean $\log_2$ FC = -1.38 and -1.45, respectively). As a result, cluster 6 transcripts were more abundant in the rescued triple than in the triple mutant (mean $\log_2$ FC = 0.68) **(Figure 3.12A)**. Transcripts in this cluster were enriched with the GO terms circadian rhythm (GO:0007623, 14 genes, 8.13E-08), response to monosaccharide (GO:0034284, 13 genes, 3.34E-06), and starch metabolic process (GO:0005982, 12 genes, 6.25E-04) **(Figure 3.12B, Table S8)**. Similar to those in cluster 6, cluster 7 mRNAs (*n* = 772) were depleted, although to a lesser extent, in the triple mutant as compared to Col-0 and *SOV*$^{L.er}$*-OX* genotypes (mean $\log_2$ FC = -1.16 and -1.23, respectively), but their abundance were unchanged/slightly depleted in the rescued triple relative to Col-0 and *SOV*$^{L.er}$*-OX* (mean $\log_2$ FC = -0.55 and -0.62, respectively) **(Figure 3.12A)**. Transcripts in this cluster represented those involved with primary metabolic process (GO:0044238, 360 genes, 2.06E-05), multidimensional cell growth (GO:0009825, 12 genes, 4.02E-04), cell wall organization or biogenesis (GO:0071554, 46 genes, 1.32E-02), and tissue development (GO:0009888, 52 genes, 4.69E-02) **(Figure 3.12B, Table S8)**. Cluster 8

represented genes of which the transcripts were slightly depleted in the triple mutant relative to Col-0 and *SOV*$^{L.er}$*-OX* (mean $\log_2$ FC = -0.92 and -0.83, respectively), but were further depleted or unchanged in the rescued triple relative to Col-0 and *SOV*$^{L.er}$*-OX* (mean $\log_2$ FC = -1.20 and -1.11, respectively) **(Figure 3.12A)**. This cluster was enriched with genes involved in the light reaction of photosynthesis (GO:0015979, 19 genes, 7.33E-08) and generation of precursor metabolites and energy (GO:0006091, 20 genes, 1.87E-03) **(Figure 3.12B, Table S8)**. By focusing on the analysis of transcripts that were induced both in transcriptome and translatome abundance **(Figure 3.8A)** in the triple mutant, we confirmed the anticipated decrease in their abundance in the rescued triple *rh6 rh8 rh12; SOV*$^{L.er}$*-OX* mutant **(Figure 3.12C)**. In line with these data, SA content in the rescued triple *rh6 rh8 rh12; SOV*$^{L.er}$*-OX* mutant was significantly diminished as compared to the triple *rh6 rh8 rh12* mutant, although it was still higher than in the wild-type Col-0 and the control *SOV*$^{L.er}$*-OX* line **(Figure 3.12D)**. Altogether, these data demonstrate that high near-constitutive expression of a functional *SOV* allele reverses the effect of loss of RH6/8/12 function on the transcriptome. These data indicate that the role of turnover of high flux RNAs mediated by RH6/8/12, as a component of the 5' to 3' decapping complex, can be assumed by the 3' to 5' decay activity of SOV. Thus, two distinct RNA turnover pathways overlap in functional specificity for maintaining the decay of transcripts associated with plant stress/defense response under non-stress conditions, and increasing the expression of those important for growth, development and primary metabolism.

3.4 DISCUSSION

The results of Chapter 2 revealed that the *Arabidopsis* DHH1/DDX6-like proteins RH6, RH8, and RH12 are integral for plant growth and development, with the triple *rh6 rh8 rh12* mutant showing several developmental phenotypes related to mRNA decapping mutants. Additionally, subcellular localization of these functionally redundant proteins determined that they are components of PB and SG, suggestive of a role in cytoplasmic mRNA metabolism. Our genetic analyses indicate nearly complete functional redundancy between *rh6, rh8* and *rh12,* with a progressive increase in the rescue of the developmental defects with each functional copy of any of these genes. The functional redundancy of the three DHH1/DDX6-like observations was further substantiated by the rescue of rosette biomass and fertility by an *RH6* transgene, driven by its native promoter. The results of this chapter establish that the *Arabidopsis* DHH1/DDX6-like RHs function in the turnover and translational repression of a subset of cellular transcripts, modulating cellular mRNA homeostasis required for normal growth and development. Key targets of RH6/8/12 turnover are transcripts associated with plant immunity.

3.4.1 Role of the *Arabidopsis* DHH1/DDX6-like family in mRNA degradation

The role of DHH1/DDX6 RNA helicase family proteins in mRNA turnover is mainly demonstrated in the yeast *S. cerevisiae*, where DHH1 promotes decapping of deadenylated mRNAs and stimulates their decay (Coller and Parker, 2005; Carroll et al., 2011; Sweet et al., 2012; Mota et al., 2014). Similar to what observed in yeast, our genome-wide analysis of mRNA decay after transcriptional arrest by cordycepin revealed that RH6, RH8, and RH12 are required for mRNA degradation, as nearly half of

the seedling transcriptome is stabilized in the triple *rh6 rh8 rh12* mutant. The 7,277 transcripts with significantly decreased decay rates in seedlings are considered RH6/8/12 decay substrates and encode for proteins with diverse biological functions. The 84% overlap between the RH6/8/12 decay substrates with 9,694 transcripts with significantly decreased decay rates in a *vcs* mutant (Sorenson et al., 2018), thereby targeted by the core decapping protein VCS, strongly supports the conclusion that RH6, RH8, and RH12 are components of the 5'-to-3' decay machinery. The functional redundancy of *RH6*, *RH8*, and *RH12* indicates that the product of only one locus is sufficient for the contribution of this helicase to the mRNA decay process. This corroborates our subcellular localization data, in which all the three RHs colocalized with DCP2 and VCS in cytoplasmic PB complexes.

Our findings also support the notion that mRNA decay does not necessary occur in PBs as the triple *rh6 rh8 rh12* mutant was impaired in the formation of visible PBs but degradation of over 3,800 VCS-specific substrates unaffected **(Figure 3.3A)**. Although we demonstrated that RH6, RH8, and RH12 associate with DCP2 and VCS complexes and that the vast majority of RH6/8/12 substrates are also targeted by VCS, it remains unclear where these helicases function. This could be in PBs, in the cytosol, and/or cotranslationally on elongating ribosomes. Future work is needed to better understand the protein-protein interactions and subcellular compartmentation of the decay apparatus.

Our study also provides new perspective on the inter-relationship between the decay apparatus. First, apart from RH6/8/12 substrates that showed increased mRNA $t_{1/2}$ and those with unaffected $t_{1/2}$, we found a considerable number of transcripts with accelerated decay, hence reduced $t_{1/2}$ in the triple mutant. This phenomenon was also

observed in *vcs* and *sov* mutants and could be due to an overcompensation of decay by other pathways (Sorenson et al., 2018). Our data on the complementation of RH6/8/12 function by SOV clearly support this possibility. Alternatively, this might represent a secondary effect caused by a stabilization of mRNAs encoding proteins involved in other decay pathways that results in increased decay rates of their mRNA clients. Second, consistent with a recent finding that RH6, RH8, and RH12 copurify with the NMD factor UPF1 (Chicois et al., 2018), our mRNA decay data showed that a significant proportion of MND substrates are stabilized in the triple *rh6 rh8 rh12* mutant. This suggests that, in addition to the general 5'-to-3' mRNA decay pathway, the *Arabidopsis* DHH1/DDX6-like RHs may also control degradation of transcripts with NMD features. On the contrary, while the human counterpart DDX6 plays a role in miRNA-mediated gene silencing (Chu and Rana, 2006; Nishihara et al., 2013; Chen et al., 2014; Mathys et al., 2014; Rouya et al., 2014), a survey of miRNA targets present in the seedling transcriptome revealed that their stability is not affect in the triple mutant. This suggests that RH6/8/12 are dispensable for miRNA-mediated mRNA decay, although it is not known whether they are involved in miRNA-mediated translational repression.

mRNA stability in eukaryotes is influenced by different *cis*- (and *trans*-) acting factors, including codon usage, secondary structures, sequence motifs in the 3' UTR, miRNA-binding sites, polyadenylation-site selection, and epitranscriptomic m^6A modification (Chen and Shyu, 2017). In plants, the presence and number of introns in the primary transcripts enhance mRNA stability (Narsai et al., 2007; Sorenson et al., 2018). mRNA $t_{1/2}$ in plants is also affected by various sequence elements in the 3' UTR. A short mRNA $t_{1/2}$ is correlated with the presence of miRNA target sites, as well as an increase in A and G content in the 5′ UTR (Narsai et al., 2007; Sorenson et al., 2018). In

this study, we found that RH6/812 substrates had short $t_{1/2}$. This was not due to a reduced statistical power to resolve the difference in decay rates of long-lived transcripts between the triple mutant and the wild-type, as our comparison of mRNA $t_{1/2}$ of RH6/8/12 substrates with those of VCS modelled by the same criteria clearly indicated that RH6/8/12 substrates had shorter $t_{1/2}$ than those specifically regulated by VCS **(Figure 3.3A)**. Consistent with the presence of introns as a mRNA-stabilizing factor as reported in other studies, we found that the number of introns was positively correlated with mRNA stability. Interestingly, RH6/8/12 substrates had fewer introns that non-RH6/8/12 substrates. It is not known how the RHs selectively regulate decay of transcripts with fewer introns, but it is possible that RNA-binding proteins associated with mRNA-splicing events might protect or redirect these transcripts from RH6/8/12-mediated decay. Apart from the number of introns, RH6/8/12 substrates also had fewer codons, hence shorter transcript lengths, than non-substrate mRNAs. In humans, but not in yeast, transcript length is negatively correlated with stability (Feng and Niu, 2007). The fact that RH6/8/12 regulate decay of short-lived and short-length mRNAs does not correspond with what was reported for humans. This could be kingdom- to species-specific and deserves further investigation.

In plants, compromised mRNA decay allows aberrant transcripts, including decay intermediates, to become substrates for small interfering (si)RNAs production that subsequently triggers silencing of homologous mRNAs (Liu and Chen, 2016). This is evident in mutants for the 5'-to-3' and/or 3'-to-5' decay machinery, such as the decapping mutants *dcp2* and *vcs* (Martínez de Alba et al., 2015), and the bidirectional decay mutant *xrn4 ski2* (Zhang et al., 2015), where loss of these genes amplifies 21-22 nt siRNA abundance. cot Surprisingly, despite the fact that nearly half of the

transcriptome of the triple *rh6 rh8 rh12* mutant was not efficiently degraded, our genetic analysis indicated that growth defects of the triple mutant is not associated with RDR6 function, suggesting that these stabilized mRNAs are not processed by RDR6. Therefore, the aberrant accumulation of these mRNAs does not appear to trigger siRNA production. This suggests that, despite the presence of stabilized mRNAs in the triple *rh6 rh8 rh12* mutant, there might be a mechanism that prevent RDR6 from accessing or processing these mRNAs. Recent evidence has established that the poly(A) tail inhibits RDR6 activity from converting endogenous mRNAs into substrates for gene silencing (Baeg et al., 2017). Both in yeast and mammals, DHH1/DDX directly interacts with the CCR4-NOT deadenylation complex. In particular, yeast DHH1 physically interacts with CAF1 (POP1) and NOT1 subunits of the CCR4-NOT complex (Hata et al., 1998; Maillet and Collart, 2002), whereas human DDX6 interacts with NOT1 (Chu and Rana, 2006; Nishihara et al., 2013; Chen et al., 2014; Mathys et al., 2014; Rouya et al., 2014). Although yeast DHH1 is not required for deadenylation (Fischer and Weis, 2002), it would be interesting to test whether the *Arabidopsis* DHH1/DDX6-like RH6, RH8, and RH12 interact with the CCR4-NOT complex and whether these proteins play a role in mRNA deadenylation. Their contribution to the regulation of deadenylation could explain the lack of influence of the *rdr6* or *sgs3* on the triple *rh6 rh8 rh12* mutant phenotype.

3.4.2 RH6, RH8, and RH12 are required for cellular transcriptome and translatome homeostasis

RNA-seq analysis of TOTAL and TRAP mRNAs demonstrated that the transcriptome and translatome profiles of the *rh6 rh8 rh12* mutant were shifted from a growth-promoting to stress-responsive state, despite the fact that the seedlings were

grown under optimal growth conditions. This was attributed by an enrichment of transcripts involved in stress and defense responses, and a depletion of those required for primary metabolic processes, growth, and development. Globally, we found that change in TRAP mRNA abundance in the triple mutant correlated well with that of the TOTAL mRNA population, albeit a subset of mRNAs displayed a discrepancy in the alteration of TRAP and TOTAL mRNA abundance. As members of the DHH1/DDX6 family in non-plant eukaryotes play a crucial role in translational repression (Coller and Parker, 2005; Boag et al., 2008; Carroll et al., 2011; Presnyak and Coller, 2013; Ayache et al., 2015), we considered that some of the altered sub-population might represent involvement of RH6/8/12 in translational regulation. For example, transcripts that were enriched in the TRAP fraction but were unchanged in the TOTAL mRNA abundance might be due to a role of RH6/8/12 in translational repression that is independent of decay **(Figure 3.5E)**.

The growth-to-stress/defense shift signature manifested by the changes in total and polysomal mRNA abundance was recognized as a significant alteration in mRNA translational status for over 200 genes **(Figure 3.6B)**. We found that mRNAs encoding proteins important for the defense response were preferentially translated, whereas those encoding for proteins related to cell wall organization and biogenesis as well as tissue development were depleted in ribosome association. Since mRNA decay and translation might act antagonistically, we hypothesized that RH6/8/12 decay substrates would have increased translational status in the triple *rh6 rh8 rh12* mutant, as their decay was compromised (hence, abundance increased). Surprisingly, our results showed that increases stability of RH6/8/12 substrates did confer increases in their translational status in the triple mutant. Conversely, we found that the overall

translational status of mRNAs in the triple mutant was reduced as compared to the wild-type. Based on the stunted growth phenotype as well as an enrichment of transcripts involved in stress/defense response in the triple mutant, we deduce that its altered translatome reflects an adjustment to stress, in which overall translation levels are reduced to reserve energy. As is typical for plant responses to both biotic and abiotic stress, global reductions in translation are associated with selective translation of individual mRNAs related with stress response and survival (Kawaguchi et al., 2004; Branco-Price et al., 2005; Moeller et al., 2012; Meteignier et al., 2016; Merchante et al., 2017; Meteignier et al., 2017).

We conjectured that stabilization of RH6/8/12 substrates would result in an increase in their steady-state transcript abundance in the triple *rh6 rh8 rh12* mutant. Unexpectedly, the majority of RH6/8/12 substrates were unchanged in both TOTAL and TRAP mRNA abundance. This has also been observed in *vcs* mutant, where stabilization of VCS substrates does not necessarily correlate with an increase in steady-state mRNA abundance of these transcripts in the *vcs* mutant (Sorenson et al., 2018). It has been proposed that this phenomenon might be mediated by a so called 'RNA buffering' mechanism, where it has been shown in yeast that changes in mRNA decay rates are generally compensated by changes in RNA Polymerase II (RNAPII) transcription activity (Haimovich et al., 2013; Sun et al., 2013). A parallel mechanism for sensing an overall alteration in mRNA decay has been observed in mammalian cells, although the transcriptional feedback operated into the opposite direction, as accelerated cytoplasmic mRNA decay resulted in a decrease in RNAPII promoter recruitment (Abernathy et al., 2015). However, the same study also suggested that decreased cytoplasmic decay may also stimulate transcription in mammalian cells

(Abernathy et al., 2015). It is unknown how changes in mRNA decay within the cytoplasm influence nuclear transcription in plants, and it would be interesting to test how compromised decay of RH6/8/12 substrates affects their nuclear transcription in the triple mutant.

Our data demonstrate a relationship between transcript decay, abundance and translation involving the DHH1/DDX-like helicases of plants. 397 RH6/8/12 substrates, defined by an increase in $t_{1/2}$, showed an enriched or depleted mRNA abundance in the triple mutant. Strikingly, despite a global decreased mRNA translation in the triple mutant, comparison of TOTAL- and TRAP-enriched mRNAs indicated that RH6/8/12 substrates have a higher translational status in the triple mutant than those non-substrate mRNAs. These stabilized, well translated mRNAs encode proteins involved in stress and defense response. This indicates that loss of RH6, RH8, and RH12 function allows translation of stress/defense-related transcripts that are otherwise degraded in the wild-type, suggesting that the DHH1/DDX6-like RHs have a crucial role in translational repression and turnover of stress- and defense-responsive mRNAs under standard growth conditions. Dysregulation of decay and translational control of these mRNAs may be the underlying cause of the growth-to-stress/defense shift in the triple *rh6 rh8 rh12* transcriptome.

This finding is reminiscent of the role of human DDX6 as a suppressor of interferon-stimulated genes (ISGs). Depletion of DDX6 in human cells induces global upregulation of ISGs and other immune genes in the absence of infection, causing resistance to RNA viruses (Lumb et al., 2017). Similarly, yeast DHH1 has been shown to associate with stress-responsive mRNAs, including those induced during nutrient starvation and those regulated by metabolic and oxygen consumption cycles (Miller et

al., 2018). In another example, DHH1 negatively regulates the lactate-proton symport-encoding *JEN1* transcripts in the presence of glucose or formic acid. Mutation of DHH1 results in an accumulation of *JEN1* transcripts in the presence of formic acid (Mota et al., 2014). Yeast DHH1 has been shown to sense codon optimality of its substrates, and trigger mRNA decay cotranslationally on elongating ribosomes (Radhakrishnan et al., 2016), yet it has not been determined if degradation of these stress/defense-related mRNAs is directly coupled with translation or it follows translation repression as separate processes. Our data indicate that this question is also relevant in plants.

Collectively, our integrative analysis of transcriptome, translatome and decay rates data demonstrated that loss of RH6, RH8, and RH12 function results in a catastrophic alteration of the seedling mRNA homeostasis, allowing the accumulation and translation of stress- and defense-responsive transcripts while dampening mRNAs important for growth and development. The regulation of mRNA turnover has long been recognized as an integral mechanism enabling rapid changes in gene expression in response to stress (Arribere et al., 2011). In this study, we presented evidence on the underappreciated contribution of mRNA decay in shaping the cellular transcriptome, translatome and ultimately proteome under optimal conditions that is critical for plant growth and development. Our data underscore the notion that stress-responsive transcripts are constitutively transcribed at some level prior to stress, but their accumulation and translation are limited by degradation and/or translational repression. This raises new questions, such as how RH6, RH8, and RH12 are modulated to allow these transcripts to become stabilized and/or translated when needed, and what determines which mRNAs will be stabilized or degraded, translated or sequestered under different conditions.

3.4.3. Constitutive immune response in the triple *rh6 rh8 rh12* mutant

Changes in TOTAL and TRAP mRNA abundance, translational status as well as preferential translation of stabilized defense-related transcripts in the triple *rh6 rh8 rh12* mutant indicated that loss of RH6/8/12 function causes a constitutive immune response. This is supported by an overaccumulation of the defense hormone SA in the triple mutant. Autoimmunity as a result of dysregulation of cytoplasmic mRNA decay and translation has been demonstrated in plants. This primarily involves misregulation of mRNAs encoding nucleotide-binding leucine-rich repeat domains (NLR) from *R* genes that results in constitutive activation of NLRs, hence autoimmunity. For example, *muse11* (mutant, *snc1*-enhancing *11*) was isolated in a forward genetic screen for enhancement of autoimmunity in an TNL protein SUPPRESSOR OF NPR1-1, CONSTITUTIVE 1 (SNC1) overexpression line (Wu et al., 2017). *muse11* is defective in the *ESSENTIAL FOR POTEXVIRUS ACCUMULATION 1* (*EXA1*) gene encoding a translational repressor glycine-tyrosine-phenylalanine (GYF) domain protein that associates with the ribosome and translation initiation factor eIF4E complexes. Loss of the *EXA1* function does not influence general protein synthesis, but causes increased accumulation of NLRs including SNC1, RESISTANT TO P. SYRINGAE 2 (RPS2), RPS4, and RESISTANCE TO P. SYRINGAE PV MACULICOLA 1 (RPM1), The autoimmunity in this mutant is partially dependent on EDS1 function (Wu et al., 2017). NMD also controls degradation of numerous mRNAs encoding Toll-like/Interleukin 1 receptors (TIR)-type NLRs (TNLs), including RESISTANT TO P. SYRINGAE 6 (RPS6), under optimal growth conditions (Gloggnitzer et al., 2014). Similarly, the *smg7* mutant impaired in NMD exhibits autoimmunity in an EDS1/PAD4-dependent, but ICS1-independent manner. By contrast, autoimmunity in a *pat1* mutant defective in mRNA

decapping is not due to overexpression of the NLR SUPPRESSOR OF MKK1 MKK2 2 (SUMM2), but can be suppressed by mutations of SUMM2 and EDS1 (Roux et al., 2015). Albeit complex, appropriate control of immunity involves the 5' to 3' decay machinery including RH6/8/12, functional NMD and some relationship to translational initiation in plants.

Several transcripts encoding NLRs were stabilized in the triple *rh6 rh8 rh12* mutant, *e.g.* SNC1, HOPZ-ACTIVATED RESISTANCE 1 (ZAR1), RESISTANCE TO LEPTOSPHAERIA MACULANS 1 (RLM1), RLM3, RECOGNITION OF PERONOSPORA PARASITICA 1 (RPP1), RPP4, RPP5, PRR13, and TARGET OF AVRB OPERATION 1 (TAO1). However, of all NLR-encoding transcripts stabilized in the triple *rh6 rh8 rh12* mutant, only 4 (At1g61300, At1g72940, At3g44630, At5g58120) showed a significant enrichment in TOTAL and TRAP mRNA abundance in the genotype, whereas another 3 (At1g72900, At5g36930, At5g66910) showed significant enrichment in abundance of TRAP but not TOTAL fraction. The increased production of these NLRs may be the cause of autoimmunity in the triple mutant. EDS1 controls defense activation and programmed cell death mediated by all TNLs characterized to date (Wiermer et al., 2005). In basal and TNL immunity, EDS1 and its direct partner PAD4 promote *ICS1* expression and SA accumulation (Rietz et al., 2011). However, despite an enrichment of EDS1/PAD4-induced transcripts in the TOTAL and TRAP fractions of the triple mutant transcriptome, our genetic analysis of the quadruple *rh6 rh8 rh12; eds1-2* and *rh6 rh8 rh12; pad4-1* mutants indicated that the autoimmune phenotype displayed in the triple mutant is partially dependent on PAD4, but not EDS1 function. However, SA accumulation in the triple mutant was independent of EDS1 and PAD4 functions. Based on these data, the autoimmune response displayed in the triple *rh6 rh8 rh12* mutant may

not be associated with TNL immunity, but is conditioned by the other family of NLRs, the coiled-coil NLRs (CNLs).

The plant hormone SA plays an integral role in both local defense and SAR (Klessig et al., 2018). Through its receptor, transcriptional coregulator NPR1, SA initiates transcriptional reprogramming leading to induction of numerous antimicrobial genes, including *PR1* (Fu and Dong, 2013). Interestingly, our genetic analysis showed that mutations of *NPR1* and *ICS1* resulted in a significant reduction of *PR1* transcripts **(Figure 3.9D)**, but they were not sufficient to abolish *PR1* transcript induction to the wild-type levels, nor did they rescue the triple mutant phenotype. On the contrary, constitutive removal of SA by *NahG* expression efficiently limited *PR1* transcript induction and suppressed the triple mutant phenotype **(Figure 3.9D)**. These data suggest that the constitutive immune response in the triple mutant partly occurs in a NPR1-independent pathway and that not only does the triple mutant overacumulate SA, the genotype might be also hypersensitive to SA since the triple mutant phenotype was rescued only when SA was completely removed. However, since the rosette growth of *rh6 rh8 rh12; NahG* genotype remained much lower than the wild-type and the *NahG* control line, we speculate that growth defects displayed in the triple mutant are not entirely due to a SA-mediated constitutive immune response. This is also supported by the fact that the *rh6 rh8 rh12; pad4* genotype showed a partially rescued phenotype even though SA content in this genotype was as high as in the triple *rh6 rh8 rh12* mutant.

3.4.4 SOV compensates RH6, RH8 and RH12 function

The 3'-to-5' exoribonuclease SOV has been shown to compensate for VCS function in mRNA degradation and rescue growth defects in the *vcs* mutant (Zhang et al., 2010). In this study, we found that a considerable proportion of RH6/8/12 substrates overlapped with SOV substrates as well as those of VCS that are compensated by SOV in the *vcs* genotype, suggesting that SOV might also compensate RH6, RH8, and RH12 function in mRNA decay. Using a genetic approach, we found that expression of the functional L.*er* allele of *SOV* was able to rescue the triple mutant phenotype. Interestingly, the complementation of the triple mutant phenotypes by SOV was further enhanced when the gene expression was driven by the near-constitutive 35S promoter. We reasoned that ectopic expression of SOV may overcome the spatial difference of SOV and RH6/8/12 expression, hence allowing SOV to compensate RH6/8/12 function more efficiently. Another possibility which is not exclusive from the former one might be that, since RH6, RH8, and RH12 are highly abundance, overexpression of SOV may improve the protein-mRNA substrate stoichiometry, increasing the efficiency of mRNA degradation. In support of the growth phenotypes, our comparative RNA-seq analysis of the rescued triple *rh6 rh8 rh12; SOV$^{L.er}$-OX* and its counterpart *rh6 rh8 rh12* demonstrated that overexpression of SOV partially alleviated the change in the triple mutant transcriptome in a direction that reduces the accumulation of stress- and defense-responsive transcripts and elevates the abundance of those encoding proteins important for growth and primary metabolisms. This included a reduction in transcripts encoding PR1 and other key immune response regulators, which is consistent with the diminished SA accumulation in the *rh6 rh8 rh12; SOV$^{L.er}$-OX* genotype as compared to *rh6 rh8 rh12* **(Figure 3.12D)**.

Altogether, our data demonstrate that the DHH1/DDX6-like RH6, RH8, and RH12 of plants functions in mRNA-decay to control homeostasis of the seedling transcriptome in a manner that maintains the growth-defense response balance under optimal growth conditions, and that this process can be complemented by the 3'-to-5 exoribonuclease SOV when the most-likely 5'-to-3' RH-mediated decay pathway are not functional.

3.5 MATERIALS AND METHODS

3.5.1 Genetic material and growth condition

Arabidopsis thaliana mutants and transgenics are in the Columbia-0 (Col-0) ecotype. Mutants *rdr6*$^{sgs2\text{-}1}$ and *sgs3-1* were as described in (Mourrain et al., 2000; Martínez de Alba et al., 2015); *eds1-2* and *pad4-1* were kindly provided by Dr. Jane Parker (Gloggnitzer et al., 2014); *npr1-3* mutant and the *NahG* transgenic line were kindly provided by Dr. Thomas Eulgem (Cao et al., 1997; Bektas et al., 2016); *ics1* (SALK_133146C) was obtained from the *Arabidopsis* Biological Resource Center (ABRC) and was described previously (Chen et al., 2015). Col-0 *SOV*$^{L.er}$ and *SOV*$^{L.er}$*-OX* (*pro35S:SOV*$^{L.er}$*-CFP*) genotypes were gifts from Dr. Leslie Sieburth (Zhang et al., 2010; Sorenson et al., 2018); *pro35S:HF-GFP-RPL18* (Col-0) was described previously (Mustroph et al., 2009b). Genotypes with mutant *rh6, rh8* and *rh12* alleles are described in Chapter 2. Primers used for genotyping of mutant alleles are listed in **Table 3.1**. Primers used for genotyping of *rh6, rh8* and *rh12* alleles are described in **Table 2.1**.

Seeds were surface-sterilized by incubation in 70% (v/v) ethanol for 5 minutes, 20% (v/v) household bleach plus 0.01% (v/v) Tween-20 for 5 minutes, and rinsed 5 times with sterile water. Unless otherwise stated, all sterilized seeds were plated on solid Murashige and Skoog (MS) medium containing 0.5x MS salts (Caisson Laboratories),

0.5% (w/v) Sucrose, 0.4% (w/v) Phytagel (Sigma) [pH 5.7-5.8], followed by stratification at 4°C in complete darkness for 2 days. Seedlings were vertically grown in a growth chamber (Percival) under a 16-hour light (~120 µmol photons·s^{-1}·m^{-2}) and 8-hour dark cycle (long-day) at a constant 23°C. Seven-day-old seedlings were transferred to soil containing Sunshine LC1 soil mix (JM McConkey) with 1.87 g/L Marathon insecticide (Crop Production Services, Riverside, California) and 1.4 g/L osmocote 14-14-14 fertilizer, and grown in a growth room under long-day conditions. Plants were imaged using a Canon camera (Canon, USA). Images were processed using Fiji software (Schindelin et al., 2012).

Sterilized seeds of *rh6*$^{(+/-)}$ *rh8 rh12; pro35S:HF-GFP-RPL18* genotype plated on sterile solid medium were transferred after stratification to the growth chamber 12 hours in advance of the *pro35S:HF-GFP-RPL18* seeds to compensate for their delayed germination. To prevent disturbance of seedlings and hasten tissue collection, seedlings of wild-type phenotype were removed from the segregating population of *rh6*$^{(+/-)}$ *rh8 rh12; pro35S:HF-GFP-RPL18* progeny after 4 days. Five-day-old seedlings of the *pro35S:HF-GFP-RPL18* and *rh6 rh8 rh12; pro35S:HF-GFP-RPL18* genotypes were harvested and flash frozen in liquid nitrogen, and stored at -80°C until used. All sample preparations were carried out in at least three independent biological replicates. Similarly, sterilized seeds of Col-0, *SOV*$^{L.er}$*-OX* (*pro35S:SOV*$^{L.er}$*-CFP*), *rh6*$^{(+/-)}$ *rh8 rh12*, and *rh6 rh8 rh12; SOV*$^{L.er}$*-OX* genotypes plated, stratified and grown 5 days before removal seedlings of wild-type phenotype from the segregating population of *rh6*$^{(+/-)}$ *rh8 rh12* progeny. Seven-day-old seedlings of Col-0, *SOV*$^{L.er}$*-OX*, *rh6 rh8 rh12*, and *rh6 rh8 rh12; SOV*$^{L.er}$*-OX* genotypes were harvested as described.

3.5.2 Global mRNA decay analysis

Col-0 wild-type and *rh6*$^{(+/-)}$ *rh8 rh12* plated on sterile solid medium, and stratified for 2 days were grown vertically at 22°C in a Conviron growth chamber under ~75 µmol photons·s^{-1}·m^{-2} constant illumination for 5 days. Seedlings with clear triple *rh6 rh8 rh12* mutant phenotypes (~12-15%) were placed on fresh growth media before cordycepin treatment. Col-0 seedlings were similarly handled to standardize the treatment. The experiment was performed in 3 independent biological replicates with ~100 *rh6 rh8 rh12* seedlings and ~50 Col-0 seedlings per sample.

Cordycepin treatment was carried out as described (Sorenson et al., 2018). Briefly, seedlings were preincubated in 3 mL of incubation buffer (15 mM sucrose, 1 mM KCl, 1 mM PIPES pH 6.25, 1 mM sodium citrate) with rotation at 100 rpm in 35 mm x 10 mm Petri dishes for 15 minutes prior to replacement of the bathing solution with 3 mL of fresh buffer containing 1 mM cordycepin (Chengdu Biopurify Phytochemicals), followed by vacuum infiltration for 1 minute. T_0 samples were harvested and frozen immediately, with the remaining samples subjected immediately to two additional vacuum infiltrations of 1 minute-vacuum with 1 minute-decompression intervals. Tissues were collected 15, 30, 60, and 120 minutes following the first vacuum infiltration, frozen in liquid nitrogen, and stored at −80 °C.

Total RNA was isolated from pulverized tissues by addition of 500 µL PureLink™ Plant RNA Reagent (Invitrogen). The samples were vortexed and incubated at room temperature for 5 minutes, followed by centrifugation at 12,000*g* for 2 minutes at room temperature. The supernatant was transferred to a tube containing 5 M NaCl (equal volume). Chloroform (300 µL) was added and the sample was mixed thoroughly before centrifugation at 12,000*g* for 10 minutes at 4ºC, and transfer of the upper aqueous phase

to a new tube. RNA was precipitated by addition of isopropanol (equal volume), thorough mix, incubation at room temperature for 10 minutes, and pelleted by centrifugation at 12,000*g* for 10 min at 4°C. The supernatant was removed, and the pellet was washed with 1 mL 70% (v/v) ethanol and resuspended in 30 µL RNAsecure™ Resuspension Solution (Invitrogen), and DNase I digested with with 1 µL of TURBO DNase (Invitrogen) for 15 minutes at 37°C. The RNA was precipitated in 0.1 volume of 5 M ammonium acetate and 2.5 volumes of ethanol, and pelleted by centrifugation at 12,000*g* for 20 minutes at 4°C. DNase-treated RNA was resuspended in RNase-free water, and submitted to the University of Utah Genomics core for RNA-seq library preparation and sequencing. RNA-seq libraries were constructed using the Illumina TruSeq Total RNA Sample Prep Kit with Ribo-Zero (Plant) (Illumina). A total of 30 libraries was multiplexed so that all time course and genotype samples in each biological replicate (10 samples) were loaded onto a single lane.

Analysis of RNA-seq data was performed on a Linux cluster using a combination of command-line software and R packages including the RNA-Seq data analysis pipeline package systemPipeR (H Backman and Girke, 2016). Multiplexed libraries were demultiplexed using their unique barcodes. Reads were trimmed to correct for adapter contamination with standard settings. Bowtie 2 (v2.2.5) was used to build the TAIR10 reference genome from individual chromosome Fasta files downloaded from www.araport.org. Reads were aligned to this assembled Arabidopsis genome using Bowtie2 (v2.2.5) /Tophat (v2.0.14). Aligned reads were counted against the Araport11 genome release 201606 using the summarizeOverlaps function (Lawrence et al., 2013) in “union” mode. Data normalization as well as modeling of mRNA decay and genotype effect were performed according to (Sorenson et al., 2018) using the Bioconductor

RNAdecay package (Sorenson, 2018). Genotypic effect on mRNA decay for each transcript was fitted to 6 possible exponential decay models with α as an estimated parameter of the initial primary decay rate and β as an estimated parameter of the secondary decay of the α decay rate, using likelihood functions. The model with the lowest Akaike information criterion (AICc) was selected for each transcript. Only the model with the estimated parameter of variance (σ^2) less than 0.065 was accepted for a downstream analysis. mRNA half-life was calculated as $t_{1/2} = \ln(2)/\alpha$.

3.5.3 Translating ribosome affinity purification (TRAP)

TRAP of polysomes was performed as described previously (Mustroph et al., 2009a). Briefly, 1 mL of pulverized tissue was added to a 15 mL tube containing 5 mL of polysome extraction buffer (PEB: 200 mM Tris, pH 9.0, 200 mM KCl, 25 mM EGTA, 35 mM $MgCl_2$, 1% PTE, 1 mM DTT, 1 mM PMSF, 100 µg/mL cycloheximide, 50 µg/mL chloramphenicol) and 1% detergent mix [20% (w/v) polyoxyethylene(23)lauryl ether, 20% (v/v) Triton X-100, 20% (v/v) Octylphenyl-polyethylene glycol, 20% (v/v) Polyoxyethylene sorbitan monolaurate 20] and incubated until thawed on ice, before homogenized with a glass homogenizer. The homogenized mixture was incubated on ice for 10 minutes, and centrifuged at 16,000*g* at 4°C for 15 minutes. After centrifugation, the supernatant was transferred to a new tube and filtered through sterilized Miracloth (Millipore) to produce a clarified extract.

The clarified extract was added to Anti-FLAG M2 Protein G Dynabeads (1.5 mL) that was pre-washed twice with wash buffer [WB; 200 mM Tris (pH 9.0), 200 mM KCl, 25 mM EGTA, 35 mM $MgCl_2$, 1 mM DTT, 1 mM PMSF, 100 µg/mL cycloheximide, 50 µg/mL chloramphenicol]. Binding of FLAG epitope-tagged ribosome-mRNA complexes was

accomplished by incubation at 4°C for 2 hours with gentle rocking. The beads were magnetically captured, the supernatant was removed, and the beads were gently resuspended in 6 mL WB for 2 minutes at 4°C with rocking. This step was repeated two additional times, before the beads were resuspended in 1 mL WB. The beads were washed two additional times with 1 mL WB, and the supernatant was removed. The beads were stored at -80°C until used.

3.5.4 Total RNA isolation and quantitative RT-PCR

Total RNA was extracted from indicated tissues using TRIzol™ reagent (Invitrogen), and purified using the Direct-zol™ RNA MiniPrep (Zymo Research) according to the manufacturer's instructions. Total RNA was treated with DNase I (New England Biolabs), and cDNAs were prepared from 2 µg of DNase-free total RNA using an oligo(dT) primer (Integrated DNA Technologies) and Maxima Reverse Transcriptase (Thermo Fisher Scientific) following the manufacturer's instructions. For RT-qPCR analysis of *PR1* transcripts, amplification was performed in 2 technical replicates in the CFX Connect™ Real-Time PCR Detection System (Bio-Rad Laboratories) using 2 µL of 5x diluted cDNA. Real-time PCR was performed using iQ™ SYBR® Green Supermix (Bio-Rad Laboratories) in a 15-µL reaction volume with 0.67 µM of each primer. The program for running qPCR was initiated at 95°C for 3 minutes followed by 40 cycles at 95°C for 15 seconds, at Tm for 15 seconds, and at 72°C for 15 seconds. *ACTIN1* (At2g37620) was used as a reference. Relative transcript fold-change was calculated by the ΔΔCt method (Pfaffl, 2001).Primers used are as follows: PR1-qF, 5'-TTC TTC CCT CGA AAG CTC AA-3'; PR1-qR 5'-AAG GCC CAC CAG AGT GTA TG-3'; ACT1-qF, 5'-GGC GAT GAA GCT CAA TCC AAA CG-3'; ACT1-qR, 5'-GGT CAC GAC CAG CAA

GAT CAA GAC G-3'.

3.5.5 Poly(A)$^+$ RNA affinity purification

Purification of Poly(A)$^+$ RNA was carried out according to (Townsley et al., 2015). Briefly, total and TRAP purified RNA were resuspended in 200 µL of Lysis binding buffer (LBB: 100 mM Tris-HCl, pH 8.0, 1000 mM LiCl, 10 mM EDTA, 1% (w/v) SDS, 5 mM DTT, 1.5% (v/v) Antifoam A, 5 µL/mL 2- mercaptoethanol) followed by vortexing for 5 min. Samples were incubated for 10 minutes at room temperature, followed by centrifugation at 13,000*g* for 10 minutes at room temperature. The supernatant was transferred to a new tube, and 1 µL of 12.5 µM biotin-20nt-dT oligos (Integrated DNA Technologies) was added and incubated at room temperature for 10 minutes. In a separate tube, 10 µL of magnetic streptavidin beads (New England Biolabs) were washed with 200 µL LBB. The sample was added to the washed beads and incubated at room temperature for 10 minutes with agitation. The beads were magnetically collected and washed with 200 µL of wash buffer A (WBA:10 mM Tris-HCl, pH 8.0, 150 mM LiCl, 1 mM EDTA, 0.1% (w/v) SDS), followed by wash buffer B (WBB:10 mM Tris-HCl, pH 8.0, 150 mM LiCl, 1 mM EDTA), and low-salt buffer (LSB: 20 mM Tris, pH 8.0, 150 mM NaCl, 1 mM EDTA). Subsequently, the pellet was resuspended in 10 µL of 10 mM Tris, pH 8.0 containing 1 mM 2-Mercaptoethanol, and heated at 80^{o}C for 2 minutes. The beads were magnetically separated, and the supernatant was quickly transferred to a new tube. The poly(A)$^+$ RNA selection process was repeated another time, and the samples were combined in a new tube before storage at -80^{o}C.

3.5.6 Library preparation, RNA-seq data processing, and differential gene expression analysis

Non-strand specific RNA-seq libraries were prepared according to (Kumar et al., 2012; Townsley et al., 2015). Briefly, the purified poly(A)$^+$ RNA (~50 ng) was used for fragmentation and cDNA priming by incubating with 1.5 µL 5x RT buffer (Thermo Scientific) and 0.5 µL of 3 µg/µL random hexamer primers (Invitrogen) in a final reaction volume of 10 µL at 94 °C for 1.5 minutes followed by 4°C for 5 minutes. The fragmented RNA was used as the template for first strand cDNA synthesis by addition of 1.5 µL 5x RT buffer, 1.5 µL of 0.1 M DTT (Invitrogen), 0.25 µL water, 0.5 µL RevertAid RT (Thermo Scientific), and 1.25 µL 10 mM dNTPs (Promega). This synthesis step was performed by incubation at 25, 42, 50 and 70°C for 10, 50, 10 and 10 minutes, respectively. Second strand synthesis, end preparation, and A-tailing of the first strand cDNA (15 µL) were performed in a reaction containing 1.4 µL end repair buffer (New England Biolabs), 1 µL DNA Polymerase I (Enzymatics), 0.1 µL RNaseH (Enzymatics), 0.4 µL T4 Pol + PNK mix (end repair module, New England Biolabs), 0.2 µL Taq DNA polymerase (GBioscience), 1 µL 10 mM dNTPs (Promega), and 0.9 µL water with the following program: 16°C for 20 minutes, 20°C for 20 minutes, and 72°C for 20 minutes. The cDNA was purified using 30 µL AMPure XP beads (Beckman), washed twice with 120 µL 80% ethanol, and used in the adaptor ligation step. Adaptor ligation was accomplished using 5 µL of 2x Rapid T4 ligase buffer (Enzymatics), 3 µL 1 µM annealed universal Y-shaped adapter, 0.25 µL T4 DNA Ligase HC (Enzymatics), 1.75 µL water with incubation at room temperature for 15 minutes. Next, 25 µL of Ampure XP Bead Resuspension buffer (ABR: 15% PEG 8000, 2.5M NaCL) was added to the reaction and incubated for 5 minutes at room temperature. The beads were magnetically separated,

washed twice with 200 µL 80% ethanol, and resuspended in 10 µL water. Following incubation for 2 minutes at room temperature, the beads were magnetically separated, and the supernatant was transferred to a new tube. Thia adapter-coupled cDNA (10 µL) was used for PCR enrichment and adapter extension in a reaction containing 4 µL 5X Kapa HiFi Fidelity buffer (Kapa Biosystems), 1 µL of 2 µM indexed primer, 1 µL of 2 µM PE1 primer, 1 µL of 8 µM EnrichS1 and EnrichS2 primers, 0.2 µL Kapa HiFi DNA polymerase (Kapa Biosystems), 0.5 µL of 10 mM dNTPs (Promega), and 2.3 µL water. The PCR reactions included denaturation by incubation at 98°C for 30 seconds, followed by 15 cycles of denaturation at 98°C for 10 seconds, annealing at 65°C for 30 seconds, extension at 72°C for 30 seconds, and a final extension at 72°C for 5 minutes. The amplified cDNA libraries of 200-300 bp were purified using acrylamide gel electrophoresis and elution. Library yield and concentration were checked by Qubit 2.0 Fluorometer (Life Technologies) and Bioanalyzer. The libraries were multiplexed and sequenced on short-read Illumina sequencers at the UC Riverside Institute for Integrative Genome Biology Genomics Core facility.

Processing of RNA-seq data was performed using the package systemPipeR (H Backman and Girke, 2016), with the same settings as in the mRNA decay analysis. Differential gene expression analysis was performed using the generalized linear model within the edgeR package. Genes that contained ≤ 2 counts per million (CPM) in at least two samples were removed. Genes which passed the first filter were passed through a second filter that retained only those with RPKM > 5 in at least two samples. The calculated *p* value for each gene was corrected by applying the Benjamini-Hochberg method, to provide a false discovery rate (FDR). Genes with fold change > |2| and FDR

< 0.01 were considered differentially expressed. GO analysis was conducted in R using the systemPipeR package environment (H Backman and Girke, 2016).

3.5.7 SA quantification

Quantification of SA in was carried out by Dr. Haiyan Ke of the group of Dr. Katayoon Dehesh at UC Riverside by gas chromatography–mass spectrometry (GC-MS), using deuterated SA as internal standard. Extraction and quantification were performed as previously described (Savchenko et al., 2010).

3.6 ACKNOWLEDGEMENTS

mRNA decay analysis was performed in collabroation with Dr. Reed Sorenson. We thank Dr. Maureen Hummel and Dr. Haiyan Ke for assistance in bioinformatic analyses and SA quantification, respectively. We thank Dr. Jeremie Bazin for kindly providing *rdr6*$^{sgs2\text{-}1}$ and *sgs3-1* seeds, Dr. Jane Parker for *eds1-2* and *pad4-1* seeds, Dr. Thomas Eulgem for *npr1-3* and *NahG* seeds, and Dr. Leslie Sieburth for Col-0 *SOV*$^{L.er}$ and *pro35S:SOV*$^{L.er}$*-CFP* seeds. This work was supported by the United States National Science Foundation grant no. MCB-1716913 to J.B.-S. and a Royal Thai Government's Development and Promotion of Science and Technology Talents Project scholarship to T.C.

3.7 REFERENCES

Abernathy E, Gilbertson S, Alla R, Glaunsinger B (2015) Viral Nucleases Induce an mRNA Degradation-Transcription Feedback Loop in Mammalian Cells. Cell Host Microbe **18**: 243–253

Akao Y, Marukawa O, Morikawa H, Nakao K, Kamei M, Hachiya T, Tsujimoto Y (1995) The rck/p54 Candidate Proto-oncogene Product Is a 54-Kilodalton D-E-A-D Box Protein Differentially Expressed in Human and Mouse Tissues. Cancer Res **55**: 3444–3449

Arribere JA, Doudna JA, Gilbert WV (2011) Reconsidering movement of eukaryotic mRNAs between polysomes and P bodies. Mol Cell **44**: 745–758

Ayache J, Bénard M, Ernoult-Lange M, Minshall N, Standart N, Kress M, Weil D (2015) P-body assembly requires DDX6 repression complexes rather than decay or Ataxin2/2L complexes. Mol Biol Cell **26**: 2579–2595

Baeg K, Iwakawa H-O, Tomari Y (2017) The poly(A) tail blocks RDR6 from converting self mRNAs into substrates for gene silencing. Nat Plants **3**: 17036

Bektas Y, Rodriguez-Salus M, Schroeder M, Gomez A, Kaloshian I, Eulgem T (2016) The Synthetic Elicitor DPMP (2,4-dichloro-6-{(E)-[(3-methoxyphenyl)imino]methyl}phenol) Triggers Strong Immunity in Arabidopsis thaliana and Tomato. Sci Rep **6**: 29554

Bergkessel M, Reese JC (2004) An Essential Role for the Saccharomyces cerevisiae DEAD-Box Helicase DHH1 in G1/S DNA-Damage Checkpoint Recovery. Genetics **167**: 21–33

Boag PR, Atalay A, Robida S, Reinke V, Blackwell TK (2008) Protection of specific maternal messenger RNAs by the P body protein CGH-1 (Dhh1/RCK) during Caenorhabditis elegans oogenesis. J Cell Biol **182**: 543–557

Branco-Price C, Kawaguchi R, Ferreira RB, Bailey-Serres J (2005) Genome-wide analysis of transcript abundance and translation in Arabidopsis seedlings subjected to oxygen deprivation. Ann Bot **96**: 647–660

Cao H, Glazebrook J, Clarke JD, Volko S, Dong X (1997) The Arabidopsis NPR1 gene that controls systemic acquired resistance encodes a novel protein containing ankyrin repeats. Cell **88**: 57–63

Carroll JS, Munchel SE, Weis K (2011) The DExD/H box ATPase Dhh1 functions in translational repression, mRNA decay, and processing body dynamics. J Cell Biol **194**: 527–537

Chantarachot T, Bailey-Serres J (2018) Polysomes, Stress Granules, and Processing Bodies: A Dynamic Triumvirate Controlling Cytoplasmic mRNA Fate and Function. Plant Physiol **176**: 254–269

Chen C-YA, Shyu A-B (2017) Emerging Themes in Regulation of Global mRNA Turnover in cis. Trends Biochem Sci **42**: 16–27

Cheng Z, Coller J, Parker R, Song H (2005) Crystal structure and functional analysis of DEAD-box protein Dhh1p. RNA **11**: 1258–1270

Chen L, Liao B, Qi H, Xie L-J, Huang L, Tan W-J, Zhai N, Yuan L-B, Zhou Y, Yu L-J, et al (2015) Autophagy contributes to regulation of the hypoxia response during submergence in Arabidopsis thaliana. Autophagy **11**: 2233–2246

Chen Y, Boland A, Kuzuoğlu-Öztürk D, Bawankar P, Loh B, Chang C-T, Weichenrieder O, Izaurralde E (2014) A DDX6-CNOT1 complex and W-binding pockets in CNOT9 reveal direct links between miRNA target recognition and silencing. Mol Cell **54**: 737–750

Chicois C, Scheer H, Garcia S, Zuber H, Mutterer J, Chicher J, Hammann P, Gagliardi D, Garcia D (2018) The UPF1 interactome reveals interaction networks between RNA degradation and translation repression factors in Arabidopsis. Plant J. doi: 10.1111/tpj.14022

Chu C-Y, Rana TM (2006) Translation Repression in Human Cells by MicroRNA-Induced Gene Silencing Requires RCK/p54. PLoS Biol **4**: e210

Coller JM, Tucker M, Sheth U, Valencia-Sanchez MA, Parker R (2001) The DEAD box helicase, Dhh1p, functions in mRNA decapping and interacts with both the decapping and deadenylase complexes. RNA **7**: 1717–1727

Coller J, Parker R (2005) General Translational Repression by Activators of mRNA Decapping. Cell **122**: 875–886

Ding J, Li D, Ohler U, Guan J, Zhou S (2012) Genome-wide search for miRNA-target interactions in Arabidopsis thaliana with an integrated approach. BMC Genomics **13 Suppl 3**: S3

Drechsel G, Kahles A, Kesarwani AK, Stauffer E, Behr J, Drewe P, Rätsch G, Wachter A (2013) Nonsense-mediated decay of alternative precursor mRNA splicing variants is a major determinant of the Arabidopsis steady state transcriptome. Plant Cell **25**: 3726–3742

Dutta A, Zheng S, Jain D, Cameron CE, Reese JC (2011) Intermolecular Interactions within the Abundant DEAD-box Protein Dhh1 Regulate Its Activity in Vivo. J Biol Chem **286**: 27454–27470

Ernoult-Lange M, Baconnais S, Harper M, Minshall N, Souquere S, Boudier T, Bénard M, Andrey P, Pierron G, Kress M, et al (2012) Multiple binding of repressed mRNAs by the P-body protein Rck/p54. RNA **18**: 1702–1715

Feng L, Niu D-K (2007) Relationship between mRNA stability and length: an old question with a new twist. Biochem Genet **45**: 131–137

Fischer N, Weis K (2002) The DEAD box protein Dhh1 stimulates the decapping enzyme Dcp1. EMBO J **21**: 2788–2797

Fu ZQ, Dong X (2013) Systemic acquired resistance: turning local infection into global defense. Annu Rev Plant Biol **64**: 839–863

Gloggnitzer J, Akimcheva S, Srinivasan A, Kusenda B, Riehs N, Stampfl H, Bautor J, Dekrout B, Jonak C, Jiménez-Gómez JM, et al (2014) Nonsense-Mediated mRNA Decay Modulates Immune Receptor Levels to Regulate Plant Antibacterial Defense. Cell Host Microbe **16**: 376–390

Haimovich G, Medina DA, Causse SZ, Garber M, Millán-Zambrano G, Barkai O, Chávez S, Pérez-Ortín JE, Darzacq X, Choder M (2013) Gene expression is circular: factors for mRNA degradation also foster mRNA synthesis. Cell **153**: 1000–1011

Hata H, Mitsui H, Liu H, Bai Y, Denis CL, Shimizu Y, Sakai A (1998) Dhh1p, a Putative RNA Helicase, Associates with the General Transcription Factors Pop2p and Ccr4p from Saccharomyces cerevisiae. Genetics **148**: 571–579

H Backman TW, Girke T (2016) systemPipeR: NGS workflow and report generation environment. BMC Bioinformatics **17**: 388

He W, Parker R (2001) The yeast cytoplasmic LsmI/Pat1p complex protects mRNA 3' termini from partial degradation. Genetics **158**: 1445–1455

Igreja C, Izaurralde E (2011) CUP promotes deadenylation and inhibits decapping of mRNA targets. Genes Dev **25**: 1955–1967

Kamenska A, Lu W-T, Kubacka D, Broomhead H, Minshall N, Bushell M, Standart N (2014) Human 4E-T represses translation of bound mRNAs and enhances microRNA-mediated silencing. Nucleic Acids Res **42**: 3298–3313

Kamenska A, Simpson C, Vindry C, Broomhead H, Bénard M, Ernoult-Lange M, Lee BP, Harries LW, Weil D, Standart N (2016) The DDX6-4E-T interaction mediates translational repression and P-body assembly. Nucleic Acids Res **44**: 6318–6334

Kawaguchi R, Girke T, Bray EA, Bailey-Serres J (2004) Differential mRNA translation contributes to gene regulation under non-stress and dehydration stress conditions in Arabidopsis thaliana. Plant J **38**: 823–839

Kinkelin K, Veith K, Grünwald M, Bono F (2012) Crystal structure of a minimal eIF4E-Cup complex reveals a general mechanism of eIF4E regulation in translational repression. RNA **18**: 1624–1634

Klessig DF, Choi HW, Dempsey DA (2018) Systemic Acquired Resistance and Salicylic Acid: Past, Present, and Future. Mol Plant Microbe Interact **31**: 871–888

Kumakura N, Otsuki H, Tsuzuki M, Takeda A, Watanabe Y (2013) Arabidopsis AtRRP44A Is the Functional Homolog of Rrp44/Dis3, an Exosome Component, Is Essential for Viability and Is Required for RNA Processing and Degradation. PLoS One **8**: e79219

Kumar R, Ichihashi Y, Kimura S, Chitwood DH, Headland LR, Peng J, Maloof JN, Sinha NR (2012) A High-Throughput Method for Illumina RNA-Seq Library Preparation. Front Plant Sci **3**: 202

Ladomery M, Wade E, Sommerville J (1997) Xp54, the Xenopus Homologue of Human RNA Helicase p54, is an Integral Component of Stored mRNP Particles in Oocytes. Nucleic Acids Res **25**: 965–973

Lawrence M, Huber W, Pagès H, Aboyoun P, Carlson M, Gentleman R, Morgan MT, Carey VJ (2013) Software for computing and annotating genomic ranges. PLoS Comput Biol **9**: e1003118

Linder P, Jankowsky E (2011) From unwinding to clamping — the DEAD box RNA helicase family. Nat Rev Mol Cell Biol **12**: 505–516

Liu L, Chen X (2016) RNA Quality Control as a Key to Suppressing RNA Silencing of Endogenous Genes in Plants. Mol Plant **9**: 826–836

Lumb JH, Li Q, Popov LM, Ding S, Keith MT, Merrill BD, Greenberg HB, Li JB, Carette JE (2017) DDX6 Represses Aberrant Activation of Interferon-Stimulated Genes. Cell Rep **20**: 819–831

Maekawa H, Nakagawa T, Uno Y, Kitamura K, Shimoda C (1994) Theste13+ gene encoding a putative RNA helicase is essential for nitrogen starvation-induced G1 arrest and initiation of sexual development in the fission yeastSchizosaccharomyces pombe. Mol Gen Genet **244**: 456–464

Maillet L, Collart MA (2002) Interaction between Not1p, a Component of the Ccr4-Not Complex, a Global Regulator of Transcription, and Dhh1p, a Putative RNA Helicase. J Biol Chem **277**: 2835–2842

Malamy J, Carr JP, Klessig DF, Raskin I (1990) Salicylic Acid: a likely endogenous signal in the resistance response of tobacco to viral infection. Science **250**: 1002–1004

Martínez de Alba AE, Moreno AB, Gabriel M, Mallory AC, Christ A, Bounon R, Balzergue S, Aubourg S, Gautheret D, Crespi MD, et al (2015) In plants, decapping prevents RDR6-dependent production of small interfering RNAs from endogenous mRNAs. Nucleic Acids Res **43**: 2902–2913

Mathys H, Basquin J, Ozgur S, Czarnocki-Cieciura M, Bonneau F, Aartse A, Dziembowski A, Nowotny M, Conti E, Filipowicz W (2014) Structural and biochemical insights to the role of the CCR4-NOT complex and DDX6 ATPase in microRNA repression. Mol Cell **54**: 751–765

Merchante C, Stepanova AN, Alonso JM (2017) Translation regulation in plants: an interesting past, an exciting present and a promising future. Plant J **90**: 628–653

Meteignier L-V, El Oirdi M, Cohen M, Barff T, Matteau D, Lucier J-F, Rodrigue S, Jacques P-E, Yoshioka K, Moffett P (2017) Translatome analysis of an NB-LRR immune response identifies important contributors to plant immunity in Arabidopsis. J Exp Bot **68**: 2333–2344

Meteignier L-V, Zhou J, Cohen M, Bhattacharjee S, Brosseau C, Chan C, Goretty M, Robatzek S, Moffett P (2016) NB-LRR signaling induces translational repression of viral transcripts and the formation of RNA processing bodies through mechanisms differing from those activated by UV stress and RNAi. J Exp Bot **67**: 2353–2366

Miller JE, Zhang L, Jiang H, Li Y, Franklin Pugh B, Reese JC (2018) Genome-Wide Mapping of Decay Factor–mRNA Interactions in Yeast Identifies Nutrient-Responsive Transcripts as Targets of the Deadenylase Ccr4. G3: Genes, Genomes, Genetics **8**: 315–330

Minshall N, Reiter MH, Weil D, Standart N (2007) CPEB interacts with an ovary-specific eIF4E and 4E-T in early Xenopus oocytes. J Biol Chem **282**: 37389–37401

Moeller JR, Moscou MJ, Bancroft T, Skadsen RW, Wise RP, Whitham SA (2012) Differential accumulation of host mRNAs on polyribosomes during obligate pathogen-plant interactions. Mol Biosyst **8**: 2153–2165

Mota S, Vieira N, Barbosa S, Delaveau T, Torchet C, Le Saux A, Garcia M, Pereira A, Lemoine S, Coulpier F, et al (2014) Role of the DHH1 Gene in the Regulation of Monocarboxylic Acids Transporters Expression in Saccharomyces cerevisiae. PLoS One **9**: e111589

Mourrain P, Béclin C, Elmayan T, Feuerbach F, Godon C, Morel JB, Jouette D, Lacombe AM, Nikic S, Picault N, et al (2000) Arabidopsis SGS2 and SGS3 genes are required for posttranscriptional gene silencing and natural virus resistance. Cell **101**: 533–542

Mustroph A, Juntawong P, Bailey-Serres J (2009a) Isolation of plant polysomal mRNA by differential centrifugation and ribosome immunopurification methods. Methods Mol Biol **553**: 109–126

Mustroph A, Zanetti ME, Jang CJH, Holtan HE, Repetti PP, Galbraith DW, Girke T, Bailey-Serres J (2009b) Profiling translatomes of discrete cell populations resolves altered cellular priorities during hypoxia in Arabidopsis. Proceedings of the National Academy of Sciences **106**: 18843–18848

Nakamura A, Sato K, Hanyu-Nakamura K (2004) Drosophila cup is an eIF4E binding protein that associates with Bruno and regulates oskar mRNA translation in oogenesis. Dev Cell **6**: 69–78

Narsai R, Howell KA, Millar AH, O'Toole N, Small I, Whelan J (2007) Genome-Wide Analysis of mRNA Decay Rates and Their Determinants in *Arabidopsis thaliana*. The Plant Cell Online **19**: 3418–3436

Navarro RE, Shim EY, Kohara Y, Singson A, Blackwell TK (2001) cgh-1, a conserved predicted RNA helicase required for gametogenesis and protection from physiological germline apoptosis in C. elegans. Development **128**: 3221–3232

Nelson MR, Leidal AM, Smibert CA (2004) Drosophila Cup is an eIF4E-binding protein that functions in Smaug-mediated translational repression. EMBO J **23**: 150–159

Nishihara T, Zekri L, Braun JE, Izaurralde E (2013) miRISC recruits decapping factors to miRNA targets to enhance their degradation. Nucleic Acids Res **41**: 8692–8705

Nishimura T, Padamsi Z, Fakim H, Milette S, Dunham WH, Gingras A-C, Fabian MR (2015) The eIF4E-Binding Protein 4E-T Is a Component of the mRNA Decay Machinery that Bridges the 5' and 3' Termini of Target mRNAs. Cell Rep **11**: 1425–1436

Ozgur S, Basquin J, Kamenska A, Filipowicz W, Standart N, Conti E (2015) Structure of a Human 4E-T/DDX6/CNOT1 Complex Reveals the Different Interplay of DDX6-Binding Proteins with the CCR4-NOT Complex. Cell Rep **13**: 703–711

Pfaffl MW (2001) A new mathematical model for relative quantification in real-time RT-PCR. Nucleic Acids Res **29**: e45

Presnyak V, Coller J (2013) The DHH1/RCKp54 family of helicases: An ancient family of proteins that promote translational silencing. Biochimica et Biophysica Acta (BBA) - Gene Regulatory Mechanisms **1829**: 817–823

Radhakrishnan A, Chen Y-H, Martin S, Alhusaini N, Green R, Coller J (2016) The DEAD-Box Protein Dhh1p Couples mRNA Decay and Translation by Monitoring Codon Optimality. Cell. doi: 10.1016/j.cell.2016.08.053

Riehs-Kearnan N, Gloggnitzer J, Dekrout B, Jonak C, Riha K (2012) Aberrant growth and lethality of Arabidopsis deficient in nonsense-mediated RNA decay factors is caused by autoimmune-like response. Nucleic Acids Res **40**: 5615–5624

Rietz S, Stamm A, Malonek S, Wagner S, Becker D, Medina-Escobar N, Vlot AC, Feys BJ, Niefind K, Parker JE (2011) Different roles of Enhanced Disease Susceptibility1 (EDS1) bound to and dissociated from Phytoalexin Deficient4 (PAD4) in Arabidopsis immunity. New Phytol **191**: 107–119

Robinson MD, McCarthy DJ, Smyth GK (2010) edgeR: a Bioconductor package for differential expression analysis of digital gene expression data. Bioinformatics **26**: 139–140

Roux ME, Rasmussen MW, Palma K, Lolle S, Regué ÀM, Bethke G, Glazebrook J, Zhang W, Sieburth L, Larsen MR, et al (2015) The mRNA decay factor PAT1 functions in a pathway including MAP kinase 4 and immune receptor SUMM2. EMBO J **34**: 593–608

Rouya C, Siddiqui N, Morita M, Duchaine TF, Fabian MR, Sonenberg N (2014) Human DDX6 effects miRNA-mediated gene silencing via direct binding to CNOT1. RNA **20**: 1398–1409

Savchenko T, Walley JW, Chehab EW, Xiao Y, Kaspi R, Pye MF, Mohamed ME, Lazarus CM, Bostock RM, Dehesh K (2010) Arachidonic acid: an evolutionarily conserved signaling molecule modulates plant stress signaling networks. Plant Cell **22**: 3193–3205

Schindelin J, Arganda-Carreras I, Frise E, Kaynig V, Longair M, Pietzsch T, Preibisch S, Rueden C, Saalfeld S, Schmid B, et al (2012) Fiji: an open-source platform for biological-image analysis. Nat Methods **9**: 676–682

Sengupta MS, Low WY, Patterson JR, Kim H-M, Traven A, Beilharz TH, Colaiácovo MP, Schisa JA, Boag PR (2013) ifet-1 is a broad-scale translational repressor required for normal P granule formation in C. elegans. J Cell Sci **126**: 850–859

Sharif H, Conti E (2013) Architecture of the Lsm1-7-Pat1 complex: a conserved assembly in eukaryotic mRNA turnover. Cell Rep **5**: 283–291

Sharif H, Ozgur S, Sharma K, Basquin C, Urlaub H, Conti E (2013) Structural analysis of the yeast Dhh1-Pat1 complex reveals how Dhh1 engages Pat1, Edc3 and RNA in mutually exclusive interactions. Nucleic Acids Res **41**: 8377–8390

Shaul O (2015) Unique Aspects of Plant Nonsense-Mediated mRNA Decay. Trends Plant Sci **20**: 767–779

Sorenson R, Johnson K, Adler F, Sieburth L (2018). RNAdecay: Maximum Likelihood Decay Modeling of RNA Degradation Data. R package version 1.2.0.

Sorenson RS, Deshotel MJ, Johnson K, Adler FR, Sieburth LE (2018) Arabidopsis mRNA decay landscape arises from specialized RNA decay substrates, decapping-mediated feedback, and redundancy. Proc Natl Acad Sci U S A **115**: E1485–E1494

Sun M, Schwalb B, Pirkl N, Maier KC, Schenk A, Failmezger H, Tresch A, Cramer P (2013) Global analysis of eukaryotic mRNA degradation reveals Xrn1-dependent buffering of transcript levels. Mol Cell **52**: 52–62

Sweet T, Kovalak C, Coller J (2012) The DEAD-Box Protein Dhh1 Promotes Decapping by Slowing Ribosome Movement. PLoS Biol **10**: e1001342

Tharun S, He W, Mayes AE, Lennertz P, Beggs JD, Parker R (2000) Yeast Sm-like proteins function in mRNA decapping and decay. Nature **404**: 515–518

Townsley BT, Covington MF, Ichihashi Y, Zumstein K, Sinha NR (2015) BrAD-seq: Breath Adapter Directional sequencing: a streamlined, ultra-simple and fast library preparation protocol for strand specific mRNA library construction. Front Plant Sci **6**: 366

Tritschler F, Braun JE, Eulalio A, Truffault V, Izaurralde E, Weichenrieder O (2009) Structural basis for the mutually exclusive anchoring of P body components EDC3 and Tral to the DEAD box protein DDX6/Me31B. Mol Cell **33**: 661–668

Tritschler F, Eulalio A, Helms S, Schmidt S, Coles M, Weichenrieder O, Izaurralde E, Truffault V (2008) Similar Modes of Interaction Enable Trailer Hitch and EDC3 To Associate with DCP1 and Me31B in Distinct Protein Complexes. Mol Cell Biol **28**: 6695–6708

Tsuzuki M, Motomura K, Kumakura N, Takeda A (2017) Interconnections between mRNA degradation and RDR-dependent siRNA production in mRNA turnover in plants. J Plant Res **130**: 211–226

de Valoir T, Tucker MA, Belikoff EJ, Camp LA, Bolduc C, Beckingham K (1991) A second maternally expressed Drosophila gene encodes a putative RNA helicase of the“ DEAD box” family. Proceedings of the National Academy of Sciences **88**: 2113–2117

Wang M, Ly M, Lugowski A, Laver JD, Lipshitz HD, Smibert CA, Rissland OS (2017) ME31B globally represses maternal mRNAs by two distinct mechanisms during the *Drosophila* maternal-to-zygotic transition. Elife. doi: 10.7554/eLife.27891

Westmoreland TJ, Olson JA, Saito WY, Huper G, Marks JR, Bennett CB (2003) Dhh1 regulates the G1/S-checkpoint following DNA damage or BRCA1 expression in yeast1. J Surg Res **113**: 62–73

Wiermer M, Feys BJ, Parker JE (2005) Plant immunity: the EDS1 regulatory node. Curr Opin Plant Biol **8**: 383–389

Wu Z, Huang S, Zhang X, Wu D, Xia S, Li X (2017) Regulation of plant immune receptor accumulation through translational repression by a glycine-tyrosine-phenylalanine (GYF) domain protein. Elife. doi: 10.7554/eLife.23684

Yu Y, Jia T, Chen X (2017) The “how” and “where” of plant microRNAs. New Phytol **216**: 1002–1017

Zhang W, Murphy C, Sieburth LE (2010) Conserved RNaseII domain protein functions in cytoplasmic mRNA decay and suppresses Arabidopsis decapping mutant phenotypes. Proceedings of the National Academy of Sciences **107**: 15981–15985

Zhang X, Guo H (2017) mRNA decay in plants: both quantity and quality matter. Curr Opin Plant Biol **35**: 138–144

Zhang X, Zhu Y, Liu X, Hong X, Xu Y, Zhu P, Shen Y, Wu H, Ji Y, Wen X, et al (2015) Suppression of endogenous gene silencing by bidirectional cytoplasmic RNA decay in *Arabidopsis*. Science **348**: 120–123

Figure 3.1. Degradation of diverse groups of mRNAs requires RH6, RH8 and RH12 functions. (A) Schematic representation of the experimental design for global RNA decay analysis. Five-day-old seedlings grown on 0.5x MS with 0.5% (w/v) sucrose were subjected to cordycepin treatment and sampled at times 0, 15, 30, 60 and 120 minutes, with three biological replicates. RNA-seq libraries were generated from total RNA following ribosomal RNA depletion. (B) Histograms showing mRNA half-life ($t_{1/2}$) distributions in the Col-0 wild-type and the triple *rh6 rh8 rh12* mutant. The analysis was performed on 16025 genes for both genotypes representing a high-quality decay dataset ($\sigma^2 < 0.0625$) from a total of 18092 genes. Vertical blue lines and the adjacent numbers represent the median mRNA $t_{1/2}$ in each genotype. (C) Heatmap of mRNA decay over 120 minutes and $t_{1/2}$ of individual transcripts in *rh6 rh8 rh12* by comparison to Col-0. mRNA decay is presented as change in mean relative mRNA abundance following cordycepin treatment and hierarchically clustered into three groups. Group 1 comprises mRNAs with decreased decay rates in *rh6 rh8 rh12* (putative RH6/8/12 substrates, *rh6 rh8 rh12* $t_{1/2}$ > Col-0 $t_{1/2}$); group 2 comprises mRNAs with increased decay rates in *rh6 rh8 rh12* (*rh6 rh8 rh12* $t_{1/2}$ < Col-0 $t_{1/2}$); group 3 comprises mRNAs with decay rates of unaffected in *rh6 rh8 rh12* (*rh6 rh8 rh12* $t_{1/2} \simeq$ Col-0 $t_{1/2}$). (D) Bar pot summarizing of the number of genes in different groups based on their relative $t_{1/2}$. (E) Representative Gene Ontology (GO) terms of RH6/8/12 substrates (group 1, *rh6 rh8 rh12* $t_{1/2}$ > Col-0 $t_{1/2}$). (F) Venn diagrams showing the overlap of RH6/8/12 substrates with validated micro(mi)RNA targets from the Integrated miRNA-Target Interaction Prediction (imiRTP) database (Ding et al., 2012) and nonsense mediated decay (NMD) pathway substrates (Drechsel et al., 2013). *p*-values indicates the significance of the overlap based on hypergeometric test.

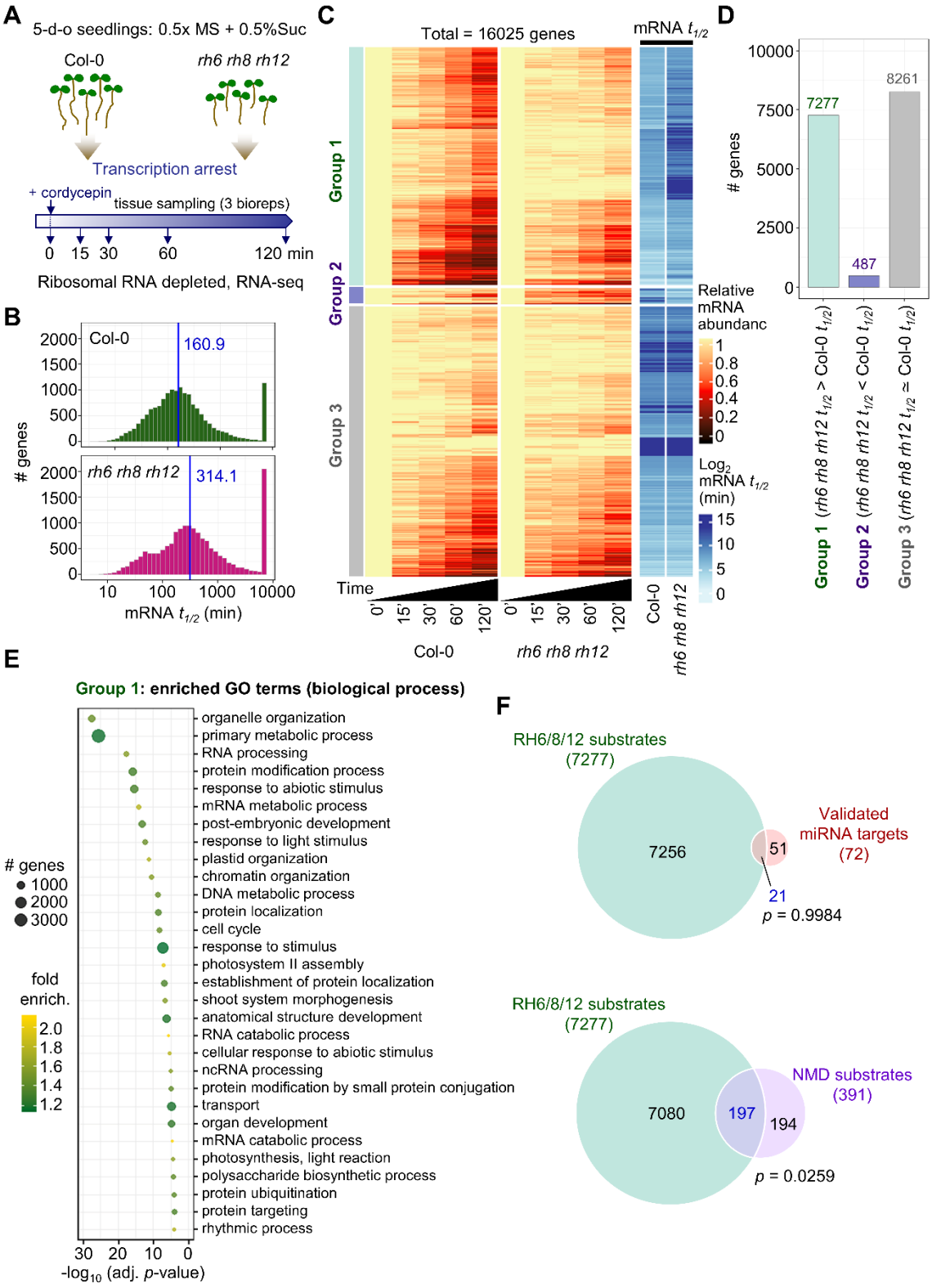
A
5-d-o seedlings: 0.5x MS + 0.5%Suc
Col-0
rh6 rh8 rh12
Transcription arrest
+ cordycepin
tissue sampling (3 bioreps)
0 15 30 60 120 min
Ribosomal RNA depleted, RNA-seq
B
Col-0
160.9
rh6 rh8 rh12
314.1
genes
mRNA $t_{1/2}$ (min)
C
Total = 16025 genes
mRNA $t_{1/2}$
Group 1
Group 2
Group 3
Relative mRNA abundanc
Log2 mRNA $t_{1/2}$ (min)
Time
Col-0
rh6 rh8 rh12
D
genes
7277
487
8261
Group 1 (rh6 rh8 rh12 $t_{1/2}$ > Col-0 $t_{1/2}$)
Group 2 (rh6 rh8 rh12 $t_{1/2}$ < Col-0 $t_{1/2}$)
Group 3 (rh6 rh8 rh12 $t_{1/2}$ ≈ Col-0 $t_{1/2}$)
E
Group 1: enriched GO terms (biological process)
organelle organization
primary metabolic process
RNA processing
protein modification process
response to abiotic stimulus
mRNA metabolic process
post-embryonic development
response to light stimulus
plastid organization
chromatin organization
DNA metabolic process
protein localization
cell cycle
response to stimulus
photosystem II assembly
establishment of protein localization
shoot system morphogenesis
anatomical structure development
RNA catabolic process
cellular response to abiotic stimulus
ncRNA processing
protein modification by small protein conjugation
transport
organ development
mRNA catabolic process
photosynthesis, light reaction
polysaccharide biosynthetic process
protein ubiquitination
protein targeting
rhythmic process
genes
fold enrich.
-log10 (adj. p-value)
F
RH6/8/12 substrates (7277)
7256
51
21
Validated miRNA targets (72)
p = 0.9984
RH6/8/12 substrates (7277)
7080
197
194
NMD substrates (391)
p = 0.0259

Figure 3.2. Characteristics of putative RH6/8/12 substrates. (A) Box-and-whisker plot comparing Col-0 mRNA $t_{1/2}$ between mRNAs that are stabilized in the triple *rh6 rh8 rh12* mutant (putative RH6/8/12 substrates; group 1, *rh6 rh8 rh12* $t_{1/2}$ > Col-0 $t_{1/2}$), mRNAs with accelerated decay in *rh6 rh8 rh12* (*rh6 rh8 rh12* $t_{1/2}$ < Col-0 $t_{1/2}$), and mRNAs the decay of which is not affected in *rh6 rh8 rh12* (*rh6 rh8 rh12* $t_{1/2} \simeq$ Col-0 $t_{1/2}$). **** denotes Benjamini & Hochberg-adjusted *p*-value < 2e-16; n.s., not significantly different (Kruskal-Wallis test followed by Wilcoxon rank sum test). (B) Summary of number of genes in each decay group binned into six classes based on mRNA $t_{1/2}$ in Col-0. (C) Box-and-whisker plots comparing mRNA features between genes that are RH6/8/12 substrates (group 1, *rh6 rh8 rh12* $t_{1/2}$ > Col-0 $t_{1/2}$) and those that are not RH6/8/12 substrates (group 3, *rh6 rh8 rh12* $t_{1/2} \simeq$ Col-0 $t_{1/2}$). * denotes *p*-value < 0.05; ** denotes *p*-value < 0.01; denotes *p*-value < 0.001; denotes *p*-value < 0.0001; n.s., not significantly different. (Wilcoxon rank sum test).

A

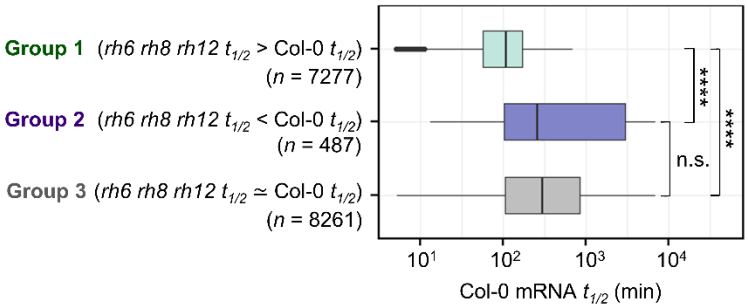

B

Col-0 mRNA $t_{1/2}$ (min)	# genes					
	[0,30]	(30,60]	(60,120]	(120,240]	(240,480]	(480,inf.)
Group 1	775	1102	2187	2282	875	56
Group 2	13	41	93	83	71	186
Group 3	414	939	868	1370	1644	3026

C

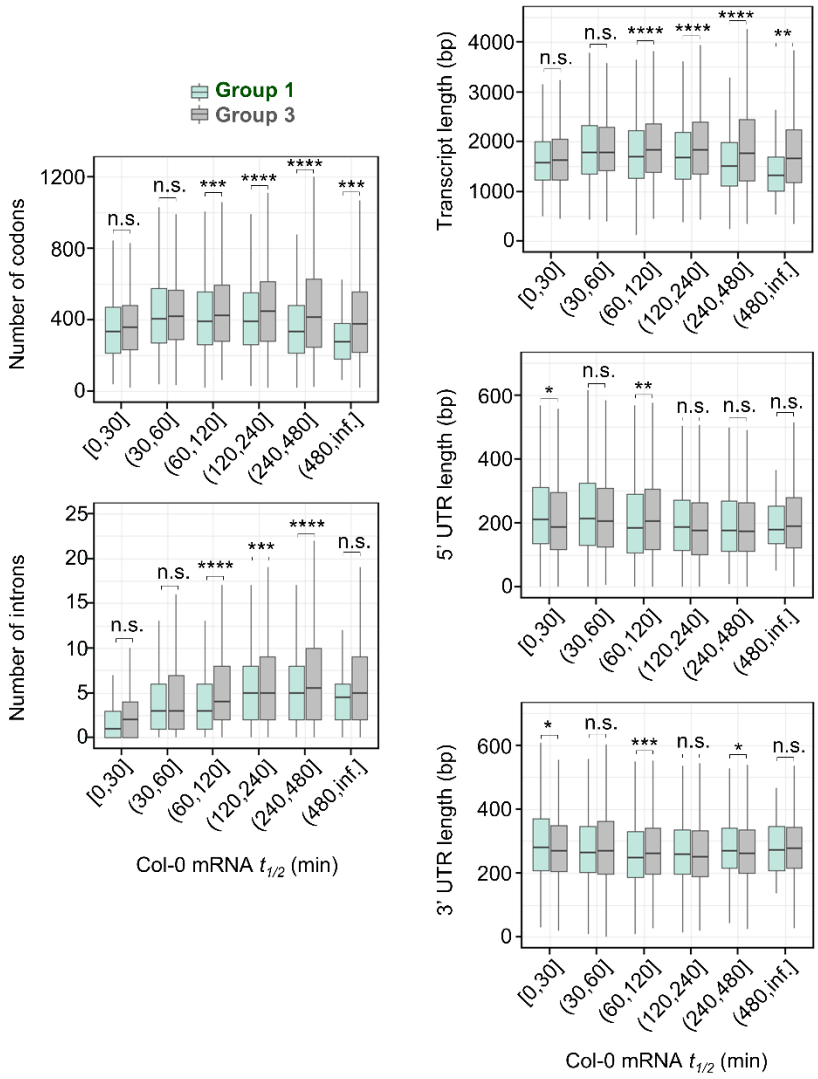

Figure 3.3 Putative RH6/8/12 substrates largely overlap with those controlled by VARICOSE. (A) Pie charts showing the proportions of genes with increased mRNA $t_{1/2}$ in the triple *rh6 rh8 rh12* and *vcs-7* mutants relative to Col-0, and Venn diagrams showing the overlap between the two populations. These mRNA cohorts were considered RH6/8/12 and VCS substrates as they are stabilized in *rh6 rh8 rh12* and *vcs-7*, respectively. *vcs-7* mRNA decay data were obtained from Sorenson et al. (2018). The data were re-modeled with the five time-points and three biological replicates as used in the *rh6 rh8 rh12* analysis. The comparison was limited to genes with the wild type mRNA $t_{1/2}$ < 12 hours because the maximum wild type mRNA $t_{1/2}$ of RH6/8/12 substrates was 690.06 minutes (11.5 hours). Both mutant genotypes are in the Col-0 background. (B) Box-and-whisker plots comparing the Col-0 $t_{1/2}$ of RH6/8/12-specific substrates (*n* = 1109), RH6/8/12 substrates that overlap with those of VCS (*n* = 5832), VCS-specific substrates (*n* = 3862), and mRNAs that are neither RH6/8/12 nor VCS substrates (*n* = 1894) as classified in (A). ***** denotes *p*-value < 2.2e-16, n.s. = no significant difference; Wilcoxon rank sum test.

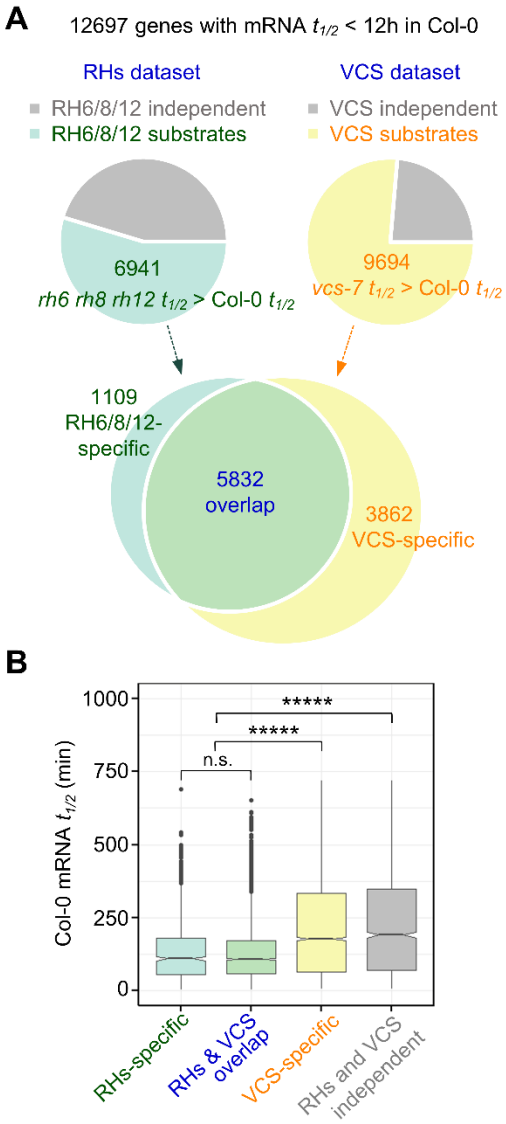
A
12697 genes with mRNA $t_{1/2}$ < 12h in Col-0
RHs dataset
VCS dataset
RH6/8/12 independent
RH6/8/12 substrates
VCS independent
VCS substrates
6941
rh6 rh8 rh12 $t_{1/2}$ > Col-0 $t_{1/2}$
9694
vcs-7 $t_{1/2}$ > Col-0 $t_{1/2}$
1109
RH6/8/12-specific
5832
overlap
3862
VCS-specific
B
Col-0 mRNA $t_{1/2}$ (min)
1000
750
500
250
0
*****
*****
n.s.
RHs-specific
RHs & VCS overlap
VCS-specific
RHs and VCS independent

Figure 3.4. The triple *rh6 rh8 rh12* mutant phenotype is *RNA-DEPENDENT RNA POLYMERASE 6/SUPPRESSOR OF GENE SILENCING 3* independent. (A) Rosette growth phenotype of 28-day-old plants of Col-0, single *rdr6*$^{sgs2\text{-}1}$ and *sgs3-1* mutants, the triple *rh6 rh8 rh12* mutant, and quadruple *rh6 rh8 rh12; rdr6*$^{sgs2\text{-}1}$ and *rh6 rh8 rh12; sgs3-1* mutants. Seeds were germinated and grown on 0.5x MS media with 0.5% (w/v) sucrose for 7 days before transfer to soil and growth for 21 days. Bar = 1 cm. All mutants are in the Col-0 background. Photos are representative of genotypes. (B) Rosette diameter and fresh weight of 28-day-old plants of the genotypes presented in (A). Statistical significance was determined by ANOVA (n = 30), followed by the Tukey's HSD test on log-transformed data. Means that are significantly different from one another ($p < 0.05$) are denoted by different letters.

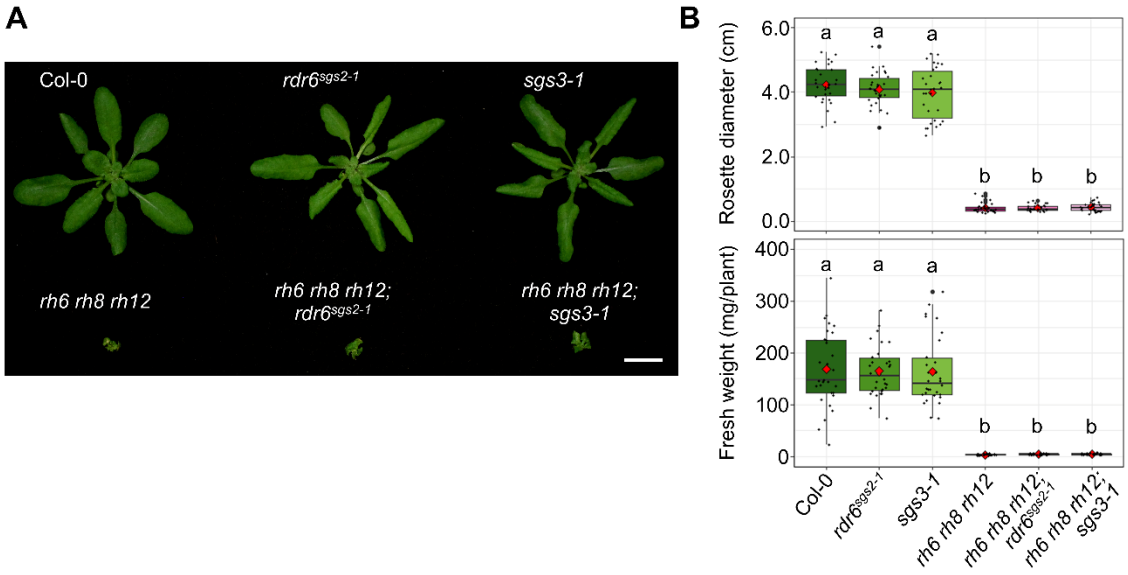
A
Col-0
rdr6sgs2-1
sgs3-1
rh6 rh8 rh12
rh6 rh8 rh12; rdr6sgs2-1
rh6 rh8 rh12; sgs3-1
B
Rosette diameter (cm)
Fresh weight (mg/plant)
a
b
Col-0
rdr6sgs2-1
sgs3-1
rh6 rh8 rh12
rh6 rh8 rh12; rdr6sgs2-1
rh6 rh8 rh12; sgs3-1

Figure 3.5. Attenuation of *RH6*, *RH8* and *RH12* function shifts the seedling steady-state transcriptome and translatome from a general growth to stress-responsive state. (A) Schematic representation of experimental setup for transcriptome and translatome analyses. For translatome analysis, ribosome-associated RNAs were isolated from developmental age-matched 5-day-old seedlings of Col-0 and the triple *rh6 rh8 rh12* mutant expressing His-FLAG-GFP tagged RIBOSOMAL PROTEIN L18 (*pro35S:HF-GFP-RPL18*) using Translating Ribosome Affinity Purification (TRAP). Total RNAs isolated in parallel from the same tissues were used for transcriptome analysis. (B) Principal component analysis of edgeR-normalized read counts (CPMs) of total and TRAP mRNAs from Col-0 and triple *rh6 rh8 rh12* mutant. PC1 and PC2 are principal components 1 and 2. (C) Volcano plots of change in TOTAL and TRAP mRNA of the triple *rh6 rh8 rh12* mutant relative to Col-0 based on differential abundance analysis by edgeR. The $\log_2$ fold-change (FC) are shown on the x-axis, and the negative $\log_{10}$ of the false-discovery rate (FDR) is shown on the y-axis. Red and blue dots represent significantly enriched and depleted mRNAs, respectively ($|\log_2 FC| \geq 1$, FDR < 0.01). Green dots represent non-differentially expressed genes. Total number of genes used in the analysis is given in parentheses. (D) Scatter plot comparison of the $\log_2$ FC between total and TRAP mRNAs in the *rh6 rh8 rh12* mutant relative to Col-0. Black line represents the linear regression fit. *R* represents Pearson correlation coefficient of significantly enriched and depleted genes (red and blue dots, $|\log_2 FC| \geq 1$, FDR < 0.01 in any of the two populations). (E) Venn diagrams showing the overlap of genes significantly enriched or depleted in *rh6 rh8 rh12* ($|\log_2 FC| \geq 1$, FDR < 0.01) between TOTAL and TRAP RNA populations. (F) GO functional categories (biological process) of gene transcripts differentially accumulated (enriched or depleted) in the triple *rh6 rh8 rh12* mutant relative to Col-0 as identified in (C). A total of 278 and 46 terms were enriched (adjusted *p*-value < 0.05) in *rh6 rh8 rh12*-enriched and -depleted genes of the TOTAL mRNA population, respectively; only 10 non-redundant terms with the lowest adjusted *p*-values are presented. A total of 278 and 154 terms were enriched (adjusted *p*-value < 0.05) in *rh6 rh8 rh12*-enriched and -depleted genes of the TRAP fraction, respectively; only 10 non-redundant terms with the lowest adjusted *p*-values are presented. Fold enrichment (fold enrich.) represents the number of genes observed relative to the expected number in each category.

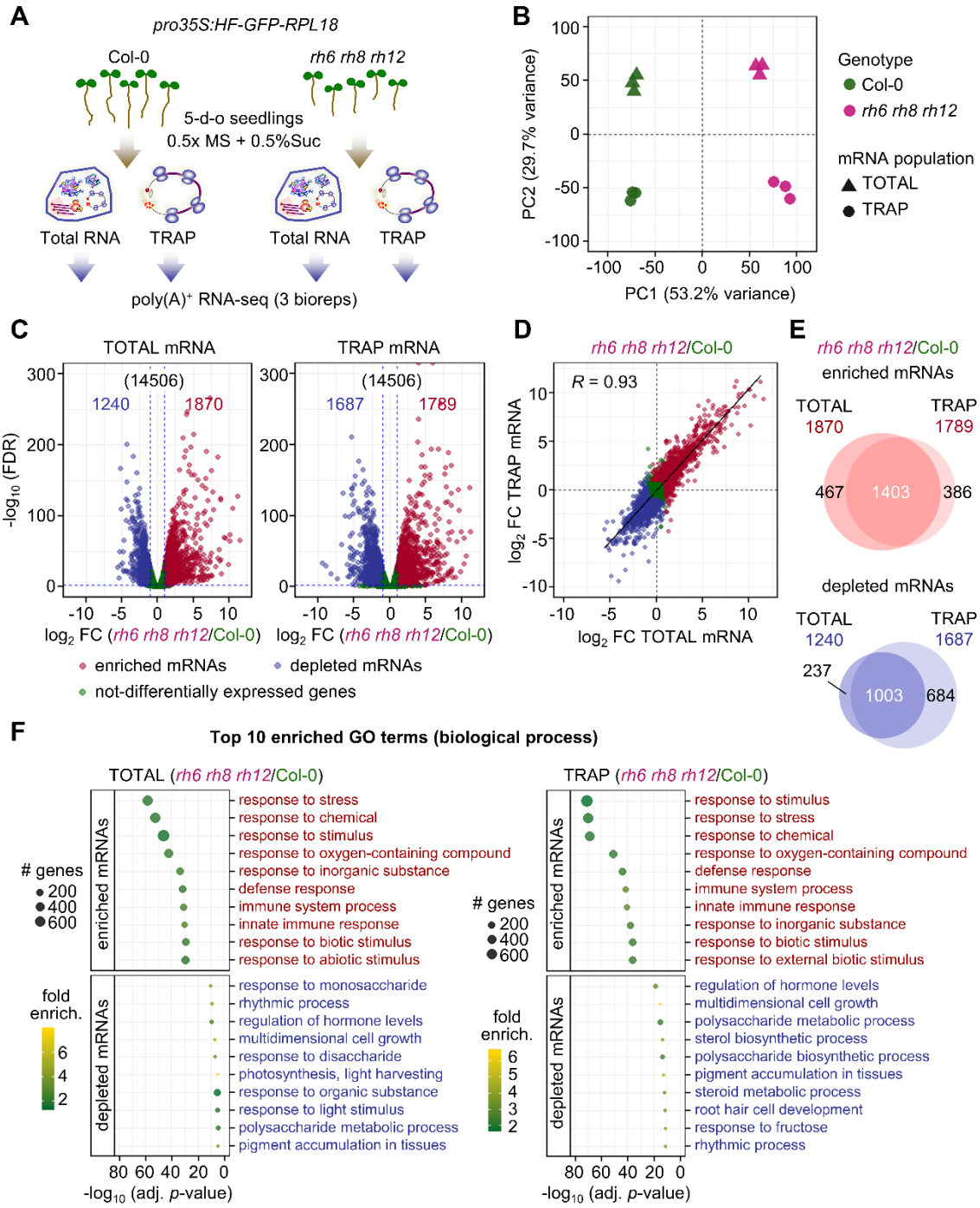
A
pro35S:HF-GFP-RPL18
Col-0
rh6 rh8 rh12
5-d-o seedlings
0.5x MS + 0.5%Suc
Total RNA
TRAP
Total RNA
TRAP
poly(A)+ RNA-seq (3 bioreps)
B
PC2 (29.7% variance)
PC1 (53.2% variance)
Genotype
Col-0
rh6 rh8 rh12
mRNA population
TOTAL
TRAP
C
TOTAL mRNA
TRAP mRNA
(14506)
1240
1870
1687
1789
-log10 (FDR)
log2 FC (rh6 rh8 rh12/Col-0)
enriched mRNAs
depleted mRNAs
not-differentially expressed genes
D
rh6 rh8 rh12/Col-0
R = 0.93
log2 FC TRAP mRNA
log2 FC TOTAL mRNA
E
rh6 rh8 rh12/Col-0
enriched mRNAs
TOTAL
1870
TRAP
1789
467
1403
386
depleted mRNAs
TOTAL
1240
TRAP
1687
237
1003
684
F
Top 10 enriched GO terms (biological process)
TOTAL (rh6 rh8 rh12/Col-0)
TRAP (rh6 rh8 rh12/Col-0)
genes
fold enrich.
enriched mRNAs
depleted mRNAs
response to stress
response to chemical
response to stimulus
response to oxygen-containing compound
response to inorganic substance
defense response
immune system process
innate immune response
response to biotic stimulus
response to abiotic stimulus
response to monosaccharide
rhythmic process
regulation of hormone levels
multidimensional cell growth
response to disaccharide
photosynthesis, light harvesting
response to organic substance
response to light stimulus
polysaccharide metabolic process
pigment accumulation in tissues
response to stimulus
response to external biotic stimulus
sterol biosynthetic process
polysaccharide biosynthetic process
pigment accumulation in tissues
steroid metabolic process
root hair cell development
response to fructose
-log10 (adj. p-value)

Figure 3.6. Directional changes in translational status of mRNAs in the triple *rh6 rh8 rh12* mutant. (A) Volcano plots of change in translational status calculated by comparison of steady-state TOTAL and TRAP mRNA abundance in Col-0 and the triple *rh6 rh8 rh12* mutant based on differential abundance analysis by edgeR. The $\log_2$ FC is shown on the x-axis, and the negative $\log_{10}$ of the FDR is shown on the y-axis. Red and blue dots represent translational status enhanced and repressed genes, respectively ($|\log_2 FC| \geq 1$, FDR < 0.01). Green dots represent genes that are not differentially associated with ribosomes relative to total transcript abundance. Total number of genes used in the analysis is presented in parentheses. (B) Venn diagrams comparing gene sets with enhanced or repressed translational status ($|\log_2 FC| \geq 1$, FDR < 0.01) between Col-0 and the triple *rh6 rh8 rh12* mutant. (C) Biological process GO categories of 216 genes in (B) with an increased translational status specifically in the triple *rh6 rh8 rh12* mutant. (D) Biological process GO categories of 424 genes in (B) with a reduced translational status specifically in the triple *rh6 rh8 rh12* mutant. (E) Scatter plot of the change in translational status of RH6/8/12 substrates (Group 1: *rh6 rh8 rh12* $t_{1/2}$ > Col-0 $t_{1/2}$) and non-substrates (Group 2 & 3: *rh6 rh8 rh12* $t_{1/2} \leq$ Col-0 $t_{1/2}$) between Col-0 and the triple *rh6 rh8 rh12* mutant. Translational status was presented as $\log_2$ FC in TRAP mRNA relative to TOTAL mRNA of genes for each genotype. The analysis was performed on the merged mRNA decay and translatome datasets comprising 12351 genes, 7185 of which with the FDR < 0.01 in at least one genotype were analyzed. Green and grey lines represent linear regression fit for RH6/8/12 substrates and non-substrates, respectively. *R*, Pearson correlation coefficient. (F) Box-and-whisker plot comparing translational status of RH6/8/12 substrates with those that are not RH6/8/12 substrates as presented in (E). **** denotes *p*-value < 2e-16, Wilcoxon signed rank test (between genotypes) or Wilcoxon rank sum test (between groups).

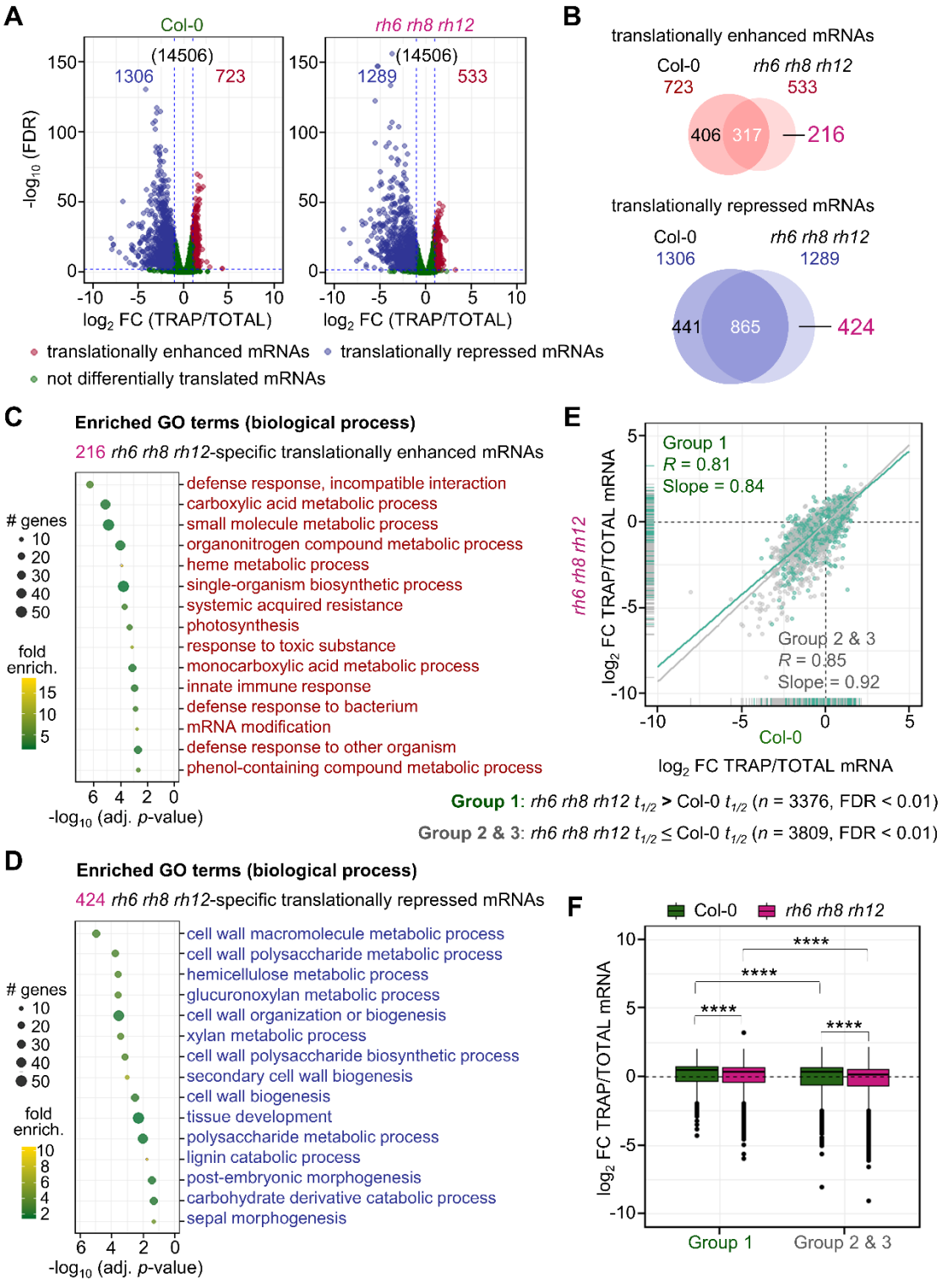
A
Col-0
rh6 rh8 rh12
(14506)
1306
723
1289
533
-log10 (FDR)
log2 FC (TRAP/TOTAL)
translationally enhanced mRNAs
translationally repressed mRNAs
not differentially translated mRNAs
B
translationally enhanced mRNAs
Col-0
723
rh6 rh8 rh12
533
406
317
216
translationally repressed mRNAs
Col-0
1306
rh6 rh8 rh12
1289
441
865
424
C
Enriched GO terms (biological process)
216 rh6 rh8 rh12-specific translationally enhanced mRNAs
genes
fold enrich.
defense response, incompatible interaction
carboxylic acid metabolic process
small molecule metabolic process
organonitrogen compound metabolic process
heme metabolic process
single-organism biosynthetic process
systemic acquired resistance
photosynthesis
response to toxic substance
monocarboxylic acid metabolic process
innate immune response
defense response to bacterium
mRNA modification
defense response to other organism
phenol-containing compound metabolic process
-log10 (adj. p-value)
D
Enriched GO terms (biological process)
424 rh6 rh8 rh12-specific translationally repressed mRNAs
genes
fold enrich.
cell wall macromolecule metabolic process
cell wall polysaccharide metabolic process
hemicellulose metabolic process
glucuronoxylan metabolic process
cell wall organization or biogenesis
xylan metabolic process
cell wall polysaccharide biosynthetic process
secondary cell wall biogenesis
cell wall biogenesis
tissue development
polysaccharide metabolic process
lignin catabolic process
post-embryonic morphogenesis
carbohydrate derivative catabolic process
sepal morphogenesis
-log10 (adj. p-value)
E
Group 1
R = 0.81
Slope = 0.84
Group 2 & 3
R = 0.85
Slope = 0.92
rh6 rh8 rh12
log2 FC TRAP/TOTAL mRNA
Col-0
log2 FC TRAP/TOTAL mRNA
Group 1: rh6 rh8 rh12 t1/2 > Col-0 t1/2 (n = 3376, FDR < 0.01)
Group 2 & 3: rh6 rh8 rh12 t1/2 ≤ Col-0 t1/2 (n = 3809, FDR < 0.01)
F
Col-0
rh6 rh8 rh12
****
log2 FC TRAP/TOTAL mRNA
Group 1
Group 2 & 3

Figure 3.7. RH6, RH8 and RH12 regulate translational status of specific stress-responsive transcripts by coupling translational repression with mRNA decay. (A) Pie charts summarizing the proportions of RH6/8/12 decay substrates with alterations in their steady-state TOTAL and TRAP mRNA abundance in *rh6 rh8 rh12* mutant relative to Col-0. The analysis was performed on a combined dataset of mRNA decay, transcriptome and translatome data comprised of 12351 genes, of which 5919 are RH6/8/12 substrates (*rh6 rh8 rh12* mRNA $t_{1/2}$ > Col-0 $t_{1/2}$). Genes with a FDR < 0.01 and fold change ≥ 2 (|log2 FC| ≥1) in *rh6 rh8 rh12* relative to Col-0 were considered *rh6 rh8 rh12*-enriched or -depleted genes. (B) Venn diagram showing the overlap between RH6/8/12 substrates and TOTAL and TRAP mRNAs that are enriched in *rh6 rh8 rh12* relative to Col-0 (log_2 FC ≥1, FDR < 0.01) from a combined analysis of mRNA decay, transcriptome and translatome data as in (A). (C) Box-and-whisker plot comparing translational status of RH6/8/12 substrates that are enriched in the triple *rh6 rh8 rh12* mutant relative to Col-0 for both TOTAL and TRAP mRNA populations [397 genes in (B)] with those that are not RH6/8/12 substrates but enriched in *rh6 rh8 rh12* for both TOTAL and TRAP mRNA populations [523 genes in (B)]. Translation status of a transcript in each genotype was determine as log_2 FC of TRAP/TOTAL mRNA. The evaluation was limited to mRNAs with translational status change (FDR < 0.01) in at least one of the genotypes (*n*= 223 for RH6/8/12 substrates; *n*= 325 for none-RH6/8/12 substrates). *** denotes *p*-value = 0.0002, **** denotes *p*-value = 0.00000009; Wilcoxon signed rank test. ** denotes *p*-value = 0.005, n.s. = no significant difference; Wilcoxon rank sum test. (D) GO functional categories (biological process) of 397 genes with stabilized transcripts in the triple *rh6 rh8 rh12* mutant concomitant with an increase in TOTAL and TRAP mRNA relative to Col-0. A total of 90 GO terms were enriched (adjusted *p*-value < 0.05); only 20 terms with the lowest adjusted *p*-values are presented. (E) Representative mRNA decay profiles of genes associated with defense response that belong to a group of 447 genes with stabilized transcripts in the triple *rh6 rh8 rh12* mutant concomitant with an increase in TOTAL and TRAP mRNA relative to Col-0. mRNA decay profile of each genotype is presented as relative mRNA abundance after inhibition of transcription by cordycepin treatment (thin line, mean ± SE, *n* =3) along with modelled value (thick line). $t_{1/2}$ for each genotype is shown. *PDF2.1*, *PLANT DEFENSIN 2.1*; *PAD4*, *PHYTOALEXIN DEFICIENT 4*; *JAZ9*, *JASMONATE-ZIM-DOMAIN PROTEIN 9*; *CORI1*, *CORONATINE-INDUCED PROTEIN 1*; *WRKY18*, *WRKY DNA-BINDING PROTEIN 18*; *WRKY33*, *WRKY DNA-BINDING PROTEIN 33*; *CYP81D11*, *CYTOCHROME P450 FAMILY 81 SUBFAMILY D POLYPEPTIDE 11*; *CAF1b*; *CCR4- ASSOCIATED FACTOR 1B*.

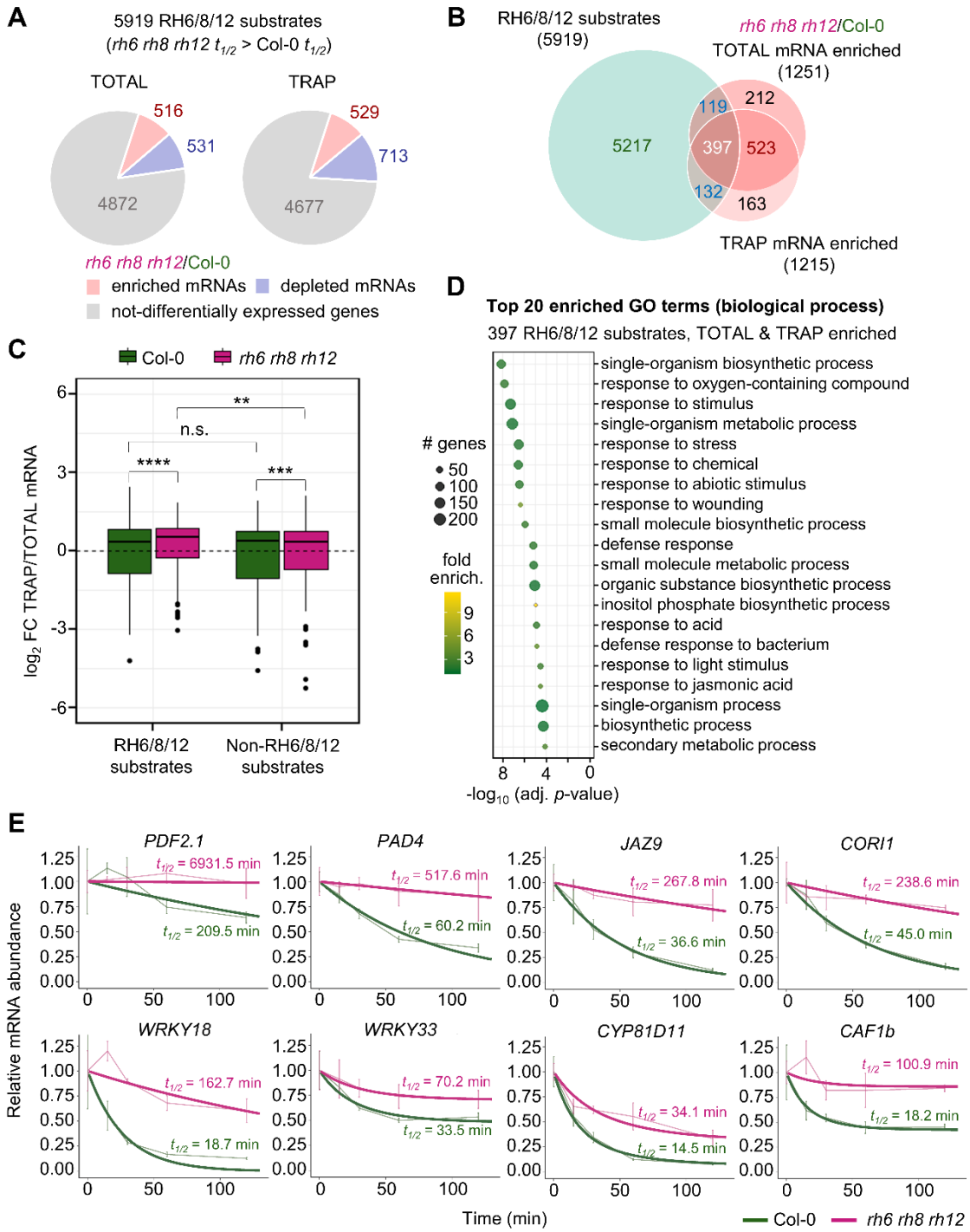
A
5919 RH6/8/12 substrates
(rh6 rh8 rh12 t1/2 > Col-0 t1/2)
TOTAL
TRAP
516
531
4872
529
713
4677
rh6 rh8 rh12/Col-0
enriched mRNAs
depleted mRNAs
not-differentially expressed genes
B
RH6/8/12 substrates
(5919)
rh6 rh8 rh12/Col-0
TOTAL mRNA enriched
(1251)
TRAP mRNA enriched
(1215)
5217
119
212
397
523
132
163
C
Col-0
rh6 rh8 rh12
log2 FC TRAP/TOTAL mRNA
n.s.
**
****
***
RH6/8/12
substrates
Non-RH6/8/12
substrates
D
Top 20 enriched GO terms (biological process)
397 RH6/8/12 substrates, TOTAL & TRAP enriched
genes
fold
enrich.
single-organism biosynthetic process
response to oxygen-containing compound
response to stimulus
single-organism metabolic process
response to stress
response to chemical
response to abiotic stimulus
response to wounding
small molecule biosynthetic process
defense response
small molecule metabolic process
organic substance biosynthetic process
inositol phosphate biosynthetic process
response to acid
defense response to bacterium
response to light stimulus
response to jasmonic acid
single-organism process
biosynthetic process
secondary metabolic process
-log10 (adj. p-value)
E
PDF2.1
PAD4
JAZ9
CORI1
WRKY18
WRKY33
CYP81D11
CAF1b
t1/2 = 6931.5 min
t1/2 = 209.5 min
t1/2 = 517.6 min
t1/2 = 60.2 min
t1/2 = 267.8 min
t1/2 = 36.6 min
t1/2 = 238.6 min
t1/2 = 45.0 min
t1/2 = 162.7 min
t1/2 = 18.7 min
t1/2 = 70.2 min
t1/2 = 33.5 min
t1/2 = 34.1 min
t1/2 = 14.5 min
t1/2 = 100.9 min
t1/2 = 18.2 min
Relative mRNA abundance
Time (min)
Col-0
rh6 rh8 rh12

Figure 3.8. The triple *rh6 rh8 rh12* mutant exhibits a constitutive immune response in a PAD4-partially dependent but EDS1-independent manner. (A) Examples of 26 defense-related genes with constitutively elevated transcripts in *rh6 rh8 rh12*. The data are presented as $\log_2$ FC of TOTAL and TRAP mRNA abundance in *rh6 rh8 rh12* relative to Col-0 with all the genes shown having an FDR < 0.01. Horizontal dashed line indicates a 2-fold change in transcript abundance ($\log_2$ FC = 1). (B) Quantification of salicylic acid (SA) in 7-day-old seedlings of *rh6 rh8 rh12* in comparison to Col-0 under standard growth conditions. Error bars represent the SD of three biological replicates. ** denotes *p*-value = 0.001848; Welch Two Sample t-test. (C) Heatmap representing relative fold change in TOTAL and TRAP mRNA abundance for 107 of the 155 'core' EDS1/PAD-induced genes (Cui et al., 2016) of *rh6 rh8 rh12* relative to Col-0. Individual genes are presented as column with the upper two rows showing their $\log_2$ FC following 12 and 24 hours of EDS1 and PAD4 overexpression (Cui et al., 2016), whereas the lower two rows representing their $\log_2$ FC in TOTAL and TRAP populations of *rh6 rh8 rh12* relative to Col-0. (D)Rosette growth phenotype of 28-day-old plants of Col-0, single *eds1-2* and *pad4-1* mutants, triple *rh6 rh8 rh12* mutant, quadruple *rh6 rh8 rh12; eds1-2* and *rh6 rh8 rh12; pad4-1* mutants, double homozygous heterozygous triple *rh6*$^{(+/-)}$ *rh8 rh12* mutant, and triple homozygous heterozygous quadruple *rh6*$^{(+/-)}$ *rh8 rh12; eds1-2* and *rh6*$^{(+/-)}$ *rh8 rh12; pad4-1* mutants. The seeds were germinated and grown on 0.5x MS media with 0.5% (w/v) sucrose for 7 days before seedlings were transferred to soil and grown for another 21 days. Bar = 1 cm. All mutants were in the Col-0 background. (E)Rosette diameter and fresh weight of 28-day-old plants of the genotypes presented in (D). Statistical significance was determined by ANOVA (*n* = 12-30), followed by a Tukey's HSD test on log-transformed data. Means that are significantly different from one another ($p < 0.05$) are denoted by different letters. (F) Reverse transcriptase-qPCR analysis of *PATHOGENESIS-RELATED GENE 1* (*PR1*) polyadenylated (total) transcript levels in 7-day-old seedlings the triple *rh6 rh8 rh12* mutant in comparison to the quadruple mutants *rh6 rh8 rh12; eds1-2* and *rh6 rh8 rh12; pad4-1* as well as the control genotypes Col-0, *eds1-2* and *pad4-1*. Relative transcript fold-change was calculated by the ΔΔCt method using *Actin 1* (*ACT1*) as a reference. Error bars represent the SD of three biological replicates. Statistical significance between genotypes was determined by ANOVA followed by a Tukey's HSD test on log-transformed data. Means that are significantly different from each other ($p < 0.05$) are represented by different letters. (G) Comparison of SA levels in 7-day-old seedlings of the quadruple mutants *rh6 rh8 rh12; eds1-2* and *rh6 rh8 rh12; pad4-1,* the triple *rh6 rh8 rh12* mutant and the control genotypes Col-0, *eds1-2* and *pad4-1*. Error bars represent the SD of three biological replicates. Statistical significance was determined by ANOVA followed by a Tukey's HSD test on log-transformed data. Significantly difference of means ($p < 0.05$) are represented by different letters.

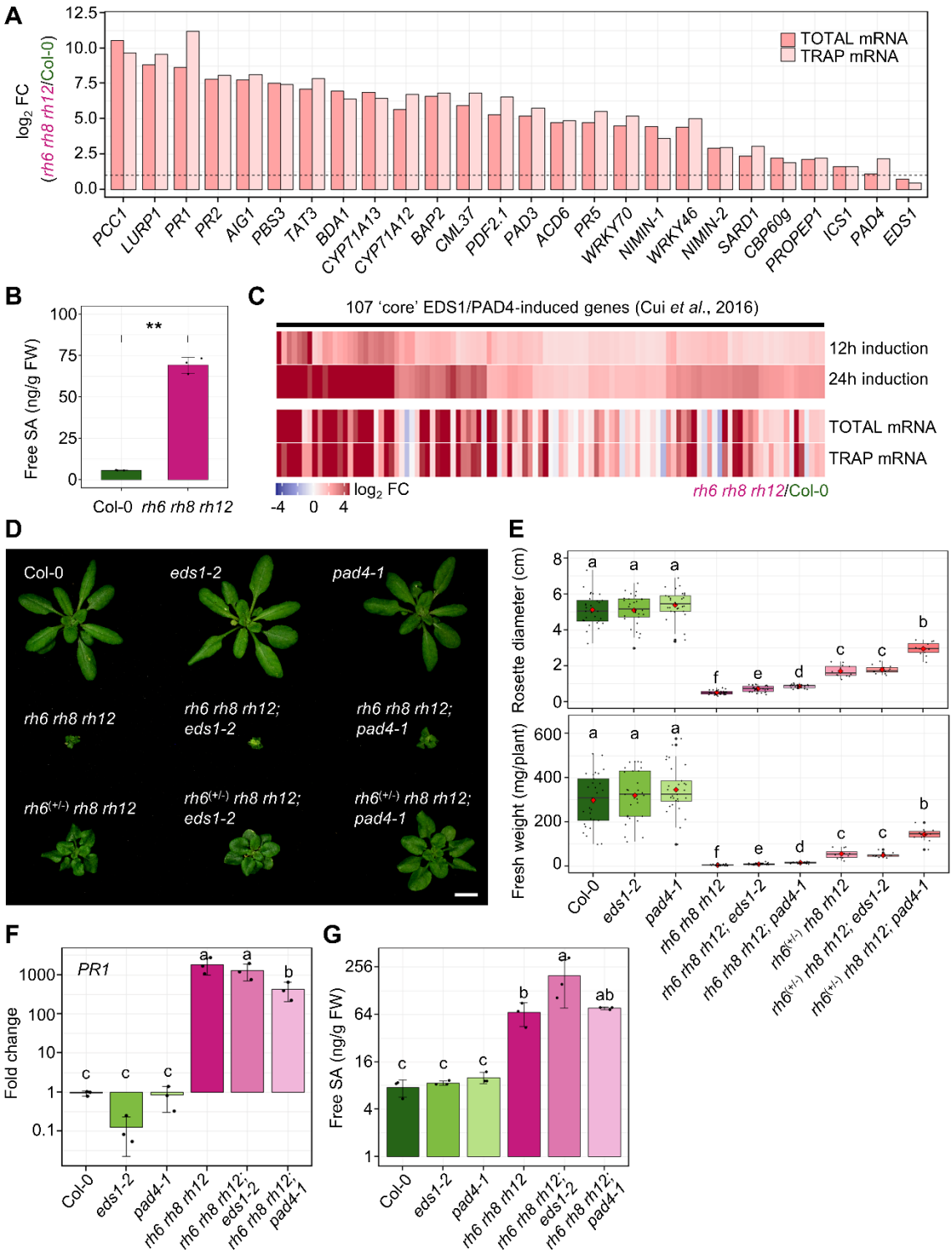
A
log2 FC (rh6 rh8 rh12/Col-0)
TOTAL mRNA
TRAP mRNA
PCC1
LURP1
PR1
PR2
AIG1
PBS3
TAT3
BDA1
CYP71A13
CYP71A12
BAP2
CML37
PDF2.1
PAD3
ACD6
PR5
WRKY70
NIMIN-1
WRKY46
NIMIN-2
SARD1
CBP60g
PROPEP1
ICS1
PAD4
EDS1
B
Free SA (ng/g FW)
Col-0
rh6 rh8 rh12
C
107 'core' EDS1/PAD4-induced genes (Cui et al., 2016)
12h induction
24h induction
TOTAL mRNA
TRAP mRNA
log2 FC
rh6 rh8 rh12/Col-0
D
Col-0
eds1-2
pad4-1
rh6 rh8 rh12
rh6 rh8 rh12; eds1-2
rh6 rh8 rh12; pad4-1
rh6(+/-) rh8 rh12
rh6(+/-) rh8 rh12; eds1-2
rh6(+/-) rh8 rh12; pad4-1
E
Rosette diameter (cm)
Fresh weight (mg/plant)
F
PR1
Fold change
G
Free SA (ng/g FW)

Figure 3.9. Suppression of the triple *rh6 rh8 rh12* mutant phenotype by ectopic overexpression of the bacterial salicylate hydroxylase *NahG*. (A) Simplified diagram of SA biosynthesis, perception and degradation. (B) Rosette growth phenotype of 28-day-old plants of Col-0, single *ics1* and *npr1-3* mutants, Col-0 overexpressing the bacterial *NahG* transgene, triple *rh6 rh8 rh12* mutant, quadruple *rh6 rh8 rh12; ics1* and *rh6 rh8 rh12; npr1-3* mutants, and triple *rh6 rh8 rh12* mutant combined with the bacterial *NahG* transgene. Seeds were germinated on 0.5x MS media with 0.5% (w/v) sucrose for 7 days before seedlings were transferred to soil and grown for another 21 days. Bar = 1 cm. All lines are Col-0 background. (C) Rosette diameter and fresh weight of 28-day-old plants of the genotypes presented in (B). Right panels are magnified plots of boxed data in the left panels. Statistical significance was determined by ANOVA (n = 25), followed by a Tukey's HSD test on log-transformed data. Means that are significantly different from each other ($p < 0.05$) are denoted by different letters. (D) RT-qPCR analysis of *PR1* transcript levels in 7-day-old seedlings of the genotypes presented in (B). Relative transcript fold-change was calculated by the ΔΔCt method using *Actin 1* (*ACT1*) as a reference. Error bars represent the SD of five biological replicates. Statistical significance between genotypes was determined by ANOVA followed by a Tukey's HSD test on log-transformed data. Significant mean differences ($p < 0.05$) are represented by different letters.

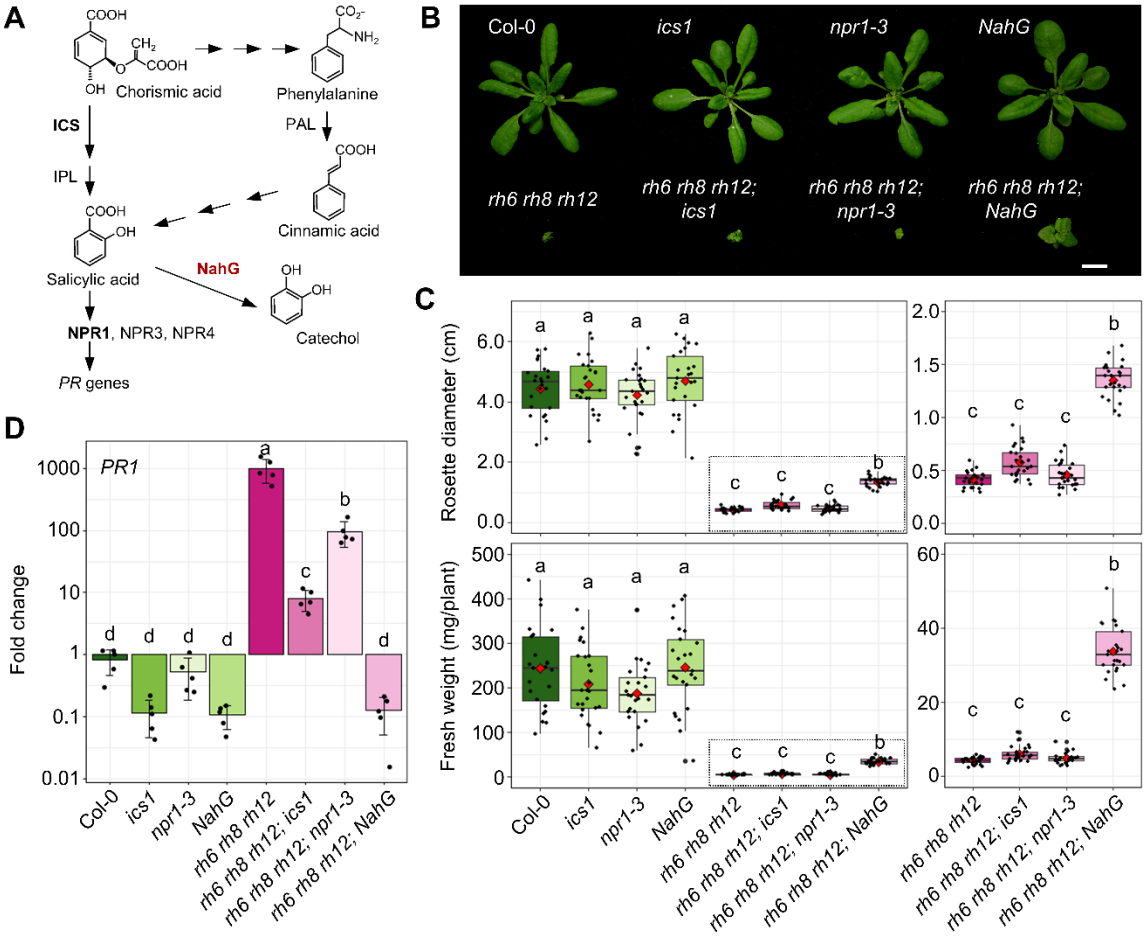
A
Chorismic acid
Phenylalanine
ICS
PAL
IPL
Cinnamic acid
Salicylic acid
NahG
Catechol
NPR1, NPR3, NPR4
PR genes
B
Col-0
ics1
npr1-3
NahG
rh6 rh8 rh12
rh6 rh8 rh12; ics1
rh6 rh8 rh12; npr1-3
rh6 rh8 rh12; NahG
C
Rosette diameter (cm)
Fresh weight (mg/plant)
D
PR1
Fold change

Figure 3.10. *SUPPRESSOR OF VARICOSE* (*SOV*) rescues the triple *rh6 rh8 rh12* mutant phenotype. (A) Venn diagrams showing the overlap of RH6/8/12 substrates with those of SOV and the overlap of RH6/8/12 substrates with those of VCS that can be degraded by SOV in the absence of VCS (Sorenson et al. 2018). The comparison was limited to the 12697 genes with mRNA $t_{1/2}$ less than 12 hours. (B) Representative rosette phenotype of 28-day-old plants of Col-0, Col-0 with the Landsberg *erecta* (L.*er*) allele of *SOV* (Col-0 $SOV^{L.er}$), the triple *rh6 rh8 rh12* mutant, and the triple mutant with the L.*er* allele of *SOV* (*rh6 rh8 rh12;* $SOV^{L.er}$). Col-0 $SOV^{L.er}$ was generated by transformation of $SOV^{L.er}$ genomic clone (native promoter) into Col-0 (Zhang et al., 2010). *rh6 rh8 rh12;* $SOV^{L.er}$ was a homozygous progeny of $rh6^{(+/-)}$ *rh8 rh12* crossed with Col-0 $SOV^{L.er}$. Seeds were germinated and grown on 0.5x MS media with 0.5% (w/v) sucrose for 7 days before seedlings were transferred to soil and grown for another 21 days. (C) and (D) Rosette diameter (C) and fresh weight (D) of 28-day-old plants of the genotypes shown in (B). Statistical significance was determined by ANOVA (n = 36), followed by a Tukey's HSD test on log-transformed data. Means that are significantly different from each other (p < 0.05) are denoted by different letters. (E) Representative rosette phenotype of 28-day-old plants of Col-0 and Col-0 overexpressing the L.*er* allele of *SOV* ($SOV^{L.er}$-*OX*), the triple *rh6 rh8 rh12* mutant, and the triple mutant overexpressing the L.*er* allele of *SOV* (*rh6 rh8 rh12;* $SOV^{L.er}$-*OX*). $SOV^{L.er}$-*OX* was generated by expression C-terminally CFP-tagged $SOV^{L.er}$ under the 35S promoter (Zhang et al., 2010). *rh6 rh8 rh12;* $SOV^{L.er}$-*OX* was a homozygous progeny of $rh6^{(+/-)}$ *rh8 rh12* crossed with $SOV^{L.er}$-*OX*. Seeds were germinated on 0.5x MS media with 0.5% (w/v) sucrose for 7 days before seedlings were transferred to soil and grown for 21 days. (F) and (G) Rosette diameter (F) and fresh weight (G) of 28-day-old plants corresponded to the genotypes shown in (E). Statistical significance was determined by ANOVA (n = 36 for rosette diameter; n = 30 for fresh weight), followed by a Tukey's HSD test on log-transformed data. Means that are significantly different from each other (p < 0.05) are denoted by different letters.

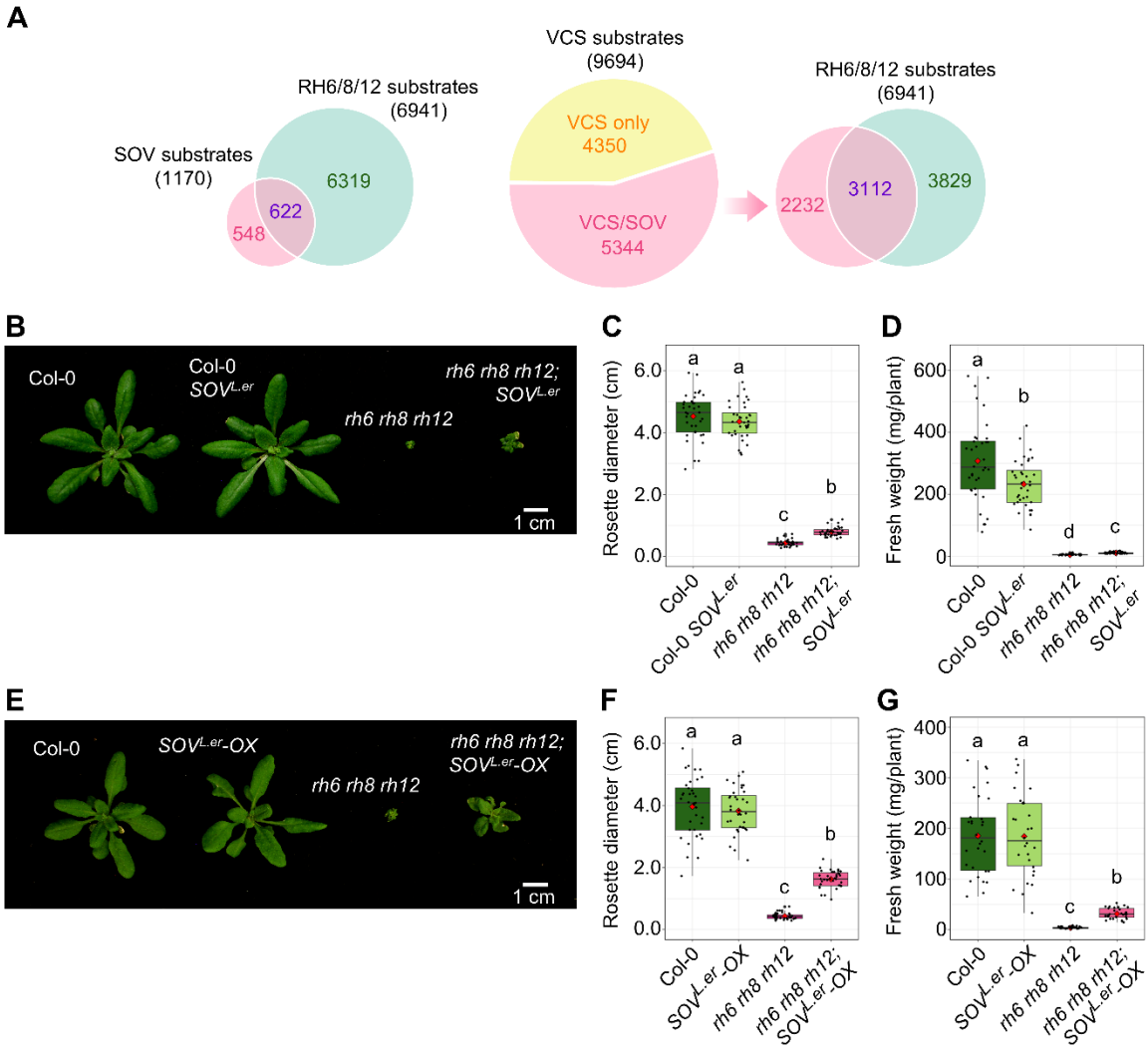
A
RH6/8/12 substrates
(6941)
SOV substrates
(1170)
6319
622
548
VCS substrates
(9694)
VCS only
4350
VCS/SOV
5344
RH6/8/12 substrates
(6941)
2232
3112
3829
B
Col-0
Col-0
SOV^L.er
rh6 rh8 rh12
rh6 rh8 rh12;
SOV^L.er
1 cm
C
Rosette diameter (cm)
6.0
4.0
2.0
0.0
a
a
b
c
Col-0
Col-0 SOV^L.er
rh6 rh8 rh12
rh6 rh8 rh12;
SOV^L.er
D
Fresh weight (mg/plant)
600
400
200
0
a
b
d
c
Col-0
Col-0 SOV^L.er
rh6 rh8 rh12
rh6 rh8 rh12;
SOV^L.er
E
Col-0
SOV^L.er-OX
rh6 rh8 rh12
rh6 rh8 rh12;
SOV^L.er-OX
1 cm
F
Rosette diameter (cm)
6.0
4.0
2.0
0.0
a
a
b
c
Col-0
SOV^L.er-OX
rh6 rh8 rh12
rh6 rh8 rh12;
SOV^L.er-OX
G
Fresh weight (mg/plant)
400
300
200
100
0
a
a
b
c
Col-0
SOV^L.er-OX
rh6 rh8 rh12
rh6 rh8 rh12;
SOV^L.er-OX

Figure 3.11. Comparative transcriptome analysis of the triple *rh6 rh8 rh12* and the rescued triple *rh6 rh8 rh12; SOV$^{L.er}$-OX* genotypes. (A) Schematic representation of genotypes and experimental strategies used in the RNA-seq analysis. Poly(A)$^+$ RNA-seq libraries were prepared in triplicate from 7-day-old seedlings of Col-0, *SOV$^{L.er}$-OX*, *rh6 rh8 rh12*, and *rh6 rh8 rh12; SOV$^{L.er}$-OX* grown on 0.5x MS media with 0.5% (w/v) sucrose under standard growth conditions. (B) Principal component analysis of edgeR-normalized read counts (CPMs) of mRNAs of the four genotypes. PC1 and PC2 are principal components 1 and 2. (C) Volcano plots of change in steady-state mRNA abundance between different pairwise comparisons of the four genotypes based on differential expression analysis by edgeR. The $\log_2$ FC is shown on the x axis, and the negative $\log_{10}$ of the FDR is shown on the y axis. Red and blue dots represent significantly enriched and depleted mRNAs, respectively ($|\log_2 FC| \geq 1$, FDR < 0.01). Green dots represent not-differentially expressed genes. Light green dot represents change in *SOV* transcript levels. Total number of genes used in the analysis presented in parentheses.

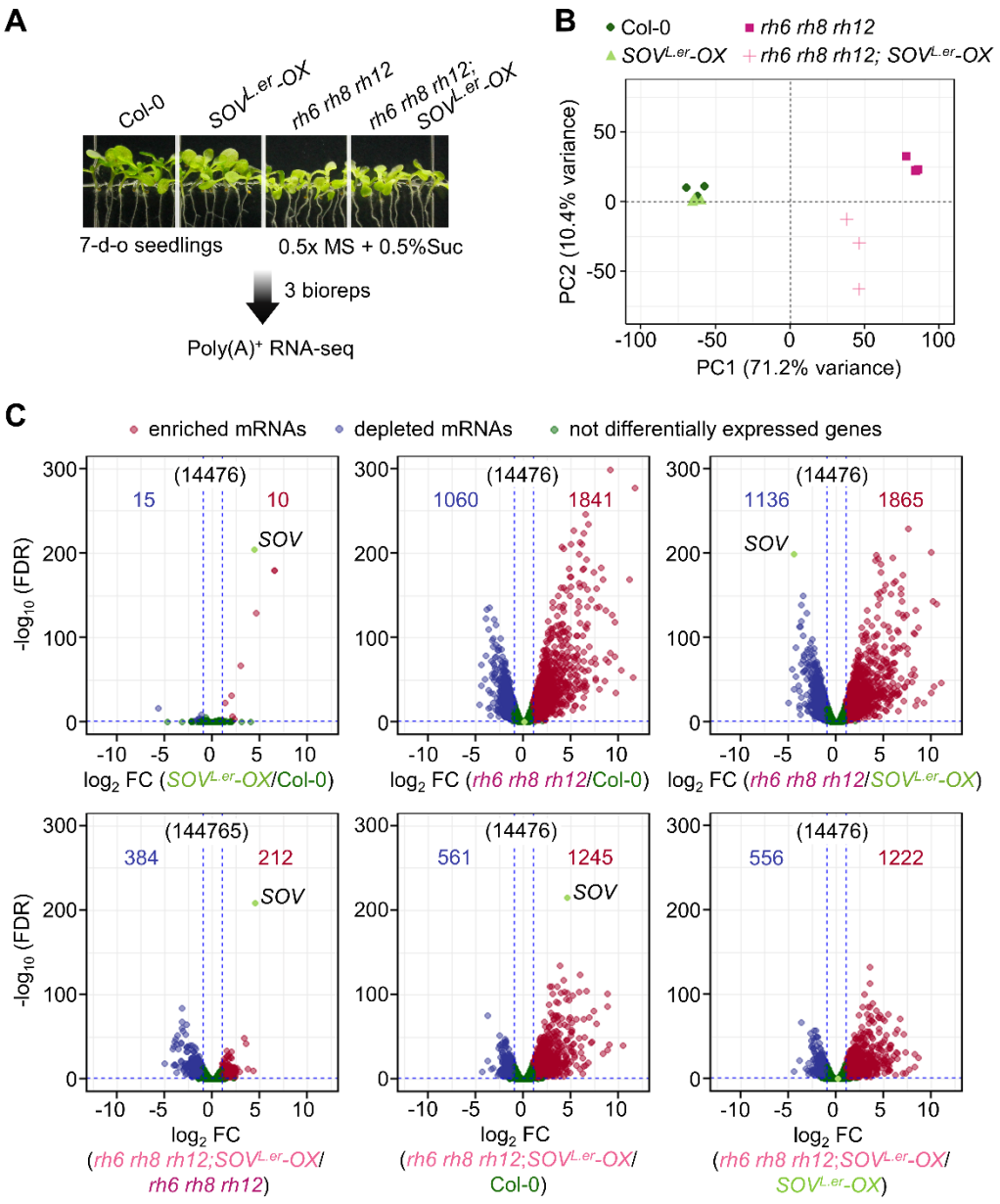
A
Col-0
SOV^L.er -OX
rh6 rh8 rh12
rh6 rh8 rh12; SOV^L.er -OX
7-d-o seedlings
0.5x MS + 0.5%Suc
3 bioreps
Poly(A)+ RNA-seq
B
Col-0
rh6 rh8 rh12
SOV^L.er-OX
rh6 rh8 rh12; SOV^L.er-OX
PC2 (10.4% variance)
PC1 (71.2% variance)
C
enriched mRNAs
depleted mRNAs
not differentially expressed genes
-log10 (FDR)
(14476)
15
10
SOV
log2 FC (SOV^L.er-OX/Col-0)
(14476)
1060
1841
log2 FC (rh6 rh8 rh12/Col-0)
(14476)
1136
1865
SOV
log2 FC (rh6 rh8 rh12/SOV^L.er-OX)
(144765)
384
212
SOV
log2 FC (rh6 rh8 rh12;SOV^L.er-OX/ rh6 rh8 rh12)
(14476)
561
1245
SOV
log2 FC (rh6 rh8 rh12;SOV^L.er-OX/ Col-0)
(14476)
556
1222
log2 FC (rh6 rh8 rh12;SOV^L.er-OX/ SOV^L.er-OX)

Figure 3.12. *SOV* overexpression mitigates the growth-to-defense shift in the *rh6 rh8 rh12* triple mutant. (A) Partitioning around medoids clustering of differentially expressed mRNAs (|log2 FC| ≥ 1, FDR < 0.01) based on the pairwise comparisons between Col-0, SOVL.er-OX, rh6 rh8 rh12 and rh6 rh8 rh12; SOVL.er-OX genotypes. Each column represents a pairwise comparison of mRNA FC between two genotypes. The heatmap scale is log2 FC. Number of genes in each cluster is shown to the left of the heatmap. (B) Biological process GO functional categories of genes from each cluster in (A). Only five terms with the lowest adjusted p-value from each cluster are presented. (C) Examples of mRNAs of genes involved in defense response that are enriched in the triple rh6 rh8 rh12 mutant relative to Col-0 and SOVL.er-OX genotypes and depleted in the complemented triple rh6 rh8 rh12; SOVL.er-OX line relative to the rh6 rh8 rh12 mutant (log2 FC ≥ 1, FDR < 0.01). Each row of the heatmap represents the z-score of read counts (read per kilobase per million, RPKM) for a gene with three biological replicates. (D) Quantification of SA levels in the complemented triple rh6 rh8 rh12; SOVL.er-OX line in comparison to the rh6 rh8 rh12 mutant, and Col-0 and SOVL.er-OX lines. Error bars represent the SD of three biological replicates. Statistical significance was determined by ANOVA followed by a Tukey's HSD test on log-transformed data. Significant difference of means ($p < 0.05$) are represented by different letters.

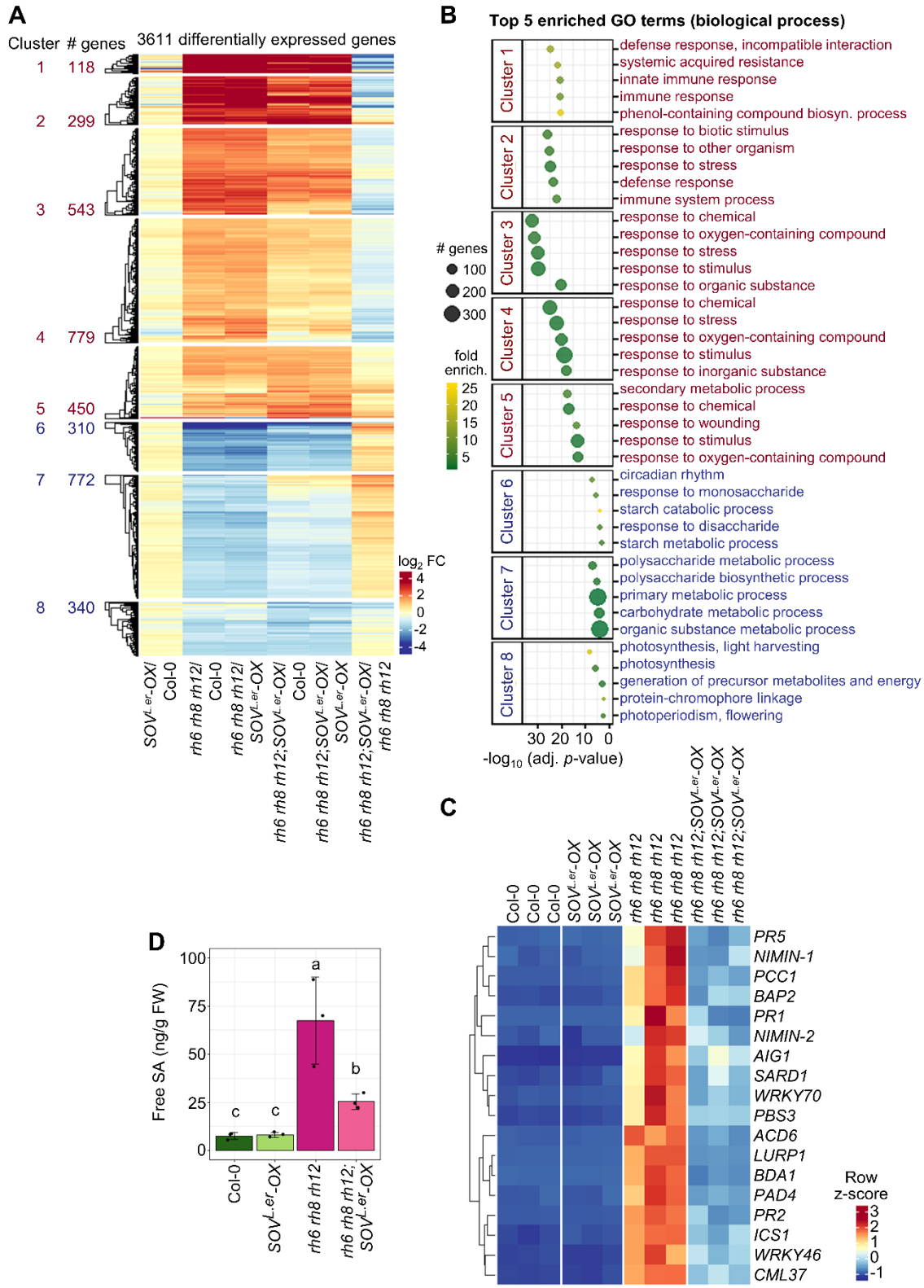
A
Cluster # genes
3611 differentially expressed genes
1 118
2 299
3 543
4 779
5 450
6 310
7 772
8 340
log2 FC
4
2
0
-2
-4
Col-0
SOVL.er-OX/ Col-0
rh6 rh8 rh12/ Col-0
rh6 rh8 rh12/ SOVL.er-OX
rh6 rh8 rh12;SOVL.er-OX/ Col-0
rh6 rh8 rh12;SOVL.er-OX/ SOVL.er-OX
rh6 rh8 rh12;SOVL.er-OX/ rh6 rh8 rh12
B
Top 5 enriched GO terms (biological process)
Cluster 1
defense response, incompatible interaction
systemic acquired resistance
innate immune response
immune response
phenol-containing compound biosyn. process
Cluster 2
response to biotic stimulus
response to other organism
response to stress
defense response
immune system process
Cluster 3
response to chemical
response to oxygen-containing compound
response to stress
response to stimulus
response to organic substance
Cluster 4
response to chemical
response to stress
response to oxygen-containing compound
response to stimulus
response to inorganic substance
Cluster 5
secondary metabolic process
response to chemical
response to wounding
response to stimulus
response to oxygen-containing compound
Cluster 6
circadian rhythm
response to monosaccharide
starch catabolic process
response to disaccharide
starch metabolic process
Cluster 7
polysaccharide metabolic process
polysaccharide biosynthetic process
primary metabolic process
carbohydrate metabolic process
organic substance metabolic process
Cluster 8
photosynthesis, light harvesting
photosynthesis
generation of precursor metabolites and energy
protein-chromophore linkage
photoperiodism, flowering
genes
100
200
300
fold enrich.
25
20
15
10
5
30 20 10 0
-log10 (adj. p-value)
C
Col-0
Col-0
Col-0
SOVL.er-OX
SOVL.er-OX
SOVL.er-OX
rh6 rh8 rh12
rh6 rh8 rh12
rh6 rh8 rh12
rh6 rh8 rh12;SOVL.er-OX
rh6 rh8 rh12;SOVL.er-OX
rh6 rh8 rh12;SOVL.er-OX
PR5
NIMIN-1
PCC1
BAP2
PR1
NIMIN-2
AIG1
SARD1
WRKY70
PBS3
ACD6
LURP1
BDA1
PAD4
PR2
ICS1
WRKY46
CML37
Row z-score
3
2
1
0
-1
D
Free SA (ng/g FW)
100
75
50
25
0
a
b
c
c
Col-0
SOVL.er-OX
rh6 rh8 rh12
rh6 rh8 rh12; SOVL.er-OX

Table 3.1. Primers used for genotyping of mutant alleles

Allele	Primer	Sequence (5'-3')	Note
rdr6^{sgs2-1}	Primer 1	GCCTAGACGAAGCAGGGATACT	CAPS marker: *Mnl*I cuts the *rdr6*$^{sgs2-1}$ mutant allele
	Primer 2	TTGACCTGGTGGTTGACAGC	
sgs3-1	Primer 1	GCTTCTTCACAAGATGATCCAGGAGAGT	dCAP marker: *Bst*XI cuts the wild-type allele
	Primer 2	CGACCATTGCCGTTACCTCTC	
eds1-2	Primer 1	ACACAAGGGTGATGCGAGACA	Multiplex PCR: wild-type, 1500 bp + 750 bp; *eds1-2,* 1500 bp + 600 np (Gloggnitzer et al., 2014)
	Primer 2	GGCTTGTATTCATCTTCTATCC	
	Primer 3	GTGGAAACCAAATTTGACATTAG	
pad4-1	Primer 1	GCGATGCATCAGAAGAG	CAPS marker: *Bsm*F1 cuts the wild-type allele (Gloggnitzer et al., 2014)
	Primer 2	TTAGCCCAAAAGCAAGTATC	
ics1	Primer 1	ACGAGAGAAGAAACAGCGAG	Primer 1 + Primer 2: wild-type Primer 2 + Primer 3 (T-DNA left border): *ics1* mutant allele
	Primer 2	CAGAAGTATGAGTCATGTTCG	
	Primer 3	ATTTTGCCGATTTCGGAAC	
npr1-3	Primer 1	GGCCGACTATGTGTAGAAATACTAGCG	dCAP marker: *Hha*I cuts the wild-type allele (Ding et al., 2015)
	Primer 2	TGAGACGGTCAGGCTCGAGG	
NahG	Primer 1	CTGCCGCTACTCCCATATCCA	Specific to the *NahG* transgene
	Primer 2	TCGGCTTCGGCTCGCTAC	
SOV$^{L.er}$	Primer 1	CTGAGGTTATTTCTCAAGCACACC	dCAP marker: *Dra*III cuts the *SOV*$^{Col-0}$ allele
	Primer 2	GTCCTTCAAATTCCCAGTGCAG	

Chapter 4

General Conclusions

The fate and state of cytoplasmic mRNAs is dynamically regulated both by internal cues and external perturbations. Cytoplasmic mRNA dynamics and homeostasis are, therefore, critical for developmental progression and cellular response to the changing external environment. Central to these processes is mRNA translation, the fundamental process that decodes the genetic information in mRNAs into functional proteins. Translational regulation is intertwined with the mechanisms that funnel mRNAs into a translationally inactive state, including sequestration by RNA-binding proteins along with components of the translational apparatus into macromolecular complexes generally called stress granules (SGs) or association with one or several multi-protein decay complexes including the processing bodies (PBs) associated with 5'-to-3' mRNA catabolism following 3' deadenylation. Together, spatiotemporal fidelity of translation, sequestration, and decay allows the cells to control when, where and how many mRNAs are translated or retired, thereby contributing to the cellular proteome homeostasis.

DEAD-box RNA helicases of the DHH1/DDX6 family play a conserved role in the regulation cytoplasmic mRNA fate and function, connecting translational silencing with the process of 5'-to-3' mRNA turnover across eukaryotic organisms (Presnyak and Coller, 2013). Using a phylogenetic approach, this dissertation established that the DHH1/DDX6 family is conserved in plants. In the model plant *Arabidopsis thaliana*, we demonstrated that the DHH1/DDX6-like proteins RH6, RH8, and RH12 are functionally redundant and have a pivotal role in the maintenance of plant growth and development. Simultaneous loss/severe reduction of *RH6*, *RH8*, and *RH12* function in the triple *rh6 rh8*

rh12 mutant results in a severe reduction of growth and development that are associated an aberrant expression of stress/defense-responsive mRNAs under optimal growth conditions. This phenomenon was directly attributed to the role of RH6/8/12 in mRNA degradation as the growth defects as well as constitutive immune response of the *rh6 rh8 rh12* genotype could be partially rescued by an overexpression of a single protein decay enzyme, the 3'-to-5' exoribonuclease SOV.

The work from this study revealed that the DHH1/DDX6-like RHs specifically regulate turnover of short-lived or unstable mRNAs. In other eukaryotes, including the budding yeast *Saccharomyces cerevisiae* (Presnyak et al., 2015), the fission yeast *Schizosaccharomyces pombe* (Harigaya and Parker, 2016), the trypanosomatid *Trypanosoma brucei* (Jeacock et al., 2018), *Drosophila* (Bazzini et al., 2016), *Xenopus* (Bazzini et al., 2016), zebrafish (Bazzini et al., 2016; Mishima and Tomari, 2016), and mouse (Bazzini et al., 2016), codon optimality have been shown to be a key determinant of mRNA decay that is directly coupled with ribosome dynamics, and translation efficiency through fidelity determined by different synonymous codons together with the concentration of their cognate tRNAs. In this regard, optimal codons are associated with higher translational efficiency, more abundant cognate tRNA species, and increased stability. By contrast, non-optimal codons reduce ribosome translocation rates and causes ribosome stalling that result in a decrease in mRNA stability (Hanson and Coller, 2017). It is possible that mRNAs that require RH6/8/12 function for their decay contain non-optimal codons that reduce their translation efficiency and overall stability. Evaluation of the codon bias of these putative RH6/8/12 substrates would provide insight into the association of their codon usage and RH6/8/12-dependent decay.

Additionally, this study showed that RH6/8/12 putative substrates have shorter than average transcript lengths and encoded by genes with fewer introns. This suggests that stability and decay of this mRNA population might be dictated by the nuclear events related to their transcription and processing, such as cotranscriptional mRNA splicing. In humans, cytoplasmic DDX6 co-immunoprecipitated with the core exon junction complex proteins eIF4A3, MLN51, MAGOH, and Y14 (Ayache et al., 2015). It was suggested that DDX6 binds newly exported mRNAs. However, whereas the nuclear function of the DHH1/DDX6 protein family is unknown, the observation that DDX6 as well as RH6, RH8 and RH12 are also localized in the nucleus makes it possible that the DHH1/DDX6-like RHs might associate with nuclear mRNAs, continue their association during mRNA export from the nucleus, and control their decay during the pioneer round of translation. It is also possible that mRNA decay occurs in the nucleus, an activity typically attributed to the 3'-to-5' decay function of the exosome.

To gain more insight into the role of RH6/8/12 in mRNA decay, RH6 can be used as a representative of the three DHH1/DDX6-like RHs for a proteomic analysis of its associated proteins from the nuclear-specific and total (nucleocytoplasmic) fractions. The isolation of nuclei tagged in specific cell types (INTACT) technology (Deal and Henikoff, 2011) can be incorporated into a transgenic line expressing FLAG- or RFP-tagged RH6 to enable the purification of nuclear-localized RH6. In addition to a proteomic analysis, RH6-bound mRNAs can be isolated from the nuclear fraction through a ribonucleoprotein immunopurification (RIP) (Sorenson and Bailey-Serres, 2015) and analyzed by RNA-seq (RIP-seq) together with RH6-bound mRNAs from the total fraction. Not only would such an experiment provide a clue on the role of RH6 nuclear function and the possible relevance of its nuclear presence with its role in mRNA

decay, but the RH6 interactome will also shed light on how RH6/8/12 couple translational repression with mRNA decay.

In yeast and human, DHH1 and DDX6 have been shown to interact with the ribosome (Ayache et al., 2015; Radhakrishnan et al., 2016), and the role of DHH1/DDX6 family in translational repression is mediated by its interacting partner eIF4E transporter (4E-T) (Kinkelin et al., 2012). However, it is unlikely that true 4E-T orthologs are conserved in plants. RH6 interactome data will determine whether RH6 interacts with the ribosome and likely provide a clue on the proteins that supplant 4E-T function in *Arabidopsis* and plants in general. As an alternative to proteomic analysis, the association of the epitope tagged RH6 with ribosomes can be evaluated by sucrose density gradient purification or TRAP of ribosomes and western blotting. If RH6 association with mRNAs in the nucleus and/or with polysomes is confirmed, data of RH6 RIP-seq performed separately on nuclear and total cell extracts can be integrated into the mRNA decay, transcriptome and translatome data of the wild-type and triple *rh6 rh8 rh12* mutant generated in this dissertation. The existing data can be complemented by a transcriptome analysis of nuclear mRNAs in the wild-type and *rh6 rh8 rh12* genotypes. Together, these data could be used to delineate the connection between nuclear mRNA metabolism and cytoplasmic mRNA fates that is regulated by the DHH1/DDX6-like RHs.

In plants, inefficient mRNA decay in such decapping mutants as *dcp2* and *vcs* triggers siRNA production by RDR6. The developmental defects and premature lethality in these mutants are suppressed by mutation of *RDR6* (Martínez de Alba et al., 2015). Interestingly, the growth and developmental defects of the triple *rh6 rh8 rh12* genotype is independent of *RDR6* and *SGS3* function. It is possible that, unlike other mRNA decay mutants, stabilized mRNAs present in the triple *rh6 rh8 rh12* mutant might be

inaccessible to RDR6, hence preventing siRNA production. Based on the fact that the mRNA 3' poly(A) tail inhibits RDR6 activity (Baeg et al., 2017), and that the DHH1/DDX6-like proteins in other eukaryotes are associated with the CCR4-NOT complex, it can be hypothesized that loss of RH6/8/12 function also compromises mRNA deadenylation. Hence, the stabilized mRNAs in the *rh6 rh8 rh12* genotype are likely to be present with longer poly(A) tail as compared to those in the decapping mutants *dcp2* and *vcs*. These hypotheses can be tested by small RNA-seq profiling of 21- and 22-nt siRNAs in wild-type and the triple *rh6 rh8 rh12* mutant tissues. Changes in poly(A) tail length of putative RH6/8/12 substrates in the triple mutant compared with those of the wild-type and the decapping mutant *vcs-7* could be evaluated using the mTAIL-seq technology (Lim et al., 2016).

In this study, we determined that RH6, RH8, and RH12 are required for PB formation and degradation of subpopulation of mRNAs. However, it remains unknown in which cytoplasmic sub-compartment the decay of RH6/8/12-regulated mRNAs takes place. Does it occur in cytoplasmic complexes with all necessary protein components or is a macromolecular assembly of multiple complexes (i.e. a PB) necessary? Future work can address this question.

PBs are translationally silenced mRNPs enriched with mRNA decay factors (Mugridge et al., 2018). Our data and studies in humans indicate that the presence of PBs that can be seen by confocal microscopy are not required for 5'-to-3' mRNA decay (Eulalio et al., 2007), although it is also suggested that these mRNP assemblages are sites of accelerated decay, as the decay machinery and mRNA substrates are concentrated at the same sites (Chan et al., 2018; Sheu-Gruttadauria and MacRae, 2018). However, other studies indicate that mRNAs targeted to PBs are stabilized but

not degraded (Horvathova et al., 2017; Hubstenberger et al., 2017; Tutucci et al., 2018a). To test whether or not RH6/8/12-regulated mRNAs are degraded in PBs, dual localization and decay of a selected putative RH6/8/12 substrate can be monitored with RH6 and another core decapping protein such as DCP2 or VCS in live cells using the MS2 system that has been demonstrated to be feasible in plants (Li et al., 2015; Luo et al., 2018). An improved MS2 system with reduced affinity for the MS2 coat protein that allows mRNA decay while preserving single-molecule detection has recently been developed, and can possibly be applicable in plant cells (Tutucci et al., 2018a; Tutucci et al., 2018b). Alternatively, a multicolor riboswitch-based technology for mRNA visualization in live cells has also been developed, and it would be interesting to test this system in plants (Braselmann et al., 2018). Even with such technologies it may be difficult to confirm sites of active RH6/8/12-regulated decay.

In yeast, DHH1 has been shown to sense codon optimality, and target mRNAs with non-optimal codons that have reduced translation elongation rate for degradation (Radhakrishnan et al., 2016). In this study, we found that decay of at least 397 RH6/8/12-dependent transcripts is coupled with translational repression. It is unclear if degradation of these mRNAs occurs cotranslationally or independently after translational repression and polysome disassembly. In plants, it is well appreciated that cotranslational decay operates on a subset of transcripts and is dependent on XRN4 function (Hou et al., 2016; Yu et al., 2016). It is postulated that this process requires mRNA decapping and possibly RH6/8/12 function. A possible role of the DHH1/DDX6-like RHs in cotranslational decay could be gleaned from the existing translatome data. If decay of this mRNA population occurs on the elongating ribosome, it is most likely that the RNA-seq-mapped read distributions of TRAP mRNAs in the wild-type Col-0 would be

biased toward to 3' end of the transcript as a result of the progressive 5'-to-3' decay. This pattern may disappear in the *rh6 rh8 rh12* genotype as decay of these mRNA is impaired. Ultimately, this hypothesis can be directly tested by use of genome-wide mapping of uncapped and cleaved transcripts (GMUCT) (Willmann et al., 2014) to profile the abundance and read distribution of uncapped mRNAs in the triple *rh6 rh8 rh12* mutant. This readout would provide a global view of cotranslational decay with the signature 3-nt periodicity at the mRNA 5' end, as cotranslational decay proceeds along the transcripts in the wide-type, that might be abolished in the *rh6 rh8 rh12* genotype if cotranslational decay is compromised.

In this study, we showed in the triple *rh6 rh8 rh12* mutant that loss of the DHH1/DDX6-like RHs causes a constitutive immune response that dampens the overall growth and development associated with stabilization and ectopic translation of defense-responsive mRNAs. As overexpression of the bacterial salicylic acid hydroxylase *NahG* only partially rescues the triple mutant phenotype, it is most likely that growth reduction as a result of the impaired RH function also occurs independently of autoimmunity. This is supported by the fact that the single and double *rh* mutants displayed reduced rosette growth without an accumulation of defense-related transcripts. It would be interesting to interrogate how RH6/8/12 regulates growth. A RNA-seq analyses of single or double *rh* mutants may provide a clue on how the seedling transcriptome is altered when one or two members of the family are not functional.

In eukaryotes including plants, the circadian clock regulates a plethora of factors that affect growth (Farré, 2012). Integrated analysis of transcriptome, translatome and mRNA decay data indicated that the circadian rhythm of triple *rh6 rh8 rh12* mutant is likely altered based on the stabilization of the morning regulator *CIRCADIAN CLOCK*

ASSOCIATED 1 and *LATE ELONGATED HYPOCOTYL 1* transcripts, together with an increase in their translational status as well as TRAP and TOTAL mRNA abundance. This is concomitant with a depletion of transcripts encoding the afternoon and evening regulators in the *rh6 rh8 rh12* genotype, including *GIGANTEA*, *TIMING OF CAB EXPRESSION 1*, and *LUX ARRHYTHMO*. It is possible that the DHH1/DDX6-like RHs control plant growth homeostasis through translational regulation of these clock regulators.

While this work began to unveil the function of the *Arabidopsis* DHH1/DDX6-like RHs in plant growth and development, evidence from the protein subcellular localization as well as mRNA decay analysis suggests that this protein family may also play a role in responses to both biotic and abiotic stresses. Given that RH6, RH8, and RH12 regulate translational repression and decay of defense-responsive mRNAs, the question remains as to how the RHs regulate decay and translation of these mRNAs in the presence of pathogen, and how they contribute to plant defense against pathogen infections. In fact, RH8 has been shown to be a critical factor required for potyvirus infection (Huang et al., 2010). Manipulation of the mRNA decay machinery as well as host mRNP complexes by viruses has emerged as an exciting area of research on plant-pathogen interactions (Reineke and Lloyd, 2013; Tsai and Lloyd, 2014). This might be relevant with RH6/8/12 function. Additionally, the fact that RH6, RH8, and RH12 complexes are induced by under-coverslip hypoxia treatment and that these complexes can associate with UBP1C SGs suggest that the function of DHH1/DDX6-like RHs might be relevant to translational repression and decay of hypoxia-regulated mRNAs. Association of RH6/8/12 complexes with UBP1C SGs supports the notion that mRNAs bound by UBP1C under hypoxia can be routed to degradation both during hypoxic conditions and during recovery periods

(Sorenson and Bailey-Serres, 2014). As translational repression and mRNA sequestration by UBP1C are critical to plant survival under hypoxia, it would be interesting to test how the RHs affect the stability and translational status of UBP1C-associated mRNAs, and how this protein family contributes to plant fitness under hypoxic conditions.

The discovery that the RH6/8/12 proteins are a component of the decapping complex that controls the turnover of high-flux RNAs associated with abiotic and biotic stress, as well as other processes, provides new opportunities for fine tuning gene activity to enhance plant fitness under stress conditions.

4.1 REFERENCES

Ayache J, Bénard M, Ernoult-Lange M, Minshall N, Standart N, Kress M, Weil D (2015) P-body assembly requires DDX6 repression complexes rather than decay or Ataxin2/2L complexes. Mol Biol Cell **26**: 2579–2595

Baeg K, Iwakawa H-O, Tomari Y (2017) The poly(A) tail blocks RDR6 from converting self mRNAs into substrates for gene silencing. Nat Plants **3**: 17036

Bazzini AA, Del Viso F, Moreno-Mateos MA, Johnstone TG, Vejnar CE, Qin Y, Yao J, Khokha MK, Giraldez AJ (2016) Codon identity regulates mRNA stability and translation efficiency during the maternal-to-zygotic transition. EMBO J **35**: 2087–2103

Braselmann E, Wierzba AJ, Polaski JT, Chromiński M, Holmes ZE, Hung S-T, Batan D, Wheeler JR, Parker R, Jimenez R, et al (2018) A multicolor riboswitch-based platform for imaging of RNA in live mammalian cells. Nat Chem Biol **14**: 964–971

Chan LY, Mugler CF, Heinrich S, Vallotton P, Weis K (2018) Non-invasive measurement of mRNA decay reveals translation initiation as the major determinant of mRNA stability. Elife. doi: 10.7554/eLife.32536

Deal RB, Henikoff S (2011) The INTACT method for cell type-specific gene expression and chromatin profiling in Arabidopsis thaliana. Nat Protoc **6**: 56–68

Eulalio A, Behm-Ansmant I, Schweizer D, Izaurralde E (2007) P-body formation is a consequence, not the cause, of RNA-mediated gene silencing. Mol Cell Biol **27**: 3970–3981

Farré EM (2012) The regulation of plant growth by the circadian clock: Circadian regulation of plant growth. Plant Biol **14**: 401–410

Hanson G, Coller J (2017) Codon optimality, bias and usage in translation and mRNA decay. Nat Rev Mol Cell Biol. doi: 10.1038/nrm.2017.91

Harigaya Y, Parker R (2016) Analysis of the association between codon optimality and mRNA stability in Schizosaccharomyces pombe. BMC Genomics **17**: 895

Horvathova I, Voigt F, Kotrys AV, Zhan Y, Artus-Revel CG, Eglinger J, Stadler MB, Giorgetti L, Chao JA (2017) The Dynamics of mRNA Turnover Revealed by Single-Molecule Imaging in Single Cells. Mol Cell. doi: 10.1016/j.molcel.2017.09.030

Hou C-Y, Lee W-C, Chou H-C, Chen A-P, Chou S-J, Chen H-M (2016) Global Analysis of Truncated RNA Ends Reveals New Insights into Ribosome Stalling in Plants. The Plant Cell Online **28**: 2398–2416

Huang T-S, Wei T, Laliberté J-F, Wang A (2010) A Host RNA Helicase-Like Protein, AtRH8, Interacts with the Potyviral Genome-Linked Protein, VPg, Associates with the Virus Accumulation Complex, and Is Essential for Infection. Plant Physiol **152**: 255–266

Hubstenberger A, Courel M, Bénard M, Souquere S, Ernoult-Lange M, Chouaib R, Yi Z, Morlot J-B, Munier A, Fradet M, et al (2017) P-Body Purification Reveals the Condensation of Repressed mRNA Regulons. Mol Cell. doi: 10.1016/j.molcel.2017.09.003

Jeacock L, Faria J, Horn D (2018) Codon usage bias controls mRNA and protein abundance in trypanosomatids. Elife. doi: 10.7554/eLife.32496

Kinkelin K, Veith K, Grünwald M, Bono F (2012) Crystal structure of a minimal eIF4E-Cup complex reveals a general mechanism of eIF4E regulation in translational repression. RNA **18**: 1624–1634

Lim J, Lee M, Son A, Chang H, Kim VN (2016) mTAIL-seq reveals dynamic poly(A) tail regulation in oocyte-to-embryo development. Genes Dev **30**: 1671–1682

Li W, Ma M, Feng Y, Li H, Wang Y, Ma Y, Li M, An F, Guo H (2015) EIN2-Directed Translational Regulation of Ethylene Signaling in Arabidopsis. Cell **163**: 670–683

Luo K-R, Huang N-C, Yu T-S (2018) Selective targeting of mobile mRNAs to plasmodesmata for cell-to-cell movement. Plant Physiol. doi: 10.1104/pp.18.00107

Martínez de Alba AE, Moreno AB, Gabriel M, Mallory AC, Christ A, Bounon R, Balzergue S, Aubourg S, Gautheret D, Crespi MD, et al (2015) In plants, decapping prevents RDR6-dependent production of small interfering RNAs from endogenous mRNAs. Nucleic Acids Res **43**: 2902–2913

Mishima Y, Tomari Y (2016) Codon Usage and 3′ UTR Length Determine Maternal mRNA Stability in Zebrafish. Mol Cell **61**: 874–885

Mugridge JS, Coller J, Gross JD (2018) Structural and molecular mechanisms for the control of eukaryotic 5'-3' mRNA decay. Nat Struct Mol Biol. doi: 10.1038/s41594-018-0164-z

Presnyak V, Alhusaini N, Chen Y-H, Martin S, Morris N, Kline N, Olson S, Weinberg D, Baker KE, Graveley BR, et al (2015) Codon Optimality Is a Major Determinant of mRNA Stability. Cell **160**: 1111–1124

Presnyak V, Coller J (2013) The DHH1/RCKp54 family of helicases: An ancient family of proteins that promote translational silencing. Biochimica et Biophysica Acta (BBA) - Gene Regulatory Mechanisms **1829**: 817–823

Radhakrishnan A, Chen Y-H, Martin S, Alhusaini N, Green R, Coller J (2016) The DEAD-Box Protein Dhh1p Couples mRNA Decay and Translation by Monitoring Codon Optimality. Cell. doi: 10.1016/j.cell.2016.08.053

Reineke LC, Lloyd RE (2013) Diversion of stress granules and P-bodies during viral infection. Virology **436**: 255–267

Sheu-Gruttadauria J, MacRae IJ (2018) Phase Transitions in the Assembly and Function of Human miRISC. Cell **173**: 946–957.e16

Sorenson R, Bailey-Serres J (2015) Rapid immunopurification of ribonucleoprotein complexes of plants. Methods Mol Biol **1284**: 209–219

Sorenson R, Bailey-Serres J (2014) Selective mRNA sequestration by OLIGOURIDYLATE-BINDING PROTEIN 1 contributes to translational control during hypoxia in Arabidopsis. Proceedings of the National Academy of Sciences **111**: 2373–2378

Tsai W-C, Lloyd RE (2014) Cytoplasmic RNA Granules and Viral Infection. Annu Rev Virol **1**: 147–170

Tutucci E, Vera M, Biswas J, Garcia J, Parker R, Singer RH (2018a) An improved MS2 system for accurate reporting of the mRNA life cycle. Nat Methods **15**: 81–89

Tutucci E, Vera M, Singer RH (2018b) Single-mRNA detection in living S. cerevisiae using a re-engineered MS2 system. Nat Protoc **13**: 2268–2296

Willmann MR, Berkowitz ND, Gregory BD (2014) Improved genome-wide mapping of uncapped and cleaved transcripts in eukaryotes--GMUCT 2.0. Methods **67**: 64–73

Yu X, Willmann MR, Anderson SJ, Gregory BD (2016) Genome-Wide Mapping of Uncapped and Cleaved Transcripts Reveals a Role for the Nuclear mRNA Cap-Binding Complex in Co-translational RNA Decay in Arabidopsis. The Plant Cell Online tpc.00456.2016